Middle Rio Grande San Acacia Reach: Morphodynamic Processes and Silvery Minnow Habitat from San Acacia Diversion Dam to Escondida Bridge 1918-2018

Final report prepared for:
United States Bureau of Reclamation
Award Number R17AC00064
Period 10/1/2018 – 9/30/2019
June 2020

Sydney Doidge
Caitlin Fogarty
Tori Beckwith
Dr. Pierre Julien

Colorado State University
Engineering Research Center
Department of Civil and Environmental Engineering
Fort Collins, Colorado 80523

Abstract

The San Acacia reach spans 11.6 miles of the Middle Rio Grande (MRG), from the San Acacia Diversion Dam to the Escondida Bridge in central New Mexico. This reach report, prepared for the United States Bureau of Reclamation (USBR), aims to better understand the morphodynamic processes of this reach. The reach is divided into four subreaches (SA1, SA2, SA3 and SA4) to better recognize the spatial and temporal trends in channel geometry and morphology.

The river is dynamic, still changing in response to anthropogenic impacts over the last century (Makar 2006). A decline in mean annual discharge and suspended sediment discharge has resulted in significant channel degradation in all subreaches. In subreach SA1, immediately downstream of the diversion dam, there has been over 10 feet of degradation since 1962. Analysis of the bed material also shows evidence of bed fining throughout time downstream of the San Acacia Diversion Dam. Coarser material was found closer to the dam, but bed material samples with d_{50} larger than 1 mm are not found beyond 22,000 ft downstream of the dam (close to agg/deg line 1246).

GIS analysis of digitized aerial photographs dating back to 1918 was also performed. The channel width has decreased over time. The width of subreach SA3 is currently one tenth of the width in 1918. Other reaches have exhibited a similar but less drastic transformation. By 2012, all subreaches are within 50% of the Julien-Wargadalam equation predicted width. Sinuosity drops for all subreaches after 1949. Beginning in 1985, sinuosity begins to increase for all subreaches, except SA4 which maintains a value of around 1.02.

Massong et al.’s 2010 geomorphic conceptual model for the Middle Rio Grande was used to classify representative cross-sections in the San Acacia reach. These cross-sections were then compared to aerial imagery and habitat curves to link trends between geomorphology, biology, and hydraulics. Application of the model finds that most subreaches are currently in the M4 stage, which represents excessive transport capacity and constraint by vegetation.

HEC-RAS analysis was performed to better understand habitat conditions for the endangered Rio Grande Silvery Minnow (RGSM). Subreach SA3 contained the most habitat when normalized by reach length across all years compared (1962, 1972, 1992, 2002 and 2012). Comparing across years found differences in habitat-discharge curves, suggesting that changes to geomorphology have impacted hydraulically suitable habitat. Overall, areas with velocities suitable for silvery minnow habitat were the limiting factor compared to depth in the availability of total habitat.

Finally, a time integrated habitat metric (TIHM) was used to predict habitat on an annual basis depending on the daily discharge and the RGSM life stage. Interpolation between the five known habitat curves was completed using changes in cumulative sediment to create annual habitat curves. The habitat curves are adjusted according to the measured daily discharge to estimate the daily RGSM available habitat, which is then summed over the life stage representative months. Results showed that larval and juvenile stages are more sensitive to the changes in discharge.

Table of Contents

List of Tables

List of Figures

Appendix A List of Figures

Appendix B List of Figures

Appendix C List of Figures

Appendix D List of Figures

Appendix E List of Figures

Appendix F List of Figures

Appendix G List of Figures

1. Introduction

The purpose of this reach report is to evaluate the morpho-dynamic conditions on the Middle Rio Grande (MRG), which extends from the Cochiti Dam downstream to the Narrows in Elephant Butte Reservoir (Figure 1). This report focuses on the San Acacia reach which begins at the San Acacia Diversion Dam and continues downstream to the bridge near Escondida, New Mexico (Figure 1).

It is part of a series of reports commissioned by the USBR to include morpho-dynamic reach reports, reports on the biological-habitat conditions for the Rio Grande Silvery Minnow, and process linkage reports. The process linkage reports will ultimately connect morpho-dynamic conditions with the required biological-habitat conditions. This report focuses on understanding the current physical condition in the San Acacia reach. Specific objectives include:

- Delineate the reach into subreaches based on shared geomorphic characteristics;
- Summarize the flow and sediment discharge conditions and trends for the period of record available from United State Geologic Survey (USGS) gages;
- Analyze geomorphic characteristics at a subreach level (sinuosity, width, bed elevation, bed material, and other hydraulic parameters);
- Link changes in the river geomorphologics with shifts in sediment and flow trends; and
- Apply a geomorphic conceptual model to help predict future river changes.

Finally, in preparation for a future process linkage report, attempts were made to characterize fish habitat in the San Acacia reach. These methods were based on HEC-RAS one-dimensional hydraulic models to understand the conditions on the Middle Rio Grande. This series of reports will support USBR's mission on the Middle Rio Grande. Current maintenance goals for the USBR include habitat improvements for species listed by the Endangered Species Act and support of channel sustainability while continuing to provide effective water delivery (U.S. Bureau of Reclamation 2012).

Figure 1 Map with the Middle Rio Grande outlined in blue. It begins at the Cochiti Dam (top) and continues to the Narrows in Elephant Butte Reservoir (bottom). The lime green highlights the San Acacia reach.

1.1 Site Description and Background

The Middle Rio Grande (MRG) has historically been characterized by large spring flooding events from snowmelt and periods of drought. These floods often caused large scale shifts in the course of the river and rapid aggradation (Massong et al 2010). Floods helped maintain aquatic ecosystems by enabling connection between water in the main channel and the floodplains (Scurlock 1998), but these events also threatened human establishments. Beginning in the 1930s, levees were installed to prevent flooding, while dams were used to store and regulate flow in the river. In the 1950s, the USBR undertook a significant channelization effort involving jetty jacks, river straightening and other techniques (Makar, 2006). While these efforts enabled agriculture and large-scale human developments along the MRG, they have also fundamentally changed the river, reducing sediment supply downstream, and altering channel geometry and vegetation. Narrowing of the river continues, with channel degradation due to limited sediment supply and the formation of vegetated bars that encroach into the channel (Varyu 2013; Massong et al 2010). The river continues to adjust to anthropomorphic impacts (Makar 2006). These factors have created an ecologically stressed environment, as seen in the decline of species such as the Rio Grande Silvery Minnow (Mortensen et al 2019).

The San Acacia reach is part of the Middle Rio Grande located in central New Mexico. This reach begins at the San Acacia Diversion Dam in Socorro County in New Mexico. It continues approximately 11.6 miles downstream to the bridge that crosses the Rio Grande near Escondida, New Mexico.

1.2 Aggradation/Degradation Lines and Rangelines

Aggradation/degradation lines (agg/deg lines) are “spaced approximately 500-feet apart and are used to estimate sedimentation and morphological changes in the river channel and floodplain for the entire MRG” (Posner 2017). Each agg/deg line is surveyed when the USBR performs monitoring and is adapted as a cross-section into the HEC-RAS models of the Rio Grande. These are surveyed on an approximately ten-year interval, starting in 1962. The most recent entire MRG survey was performed in 2012. In addition to the agg/deg lines, there are rangelines, which preceded the creation of the agg/deg lines and have different spacing. Rangeline locations were determined in association with geomorphic factors such as migrating bends and incision, along with river maintenance issues such as threats to infrastructure.

Cross-section geometry at each agg/deg line is available from models developed by the Technical Service Center. Models are available for 1962, 1972, 1992, 2002 and 2012. The 2012 model was developed from LiDAR data, but models prior to 2012 used photogrammetry techniques. All models use the NADV88 vertical datum.

1.3 Subreach Delineation

To analyze hydraulic trends, the reach was subdivided into four sections. These subreaches were primarily delineated by confluences or by cumulative plots of hydraulic variables such as channel top width and flow depth. Subreaches were designated when there was a noticeable change in the slope of the cumulative plots. These plots were developed using a HEC-RAS model with 2002 and 2012 geometry. A flow of 3,000 cfs was selected for cumulative plots of hydraulic variables to be consistent with previous reach reports (LaForge et al. 2019; Yang et al. 2019). This is the nominal discharge that fills the main channel without overbanking. The percent exceedance for 3,000 cfs is approximately 9.3% at the Rio Grande Floodway near San Acacia, NM.

Subreach SA1 (San Acacia 1) begins at the San Acacia Diversion Dam and continues downstream to the confluence with the Alamillo Arroyo, encompassing agg/deg lines 1207-1245. SA2 begins at the confluence with the Alamillo Arroyo and continues until a cumulative change in depth was seen (i.e. this subreach is deeper than the downstream subreach). SA2 includes agg/deg lines 1245-1264. SA3 begins where the cumulative depth plots indicate that the river is shallower, and continues until the cumulative width plot indicates narrowing, agg/deg lines 1264-1300. SA4 is a narrower section of the river and continues until Escondida Bridge at the conclusion of the entire San Acacia reach and at agg/deg line 1313. See Appendix A Subreach Delineation for all cumulative mass plots used in these determinations. Table 1 describes these delineations along with the mean and median widths from the HEC-RAS results in feet and Figure 2 through Figure 5 show maps of the subreach delineations.

Table 1 San Acacia Subreach Delineation

San Acacia Reach			Width in 2012		
Subreach	Agg/deg lines	Justification	Mean	Median	Standard Deviation
SA1	1207-1245	San Acacia Diversion Structure	197	179	64
SA2	1245-1264	Confluence with Alamillo Arroyo	227	216	83
SA3	1264-1300	Change in cumulative depth (shallower)	378	369	136
SA4	1300-1313	Change in cumulative width (narrower)	182	144	72

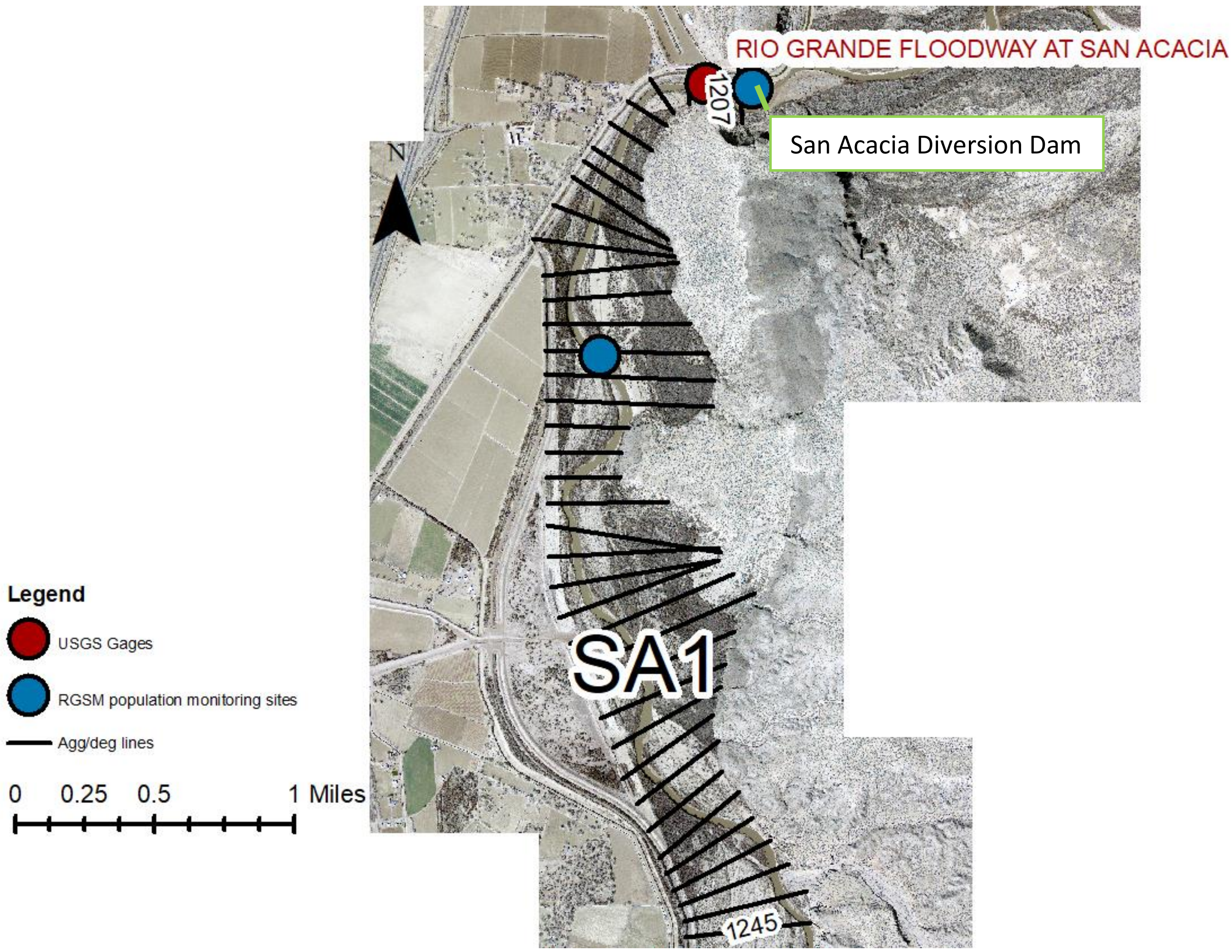

Figure 2 Subreach SA1; flow direction is north to south. The top most RGSM population monitoring site is downstream of the San Acacia Diversion Dam shown in green

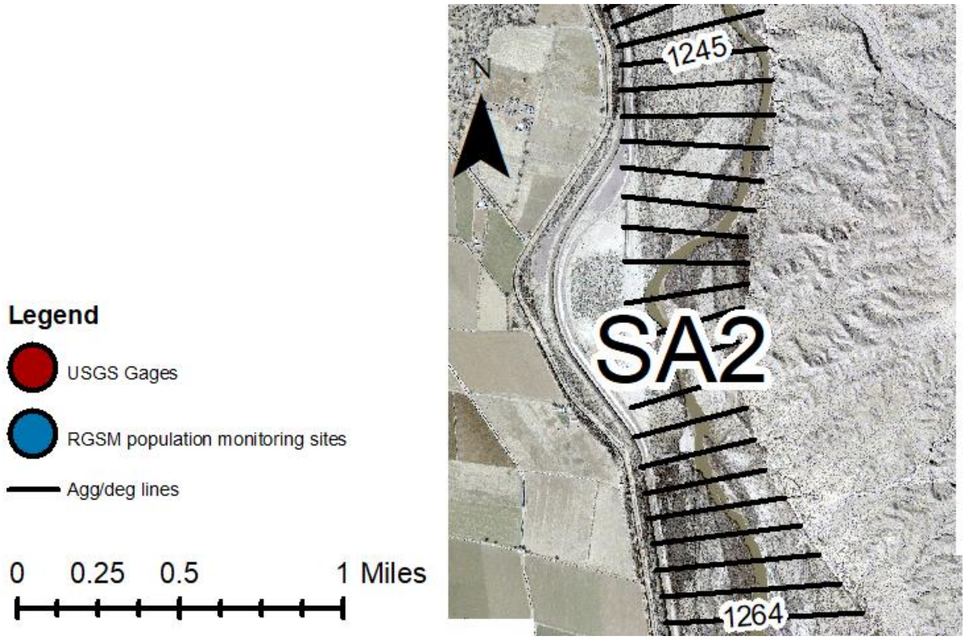

Figure 3 Subreach SA2; flow direction is north to south

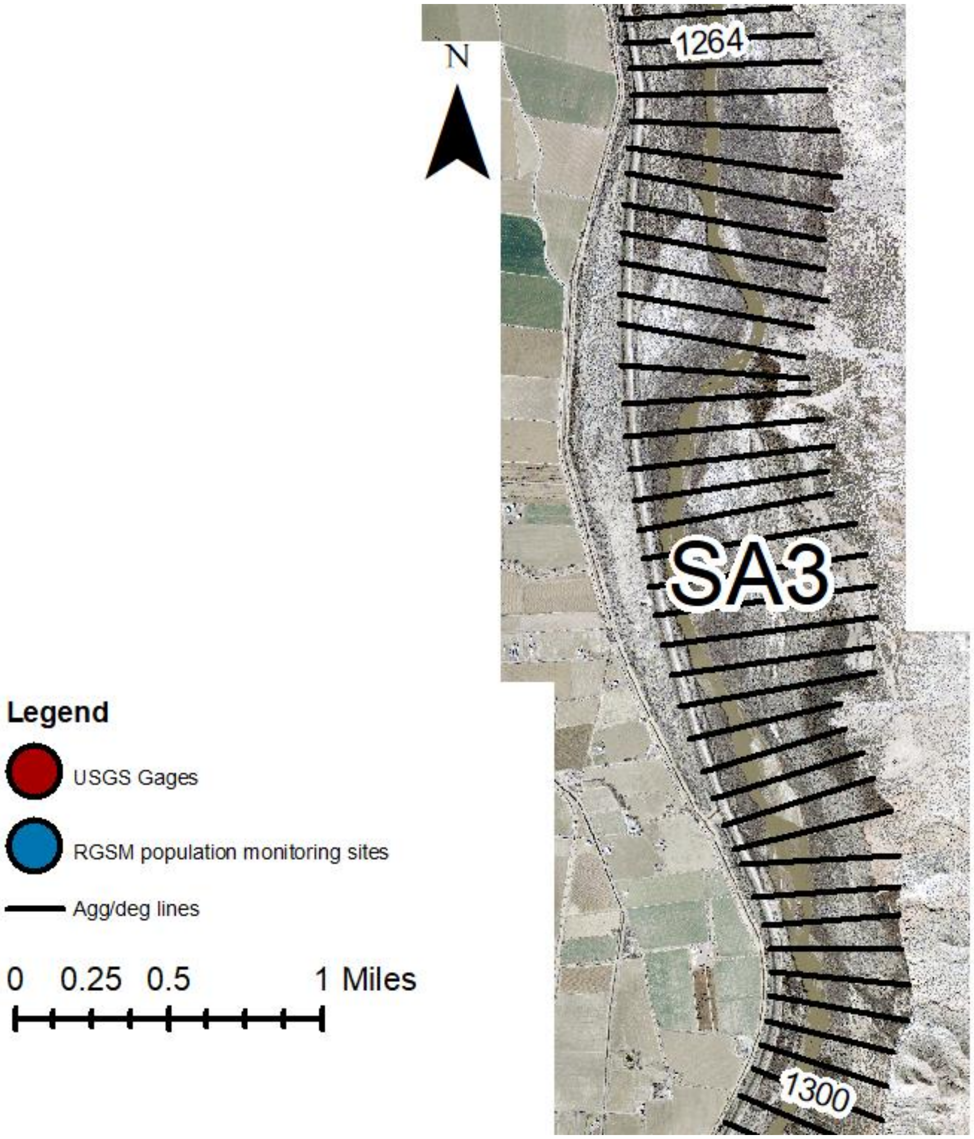

Figure 4 Subreach SA3; flow direction is north to south

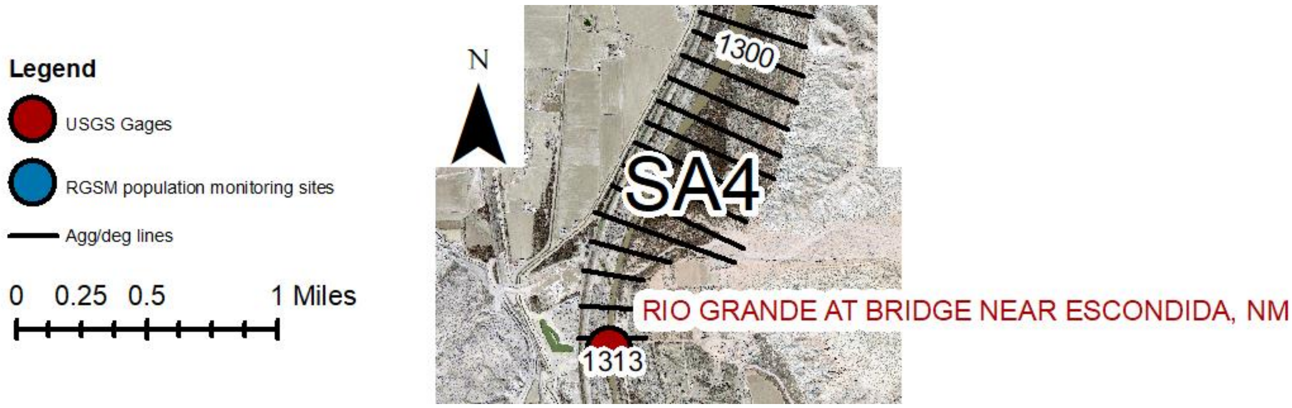

Figure 5 Subreach SA4; flow direction is north to south

2. Precipitation, Flow and Sediment Discharge Analysis

2.1 Precipitation

Precipitation data are collected along the MRG by the Bosque Ecosystem Monitoring Program from University of New Mexico (BEMP Data 2017). The locations of data collection are shown in Figure 6.

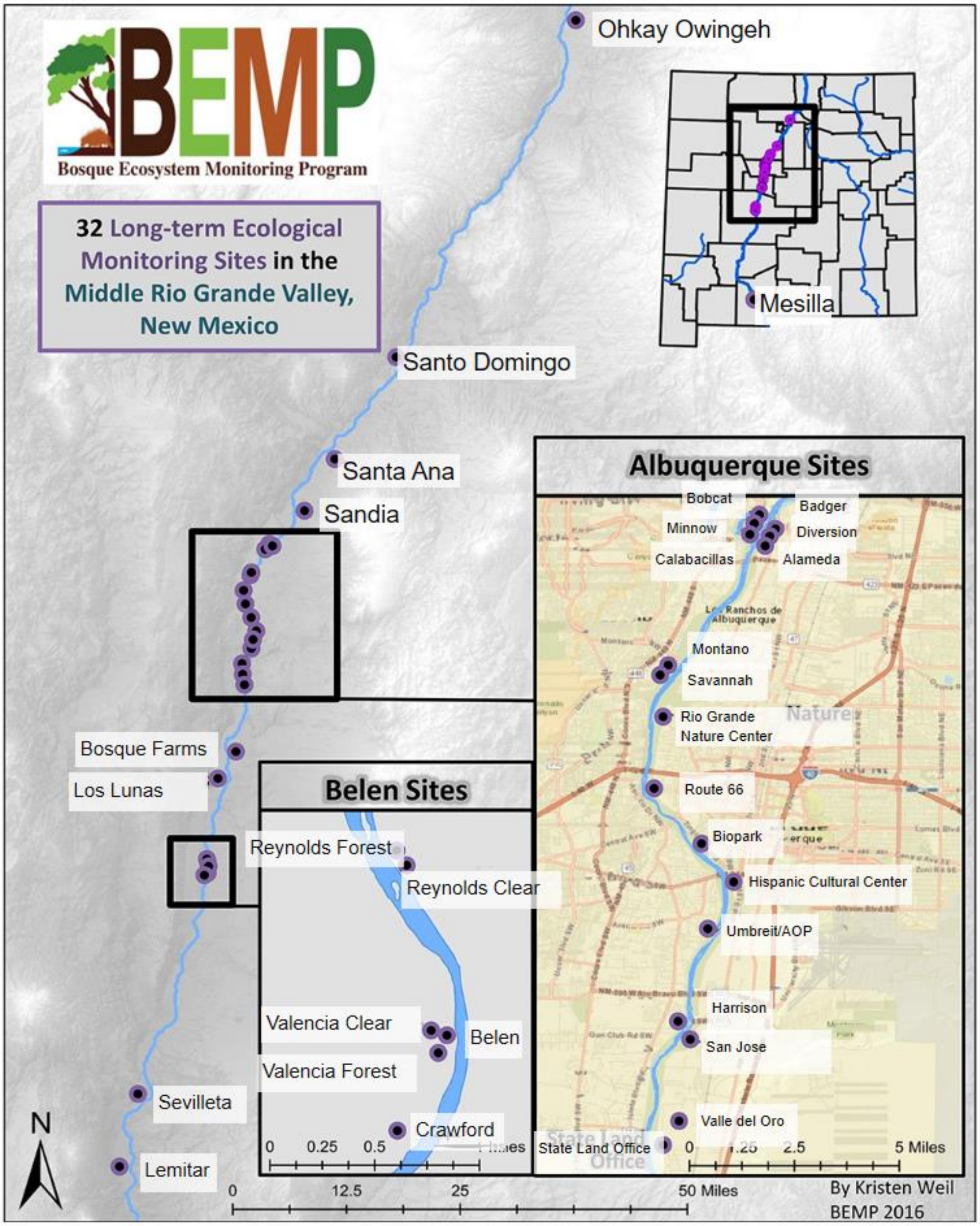

Figure 6 BEMP data collection sites (figure source: http://bemp.org)

The Sevilleta site is near the San Acacia Diversion Dam, and the Lemitar site is between the San Acacia Diversion Dam and Escondida, just outside of Lemitar, New Mexico. Both sites were used in the precipitation analysis. The precipitation data are shown in Figure 7. By far, the highest precipitation peak was in August of 2006 at the Lemitar gage, with 140.55 mm of rainfall total. A general trend was observed with highest precipitation values during monsoon season (late July through early September), although some outliers were seen. A cumulative plot of rainfall (Figure 8) shows that individual rain events can greatly affect the overall trend of the data. It further highlights the monsoonal rains, which create a “stepping” pattern with higher rainfall in August and September, and lower levels (a nearly flat trend) through the rest of the year.

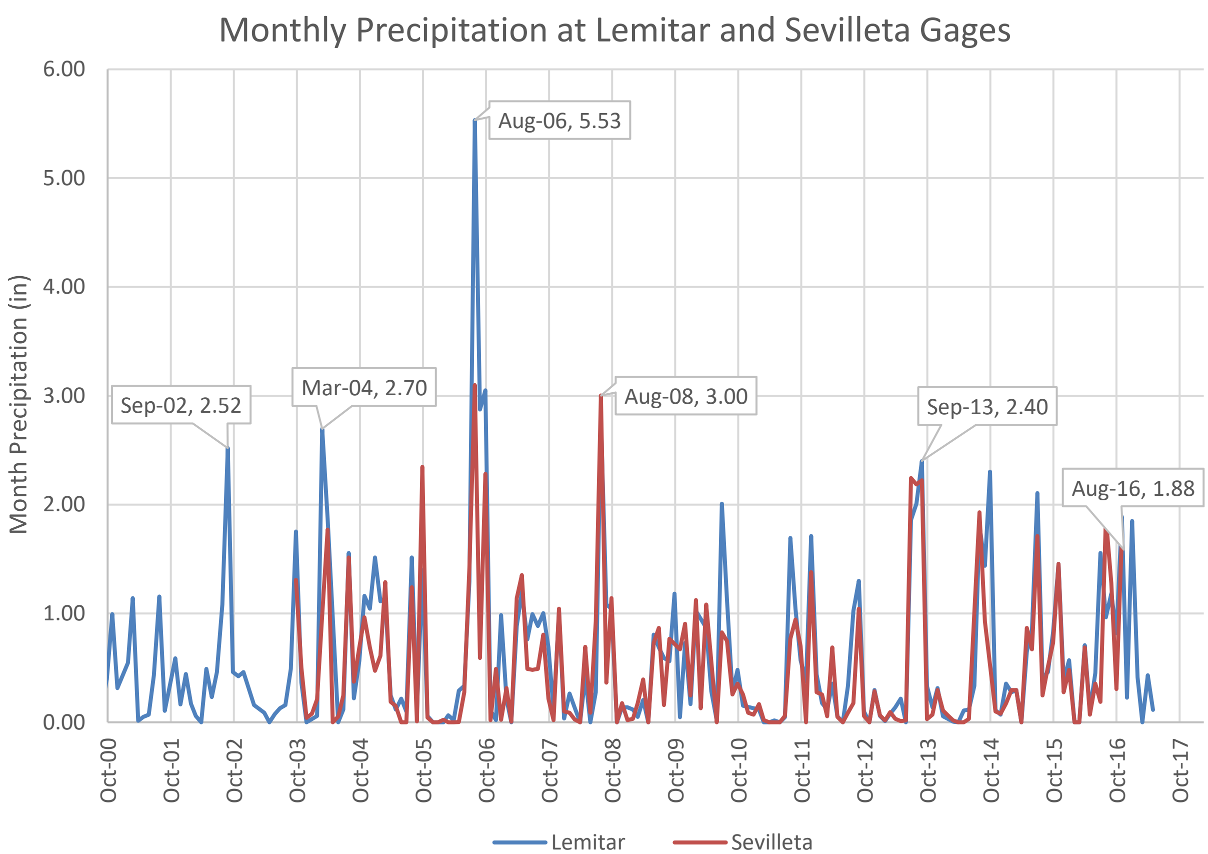

Figure 7 Monthly precipitation trends for the San Acacia reach

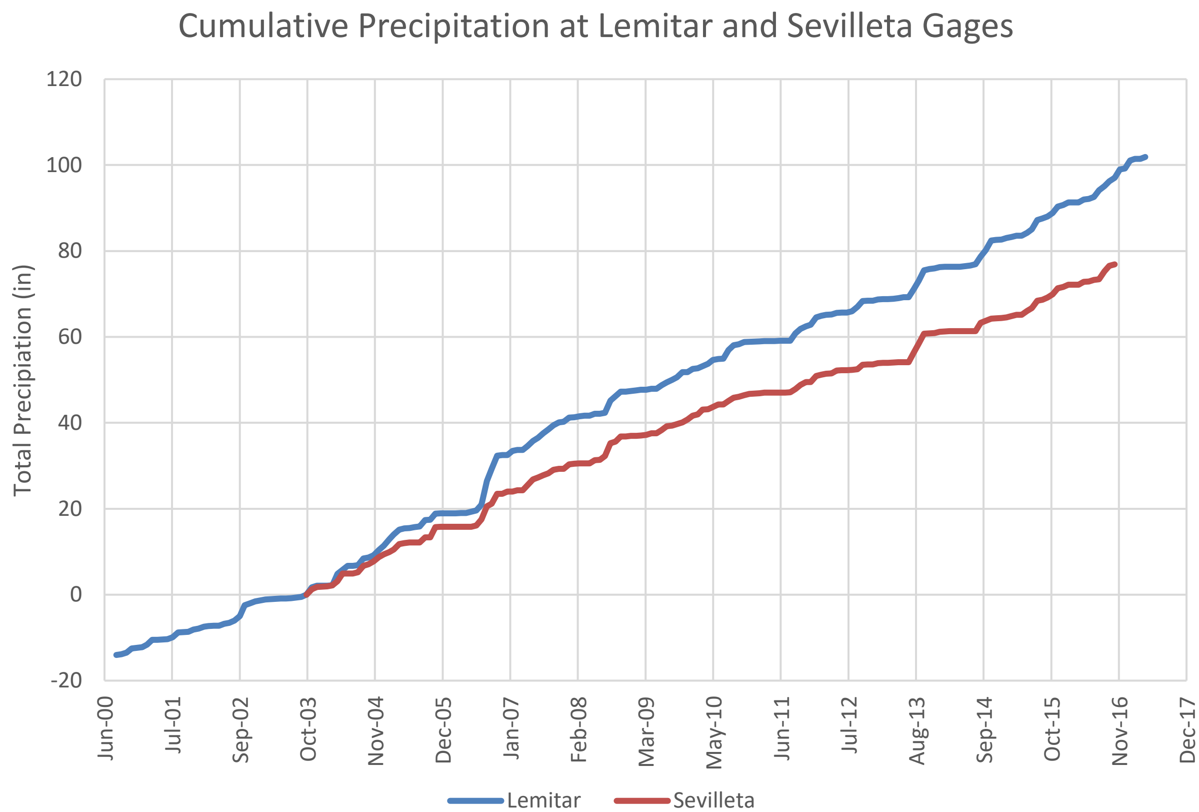

Figure 8 Cumulative precipitation for the San Acacia Reach

2.2 Flow Discharge

Available gages near the study area were found in the United State Geological Survey (USGS) National Water Information System. Table 2 lists the gages analyzed in this report. These gages can be seen relative to the reach in Figure 2 and Figure 5.

Table 2 List of gages used in this study

Station	Station Number	Mean Daily Discharge	Suspended Sediment
Rio Grande at San Acacia NM	08355000*	May 1, 1936 to September 29, 1964	No data
Rio Grande Floodway at San Acacia	08354900	October 1, 1958 to present	January 5, 1959 to September 30, 2018
Rio Grande At Bridge Near Escondida, NM	08355050	September 30, 2005 to present	No data

*Indicates a historical gage that was renamed

The daily discharge of the San Acacia (08355000* and 08354900) and Escondida (08355050) gages are shown in Figure 9 through Figure 11. These show seasonal flow patterns, with peak flow occurring during snowmelt runoff April through June, low flow through much of the rest of the summer, and then medium flow from November onwards, representing the end of the irrigation season.

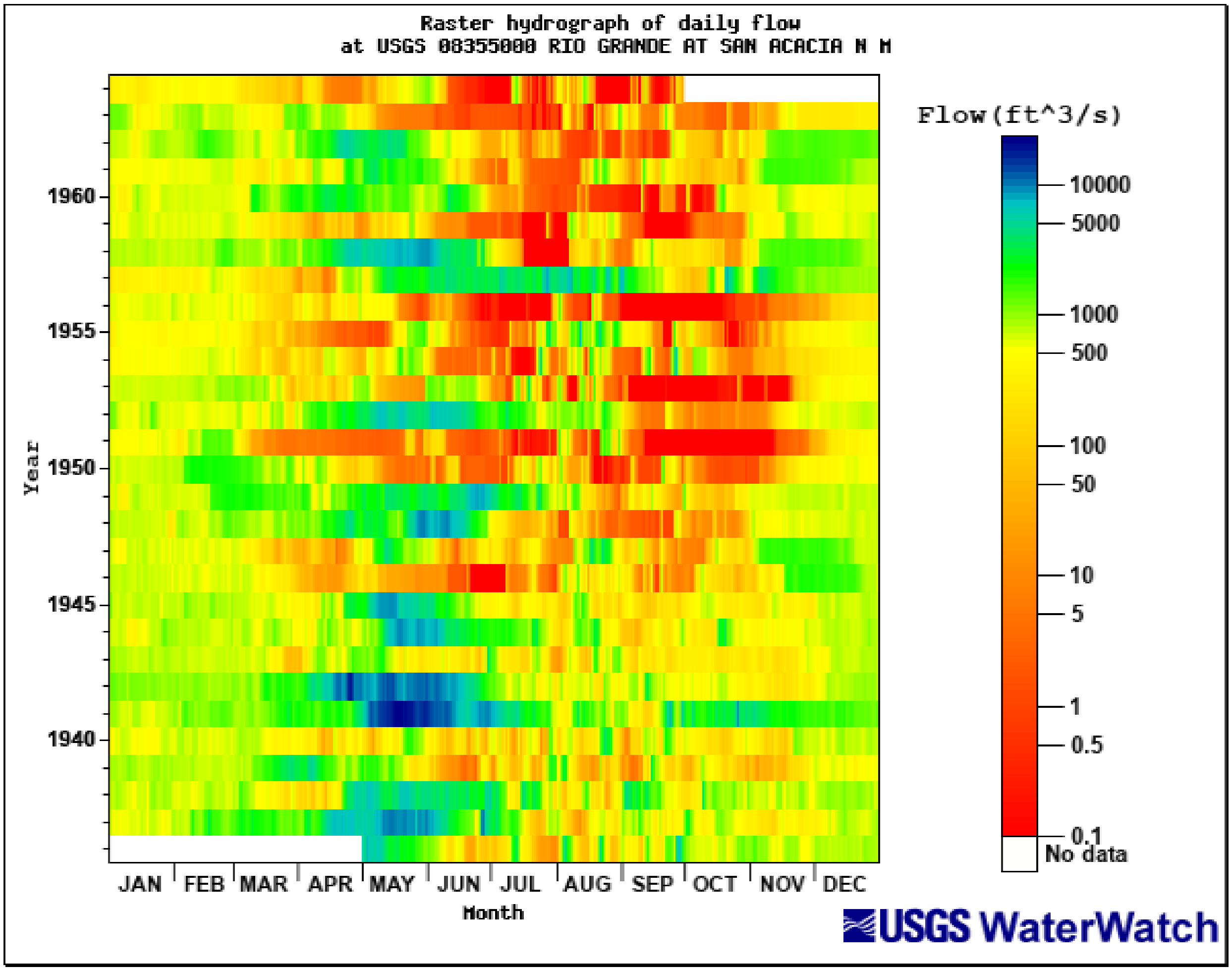

Figure 9 Raster hydrograph of daily discharge at USGS station 08355000

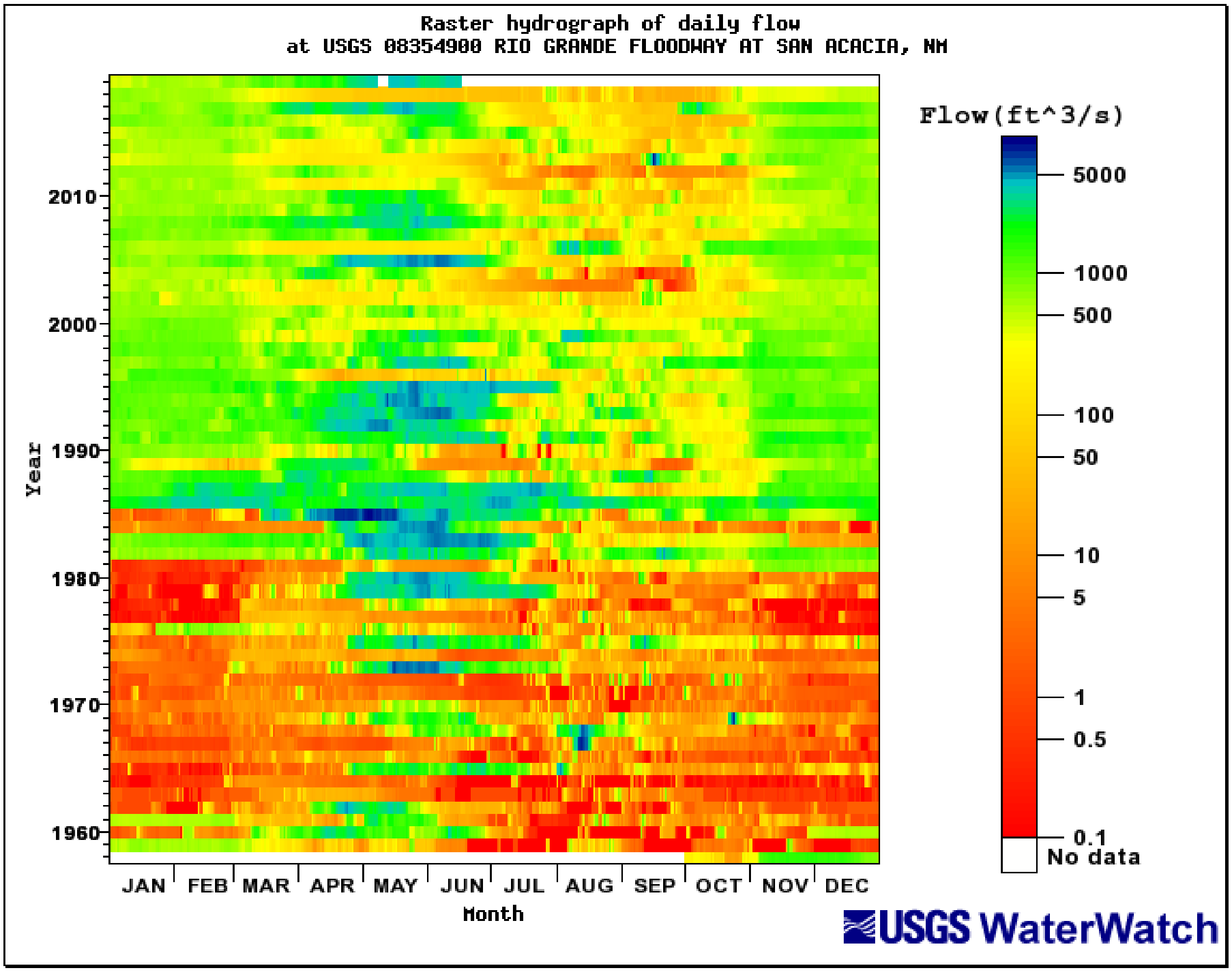

Figure 10 Raster hydrograph of daily discharge at USGS Station 08354900

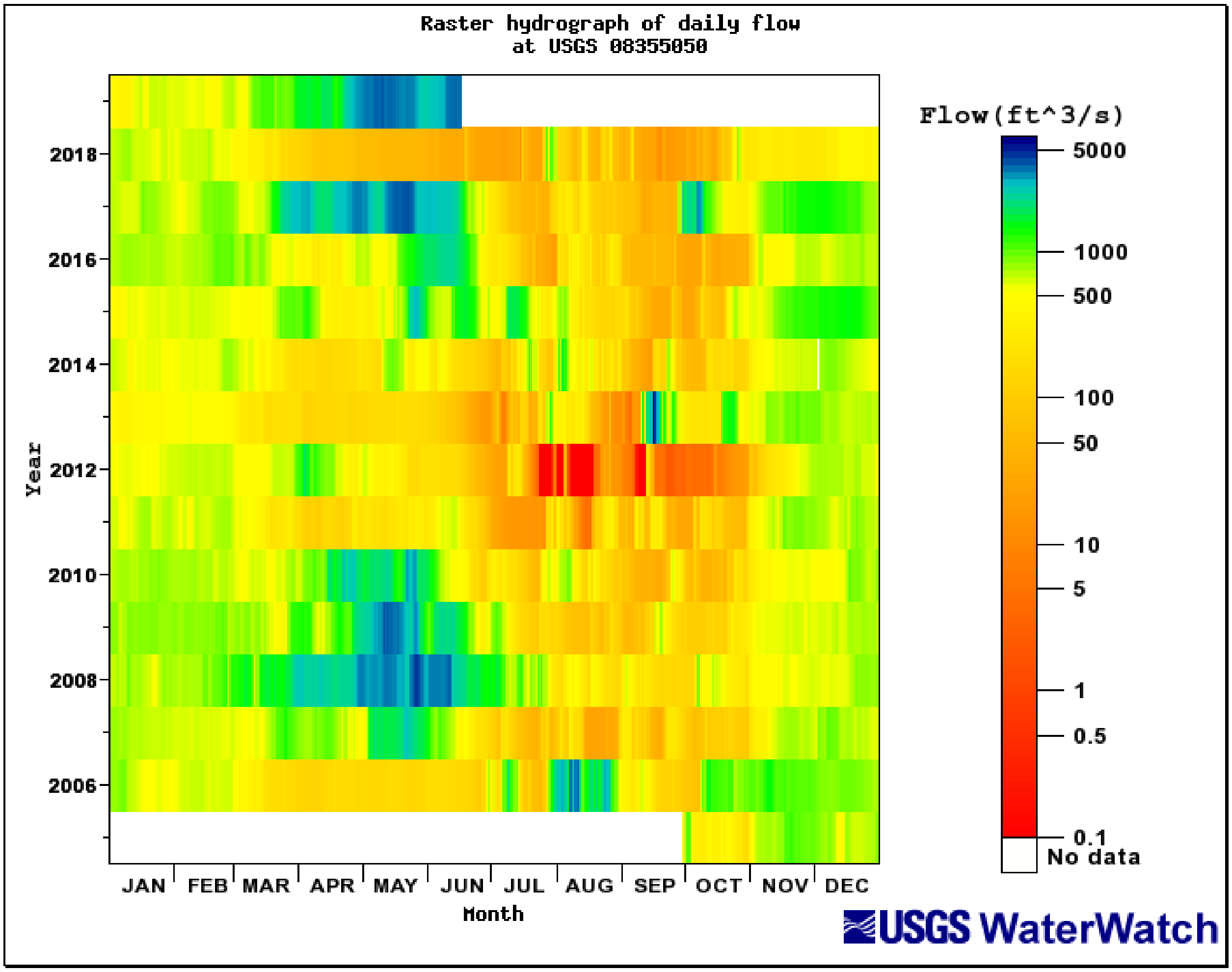

Figure 11 Raster hydrograph of daily discharge at USGS Station 08355050

Figure 12 shows the annual peak discharges for the Rio Grande Floodway at San Acacia, NM (08354900) gage and whether the largest instantaneous peak occurs during spring runoff or summer monsoons. In this case, snowmelt (shown in green) represents the months of January to June, while storms (shown in orange) represents the months June to December. Notice that from 1958 to 2018, the largest instantaneous peaks more frequently occur during summer monsoons than spring runoff.

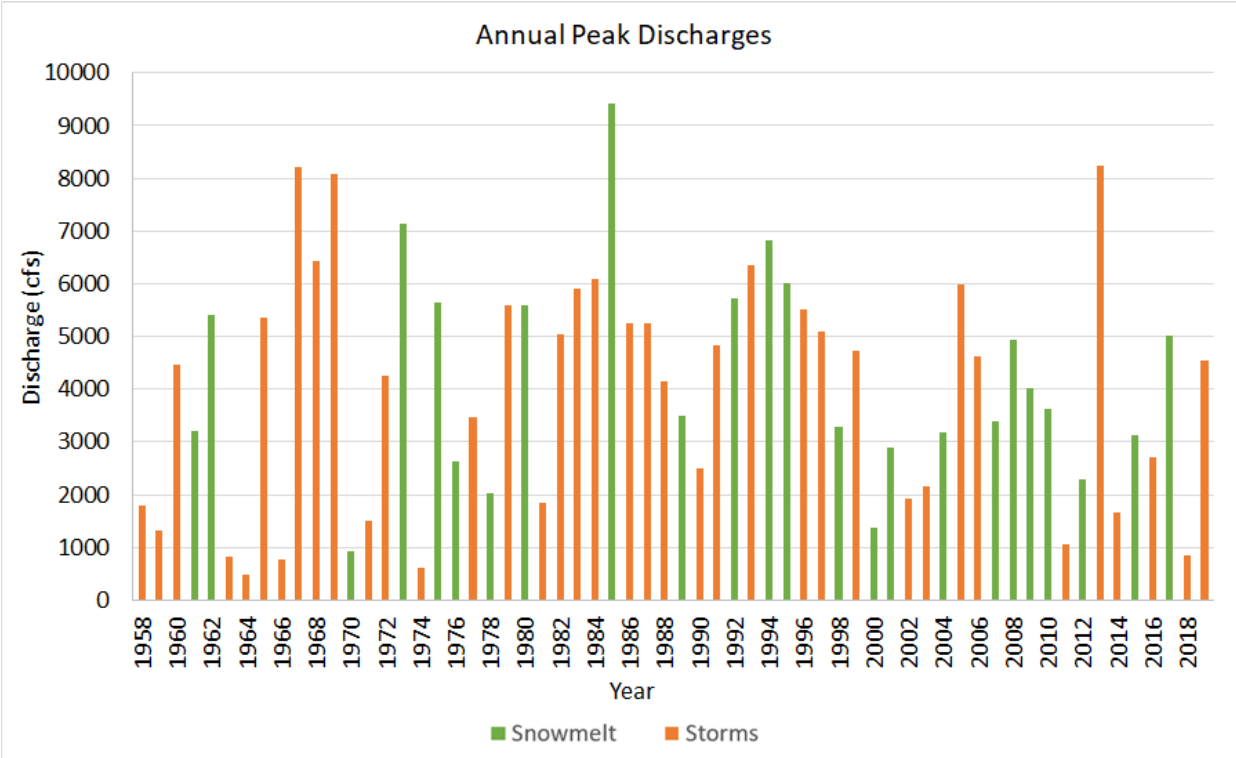

Figure 12 Peak discharge for Rio Grande Floodway at San Acacia, NM (08354900)

2.2.1 Cumulative Discharge Curves

Cumulative discharge curves can show changes in annual flow volume over time. The slope of the line of the mass curve gives the mean annual discharge, where breaks in slope show changes in flow volume. Figure 13 shows the flow mass curves of gages at San Acacia and Escondida. The mass curves were divided into the following time periods in water years: 1958 to 1978, 1978 to 1995, 1995 to 2018, 2005 to 2011, and 2011 to 2018. For each of these time periods the mean annual discharge in million acre-feet was calculated.

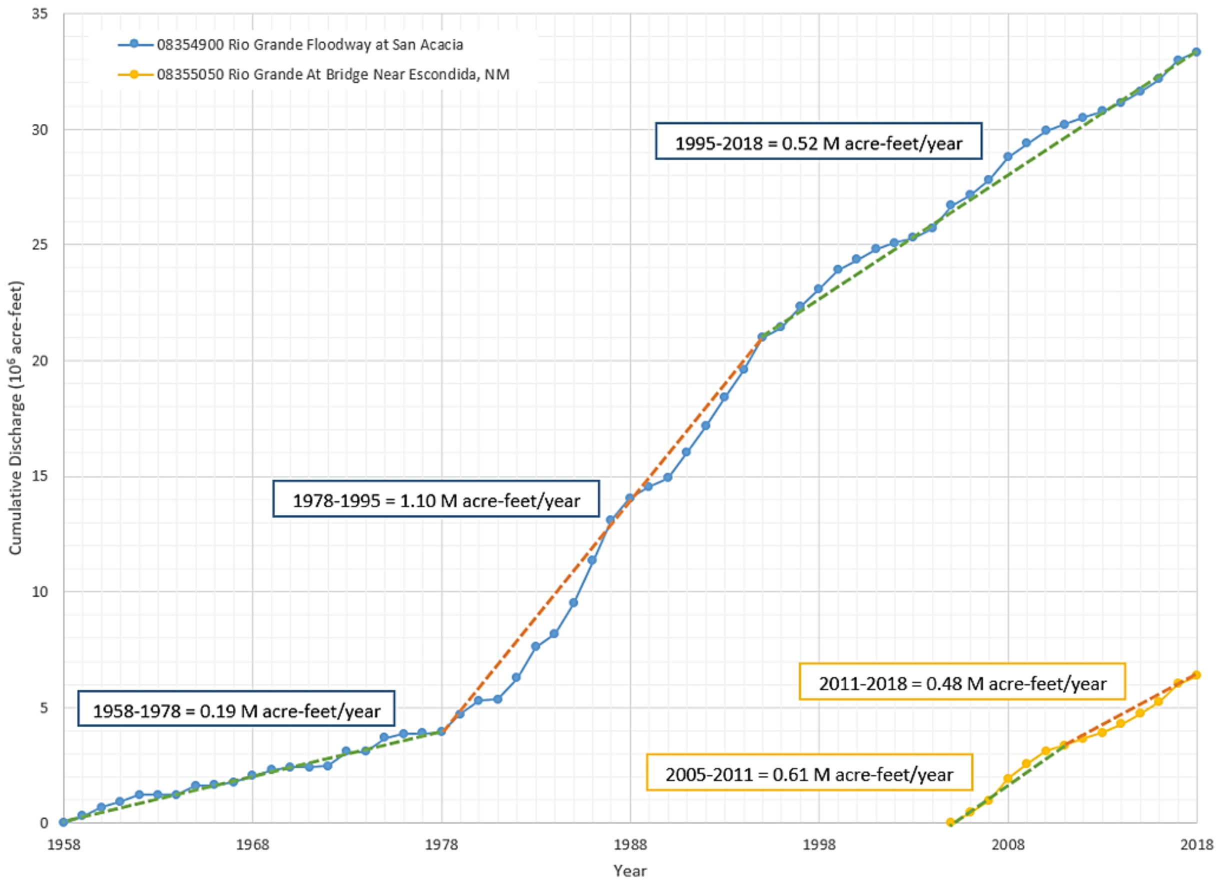

Figure 13 Discharge single mass curve at San Acacia and Escondida gages

Figure 14 below shows the flow mass curves of gages at San Acacia and Escondida for the Escondida period of record. Note that there is a loss of cumulative discharge between gages from 2005 to 2018 of 0.02 million acre-feet/year.

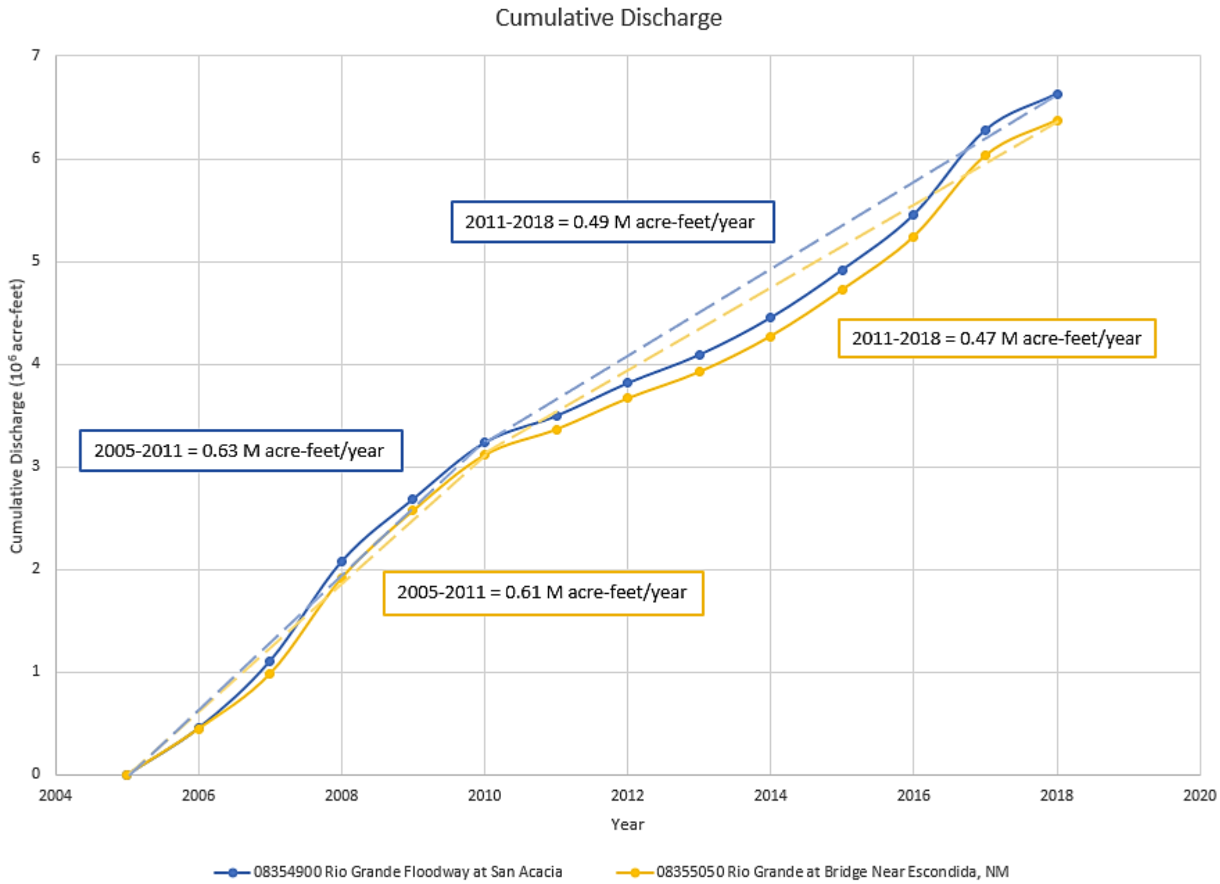

Figure 14 Discharge single mass curve for San Acacia and Escondida gages for 2005 to 2018

2.2.2 Flow Duration

A flow duration curve was developed for the San Acacia gages for the time periods 1937 to 1964 and 1975 to 2018 and for the Escondida gage for the entire record, 2011 to 2018. Figure 15 through Figure 17 show the flow duration curves for each of the USGS gages. Table 3 shows exceedance values calculated from these flow duration curves. When comparing the post-Cochiti flow conditions, the values for the Escondida gage are lower except for 90% exceedance. There is a shorter period of record for the Escondida gage; as a result, it has not experienced as many high flow events since recording began at the San Acacia gage. The higher flow value calculated at Escondida for the 90% exceedance may also be attributed to a station that pumps water into the river near agg/deg line 1300, just upstream of the gaging location, thus ensuring that this section of the river maintains a higher level of flow regardless of upstream flow conditions.

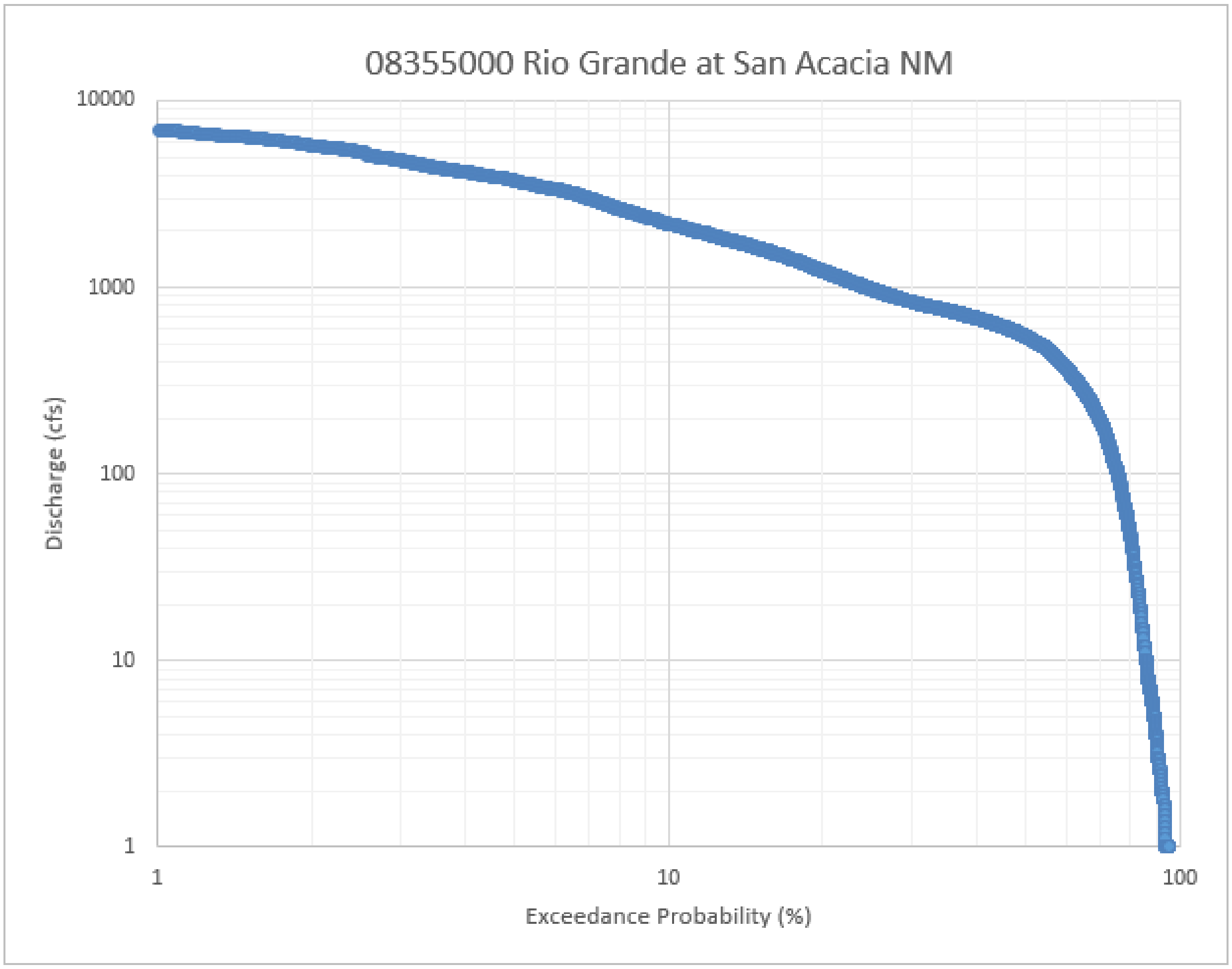

Figure 15 Flow duration curve for USGS gage 08355000 using mean daily flow discharge values

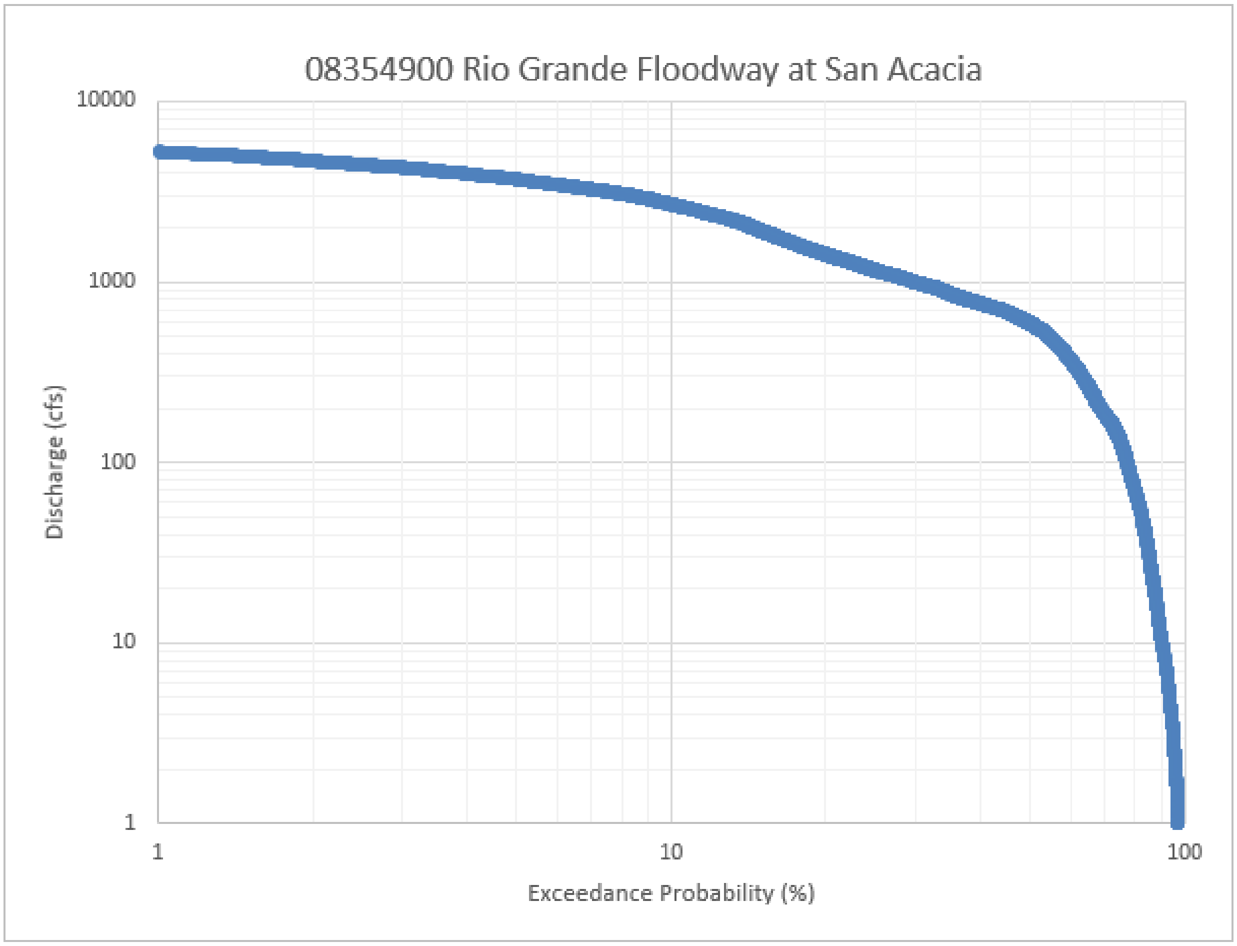

Figure 16 Flow duration curve for USGS gage 08354900 using mean daily flow discharge values

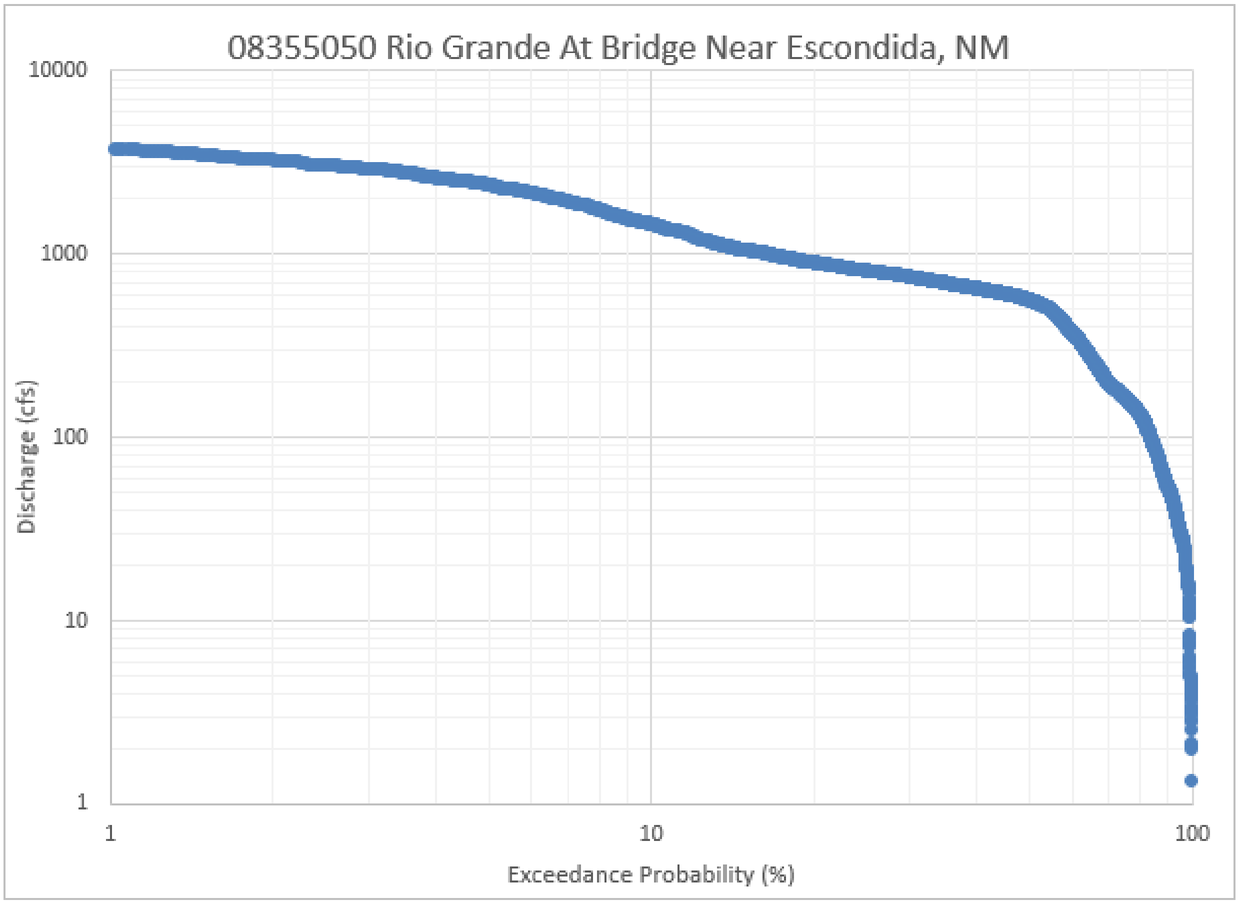

Figure 17 Flow duration curve for USGS gage 08355050 using mean daily flow discharge values

Table 3 Probabilities of exceedance for gages from the flow duration curves

	08355000 Rio Grande at San Acacia NM	08354900 Rio Grande Floodway at San Acacia	08355050 Rio Grande At Bridge Near Escondida, NM
Probability of Exceedance	Flow (cfs)		
1%	7000	5270	3760
10%	2200	2690	1470
25%	978	1160	815
50%	545	587	565
75%	107	129	164
90%	3.5	11	55

In addition to flow duration curves, the number of days in the water year exceeding identified flow values (500 cfs, 1000 cfs, 2000 cfs, 3000 cfs, 4000 cfs, 5000 cfs and 6000 cfs) at each gage was analyzed. This is purely a count of days and does not consider consecutive days. Analysis was performed for the years 1992 to 2018 for the San Acacia gage, and for the entire record for the Escondida gage. Figure 18 and Figure 19 show the number of days over these identified values. There are two periods of lower peak flows, from 2002 to 2003 and from 2011 to 2013. 2013 is a particularly interesting year in that the fewest number of days over 500 cfs were seen while the greatest number of days over 6000 cfs were seen. These outlying high values are not from snowmelt but are associated with a storm event in September of 2013.

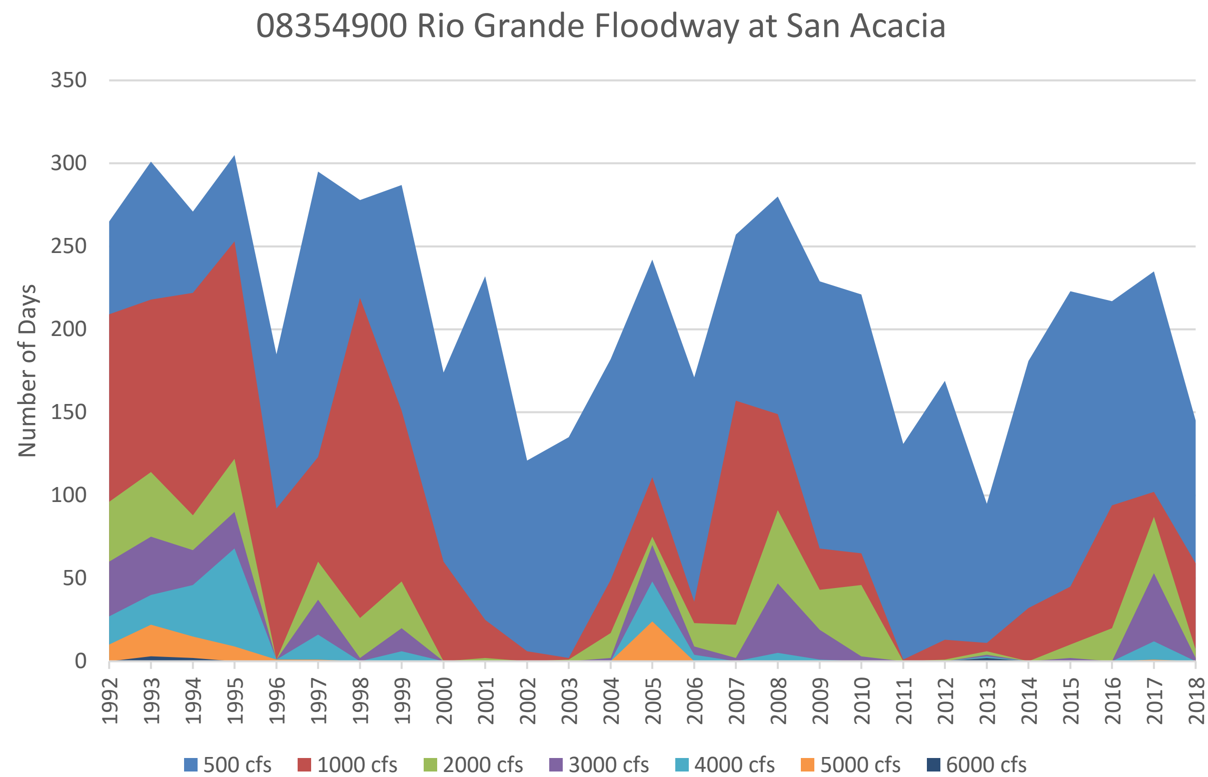

Figure 18 Number of days over the identified discharge at the San Acacia gage

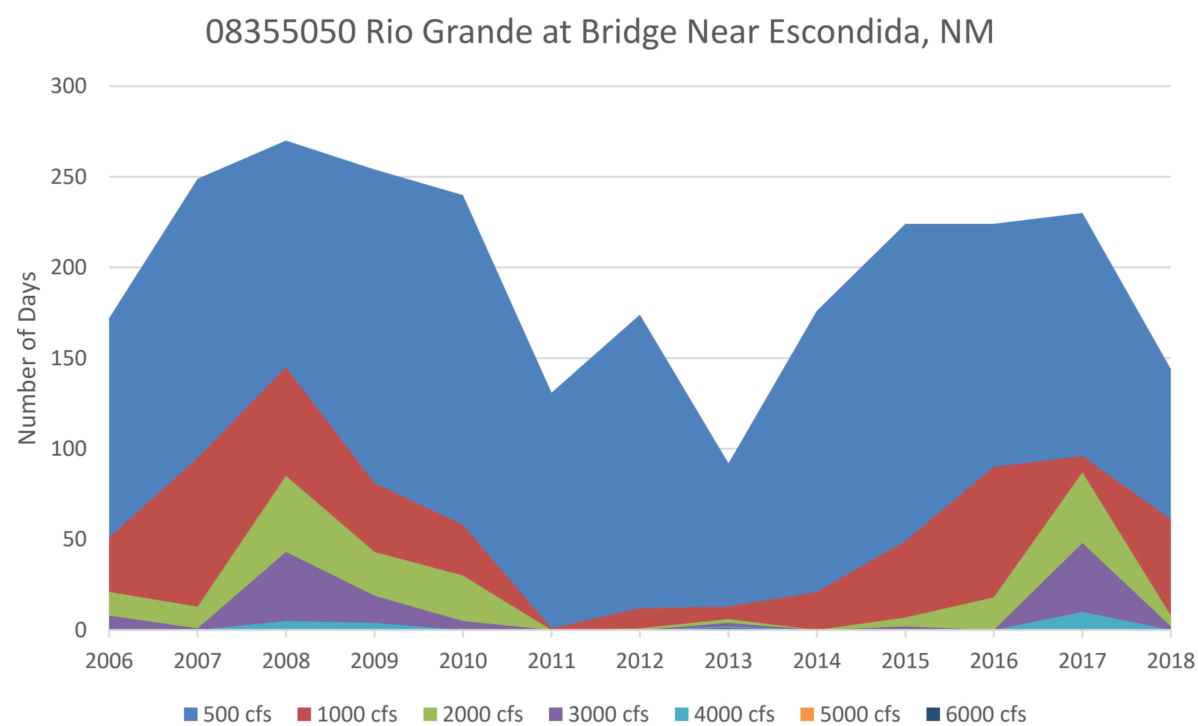

Figure 19 Number of days over the identified discharge at the Escondida gage

2.3 Suspended Sediment Load

2.3.1 Single Mass Curve

Single mass curves of cumulative suspended sediment (in millions of tons) are shown in Figure 20. Breaks in slope show the changes in flux. Data comes from the USGS gage at San Acacia (08354900) alone, as there is no sediment monitoring at the USGS gage at Escondida. Analysis is performed in water years. Years 1997 through 2000 were removed from the record as the data for those years is incomplete, some even missing several months of suspended sediment data. Since 2006, there has been an average of 2.1 million tons of sediment passing through the gage each year.

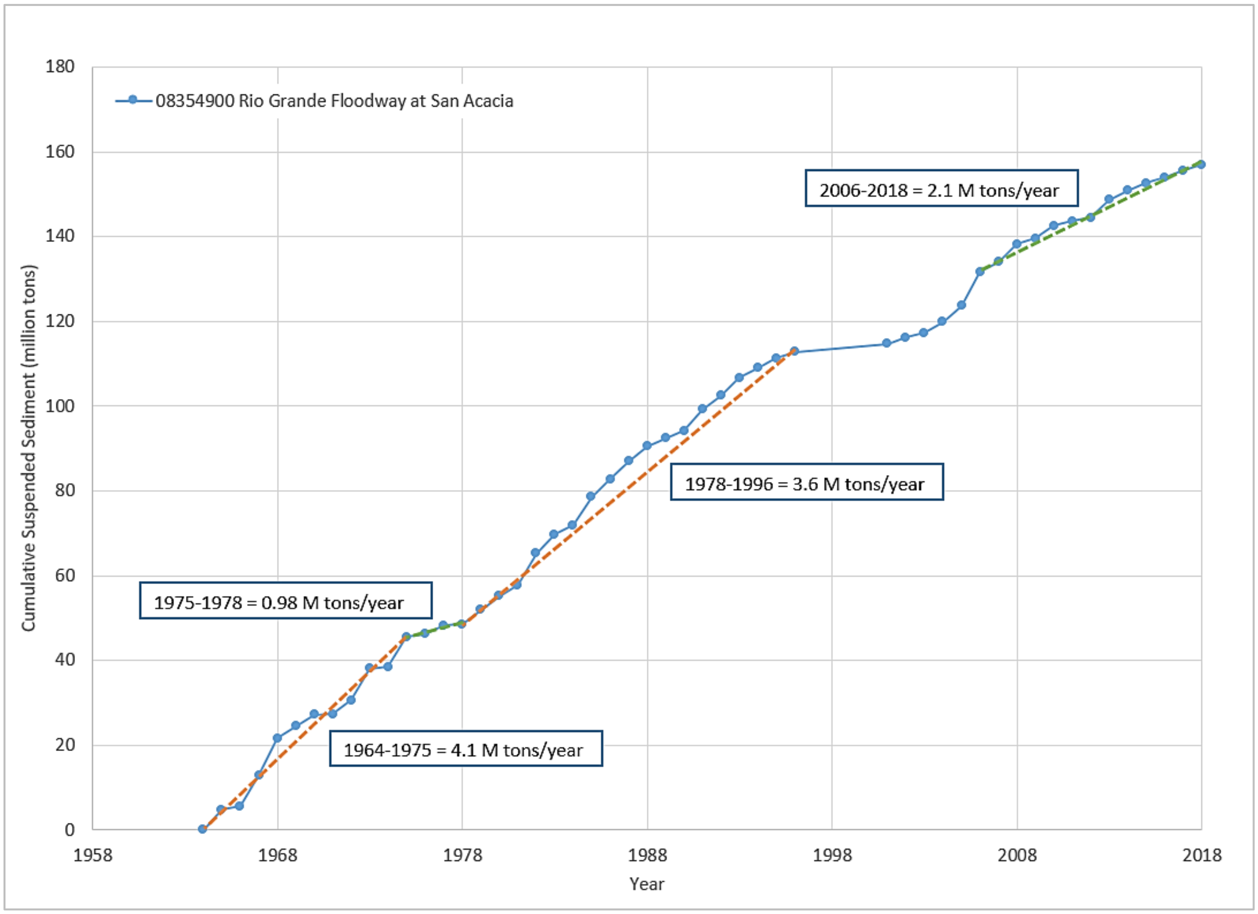

Figure 20 Suspended sediment discharge single mass curve for the San Acacia gage

2.3.2 Double Mass Curve

Double mass curves show how suspended sediment volume pairs with annual discharge volume. The slope of the double mass curve represents the mean sediment concentration. The double mass curve in Figure 21 is for USGS gage at San Acacia (08354900). Overall, the mean annual suspended sediment concentration has decreased since the 1960s.

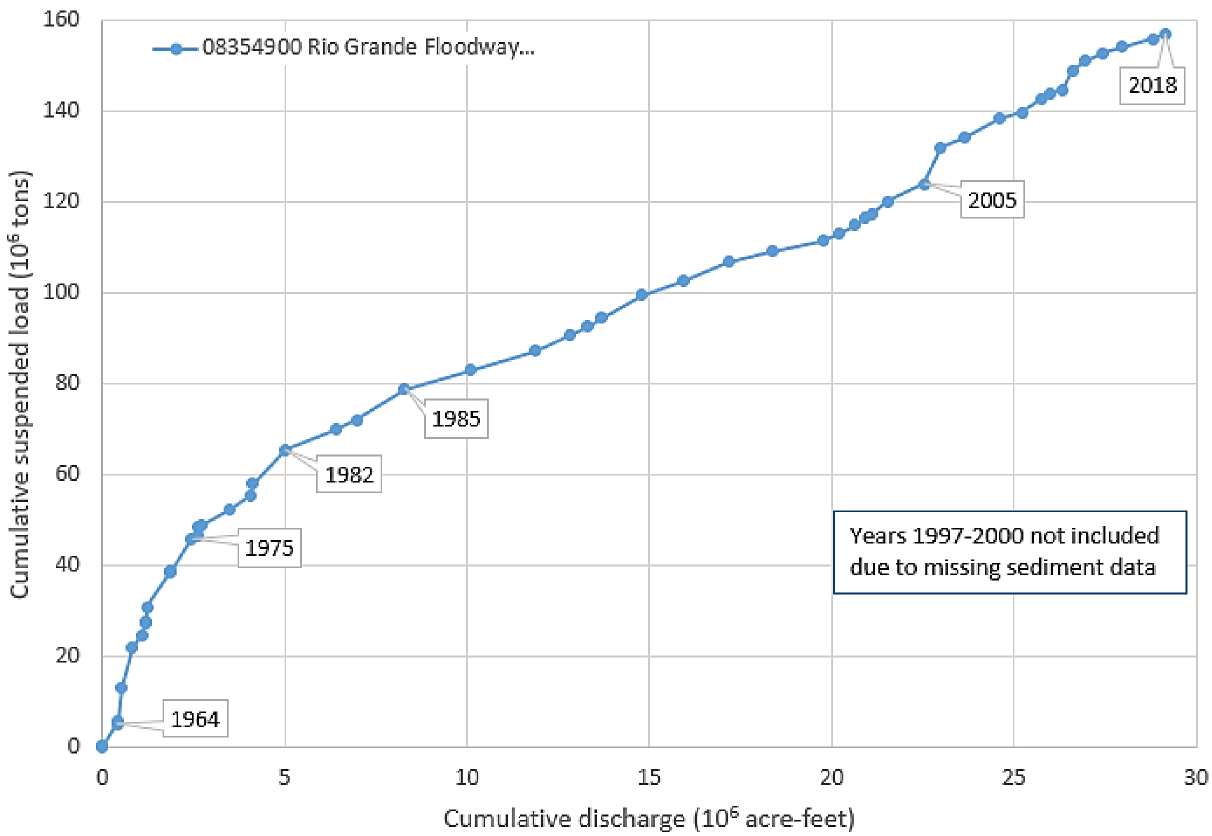

Figure 21 Double mass curve for the Rio Grande Floodway at San Acacia (08354900) gage

Table 4 shows the average suspended sediment concentration of groupings of years compared. Cochiti dam began operation in the early 1970's. Prior to operation of the dam, there was a high ratio of suspended sediment to cumulative discharge resulting in the steep slope at the beginning of the double mass curve. Throughout this time period, the average suspended sediment concentration was 4,150 mg/L. Following the operation of Cochiti dam, average suspended sediment concentration did not change much, but slightly increased to 4,161 mg/L. In the late 1980s, 1990s, and early 2000s this was reduced to an average of only 2,468 mg/L. Since 2006, the average suspended sediment concentration has been 3,186 mg/L.

Table 4 Change in average suspended sediment concentration over time at the San Acacia gage

Years	Average Suspended Sediment Concentration (mg/L)
1964-1975	4150
1975-1982	4161
1982-1985	4341
1985-2005	2468
2005-2018	3186

It is important to note that with the closure of the Cochiti Dam, the main source of new sediment for the Rio Grande is the Rio Puerco. The confluence with the Rio Puerco occurs just upstream of the San Acacia reach. The Rio Puerco is undammed and still carries high sediment loads. Historic estimates indicate that values of sediment concentration in the Rio Puerco approached 150,000 to 165,000 mg/L in the 1940s and 1950s (MEI 2002); this has since been substantially reduced to only around 15,120 mg/L (Klein et al. 2018a).

2.3.3 Monthly Average Histogram

Figure 22 shows a monthly average discharge histogram and monthly average suspended sediment concentration (mg/L) for the San Acacia gage from 1980 to the present. Figure 23 shows the same type of graph versus suspended sediment discharge (tons/day). A decadal time scale was chosen to analyze and compare important seasonal trends.

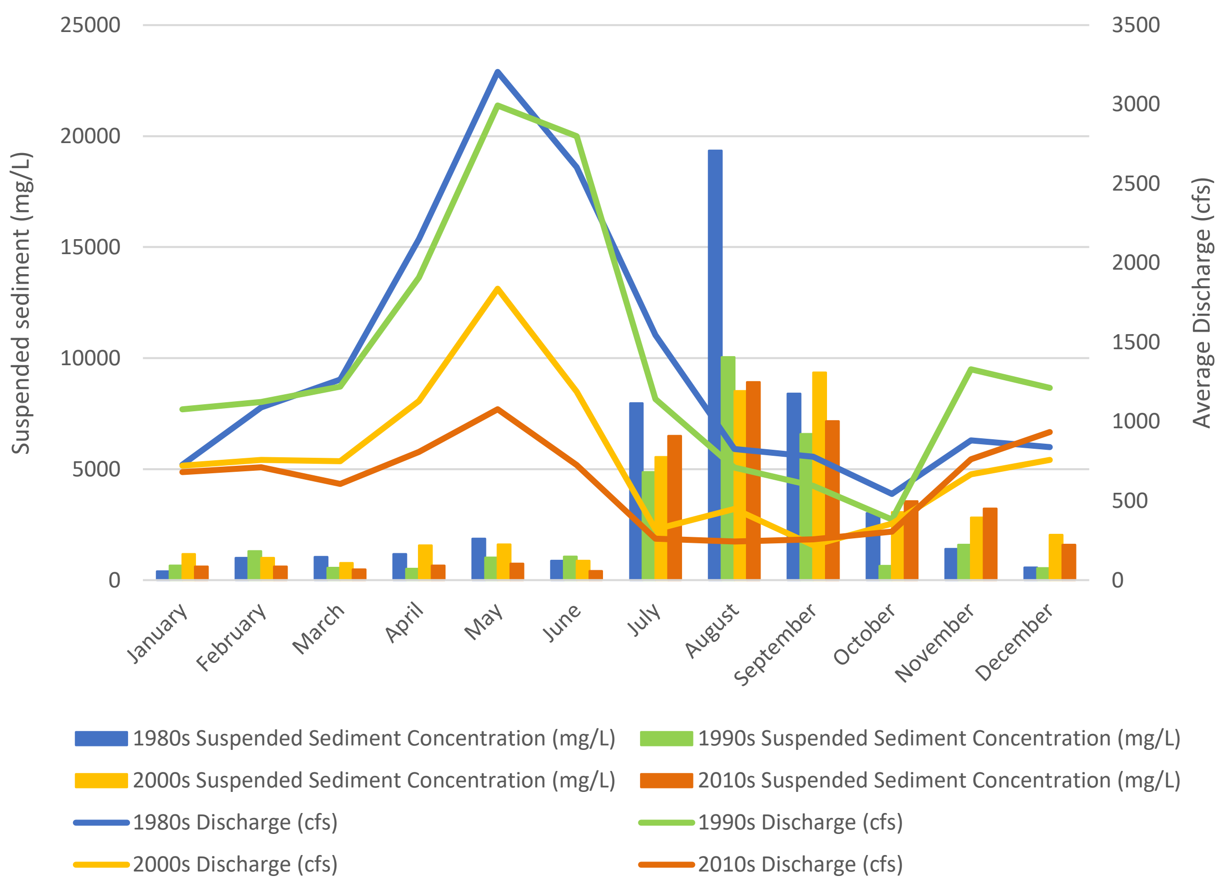

Figure 22 Monthly average histogram of discharge and suspended sediment concentration (mg/L) at the San Acacia gage

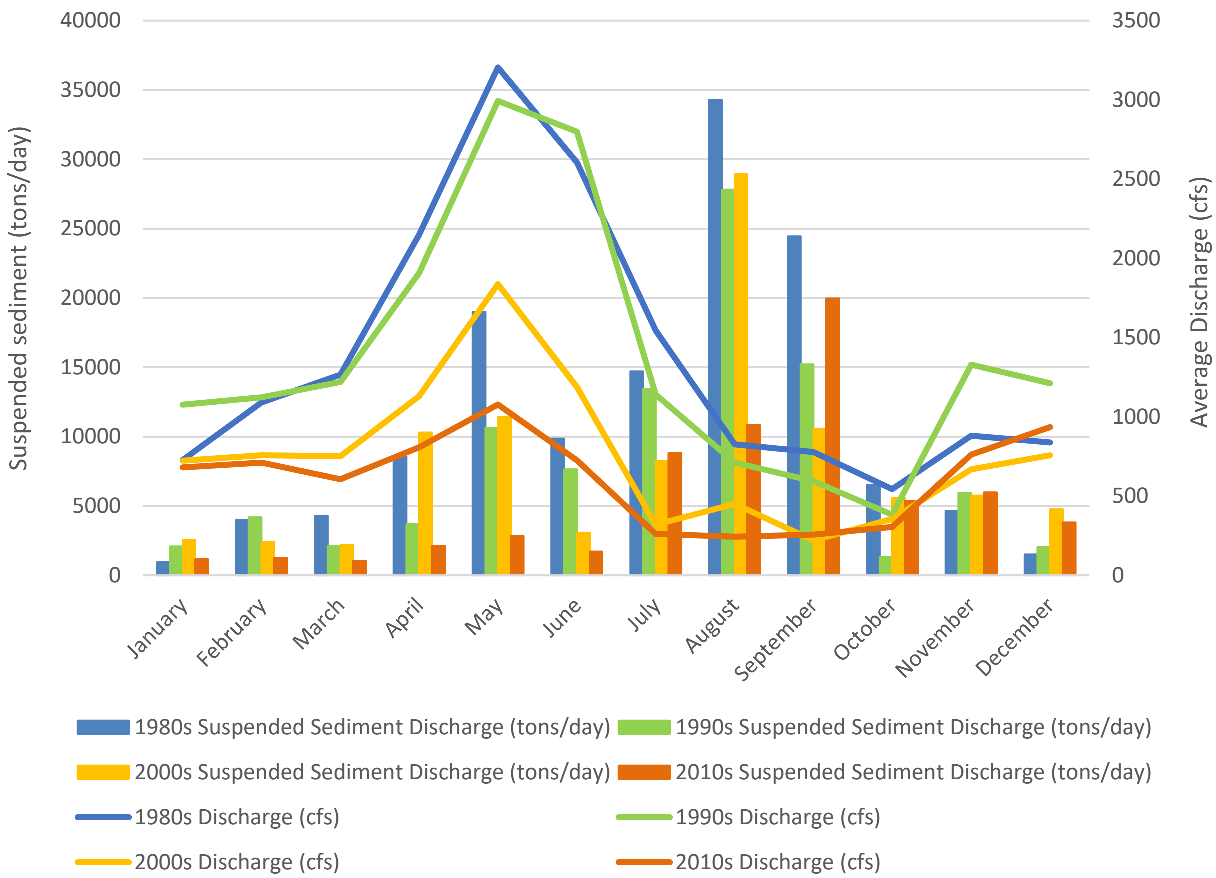

Figure 23 Monthly average histogram of discharge and suspended sediment discharge (tons/day) at the San Acacia gage

Although discharge peaks in late spring, April through June, the highest suspended sediment load occurs July through September. These high levels of transport are associated with monsoon events, which tend to be sudden and severe and cause widespread deposition in tributary arroyos. In flows associated with spring snowmelt during April, May and June, concentrations remain similar to what they are October through March, even though the total sediment discharge is higher than in the rest of the year. In contrast, the monsoon events have higher concentrations of sediment. Generally, average flows have been lower in the 2000s and 2010s.

To further demonstrate the effects of monsoon-related sediment movement, figures of precipitation versus discharge and precipitation versus suspended sediment discharge were generated. In Figure 24, when the line moves upward without moving across in the horizontal direction (as it does between April 2005 and August 2005, it means that there is a significant amount of discharge in the river despite a lack of rainfall (i.e. snowmelt related discharge can be seen). In contrast, from July 2006 to November 2006, there was a substantial increase in the amount of cumulative rainfall, while there was little change in the discharge. Figure 25 compares the suspended sediment discharge with precipitation. Specific monsoon events can be clearly seen in this figure, such as from August 2006 to September 2006, and September 2013 to October 2013. These are the events that are substantially altering what sediment is in the river.

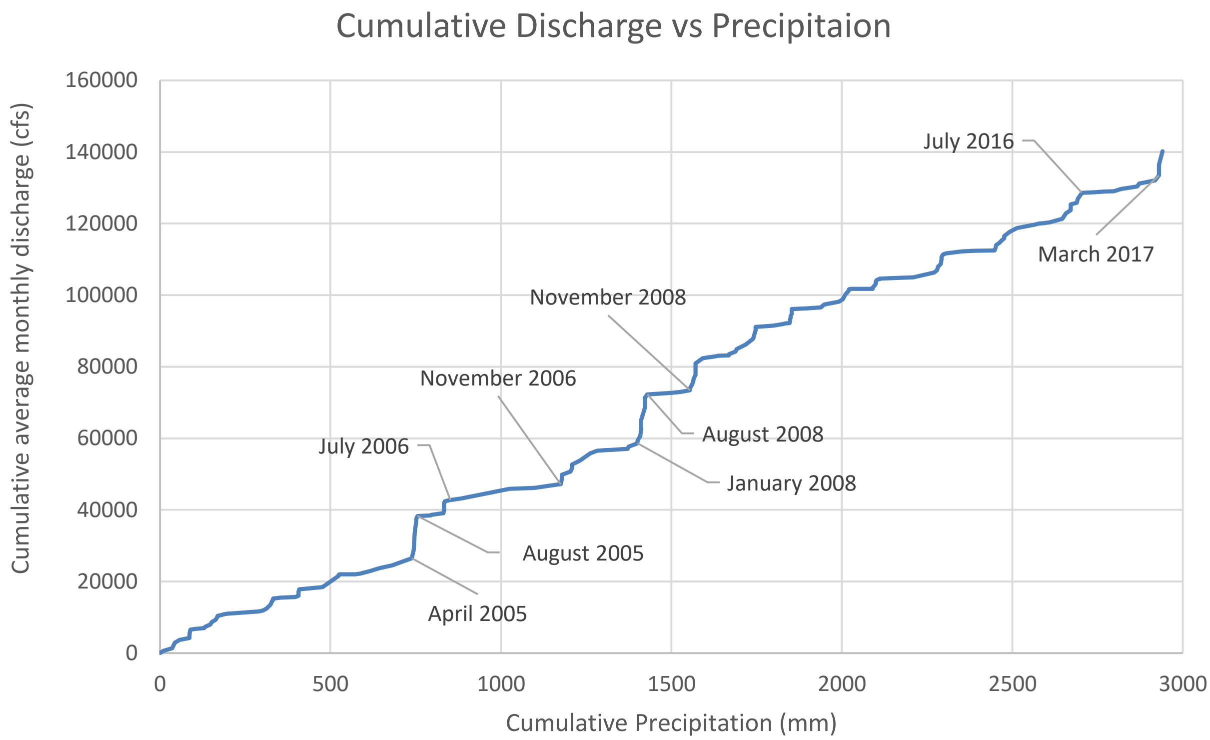

Figure 24 Cumulative discharge versus precipitation

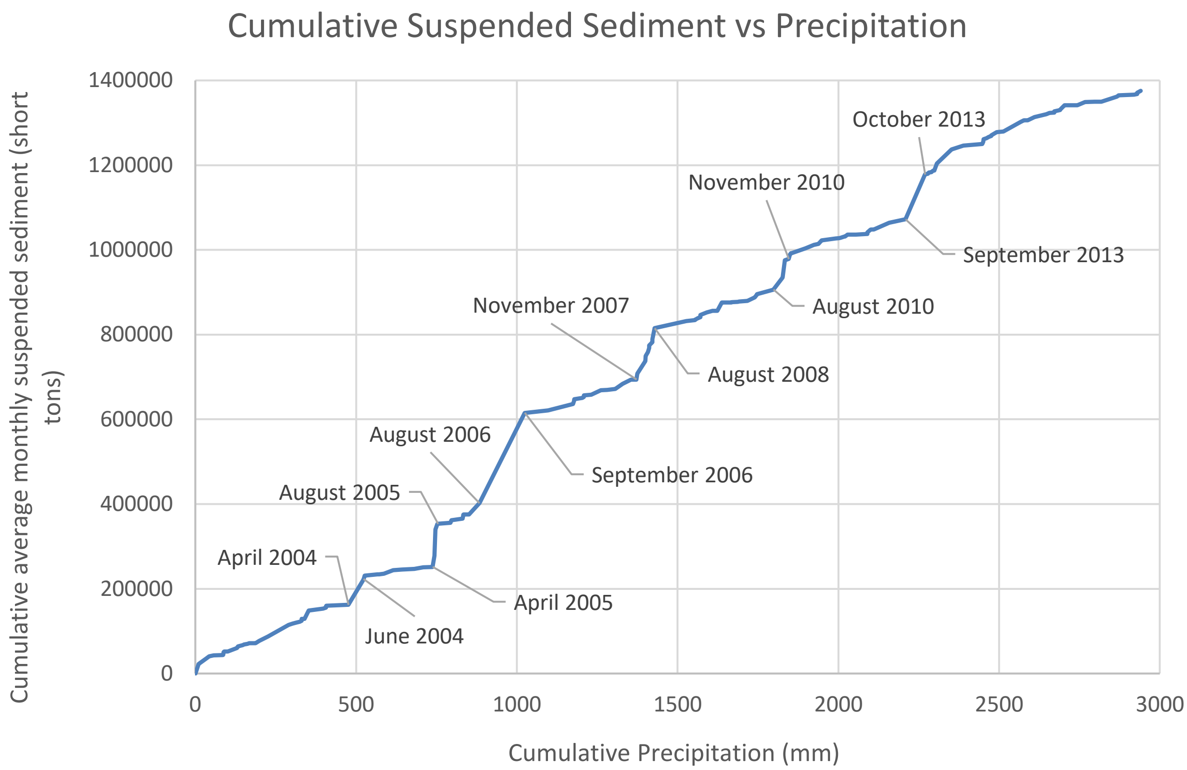

Figure 25 Cumulative suspended sediment vs precipitation

3. Geomorphic and River Characteristics

3.1 Wetted Top Width

Wetted top width can provide significant insight into at-a-station hydraulic geometry. A typical pattern would be a slow rate of width increase until connection with the floodplain is reached, when the width would increase dramatically. Then, the slow increase in width would continue. Analysis of the wetted top width can be used to help understand bankfull conditions and how they vary spatially and temporally in the San Acacia reach. A HEC-RAS model was created to analyze the top width. An increment of 500 cfs up to 10,000 cfs was used. This data was then processed to analyze a variety of top width metrics.

Figure 26 shows the wetted top width at 1,000 cfs and 3,000 cfs from HEC-RAS model results. The models shown at each agg/deg line are the moving averages from five consecutive cross sections. Additional figures from this analysis can be found in Appendix C. Figure 26 shows that 2012 is the narrowest year, with the largest difference seen in subreach SA3. Similar shapes can be seen at 3,000 cfs for 1992, 2002, and 2012, while shape varies a lot more at 1,000 cfs for all years. Figure 27 shows the differences in top width between the years 1992 and 2002, 2002 and 2012, and 1992 and 2012 at 1,000 cfs and 3,000 cfs. In this case, a positive difference represents an increase in top width, while a negative difference represents a decrease in top width.

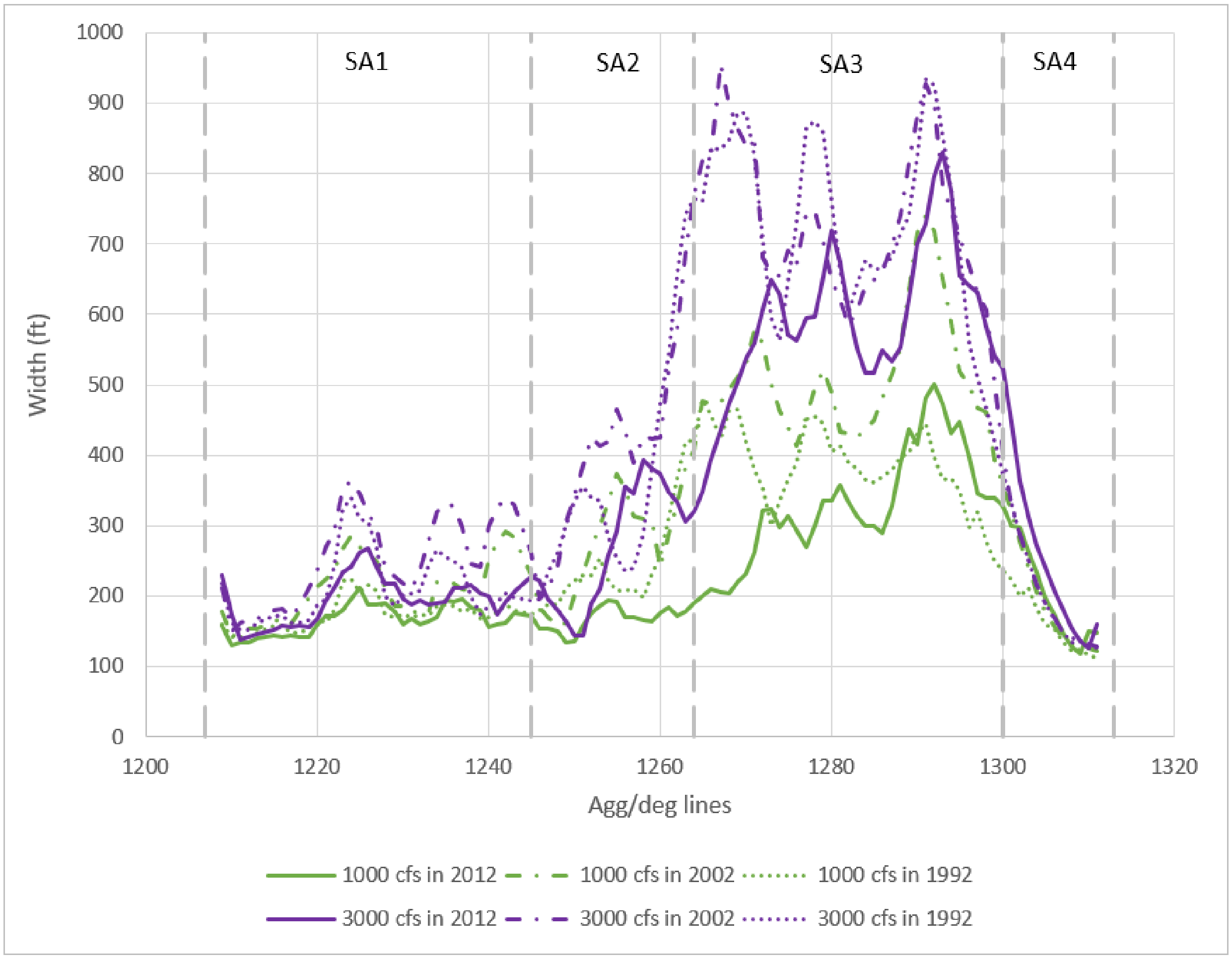

Figure 26 Five cross-section moving average width at 1,000 cfs and 3,000 cfs

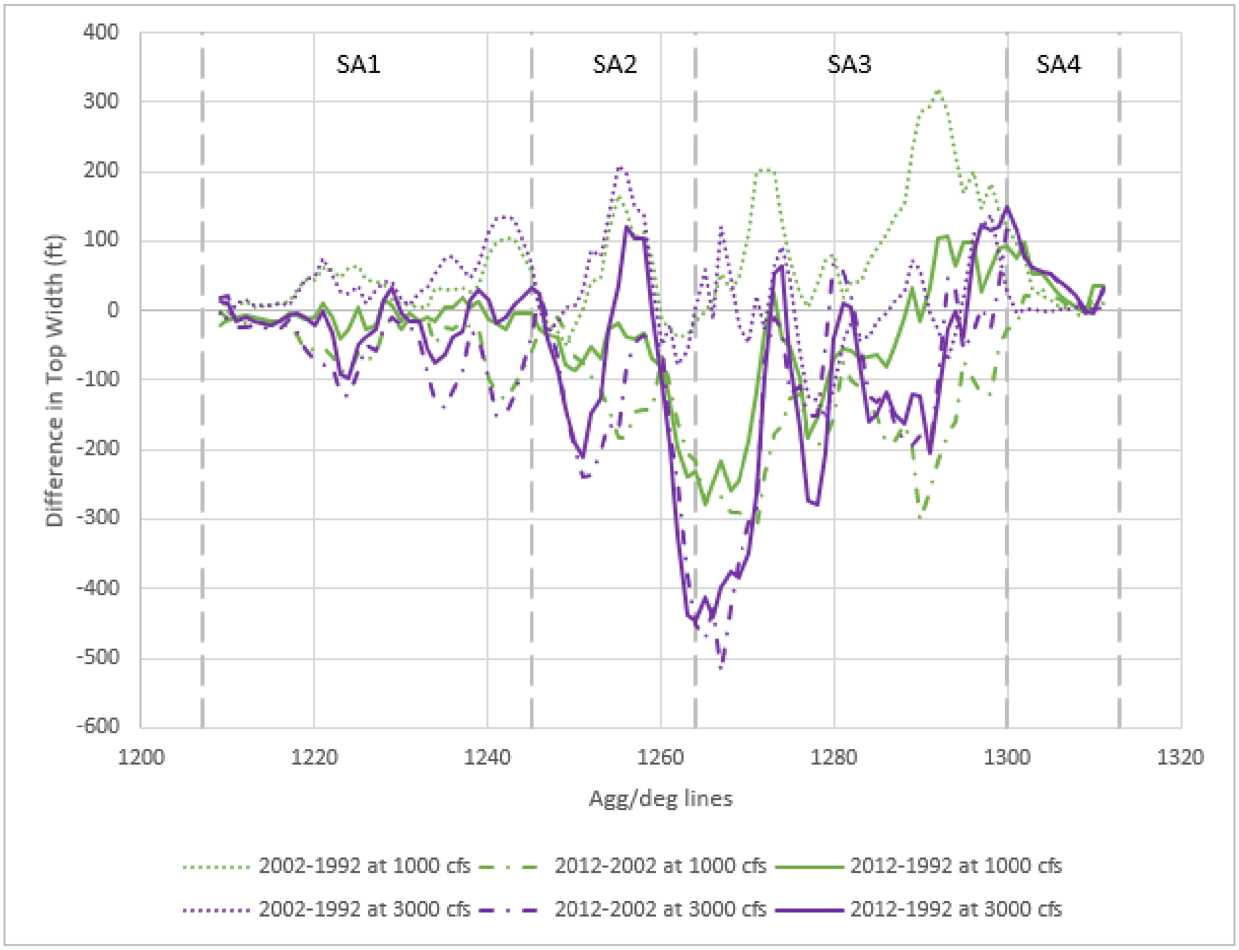

Figure 27 Differences in top width at 1,000 cfs and 3,000 cfs

Figure 28 shows the width-discharge relationship averaged across each subreach in 1992, 2002 and 2012. SA1 had a linearly increasing trend. The widest year was 2002, and the narrowest was 2012. SA2 and SA3 showed more of the expected pattern of increase associated with floodplain connection. In SA2 and SA3, narrowing occurred over time at discharges below 5,000 cfs, while widening occurred over time at discharges above 5,000 cfs. Discharges of 6,000 cfs are rarely exceeded on these sections of the river. From 1992 to 2018, discharges of 6,000 cfs only occurred in 1993, 1994, and 2013. It is likely that the narrowing reflects general trends seen with encroachment of vegetation. SA3 decreased the most from 2,000 to 4,500 cfs. Compared to the other subreaches, SA3 incised the least from 1962 to 2012 and has the widest non-vegetated width (Sections 0 Bed Elevation and 0 Width, respectively). SA4 does not begin to significantly widen until discharges of around 8,000 cfs are reached, reflecting the heavily incised nature of this subreach.

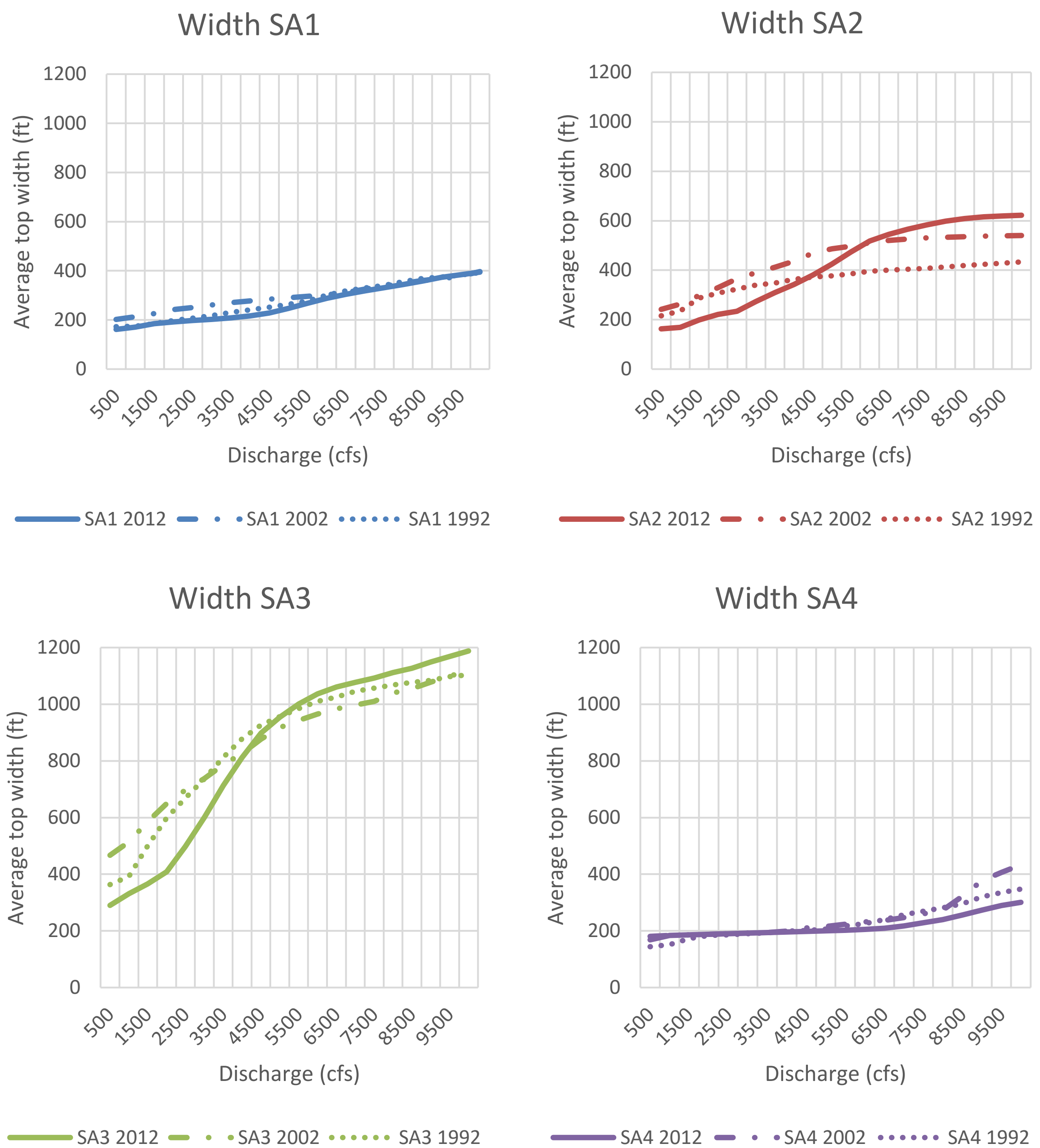

Figure 28 Subreach averaged width trends

Finally, narrow, average and wide cross-sections (25^{th}, 50^{th} and 75^{th} percentiles, respectively) were selected from the entire reach and can be seen in Figure 29. These representative cross-sections can illustrate in more detail the trends occuring at each reach. The 50^{th} percentile cross-section was represented by agg/deg line 1223, the 25^{th} percentile by agg/deg line 1248 and the 75^{th} percentile cross-section by agg/deg line 1285. The 75^{th} percentile cross-section followed a pattern of rapid increase in width before 4,000 cfs, at which point it remained mostly constant. Little change in width occurred between 1992 and 2002, but from 2002 to 2012 width decreased rather significantly at discharges less than 4,000 cfs. In 2012, the most dramatic increase happened from 2,000 to 4,000 cfs. The rapid increase indicates that bankfull has been reached, and because that occurs at a much lower discharge for this agg/deg line compared to the other representative cross sections, it can be concluded that the channel is wide and shallow at this location. The 50th percentile cross-section remained consistent until 4,000 cfs was reached, when it began to increase. Bankfull discharge in 2012 appears to be around 6,000 cfs. Finally, the 25th percentile cross-section maintained a linear trend throughout the entire range of discharges, making determining a bankfull discharge difficult. The largest increase in width in 2012 was seen at 6,000 cfs as well.

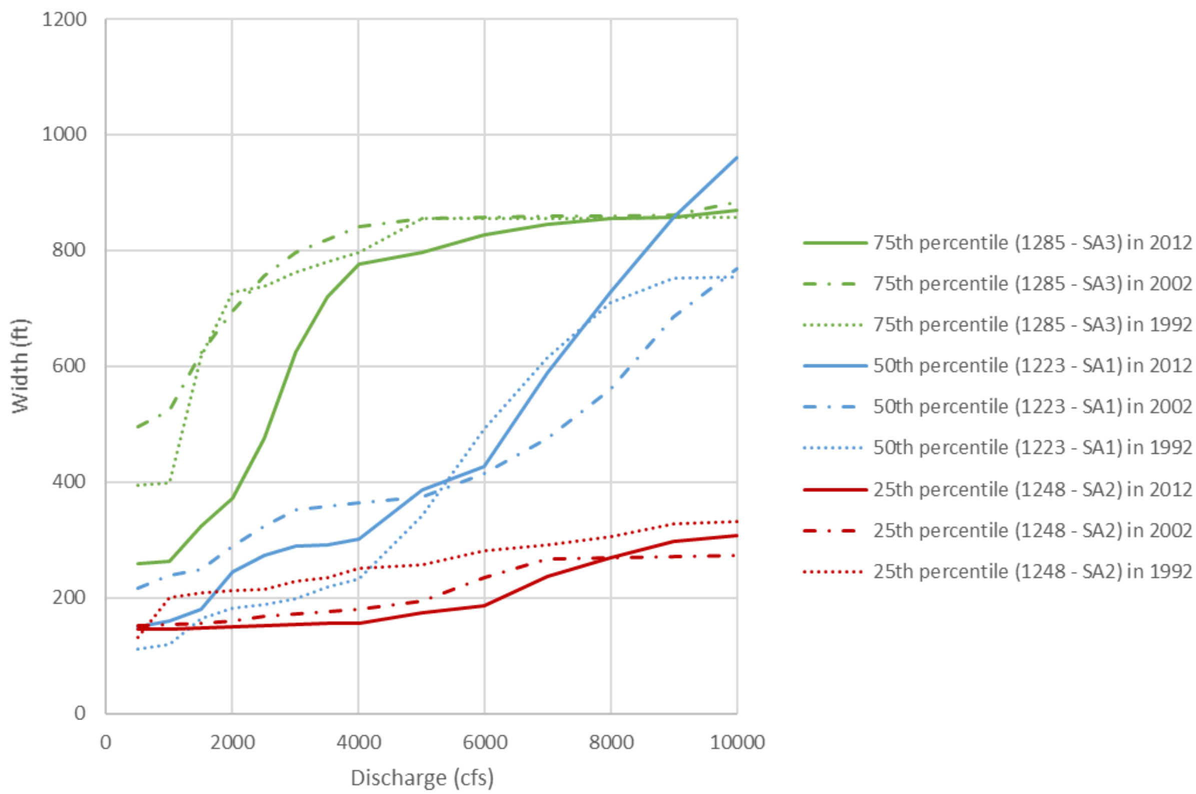

Figure 29 Width vs discharge at 25th, 50th, and 75th percentile cross-sections

3.2 Width (Defined by Vegetation)

The width of the active channel, defined as the non-vegetated channel, was found by clipping the agg/deg line with the active channel polygon provided by the USBR's GIS and Remote Sensing Group. The widths of the active channel polygon were exported from ArcMap for each agg/deg line. Then the width of each subreach was calculated by averaging the width of all agg/deg lines within the subreach. Aerial photographs and accompanying digital shapefiles were provided for years 1918, 1935, 1949, 1962, 1972, 1985, 1992, 2001, 2002, 2006, 2008, 2012 and 2016.

These results are shown in Figure 30. There is a dramatic decrease in active channel width after 1949, due to channelization efforts by the USBR in the 1950s and 1960s. Additionally, post completion of the Cochiti Dam in 1975, degradation occurred in most subreaches as a result of a reduction in sediment supply. In subreaches SA1 and SA4, after this decrease, the width of the channel stays nearly constant as the river reaches an equilibrium width. Subreaches SA2 and SA3 have a more gradual decline, but also appears to flatten out starting in the 2000s. A major realignment through SA4, where the river's course once meandered across the valley to the location of the existing Escondida lakes, straightened and increased the slope of SA4, which may have resulted in the width maintenance in SA3. In all subreaches but SA4, the narrowest year was 2016, where subreaches SA1, SA2, SA3 and SA4 had widths of 156, 171, 260 and 175 feet, respectively.

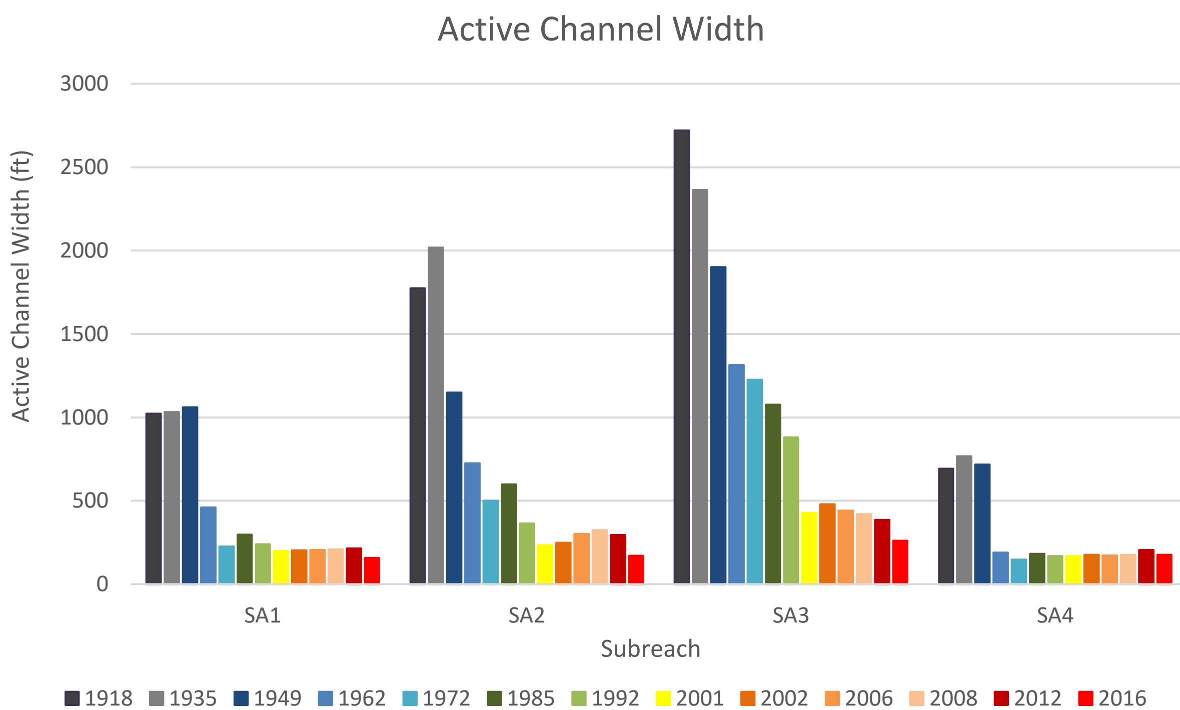

Figure 30 Averaged active channel width by subreach

3.3 Bed Elevation

The mean bed elevation is used to compare the change in longitudinal profile in this report. Mean bed elevation is then obtained from HEC-RAS as the minimum main channel elevation. Figure 31 shows the longitudinal profiles for 1962, 1972, 1992, 2002, and 2012.

The amount of degradation and aggradation by subreach can be seen in Figure 32. Subreach SA1 had the most degradation over the period from 1962 to 2012, almost 10.5 ft. SA2, SA3 and SA4 had degradation of 8.4 ft, 5.0 ft and 5.2 ft, respectively. The most severe degradation is at the upstream end of this subreach. It is possible that scour is occurring downstream of the San Acacia Diversion Dam if sediment is being contained behind the diversion structure. The only time aggradation occurred was in subreach SA4 from 1992 to 2002; all other time periods and subreaches were degradational. The most degradation occurred between 1972 and 1992, although this is a longer period than the others. Normalized to a ten-year period, the most degradation occurs between 2002 and 2012.

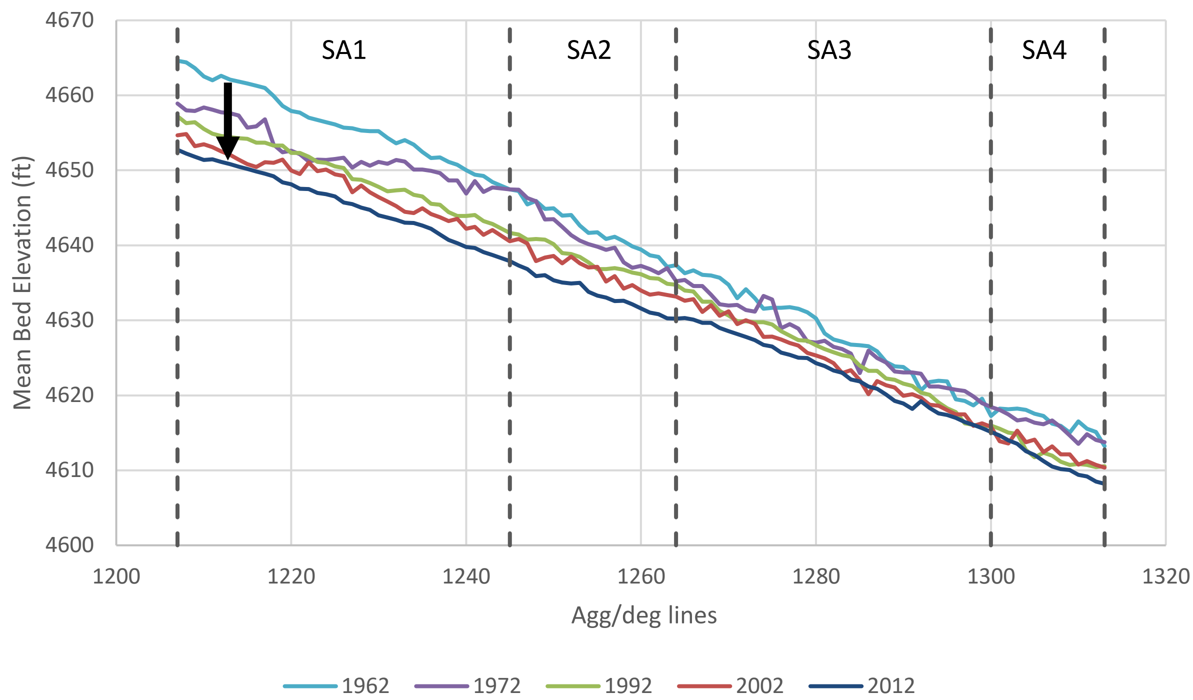

Figure 31 Longitudinal profile of bed elevations

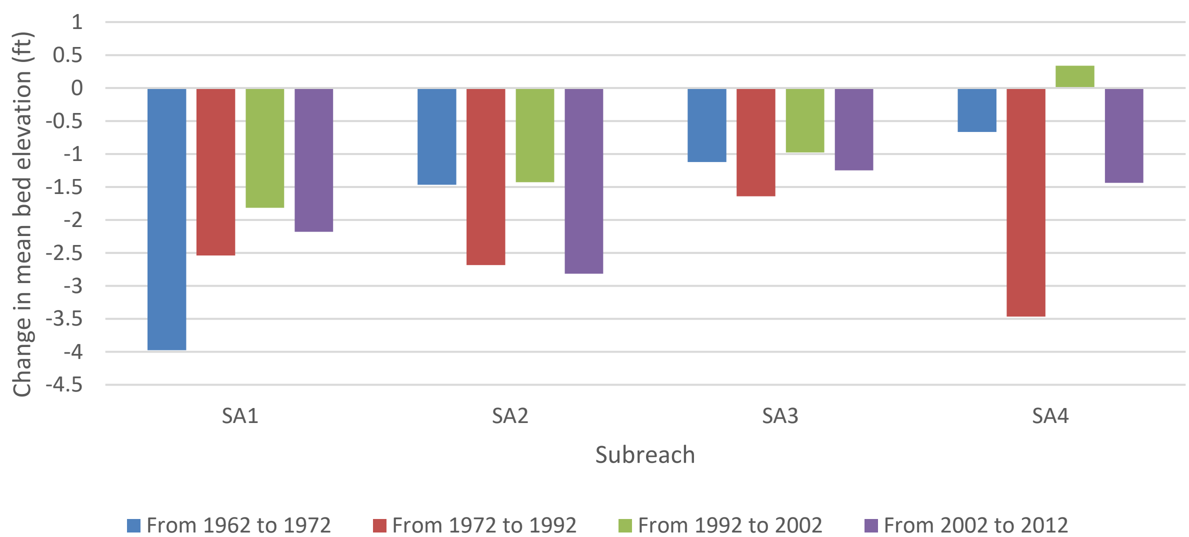

Figure 32 Degradation and aggradation by subreach

3.4 Bed Material

Bed material samples are collected at rangelines that differ from the agg/deg lines. There are samples available for analysis in the San Acacia reach for 1995, 1996, 1997, 1998, 1999, 2005 and 2014. Although samples were also collected in 2000, they were an order of magnitude larger than the mean of any other year and were sampled for the purpose of determining the size of the sediment in the gravel layer under the sand layer. Therefore, this data was not included in Figure 33. Figure 33 shows the D_{50} of each sample in mm vs the distance downstream of the San Acacia Diversion Dam (i.e. the start of the San Acacia reach). Figure 34 shows the D_{50} of each sample in mm at agg/deg lines. In both figures, the bottom dashed line represents the grain size for very fine gravel (2 mm), while the top dashed line represents the grain size for small cobbles (64 mm). Samples below the 2 mm line are classified as sand.

Some evidence of bed fining due to the San Acacia Diversion Dam is seen in the upstream third of the San Acacia reach. After 22,000 ft downstream of the diversion, no samples were collected with a D_{50} larger than 1 mm. The San Acacia Diversion Dam acts as a grade control, so immediately downstream of the dam, downcutting is occurring. The higher shear forces result in the higher grain sizes close to the dam. Actual values of D_{50} averaged over each subreach and sampling locations by agg/deg line can be seen in Table 5.

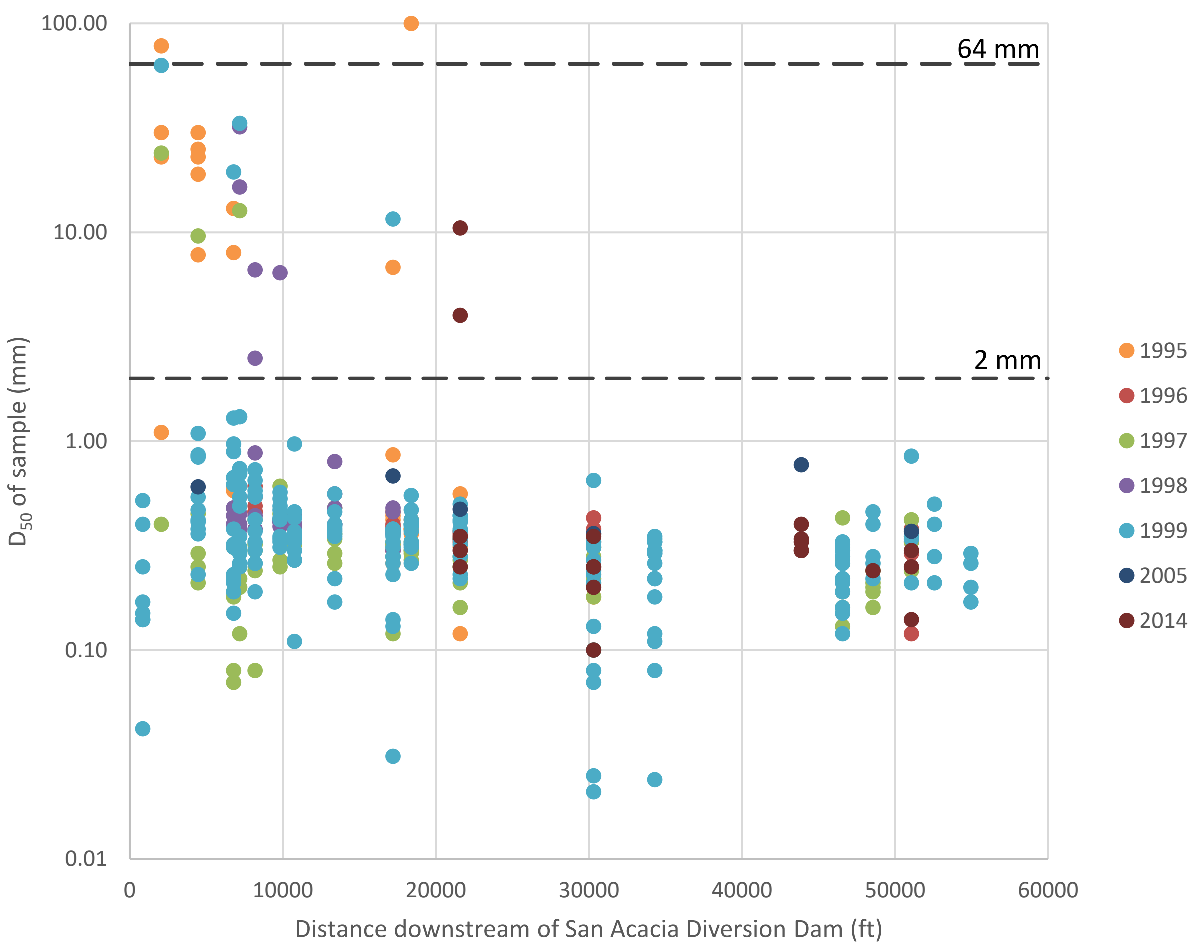

Figure 33 D_{50} measurements along the reach

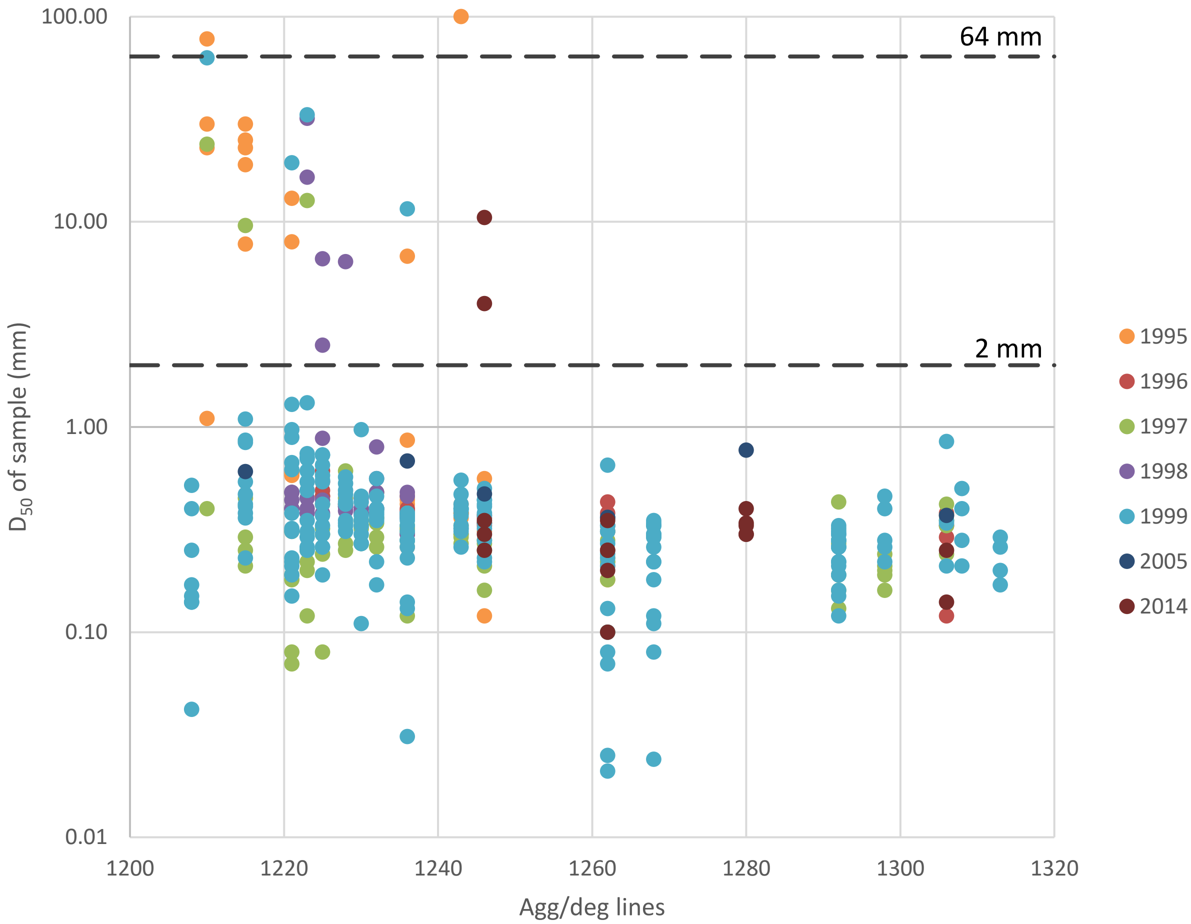

Figure 34 D_{50} measurements at agg/deg lines

Table 5 D_{50} in mm of the samples averaged by subreach and by sample year. Sampling locations are specified by agg/deg lines

		D_{50} (mm) by Subreach			
Sampling Year	**Sampling Locations**	**SA1**	**SA2**	**SA3**	**SA4**
1995	1210, 1215, 1221, 1236, 1243, 1246, 1262	14.25	0.29	--	--
1996	1225, 1236, 1246, 1262, 1306	0.45	0.36	--	0.28
1997	1210, 1215, 1221, 1223, 1225, 1228, 1230, 1232, 1236, 1243, 1246, 1262, 1292, 1298, 1306	1.26	0.22	0.22	0.34
1998	1221, 1223, 1225, 1228, 1230, 1232, 1236	2.21	--	--	--
1999	1208, 1215, 1221, 1223, 1225, 1228, 1230, 1232, 1236, 1243, 1246, 1262, 1268, 1292, 1298, 1306, 1308, 1313	1.48	0.29	0.25	0.34
2000	1207, 1209, 1212, 1215, 1218, 1221, 1223, 1224, 1225, 1228, 1229, 1231, 1243, 1246, 1252, 1256, 1262, 1268, 1280, 1298	18.27	34.25	26.00	--
2005	1215, 1236, 1246, 1262, 1280, 1306	0.64	0.42	0.77	0.37
2014	1246, 1262, 1280, 1306	--	1.66	0.33	0.20
2016	1298, 1306	--	--	0.24	0.30

3.5 Sinuosity

Sinuosity was calculated at each subreach using digitized channel centerlines provided by the USBR's GIS and Remote Sensing Group. Aerial photographs and accompanying digital shapefiles were provided for years 1918, 1935, 1949, 1962, 1972, 1985, 1992, 2001, 2002, 2006, 2008, 2012 and 2016. The centerlines were split up by subreach and divided by the length of the subreach to calculate the sinuosity. Figure 35 shows the sinuosity of each subreach from year to year.

Overall, sinuosity values are low. They are highest in SA1, staying above 1.20 and lowest in SA4, staying around 1.01 to 1.02. In SA1, SA2 and SA4, the year with the highest sinuosity is 1935. In SA1 and SA2, sinuosity decreases until 1985 due to the channelization efforts that occurred in the MRG. The sinuosity slowly increases again as a result of degradation and a reduction in sediment supply post Cochiti Dam.

SA3 shows a slight increase from 1992 onward, but it did not have the same extreme decrease in sinuosity after 1935 that occurred in the other subreaches. SA4 shows the biggest change following the deliberate channelization of the MRG that occurred in the 1950s, which included channel straightening. Up until 1949, sinuosity values were over 1.20. Beginning in 1962, sinuosity stayed around 1.02. This is the straightest subreach within the San Acacia reach and is experiencing very little change in channel centerline.

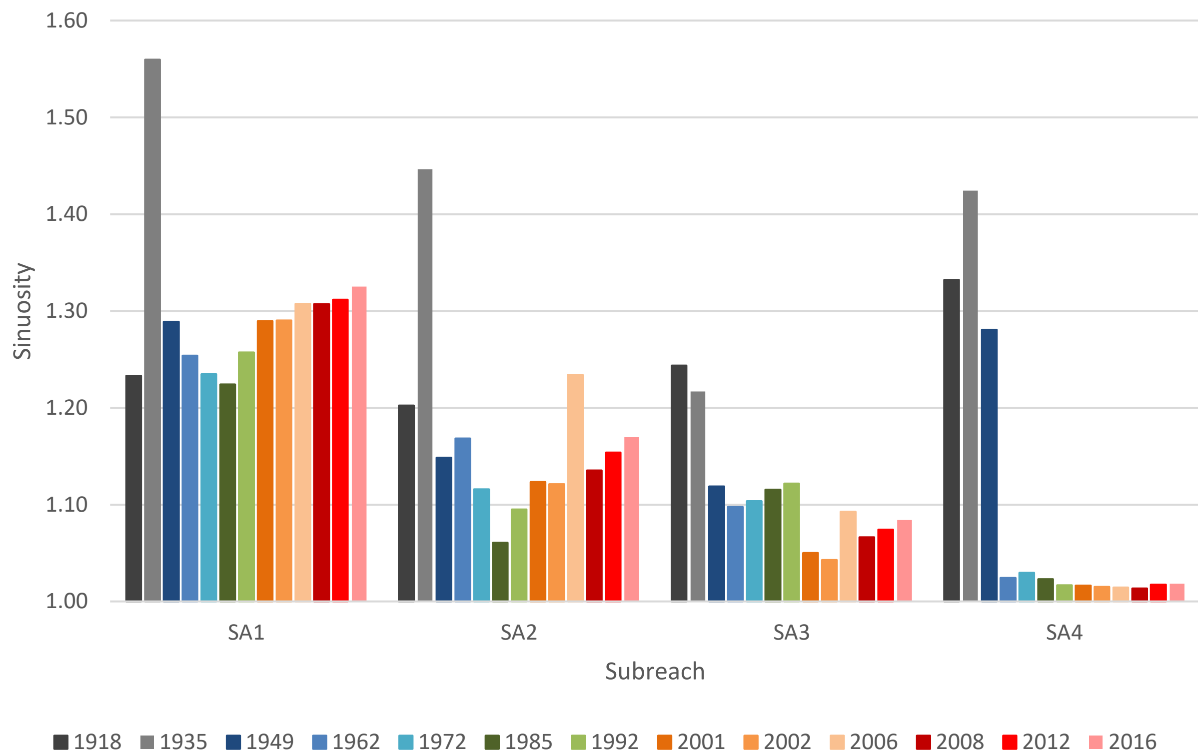

Figure 35 Sinuosity by subreach

3.6 Hydraulic Geometry

Flow depth, velocity, width, wetted perimeter, bed slope and energy slope are obtained using HEC-RAS 5.0.3 with a discharge of 3,000 cfs. A flow of 3,000 cfs, which has a recurrence interval of 11 years, was selected for plots of hydraulic variables to be consistent with previous reach reports (LaForge et al. 2019; Yang et al. 2019). This is the nominal discharge that fills the main channel without overbanking. Analysis was performed for years 1972, 1992, 2002, and 2012. Average values at each subreach are plotted in Figure 36.

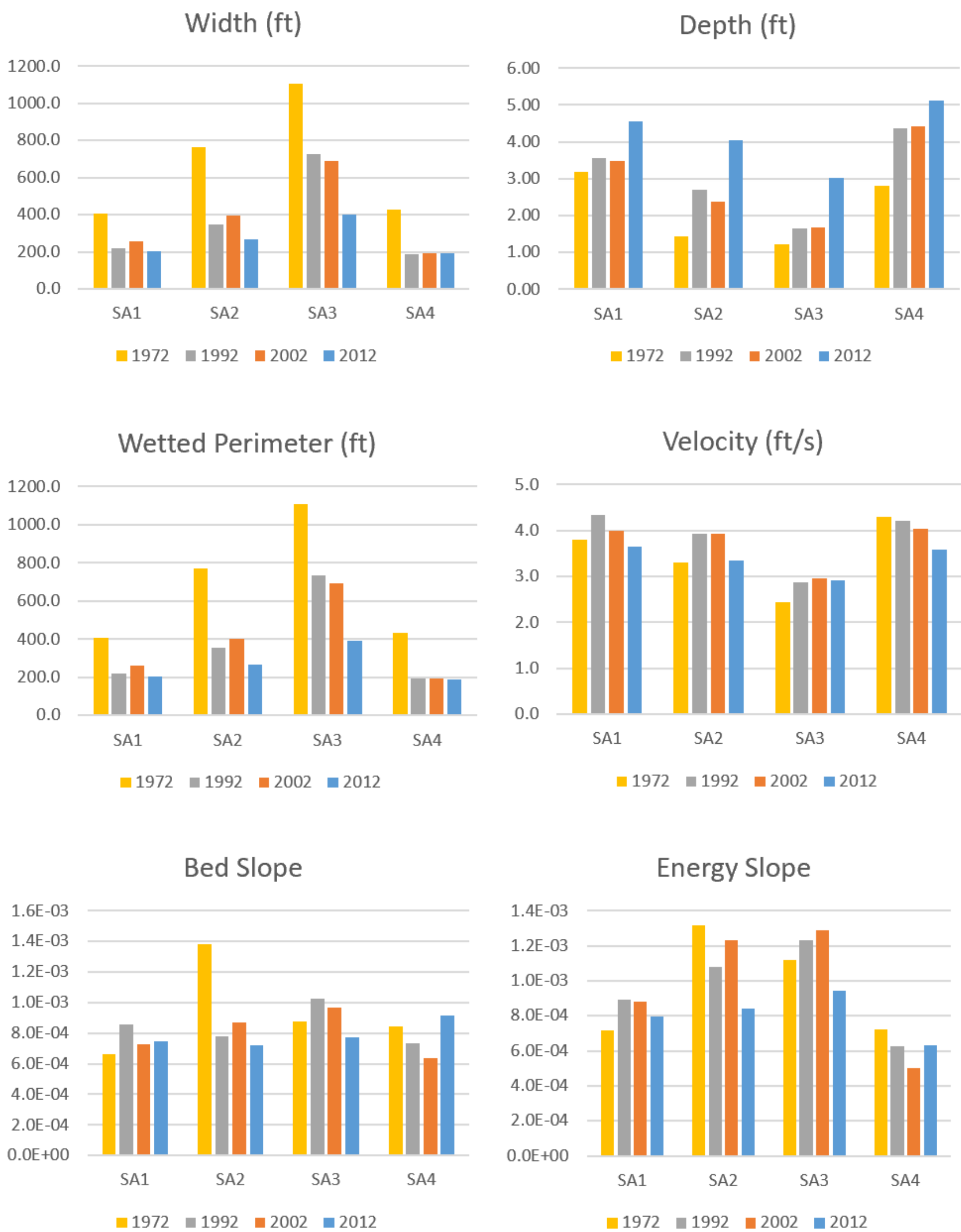

Figure 36 HEC-RAS analysis results

Narrowing is a prominent trend throughout the San Acacia reach. There are dramatic decreases in width and wetted perimeter from 1972 to 2012. Width and wetted perimeter are closely linked, which indicates a wide and shallow channel. Based on the plots generated from the HEC-RAS data, there is an inverse relationship between the depth and width. As the channel narrows from 1972 to 1992, the depth increases. From 1992 to 2002, the width only has slight changes resulting in minimal changes in depth as well. From 2002 to 2012, the channel continues to narrow throughout most of the reach. For this time period, the depth increases a greater amount, while the narrowing is not as significant as in 1972. Based on the width and depth, the flow area appears to increase in SA1, SA2, and SA4. This can also be related to the velocity. An increase in flow area could be correlated with a decrease in velocity, a decrease in bed slope, or possibly a combination of the two. The figure shows a decrease in velocity throughout SA4, which is supported by analysis showing that the width was not changing, and the depth was increasing. The bed slope throughout the reach fluctuates slightly, but overall remains fairly unchanged except in SA2 from 1972 to 1992, where the bed slope decreased leading to a much flatter subreach.

3.7 Mid-Channel Bars and Islands

At low flows, the number of mid-channel bars and islands at each agg/deg line is measured from digitized planforms from the aerial photographs provided by the USBR. In some locations, multiple channels were present at one agg/deg line due to a vegetated bar or island bifurcating the flow. Figure 37 shows the results of this analysis. Subreach SA4 never has more than one channel, while the others shift inconsistently through time. For all subreaches, years 1985 and 1992 show only one channel. Overall, these results highlight how easily a sand-bedded channel shifts over time.

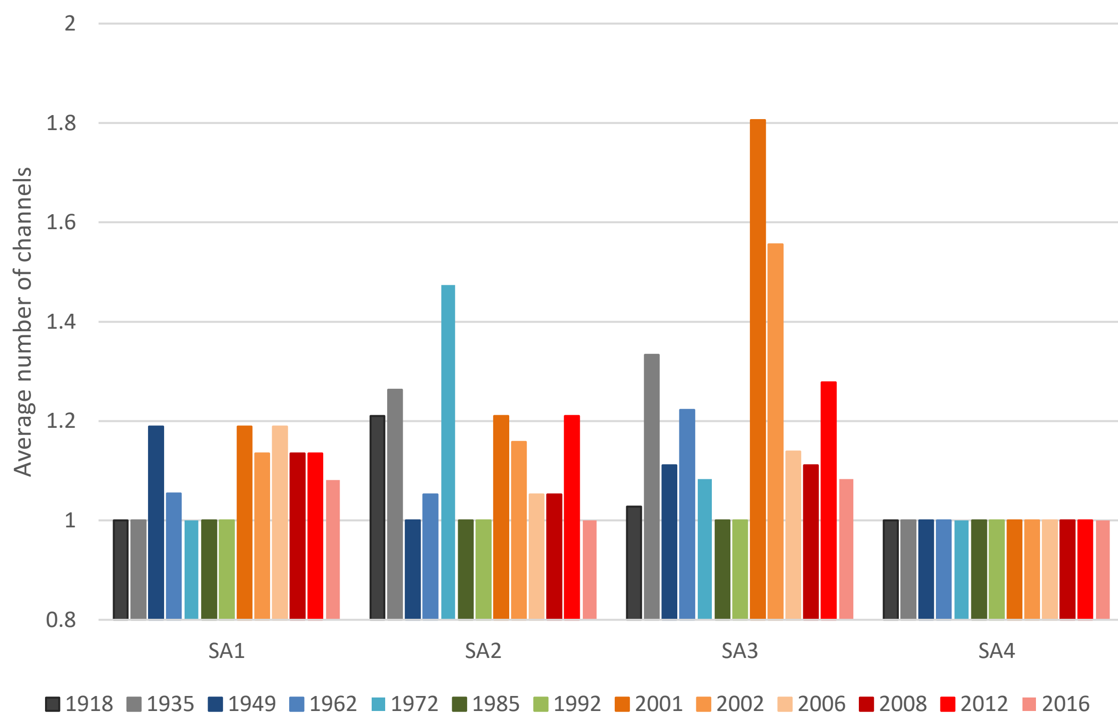

*Discharges are unknown in the aerial photographs that were used to create the digitized planforms. The number of low flow channels may be affected by varying discharge values.

Figure 37 Average number of channels at each subreach through time.

3.8 Channel Response Models

Qualitative and quantitative channel response models can be useful in understanding how river systems respond to changes in water and sediment loads.

3.8.1 Schumm's 1969 River Metamorphosis

Schumm (1969) suggested the following qualitative response model.

$$Q_t^+ \sim W^+ h^- P^- L^+ S^+$$

$$Q^+ \sim W^+ h^+ L^+ S^-$$

$$Q^- Q_t^- \rightarrow W^- h^\pm F^- L^- S^\pm P^+$$

Where Q is the flow discharge, Q_t is the percentage of the total sediment load transported as bedload, W is the channel top width, h is the flow depth, L is the meander wavelength, F is the width-depth ratio, S is the slope, and P is the sinuosity. The exponent, expressed as either a plus or minus, indicate whether the dimensions of the variables are increasing or decreasing.

Width and sinuosity came from Section 3.2 Width (Defined by Vegetation) and Section 3.5 Sinuosity respectively. The width-depth ratio, slope and flow depth were calculated using HEC-RAS in 3.6 Hydraulic Geometry. These values were then applied to Schumm's model, which predicted either an increase or decrease in sediment load and discharge (see Table 6 Summary of Schumm's model applied to the San Acacia subreaches). However, Schumm's model was a poor fit for this section of the Middle Rio Grande, and few relationships according to the model were found.

Table 6 Summary of Schumm's model applied to the San Acacia subreaches

Year	Subreach	W	h	S	F	P	Schumm's model
1972-1992	SA1	+	-	+	-	+	NA
	SA2	-	-	-	-	-	NA
	SA3	-	-	+	+	+	NA
	SA4	+	-	-	-	-	NA
1992-2002	SA1	-	-	-	+	+	NA
	SA2	-	-	+	+	+	NA
	SA3	-	-	-	+	-	NA
	SA4	+	-	-	+	=	NA
2002-2012	SA1	+	+	+	-	+	NA
	SA2	+	+	-	-	+	Q+
	SA3	-	+	-	-	+	Q-Qt-
	SA4	+	+	+	-	=	NA

3.8.2 Julien and Wargadalam Equations

Equations to predict the downstream hydraulic geometry of rivers were derived by Julien and Wargadalam (1995). These equations were based on empirical analysis of over 700 single-threaded rivers and channels, and predicted the width and depth likely to result from a certain discharge, grain size and slope:

$$h = 0.2Q^{\frac{2}{6m+5}}d_s^{\frac{6m}{6m+5}}S^{\frac{-1}{6m+5}}$$

$$W = 1.33Q^{\frac{4m+2}{6m+5}}d_s^{\frac{-4m}{6m+5}}S^{\frac{-1-2m}{6m+5}}$$

Where $m = 1/\ln\,(12.2h/d_s)$, h is the flow depth, W is the channel width, Q is the flow discharge, d_s is the median grain size and S is the slope. A discharge of 3,000 cfs, the same as the previous HEC-RAS analysis, is used. The values for grain size and slope were obtained from 3.4 Bed Material and 3.3 Bed Elevation, respectively. The mean d_{50} of the 1990s was used for 1992, 2000s for 2002 and 2010s for 2012. The flow depth was iterated to calibrate m, then the width was calculated.

Historically, these equations would not have applied to the MRG as a braided, sand-bed channel. However, as the MRG became a single-threaded channel it became more appropriate to apply these equations as a method of estimating the eventual equilibrium width of the channel. Predicted widths were generally narrower than the observed widths. Over time, the percent difference between the predicted and observed widths decreased and in 2012, all widths were within 50% of the predicted widths. The predicted widths are calculated using only the bankfull discharge, 3,000 cfs, when in reality there are various discharges flowing through the river affecting the observed widths, which could lead to discrepancies between the two. The JW equations seem to indicate that further narrowing is mostly likely to occur in subreaches SA2 and SA3. The predicted width and observed width are compared in Table 7 and Figure 38.

Table 7 Julien and Wargadalam's equations results

Year	Subreach	Q (cfs)	ds (mm)	Slope	Predicted Width (ft)	Observed Width (ft)	Percent difference
1992	SA1	3000	3.93	0.000749	210.2	239.6	-12%
	SA2	3000	0.29	0.000686	222.3	363.4	-39%
	SA3	3000	0.23	0.000991	206.9	879.5	-76%
	SA4	3000	0.32	0.000779	216.4	168.4	29%
2002	SA1	3000	0.64	0.000729	217.5	203.0	7%
	SA2	3000	0.42	0.000779	215.7	248.2	-13%
	SA3	3000	0.77	0.000885	208.6	479.3	-56%
	SA4	3000	0.37	0.000779	216.1	175.7	23%
2012	SA1	3000	1.66*	0.000734	214.3	215.1	0%
	SA2	3000	1.66	0.000736	214.1	295.8	-28%
	SA3	3000	0.29	0.000766	217.4	385.0	-44%
	SA4	3000	0.25	0.000993	206.6	204.2	1%

* 2012 grain size for SA1 not available, approximated with value from SA2

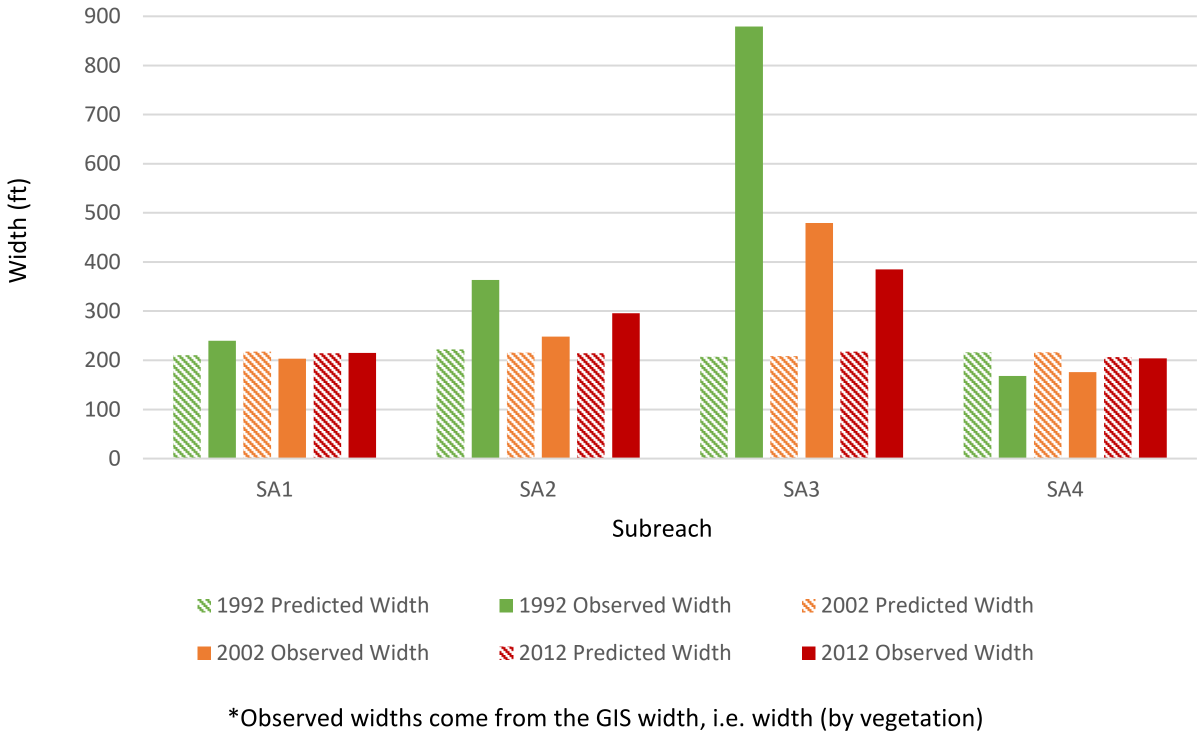

Figure 38 JW predicted and observed widths at 3,000 cfs

3.9 Geomorphic Conceptual Model

Massong et al. (2010) developed a channel planform evolution model for the Rio Grande based on historic observations. The sequence of planform evolution is outlined in Figure 39. Stage 1 describes a large channel with a high sediment load and frequent floods such that a wide, clear channel is maintained. As water levels fall, Stage 2 occurs and dunes from Stage 1 begin to stabilize into bars. In Stage 3, this stabilization is maintained by encroaching vegetation, regardless of flow levels. Only after the third stage does sediment transport become important in determining future stages. A lack of transport capacity leads to avulsion, as the channel aggrades and eventually the main flow shifts on to the now lower floodplain, processing to the A (aggrading) stages. Excessive transport capacity leads to the M (migrating) stages. Bends occur where bed and bank material erode both laterally and vertically. Transition between the M stages and the A stages can occur, but a reset to a Stage 1 requires a large, prolonged flood (Massong et al., 2010).

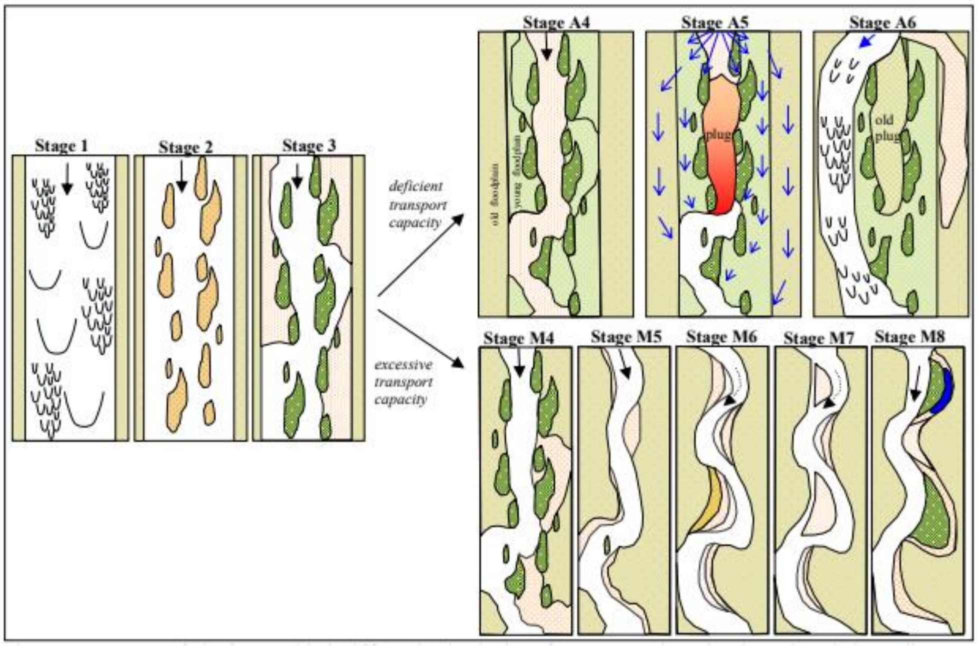

Figure 39 Planform evolution model from Massong et al. (2010). The river undergoes stages 1-3 first and then A4-A6 or M4-M8 depending on transport capacity.

Stages M4-M8 are the most relevant to the San Acacia reach because it has excess transport capacity, as shown by the degradation seen in 3.3 Bed Elevation. During the early 2000s, a drought led to flows rarely exceeding 1,000 cfs (less than 6% of the time). As flows increased during the 2005 spring runoff, many of the islands that formed in the previous five years became vegetated (Massong et al., 2010). Although this generalization holds true for much of the Rio Grande, in some areas, different patterns were seen. This evolution is demonstrated in Figure 40.

Each of the subreaches is evaluated individually in the following pages. SA1 and SA4 appear to be more entrenched compared to SA2 and SA3. SA2 shows full evolution through the M-stages. SA3 can still be classified in the early stages of the Massong model.

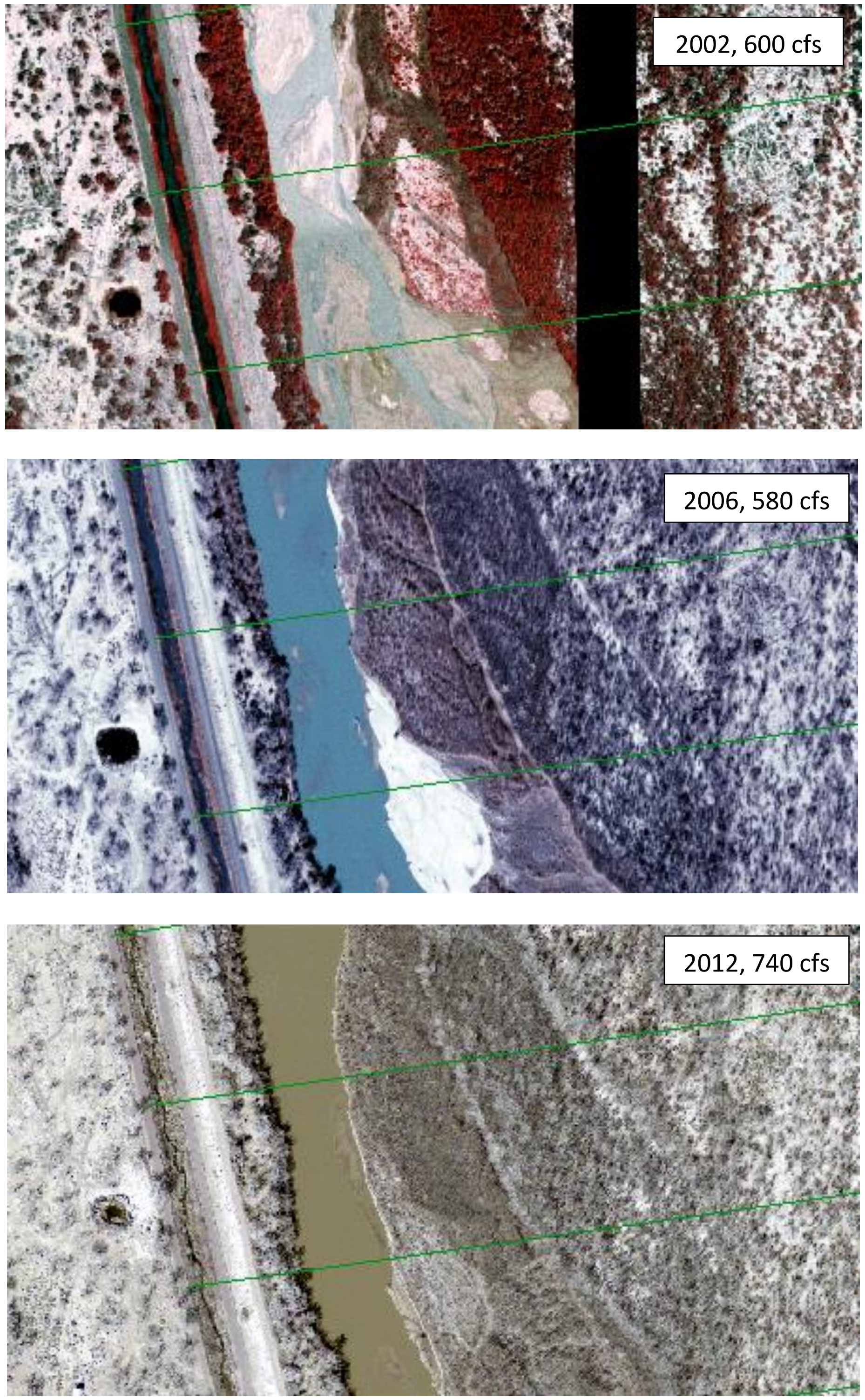

Figure 40 Geomorphic conceptual model evolution (Top: 2002; Middle: 2006; Bottom: 2012); flow direction from top to bottom

Figure 41 shows changes to Agg/deg line 1237 throughout time in subreach SA1. It shows significant incision over the time period from 1962 to 2012. Slight migration towards the levee is shown as well, although this migration is likely to slow down in the future due to the placement of Kellner jetty jacks.

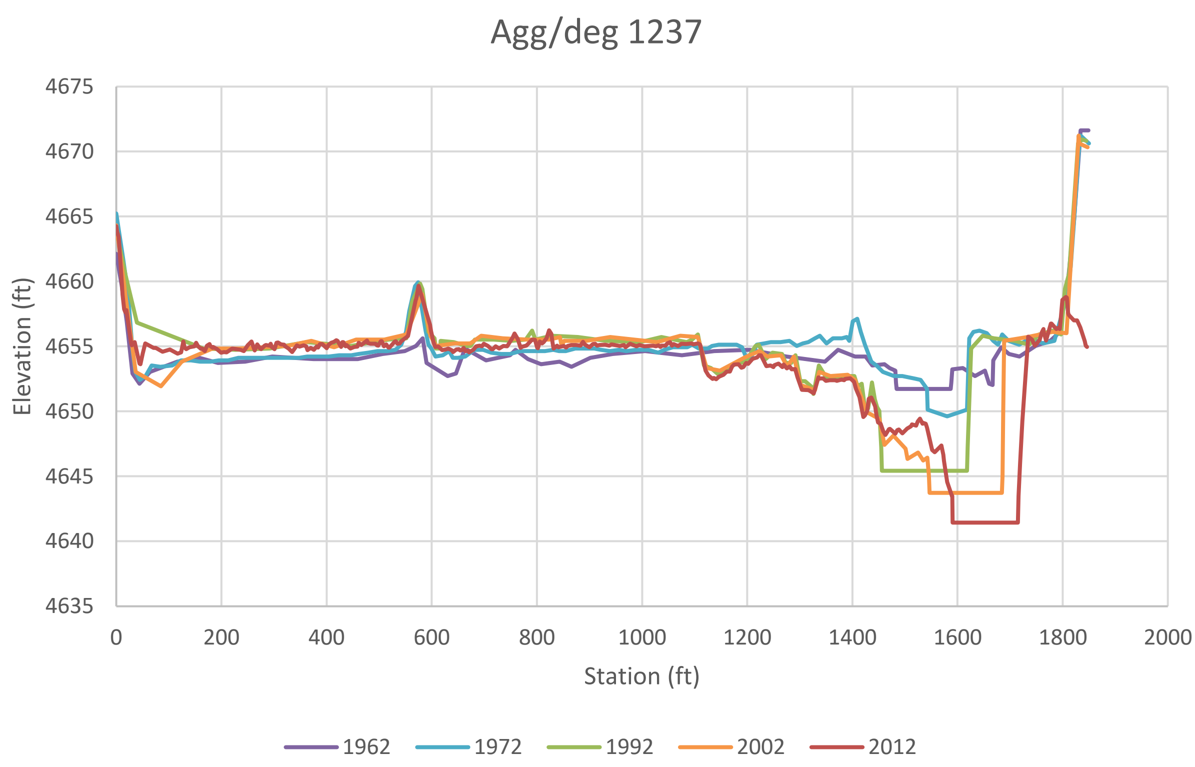

Figure 41 Evolution of cross-section 1237 from 1962 to 2012

Figure 42 on the next page shows each of these individually assigned a classification through Massong's model. In subreach SA1, the channel is eroding vertically and increasing in size, indicating that the sediment transport capacity exceeds the incoming sediment. Based on the cross-section profile and aerial photographs, a dominant main channel has formed. The side channels that were once a part of the main channel are experiencing vegetation growth and are no longer active. Based on these observations, subreach SA1 could be classified in a migrating stage, M5.

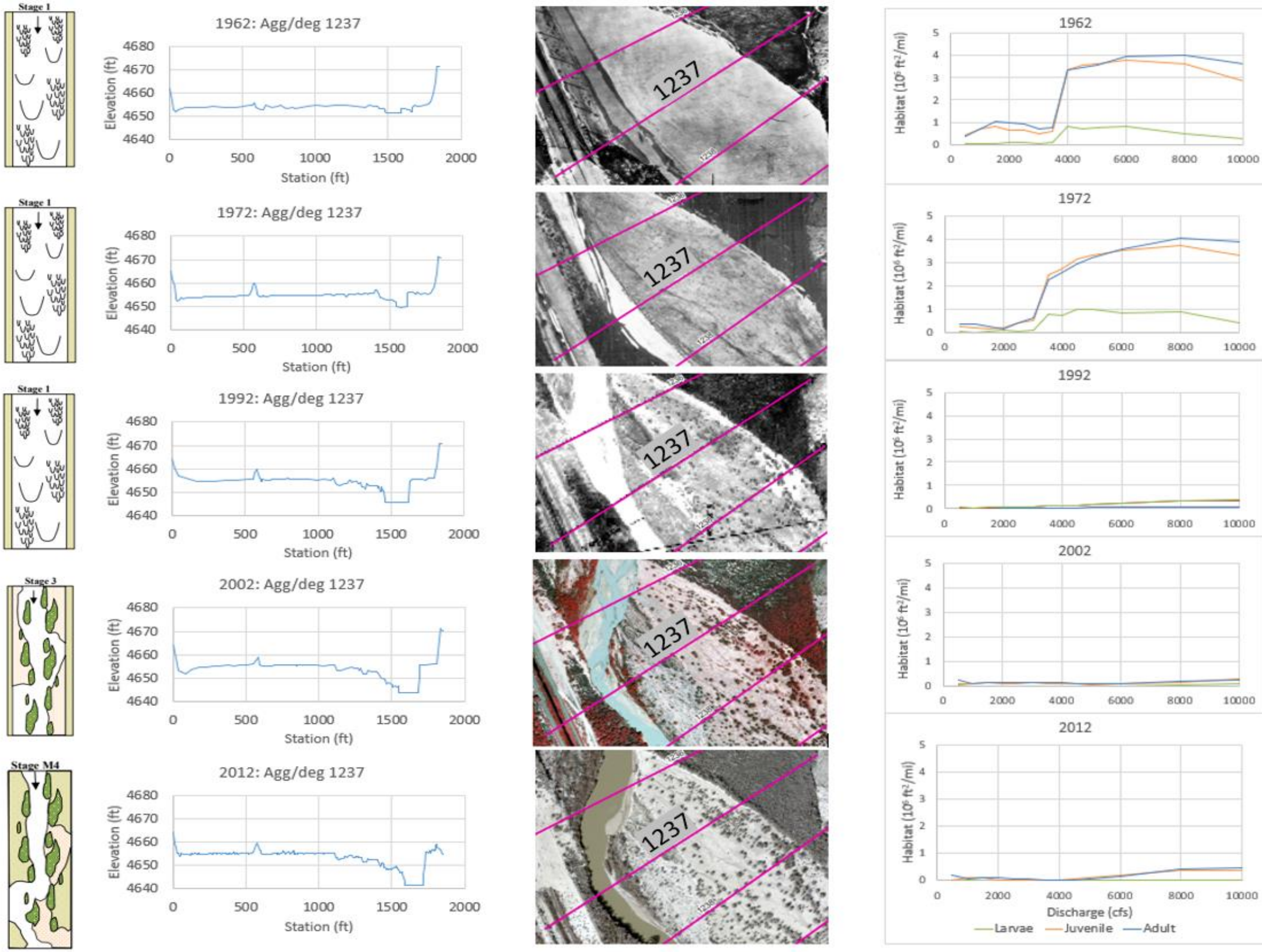

Figure 42 Evolution of cross-section 1237 from 1962 to 2012. Agg/deg line label on the aerial photographs refers to the line below

Figure 43 shows changes to Agg/deg line 1246 throughout the same time period in subreach SA2. From 1962 to 1972, the main channel (shown on the left) aggraded and became relatively flat. From 1972 to 2012, the main channel underwent significant incision, with the biggest changes occurring between 1972 and 1992 and 2002 and 2012. Figure 44 on the next page shows each of these individually assigned a classification through Massong's model.

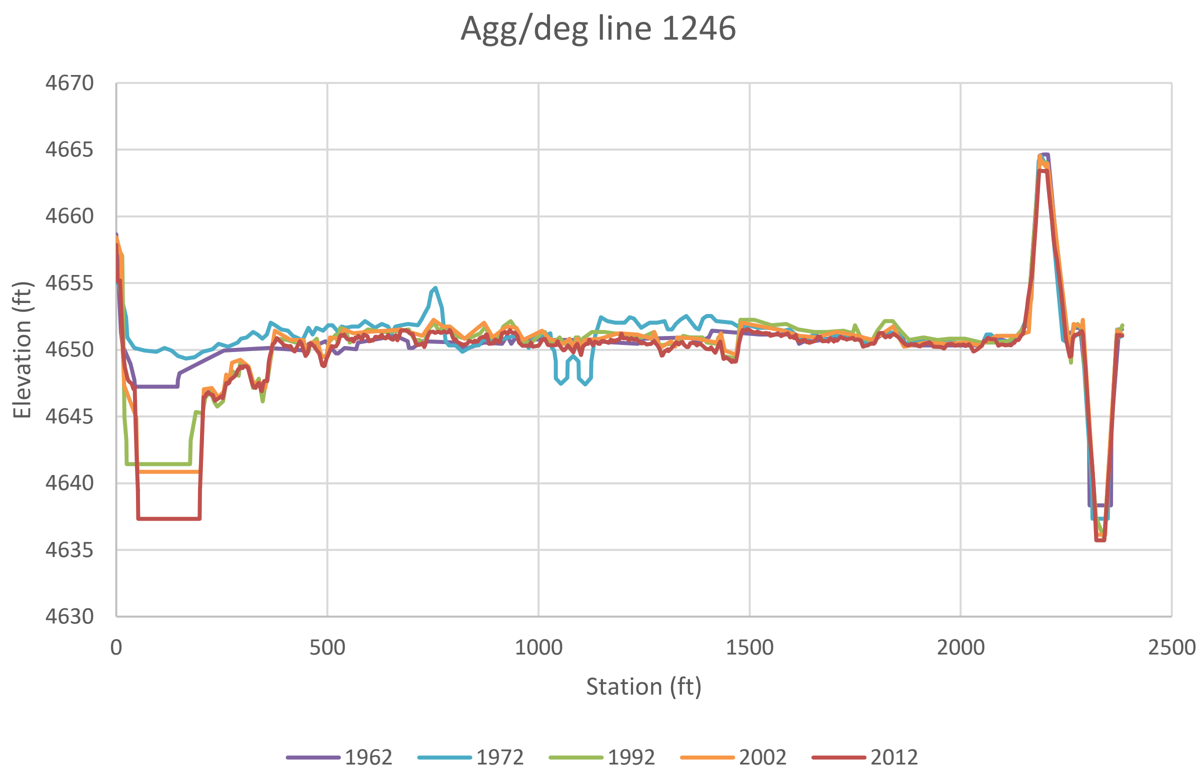

Figure 43 Evolution of cross-section 1246 from 1962 to 2012

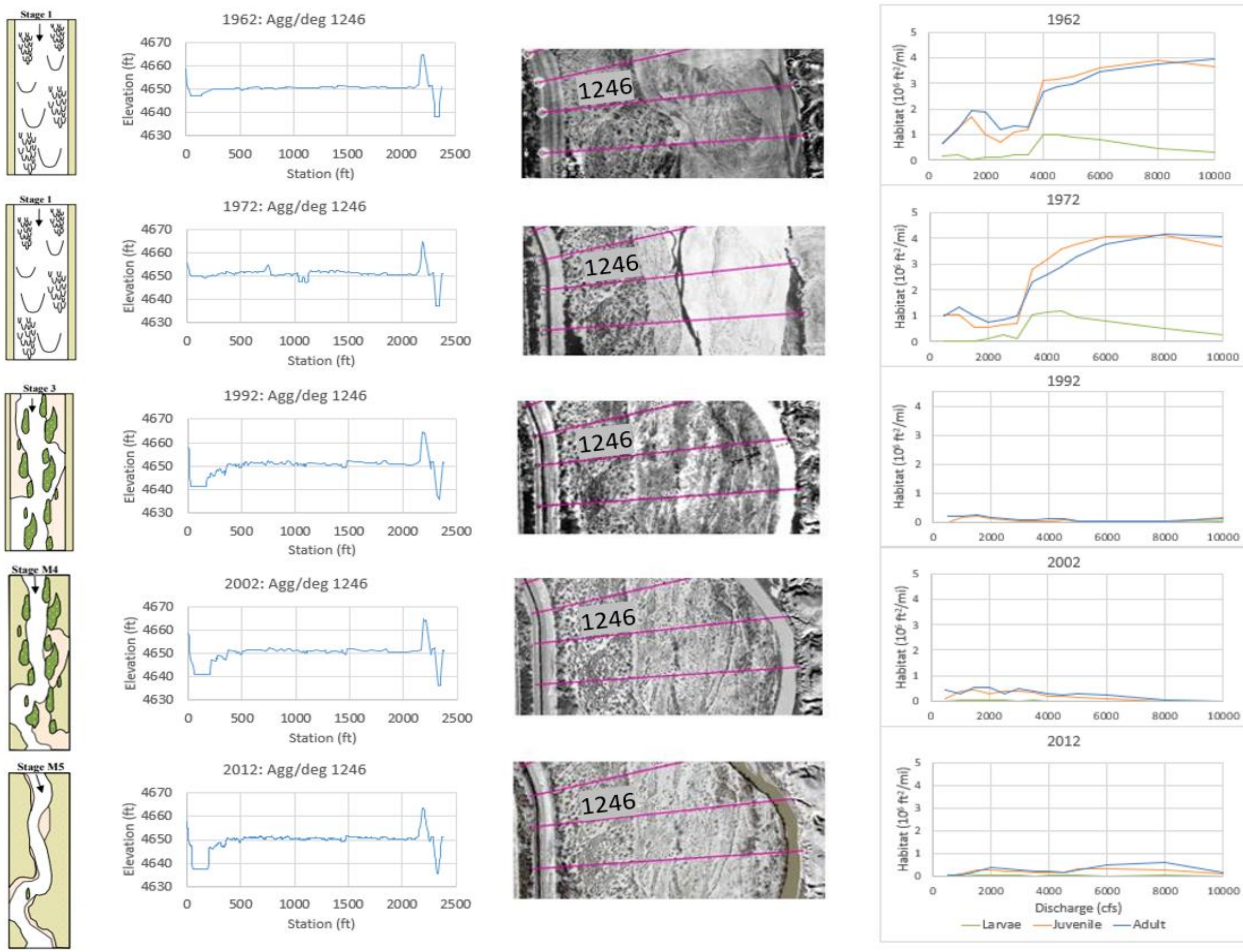

Figure 44 Evolution of cross-section 1246 from 1962 to 2012. Agg/deg line label on the aerial photographs refers to the line below

Subreach SA2 shows the full evolution through the M-stages, as seen in Figure 45 below. In 1992, this section of the river appeared to be in Stage 2, with un-vegetated bars and islands. Substantial change was then seen with a dramatic increase in the degree of sinuosity, as the bends laterally eroded. In 2005, M6 is most closely represented. Stages 3, M4 and M5 occurred in the period of time between these two images. Shortly after, in 2006, a cutoff formed, with flow split between the more direct path and the larger bend. By 2009, this bend was inactive, resembling stage M8. Sand deposits likely filled the previous channel, and vegetation continued to colonize the old bars and islands formed by this cutoff. It is likely that the channel reverted to M4, but can now be classified as M5, with smoother banks. The median width cross-section in this channel is shown in Figure 45.

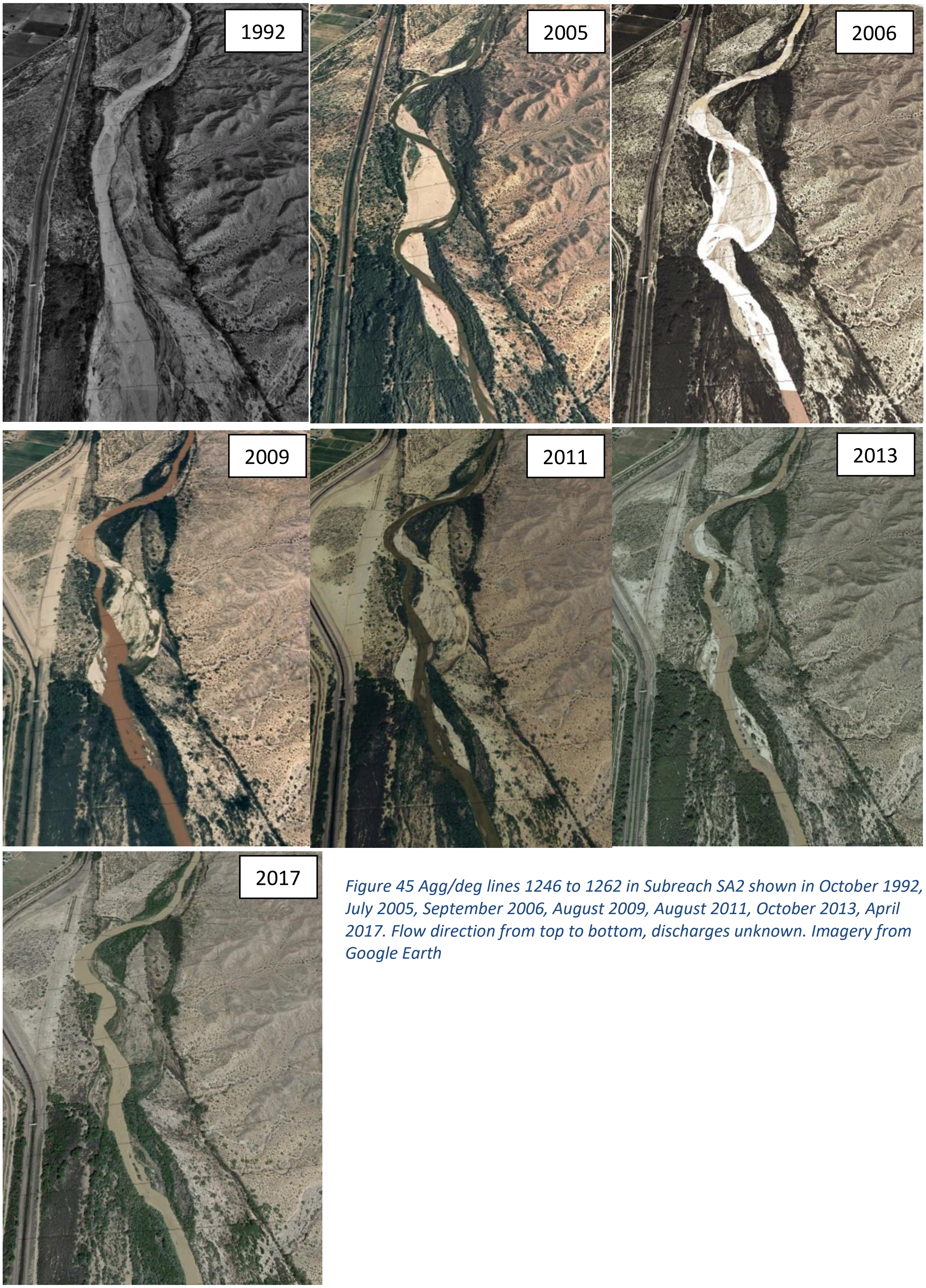

Figure 45 Agg/deg lines 1246 to 1262 in Subreach SA2 shown in October 1992, July 2005, September 2006, August 2009, August 2011, October 2013, April 2017. Flow direction from top to bottom, discharges unknown. Imagery from Google Earth

Figure 46 shows changes to Agg/deg line 1282 throughout the same time period in subreach SA3. The main channel (shown on the right) shows degradation and channel widening from 1962 to 2012. Additionally, the floodplain bed elevation has risen slightly since 1962.

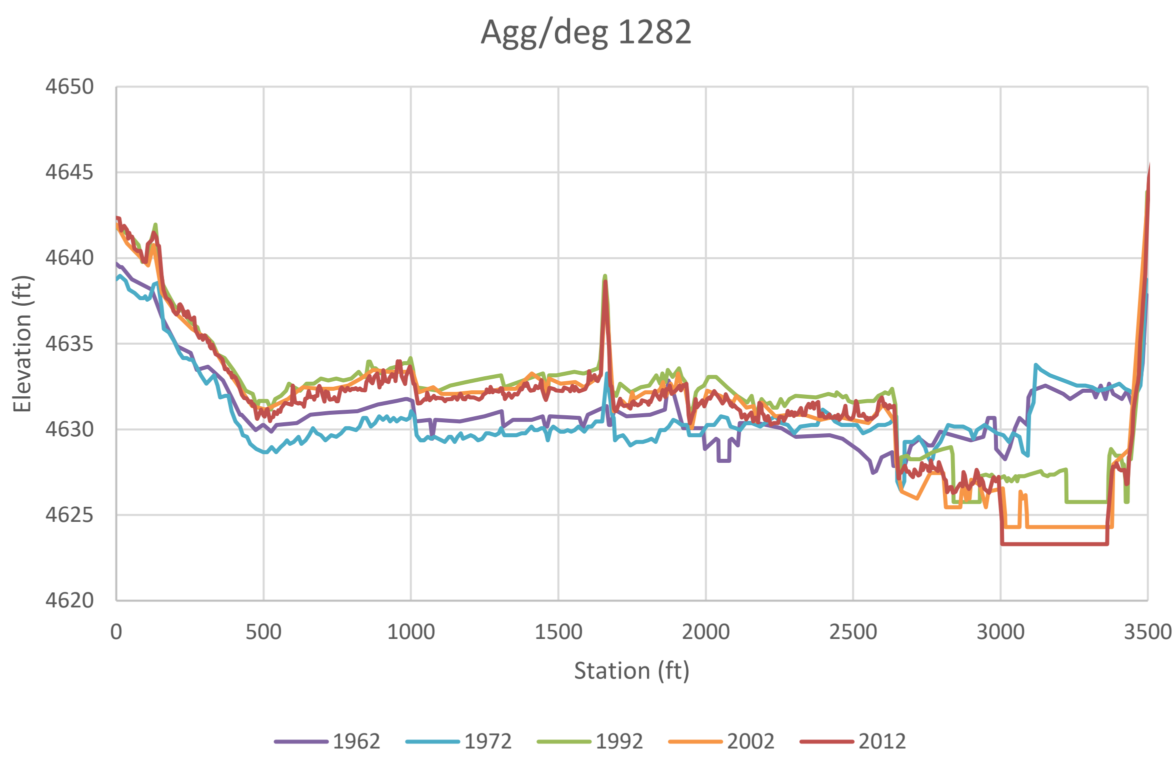

Figure 46 Evolution of cross-section 1282 from 1962 to 2012

Although Subreach SA3 has changed dramatically since 1962, in comparison to the other subreaches, it is still significantly wider, as seen in Figure 30. Therefore, through 2012, it can still be classified in the early stages of the Massong channel evolution model. However, vegetation encroachment happens rapidly from 2013 to 2017, indicating that it may be proceeding to the other M-stages relatively soon, as seen in Figure 47. Although in Figure 48, it is classified as Stage 3 in 2012, its classification today is somewhere between Stage 3 and Stage M4.

Figure 47 Subreach SA3 from October 2013 to April 2017 showing vegetation encroachment and narrowing in the main channel. Flow direction is from top to bottom, discharges unknown. Imagery from Google Earth

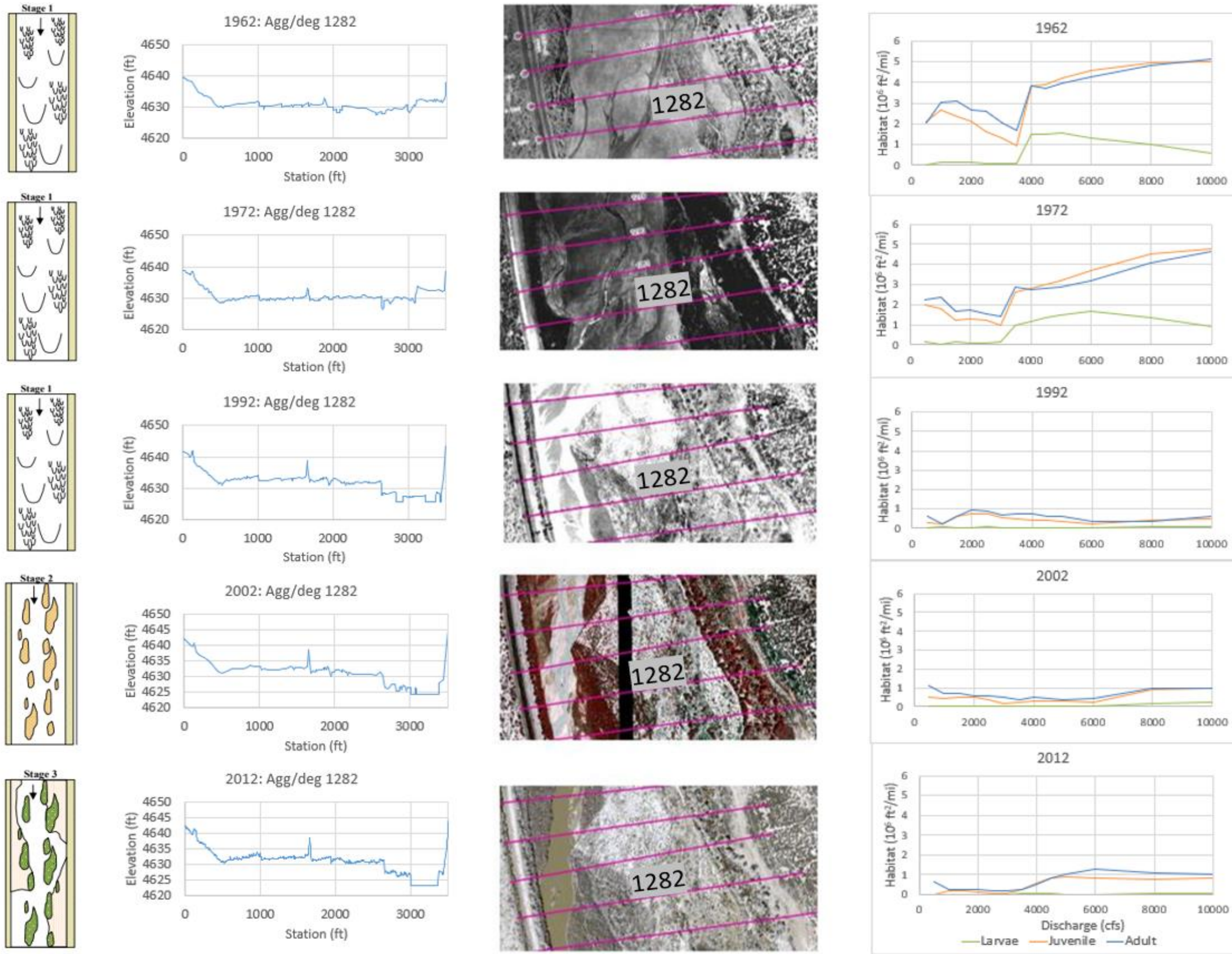

Figure 48 Evolution of cross-section 1282 from 1962 to 2012. Agg/deg line label on the aerial photographs refers to the line below

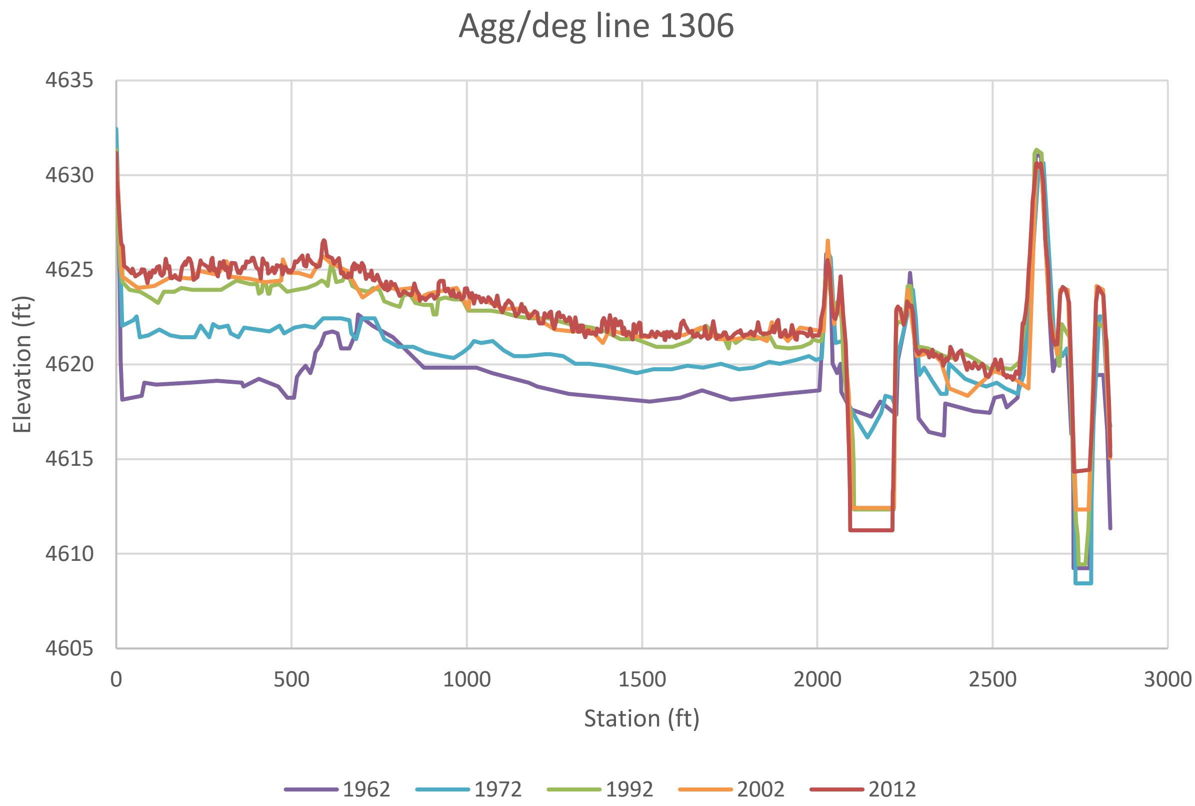

Figure 49 Evolution of cross-section 1306 from 1962 to 2012

As seen in Figure 49 above, SA4 (represented by agg/deg line 1306) shows very little movement besides incision over time and has a nearly constant average width from 1962 to the present. Although the characteristics of vegetation and the depth of the channel in that subreach have changed since 1962, the lack of meandering shows that stage M4 can have different lag times in different areas of the river. This may be so severe in this reach because the main channel of SA4 was straightened and altered away from the historic river channel. In Figure 50, the channel on the right side of each of the figures was the historic channel. After the 1950s, flow rarely passed through this channel, and instead was concentrated in the channel on the left side.

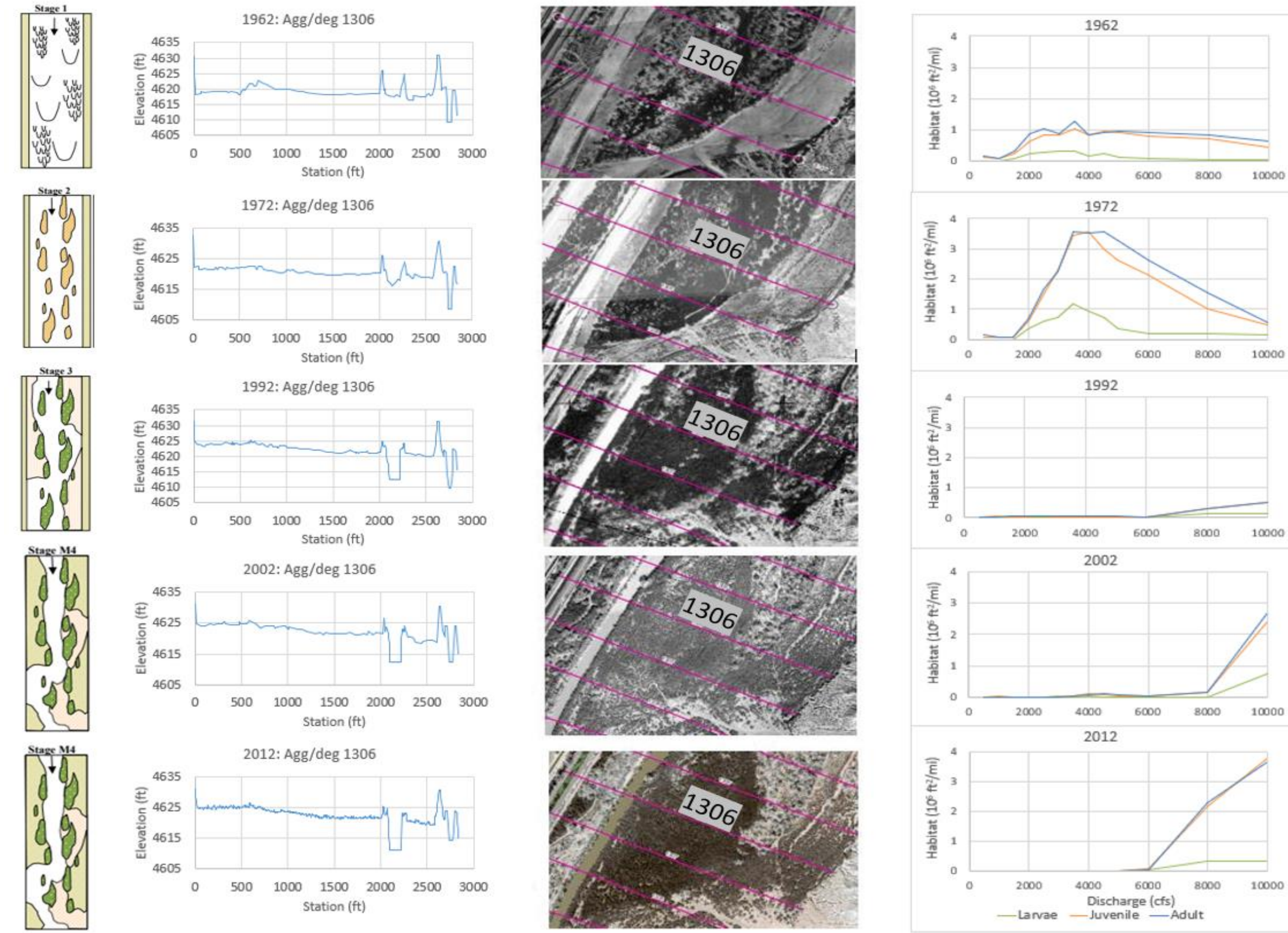

Figure 50 Evolution of cross-section 1306 from 1962 to 2012. Agg/deg line label on the aerial photographs refers to the line below

Table 8 provides a summary of the Massong geomorphic stage classifications assigned to each subreach for 1962, 1972, 1992, 2002, and 2012. Notice that earlier years (1962, 1972, 1992) tend to show stages 1 to 3, while more recent years (2002 and 2012) show migrating stages, M4 and M5. Stages 1 and 2 tend to correspond with the rounded habitat curves, while stage 3 and migrating stages tend to show habitat curves with a step at higher discharges.

Table 8 Summary of Massong's stage classifications by subreach and year

	1962	**1972**	**1992**	**2002**	**2012**
Subreach	**Stage Classification**				
SA1	1	1	1	3	M4
SA2	1	1	3	M4	M5
SA3	1	1	1	2	3
SA4	1	2	3	M4	M4

4. HEC-RAS Modeling for Silvery Minnow Habitat

The Rio Grande Silvery Minnow (RGSM or silvery minnow) is an endangered fish species that is native to the Middle Rio Grande. It currently occupies only about seven percent of its historic range (U.S. Fish and Wildlife Service, 2010). It was listed by the US Fish and Wildlife Service in 1994.

One of the most important aspects of silvery minnow habitat is the connection of the main channel to the floodplain. Spawning is stimulated by peak flows in late April to early June. These flows should create shallow water conditions on the floodplains, which are ideal nursery habitat for the silvery minnow (Mortensen et al., 2019). Silvery minnows prefer specific velocities and depths for different stages of their life histories. Table 9 outlines these velocity and depth guidelines. Fish population counts are available from 1993 to the present. Therefore, analysis of silvery minnow habitat will not extend prior to 1992.

Table 9 RGSM habitat velocity and depth requirements (from Mortensen et al., 2019)

	Velocity (cm/s)	Depth (cm)
Adult Habitat	<40	>5 and <60
Juvenile Habitat	<30	>1 and <50
Larvae Habitat	<5	<15

4.1 Modeling Data and Background

The data available to develop these models varies year by year. In 1992, 2002 and 2012 cross-sections were available in a HEC-RAS model. In 2012, additional LiDAR data of the floodplain was available, which allowed the development of a terrain for RAS-Mapper. Therefore, RAS-Mapper was used in 2012 only, while comparisons across years are done using 1-D techniques. In the development of these models, HEC-RAS levee points were set at the necessary location to prevent flow in inaccessible side channels and in the low flow channel on the other side of the levee (see Section 4.2 Bankfull Discharge).

Peak spring flows have varied drastically from 1992 to the present, with some years maintaining flows over 5,000 cfs for many days in a row, and some years where flows did not even reach 2,000 cfs. Therefore, a wide variety of flows were modeled to represent this spread of peak runoff values, using an increment of 500 cfs up to 10,000 cfs.

Although modeling was done at low flows (<1,000 cfs), these results are rather simplified. In developing the HEC-RAS geometry cross-sections, LiDAR was not available under the water surface. Therefore, an underwater prism was developed by the USBR based on water surface elevation measurements. This underwater prism was approximated as a trapezoidal cross-section and lacks the complexity of the actual channel. Those interested in understanding RGSM habitat at low flows should look at the 2008 report "Streamflow and Endangered Species Habitat in the Lower Isleta Reach of the Middle Rio Grande" by Bovee et al, which analyzed fish habitat at flows below 1,000 cfs.

4.2 Bankfull Discharge

A method was used to determine the overtopping discharge throughout a reach, which provided a discharge at which the HEC-RAS "levees" would be removed from all cross-sections in that reach. One issue with HEC-RAS one-dimensional modeling is the prediction of the water distribution as discharge increases. HEC-RAS distributes the water from the lowest elevation up. Because much of the MRG is perched, a problem arises in which HEC-RAS assumes water is in the floodplains at a much lower discharge than what would actually occur. To correct this issue, the method described in Baird and Holste, 2020 was used to determine bankfull discharge and assign HEC-RAS "levees" (top of bank (TOB) points) to prevent the floodplains from filling before expected.

First, HEC-RAS "levees" were placed at the locations that best represent the point of bank on each side of the channel. The water is contained within the main channel (between the TOB points) until there is a discharge large enough to overtop these points. HEC-RAS has the capability to calculate the left and right levee freeboard, which is the difference between water surface elevation and "levee" elevation. A negative value indicates an overtopping discharge. A sensitivity analysis was completed to determine the percentage of cross sections that should be overtopped before removing the TOB points in HEC-RAS. For this case, when 25% of the cross sections in the reach were experiencing overtopping, signifying 25% had reached bankfull discharge, the TOB points were removed, allowing water to inundate the floodplains. Figure 51 shows the percent of cross-sections overtopping the top of bank points for 1962, 1972, 1992, 2002, and 2012 and the resulting bankfull discharges.

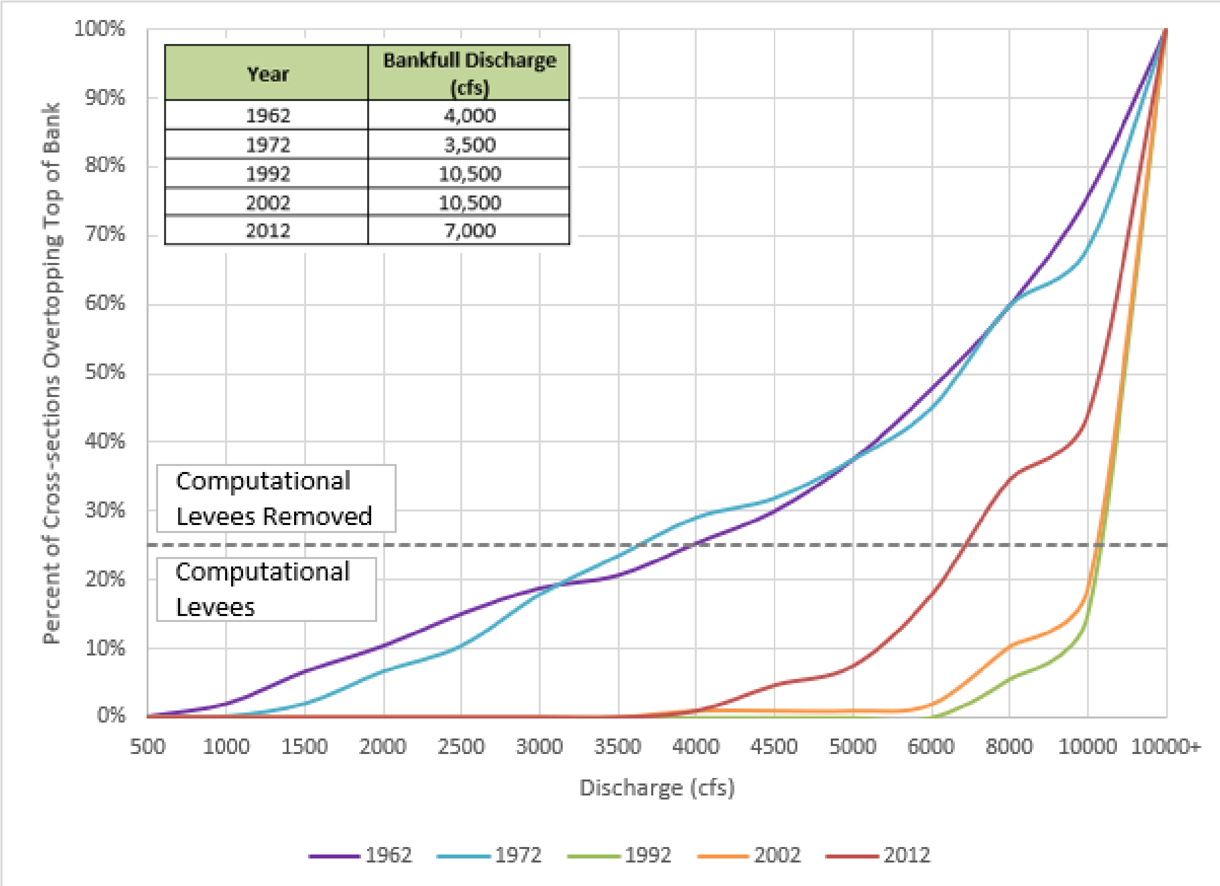

Figure 51 Percent of cross-sections overtopping top of bank points from 1962 to 2012. The gray dashed line represents the 25% threshold

4.3 RAS-Mapper Methodology

The HEC-RAS geometry data needed to use RAS-Mapper was available in 2012 only (geo-referenced cross-sections and a LiDAR surface to generate a terrain). Therefore, only 2012 results were processed in RAS-Mapper. The original 2012 LiDAR data was used to develop a terrain. The RAS-Mapper program then interpolated the areas between the cross-sections using the terrain, which resulted in a more accurate understanding of where water was present in the channel. ArcGIS was used to combine the RAS-Mapper generated rasters of velocity and depth as a grid, and the results were exported by subreach.

4.3.1 RAS-Mapper Delineation

To obtain the best resolution possible in the RAS-Mapper habitat maps, subreaches were broken up into smaller delineations. Table 10 summarizes these delineations.

Table 10 Subreach delineations for habitat mapping

Subreach	Agg/Deg Lines
SA1(a)	1207-1226
SA1(b)	1226-1245
SA2	1245-1264
SA3(a)	1264-1282
SA3(b)	1282-1300
SA4	1300-1313

4.4 Width Slices Methodology

Without a terrain for 2002 and 1992, additional methods had to be considered to determine a metric of fish habitat. HEC-RAS can analyze the lateral variability in discharge, depth, and velocity throughout a cross section as described in chapter 4 of the HEC-RAS Hydraulic Reference Manual (U.S. Army Corps of Engineers, 2016). HEC-RAS allows each cross-section to be divided into a set number of slices up to 45. 20 slices were assigned to the overbank sides and 5 were assigned to the main channel to provide the best results (see Appendix E for further insight into how this method was developed). Each slice calculates a velocity and hydraulic depth specific to that slice, where hydraulic depth is computed as the area divided by the top width of active flow. An example of cross-section 1276 is shown in Figure 52 at 10,000 cfs. These values were then taken and processed by cross-section for each flow value to compare across years. The area of hydraulically suitable habitat was calculated by summing the width slices that meet the RGSM velocity and depth requirements at a cross section. Agg/deg lines are spaced approximately 500 feet apart, so the width of hydraulically suitable habitat is multiplied by 500 feet to interpolate the area in between cross sections. For direct comparison between subreaches and other reaches of the river, the area of available habitat was divided by reach or subreach length to obtain square feet of available habitat per mile of river.

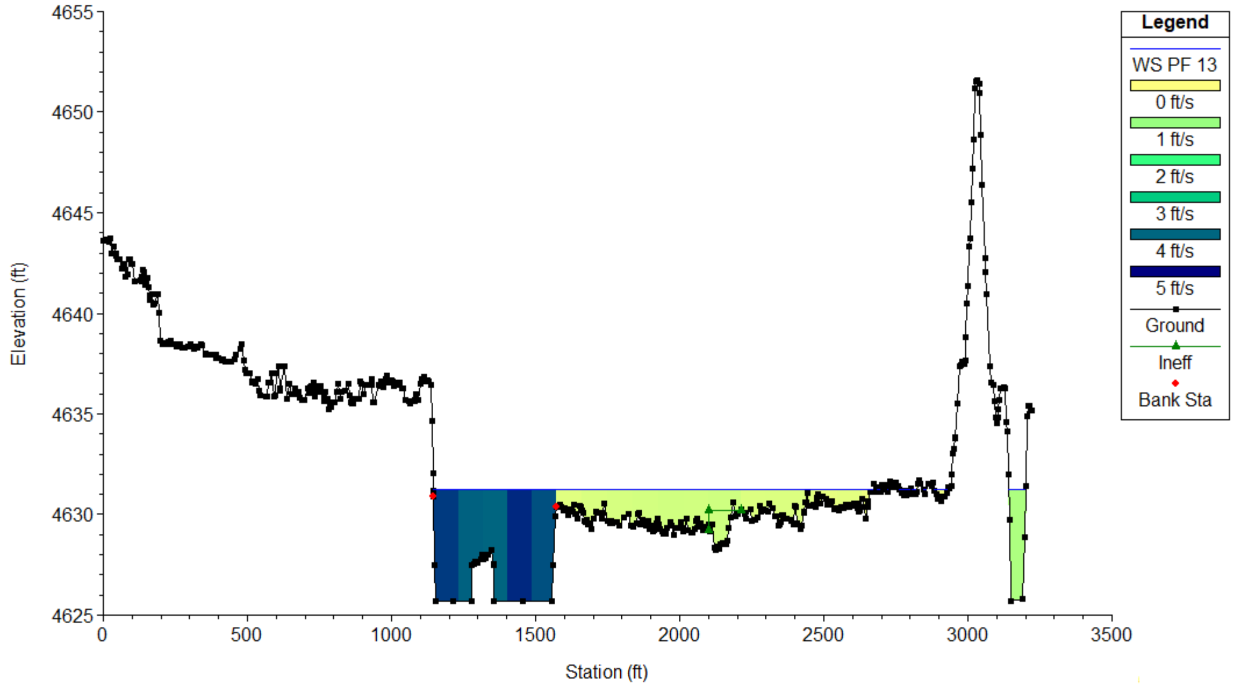

Figure 52 Cross-section 1276 showing "width slices" at 10,000 cfs

4.5 Time Integrated Habitat Metrics Methodology

Time Integrated Habitat Metrics (TIHMs) were developed to calculate habitat between 1992 and 2019 based on the previous habitat curves created, but now also considering the daily discharges of the reach. The TIHM model requires daily discharge data and yearly habitat data. Discharge data for the Rio Grande Floodway at San Acacia (08354900) was obtained for each water year, typically from October 1 to September 30, for the years 1992 to 2019. Figure 53 shows the hydrograph created for this gage separated out by representative sampling months for each of the RGSM's life stages. The representative sampling period is May to June for the larval stage, July to September for the juvenile stage, and October to April for the adult stage. Results are separated by sampling periods to allow for correlations to be made with fish population density data in the future. The habitat curves for each year are imported to the program along with the gage discharge data. A simple linear equation is determined that calculates the total habitat for each day of the year using the imported habitat and discharge data.

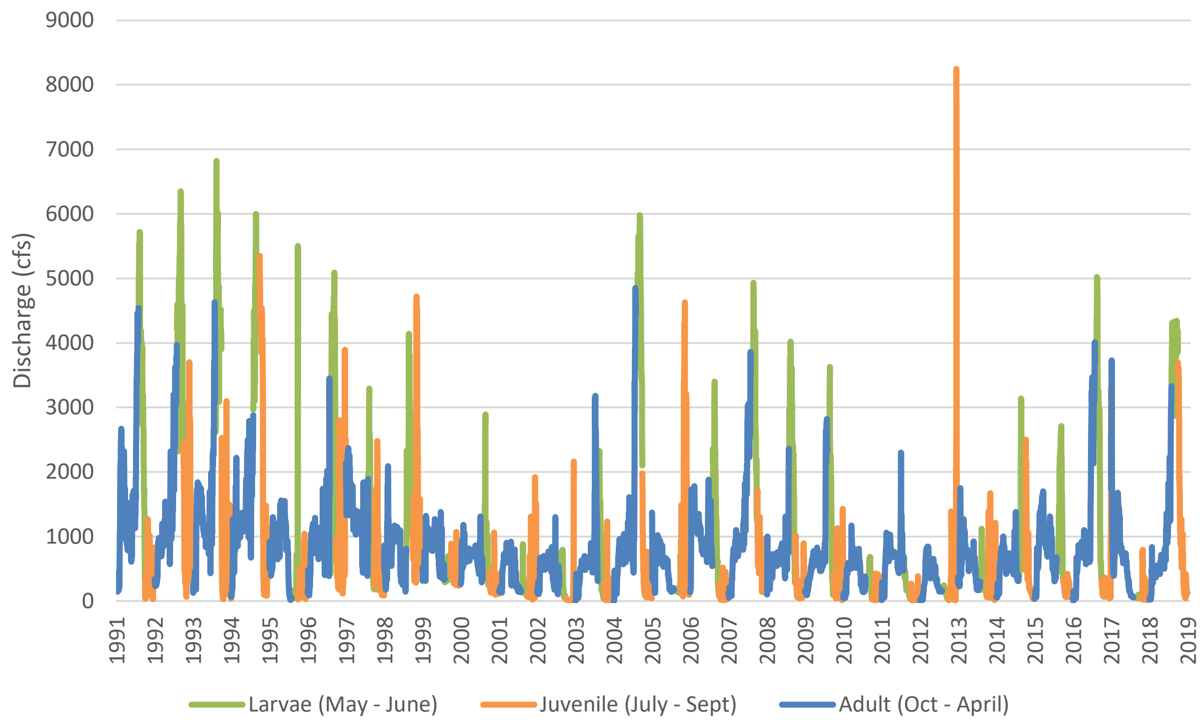

Figure 53 Rio Grande Floodway at San Acacia (08354900) hydrograph separated out by representative sampling periods

4.5.1 Temporal Interpolation of Habitat Curves

The RGSM habitat curves were developed using a temporal interpolation method, which allowed for interpolation between the known years to get a habitat curve for every year between 1992 and 2019. Cross-section geometry data, which are necessary for generating habitat curves, were available for 1962, 1972, 1992, 2002, and 2012. However, fish sampling data began in 1993 so the temporal interpolation starts with the 1992 data. To estimate the habitat for the unknown years, the habitat curves were interpolated temporally using a single mass curve, which would help identify the major changes in sediment transport, thus indicating greater changes to the cross-section geometry. Figure 54 shows the single mass curve that was created using sediment discharge data from the Rio Grande Floodway at San Acacia (08354900) USGS gage.

The interpolation method uses a variable "α" which represents the fraction of cumulative sediment transport at a given year relative to the cumulative sediment transport of the time interval. The single mass curve was divided into 10-year time periods determined by the available cross-section data (1992-2002, 2002-2012). The cumulative sediment at the end of the time period marks the max cumulative amount of sediment in that time period. The sediment discharge at any point can be divided by the max, which results in the term (1-α). The habitat curves for the years in between were interpolated by taking a fraction of the habitat from the earlier year (1-α) plus a fraction of the habitat curve from the later year (α). An example of this method can be seen in Figure 55.

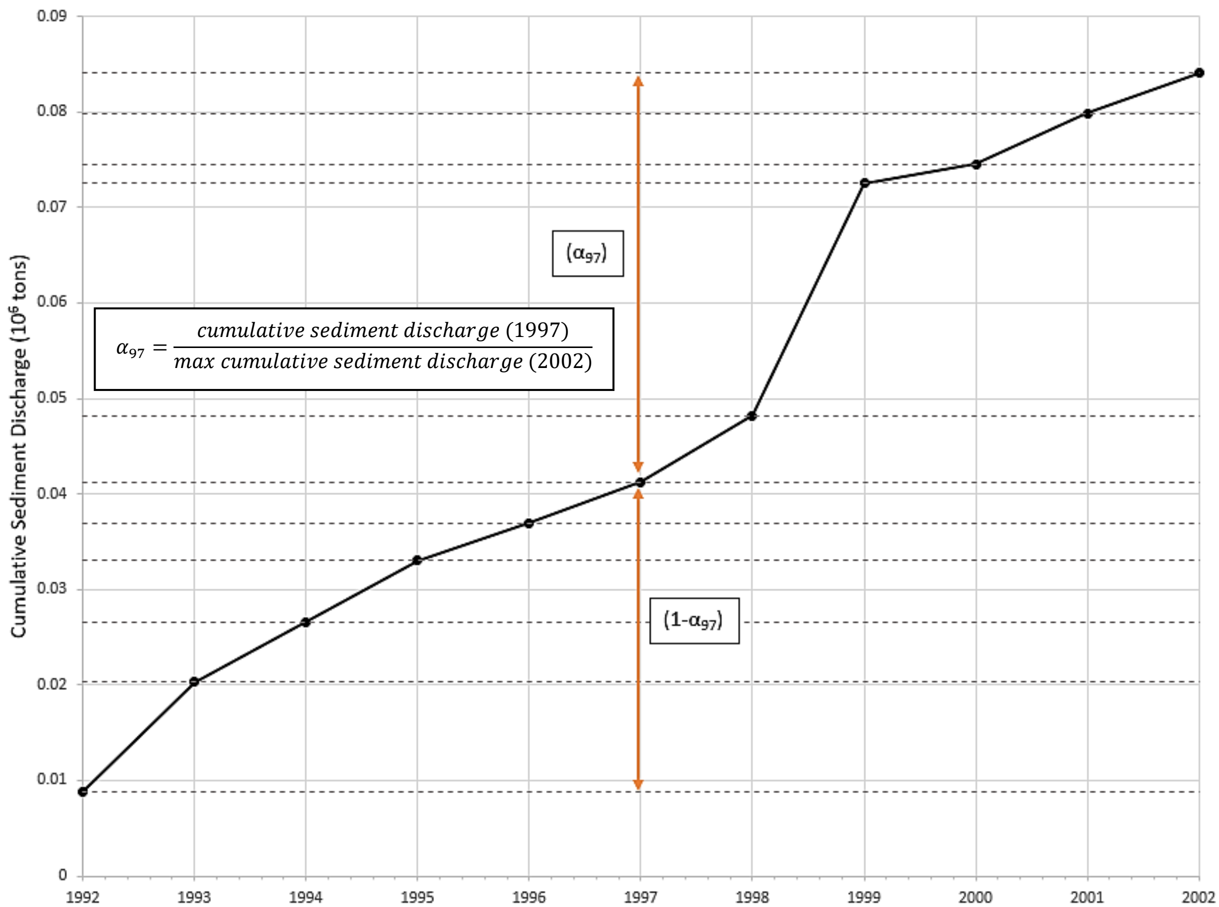

Figure 54 Temporal interpolation method using a single mass curve

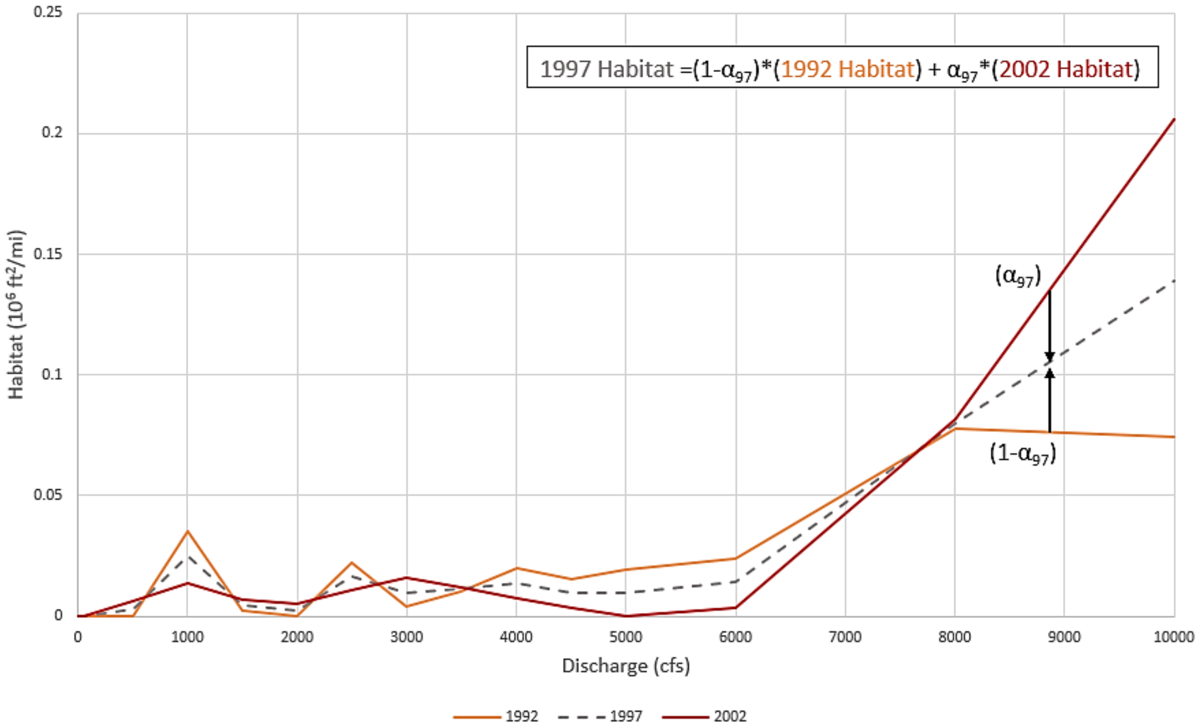

Figure 55 Example of temporal interpolation between habitat curves for 1997

4.6 RAS-Mapper Habitat Results in 2012

Mapping for larvae, juvenile, and adult habitat in SA3 can be seen in Figure 56 and Figure 57. Additional maps for the remaining subreaches can be found in Appendix C. Discharges 1,500, 3,000, and 5,000 cfs were selected for mapping. An aerial view provides further insight into the habitat conditions and where habitat conditions are being met. Note that throughout this subreach, there is minimal available habitat for the RGSM until higher flows are reached. This subreach could be considered to have poor restoration potential, as there are not many disconnected areas that are close to the main channel that would be of interest to the USBR.

.

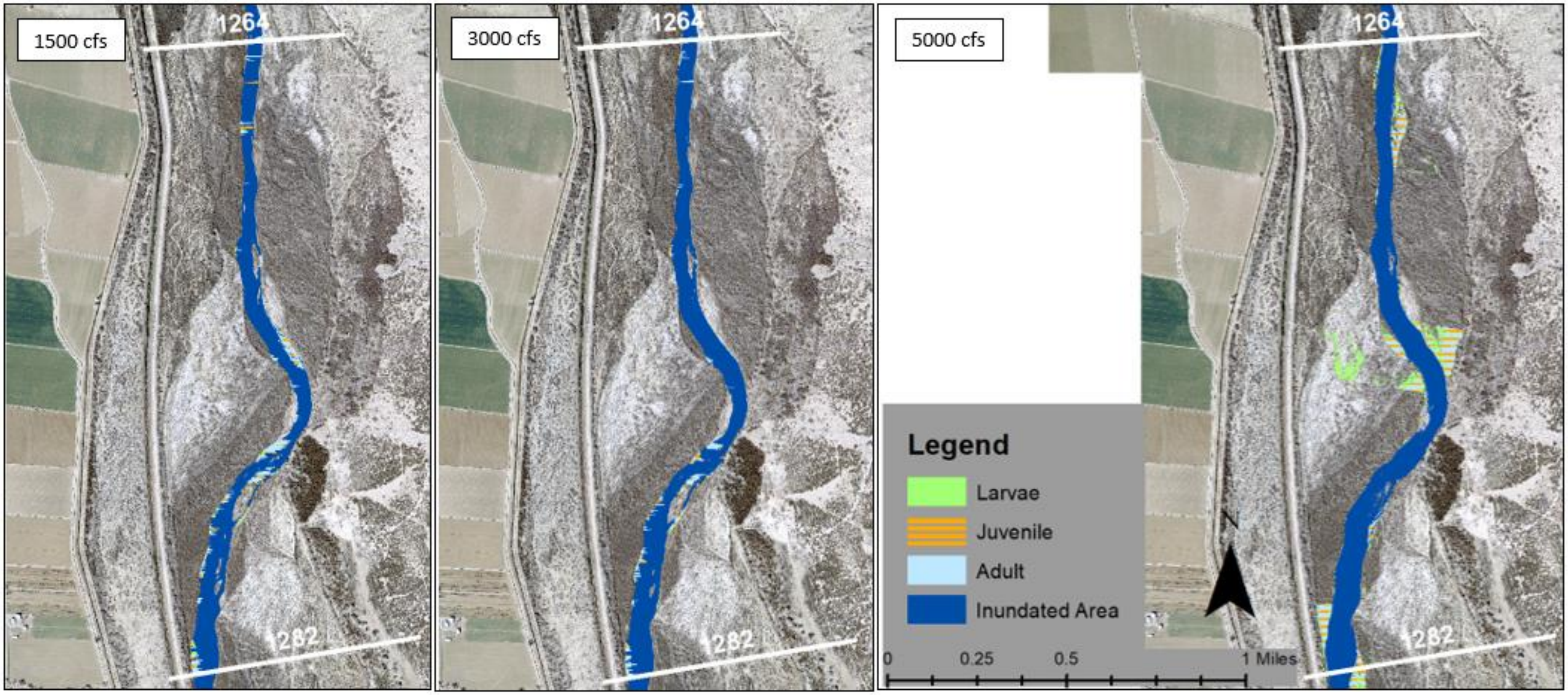

Figure 56 SA3(a) maps showing larval, juvenile, and adult habitat throughout the subreach. Flow direction is from top to bottom.

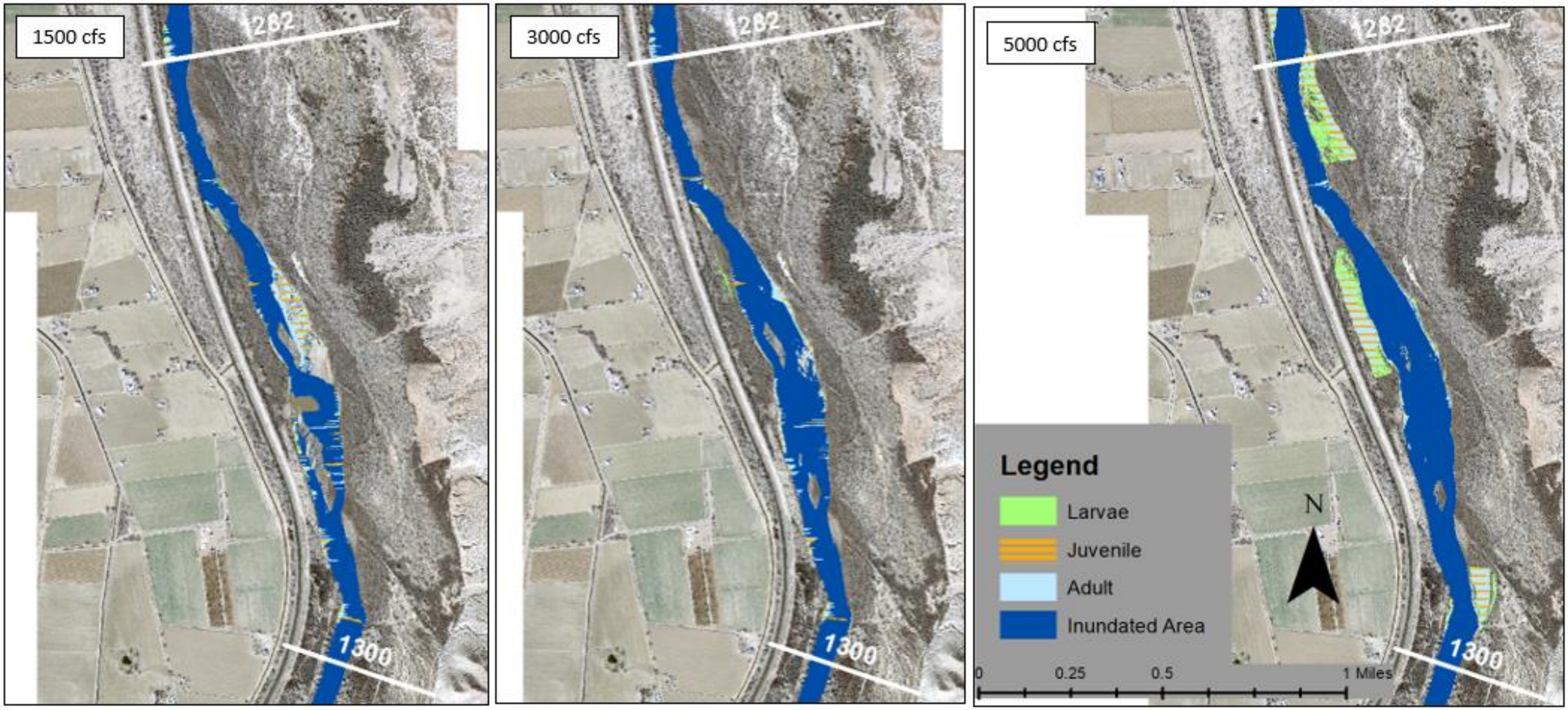

Figure 57 SA3(b) maps showing larvae, juvenile, and adult habitat throughout the subreach. Flow direction is from top to bottom

4.7 Width Slices Habitat Results

Figure 58 shows the habitat curves for larvae, juvenile, and adult for the entire San Acacia reach. Figure 59 through Figure 62 shows the habitat curves by subreach (SA1-SA4). Additional habitat curve figures can be found in Appendix C. For the overall reach, larvae have the least amount of habitat availability, while juveniles and adults have the most and are relatively similar in magnitude. For larvae, the peak habitat availability occurred in 1972 around 1.25 million ft^2/mi at a discharge of 4,500 cfs. Habitat availability greatly decreased in subsequent years (1992, 2002, and 2012) with the peak occurring at a much higher discharge of 10,000 cfs. In 2012, habitat availability was around 0.1 million ft^2/mi at 10,000 cfs. For juveniles and adults, peak habitat availability occurred in 1962 and 1972 around 4 million ft^2/mi at a discharge of 8,000 cfs. In subsequent years, habitat availability greatly declined with the maximum occurring at a discharge of 10,000 cfs. In 2012, habitat availability was around 1 million ft^2/mi at 10,000 cfs.

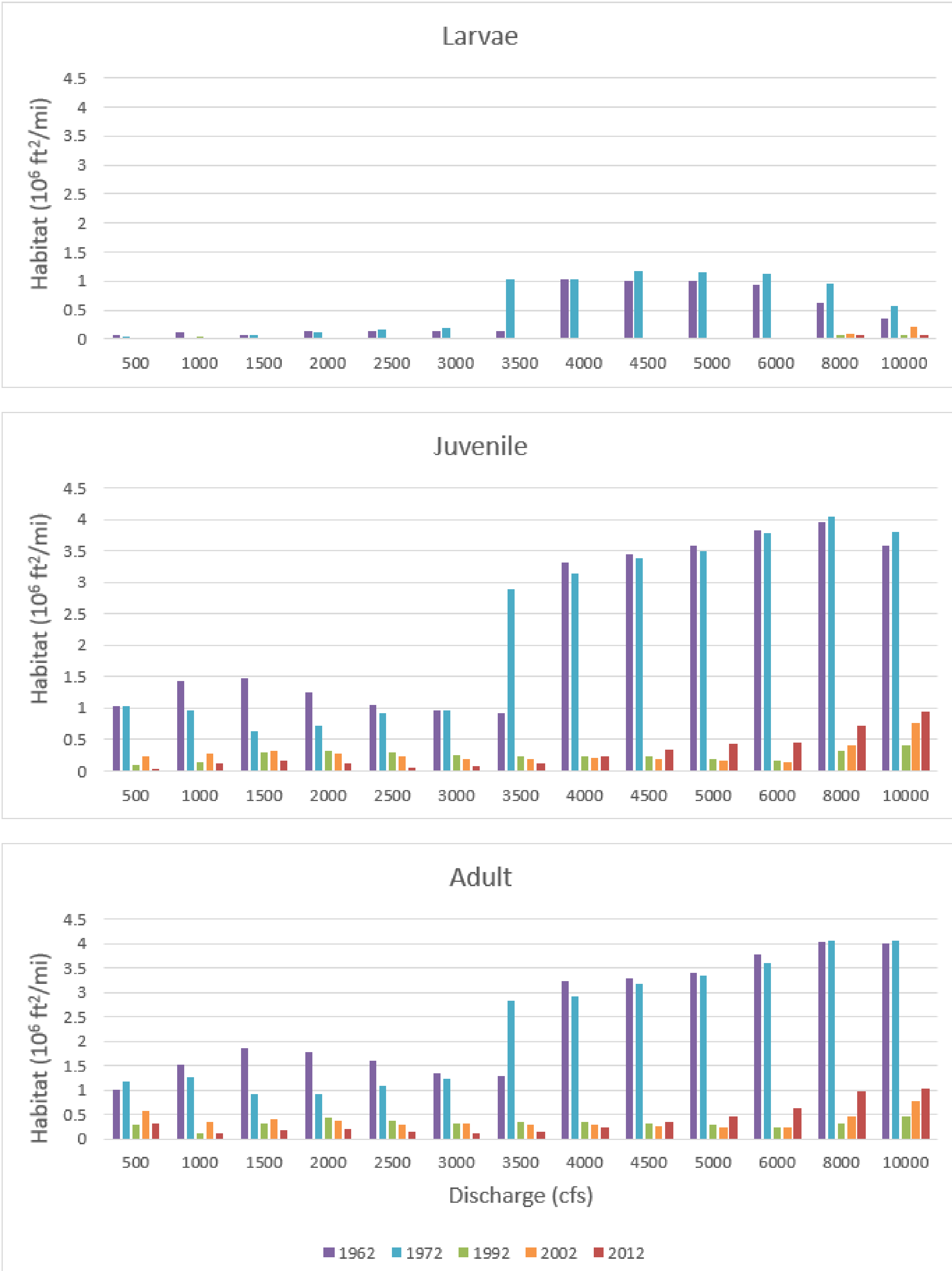

Figure 58 Larval, juvenile, and adult habitat curves for the entire San Acacia reach

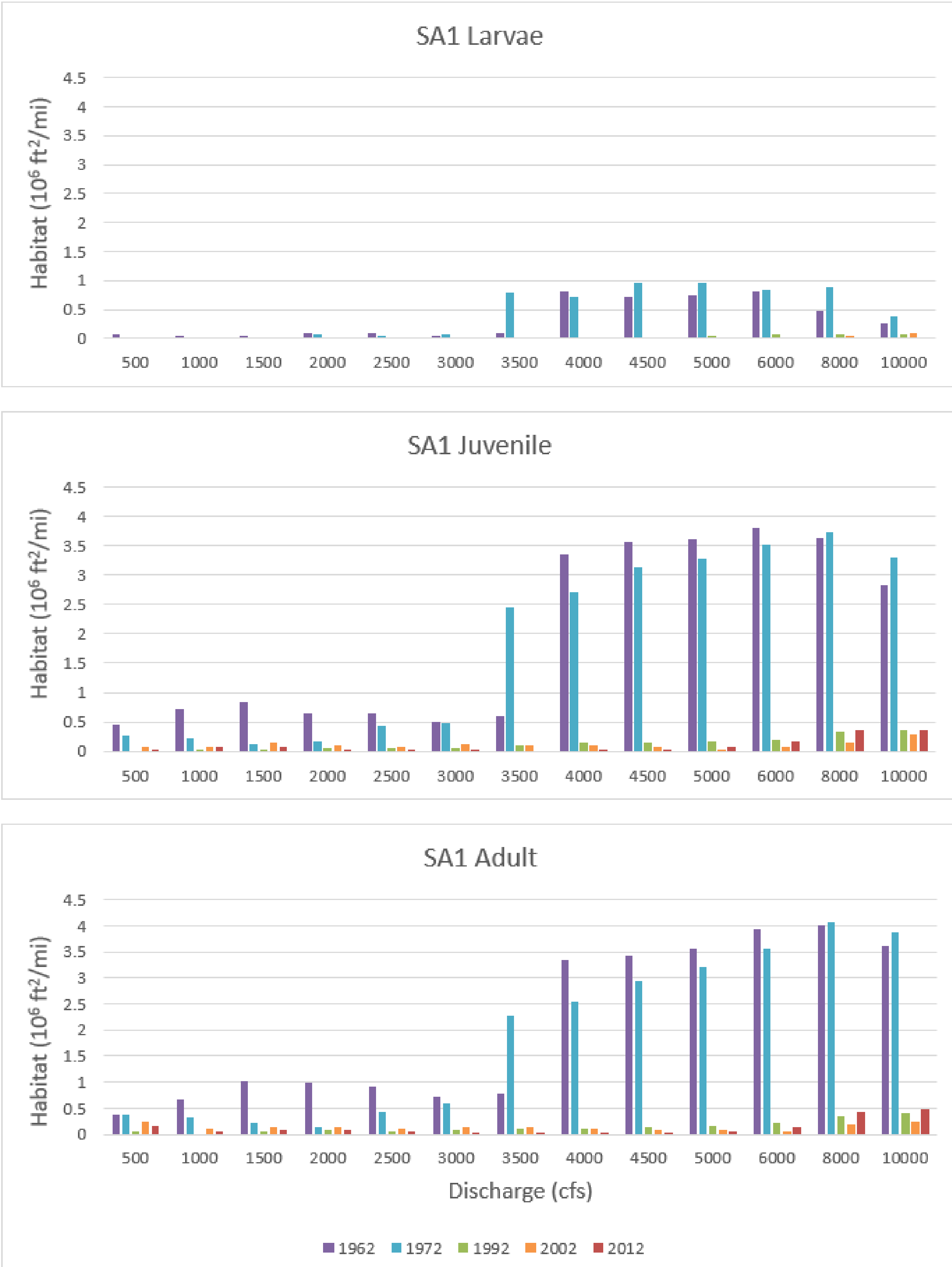

Figure 59 Larval, juvenile, and adult habitat curves for SA1

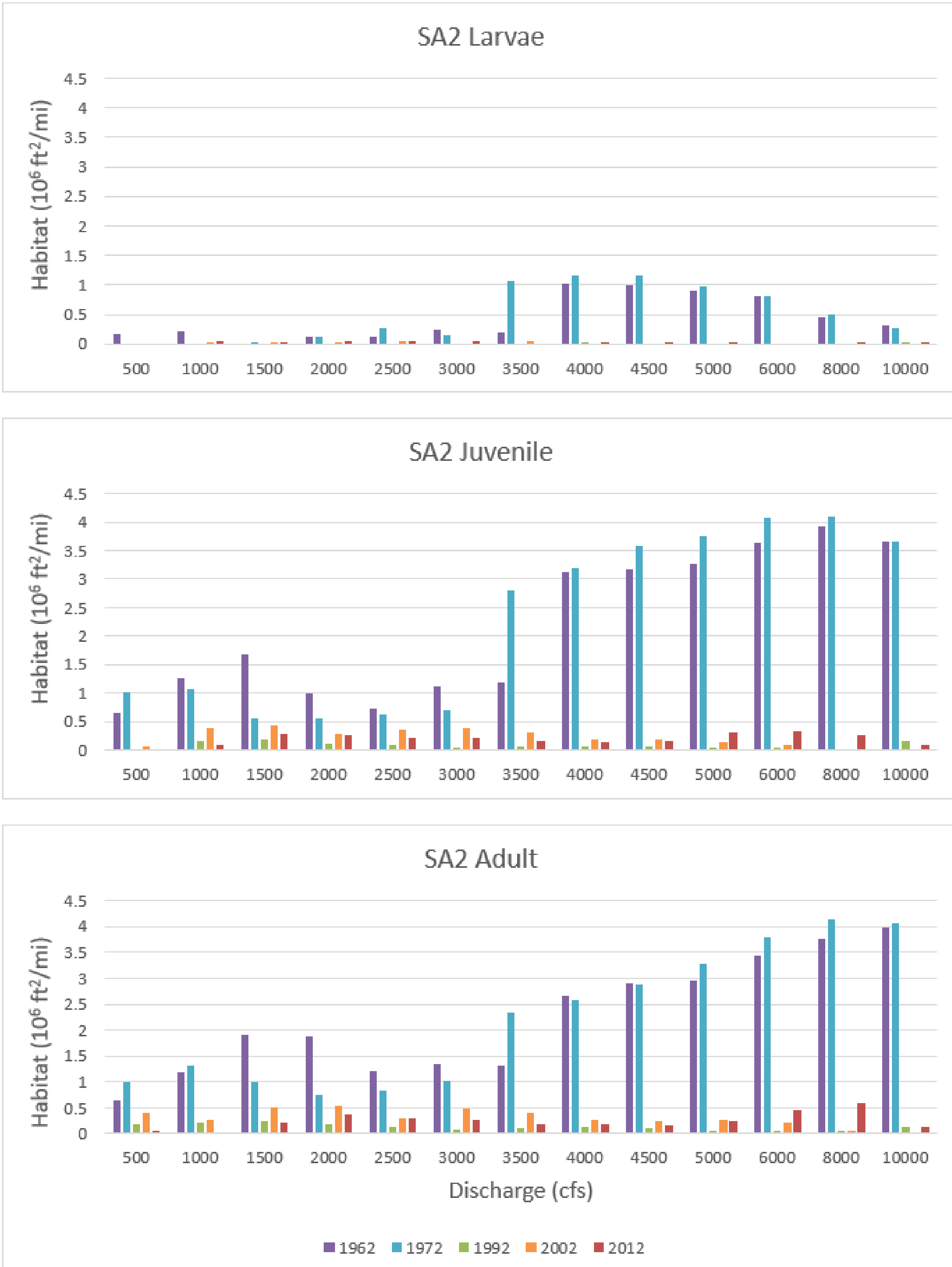

Figure 60 Larval, juvenile, and adult habitat curves for SA2

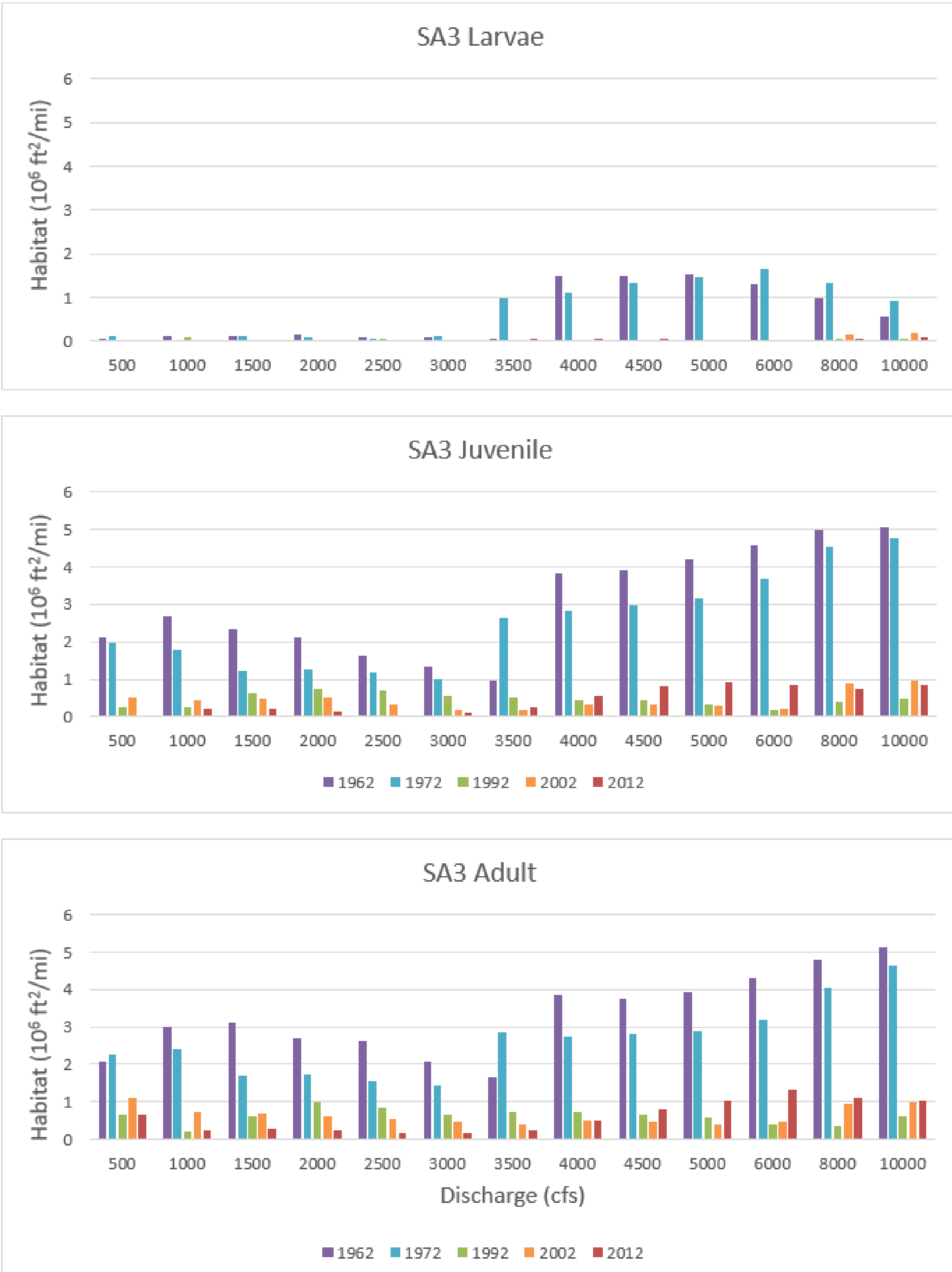

Figure 61 Larval, juvenile, and adult habitat curves for SA3

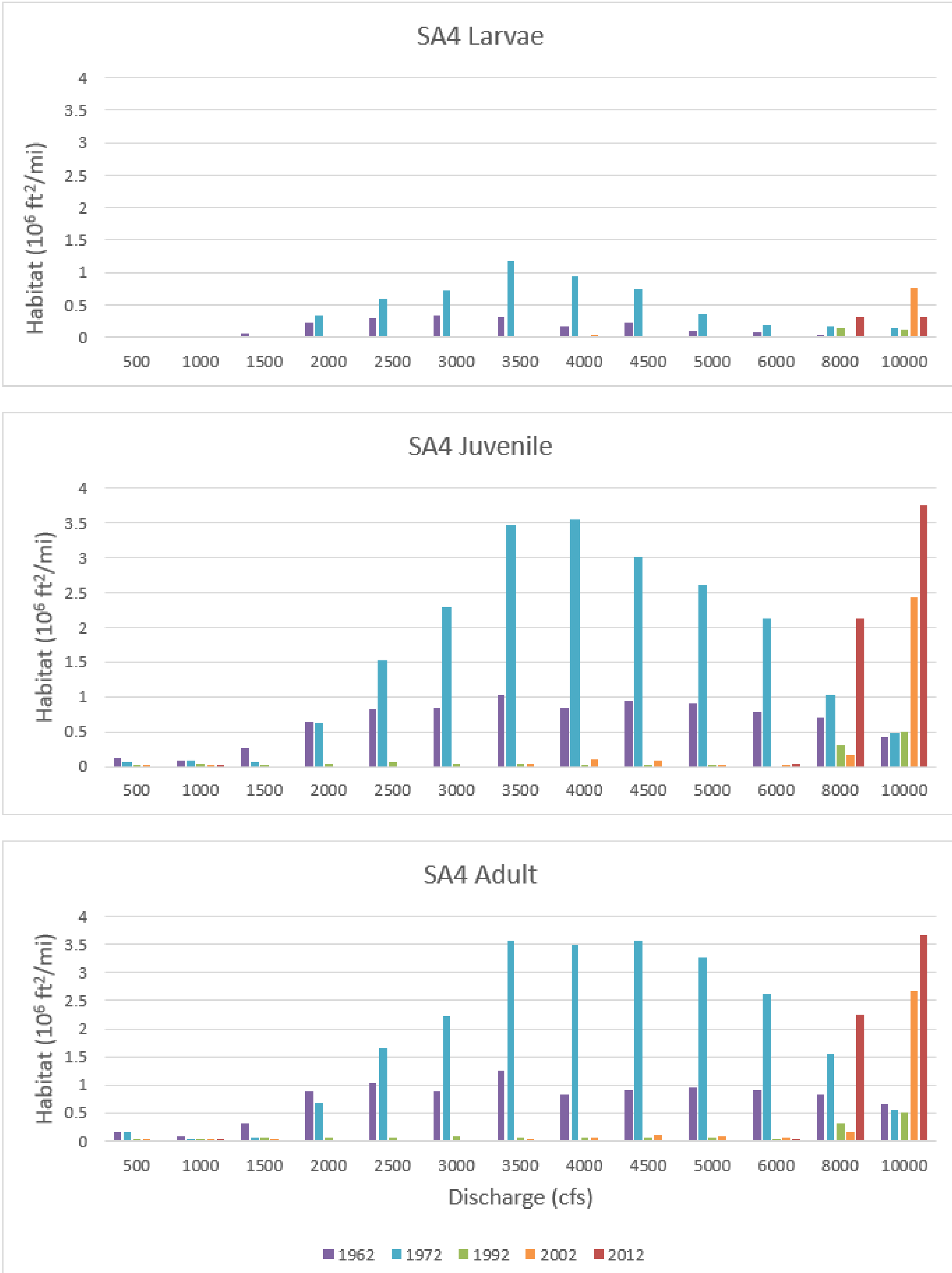

Figure 62 Larval, juvenile, and adult habitat curves for SA4

SA3 shows the most habitat availability for all three life stages, while SA4 shows the least amount of habitat availability from 1962 to 2012. This indicates that there are distinct subreach level differences in suitability for RGSM. There are potential links to the geomorphology of the subreach. Note that subreach SA3, the widest subreach historically and currently, experienced the least amount of degradation in the time period analyzed (see sections 3.2 and 3.3). SA3 can be considered the major contributor to overall habitat trends in the San Acacia reach.

While habitat availability in SA1 to SA3 for 2012 is typically low for more recent years (2002 and 2012), SA4 sees a spike in habitat availability in recent years at discharges of 8,000 and 10,000 cfs. It is important to note that while this spike is seen in SA4, this occurs at discharges that rarely occur in the reach. Subreach SA4 is very incised and did not experience any overbanking up to 10,000 cfs in the year 2012. However, because this is a short subreach with only 13 cross sections out of 107 for the reach, it did not have a large impact on determining the reaches average bankfull discharge of 7,000 cfs. This resulted in the placement of water in the floodplains in SA4 that would not have actually occurred, leading to an exaggeration of habitat. Future reports may investigate a sensitivity analysis of bankfull discharge on a subreach scale.

The shape of the habitat curves (which are enlarged in Appendix C) vary from year to year, however trends can be seen across all subreaches. This indicates that changing channel morphology has an impact on habitat availability. If results were similar from year to year, despite the changes seen in the San Acacia reach during that time, that would indicate that habitat availability is not dependent on river morphology. It is particularly indicative that the curves were not just changing magnitudes or shifting peaks but changing the shape of the curve itself. For SA1, SA2 and SA4, earlier years (1962 and 1972) tend to have a rounded shape, where habitat availability tends to rapidly increase at lower discharges and then round down at higher discharges. In SA1, SA3, and SA4, more recent years (1992, 2002, and 2012) tend to show low, constant habitat availability at lower discharges with rapid increases in habitat availability at discharges higher than 4,000 cfs. Additional work looking at the sensitivity of the width slices method and the effects of levee placement is shown in the Appendix. Please refer to Appendix D and Appendix E for more detail. The RGSM habitat was also displayed as stacked bar charts to display the spatial variation of habitat, which will be discussed in the future process linkage report. These charts were included at the end of this report in Appendix G.

4.8 Time Integrated Habitat Metrics Results

Figure 63 shows the results from the TIHMs for the San Acacia reach for each of the RGSM's life stages over their respective sampling periods. Adults show relatively constant cumulative habitat from 1992 to 2019, ranging from 35 to 95 million ft^2/mi. Juvenile and larvae tend to be more sensitive to the method, showing more fluctuations in cumulative habitat from 1992 to 2019. Juvenile cumulative habitat ranges from approximately 0.032 to 21 million ft^2/mi, while larvae ranges from 4.6×10^{-8} to 1.4 million ft^2/mi.

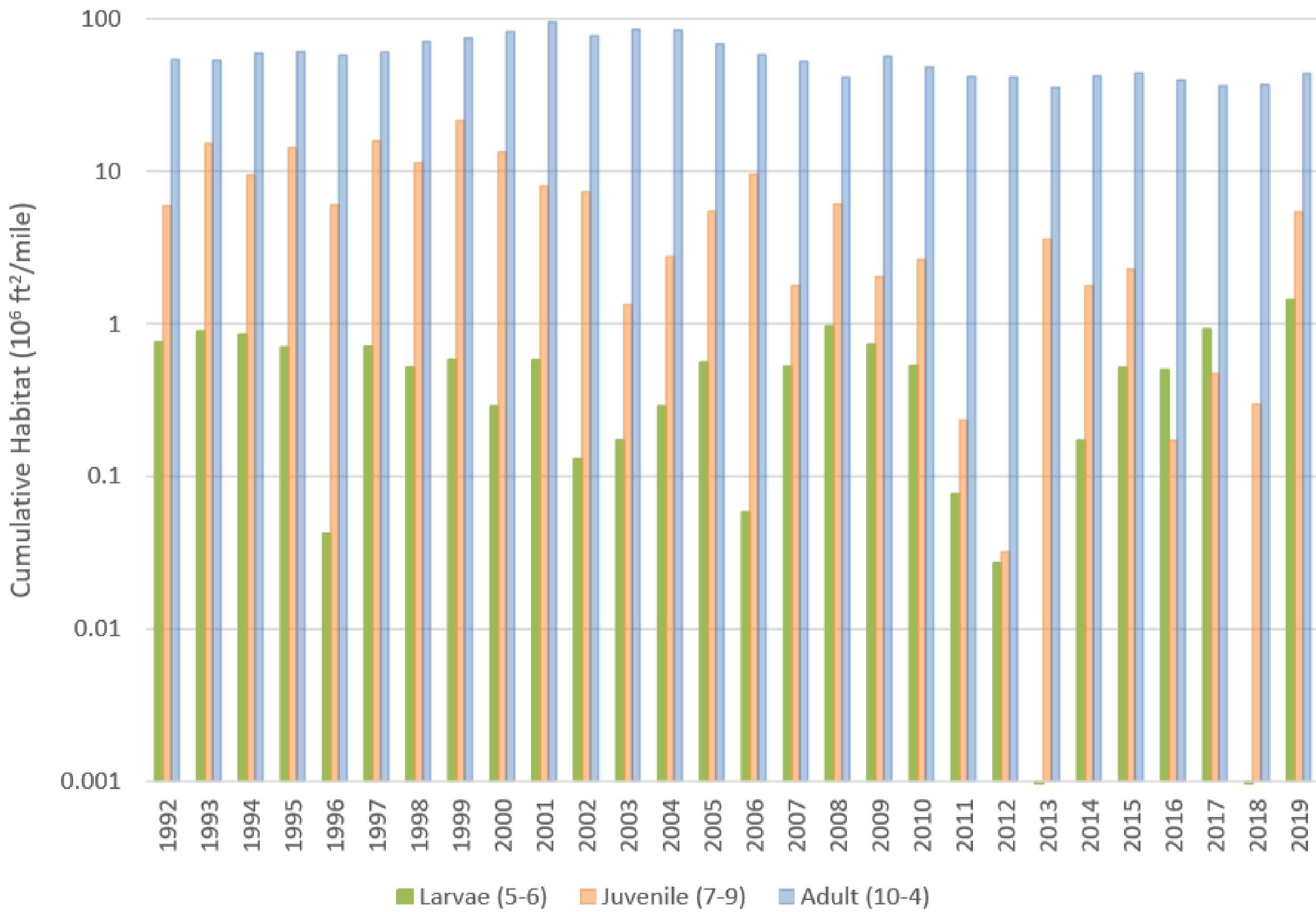

Figure 63 Cumulative habitat from the TIHMs for larvae, juvenile, and adult over representative sampling months

5 Conclusions

The San Acacia reach was analyzed for hydrologic, hydraulic and geomorphic trends between 1918 and 2018. This reach covers around 11.6 miles from the San Acacia Diversion Dam to the Escondida Bridge.

HEC-RAS and GIS were used to find geomorphic and river characteristics such as sinuosity, width, bed elevation and other hydraulic parameters. These analyses were broken down by each of the four subreaches, allowing trends to be seen on a smaller scale.

Major findings include:

- The annual water volume has been reduced since 1995. Peak discharges are lower and of shorter duration.
- The annual suspended sediment discharge in the Rio Grande has decreased since 1995.
- Significant narrowing has occurred in all subreaches, and some are approaching the theoretical equilibrium width of approximately 200 feet predicted by the JW equations.
- Sinuosity has decreased overall since 1918 but has been increasing since 1985 on subreaches SA1-SA3. Subreach SA1 has the highest sinuosity of 1.3, with each subreach becoming less sinuous. SA4 has a sinuosity of nearly 1.
- Degradation has occurred in all subreaches. Subreach SA1 had the most degradation over the period from 1962 to 2012, almost 10.5 ft. SA2, SA3 and SA4 degraded 8.4 ft, 5.0 ft and 5.2 ft, respectively.
- Vegetation encroachment and stabilization of low elevation bars and islands lead to overbanking at lower discharges.
- Most subreaches are currently in stage M4 of the geomorphic conceptual model, representing more incision and less connection to the floodplain.
- Based on the width slice method and RAS-Mapper habitat maps, subreach SA3 had the most habitat available every year and is the greatest contributor to habitat trends throughout the San Acacia reach.
- Differences are seen in the shape of the habitat-discharge curves from year to year, indicating that changing channel morphology has a significant impact on the amount of habitat available.
- Larvae and juveniles appear to be most sensitive to the TIHMs method, indicating that changes in discharge have the greatest impact on the larval and juvenile habitat.

6 Works Cited

Bovee, K.D., Waddle, T.J., and Spears, J.M. (2008). “Streamflow and endangered species habitat in the lower Isleta reach of the middle Rio Grande.” *U.S. Geological Survey Open-File Report 2008-1323*.

LaForge, K., Yang, C.Y., Julien, P.Y., and Doidge, S. (2019). Draft Report. *Rio Puerco Reach: Hydraulic Modeling and Silvery Minnow Habitat Analysis*, Colorado State University, Fort Collins, CO.

Klein, M., Herrington, C., AuBuchon, J., and Lampert, T. (2018a). *Isleta to San Acacia Geomorphic Analysis*, U.S. Bureau of Reclamation, Reclamation River Analysis Group, Albuquerque, New Mexico.

Klein, M., Herrington, C., AuBuchon, J., and Lampert, T. (2018b). *Isleta to San Acacia Hydraulic Modeling Report*, U.S. Bureau of Reclamation, Reclamation River Analysis Group, Albuquerque, New Mexico.

Julien, P.Y. (2002). *River Mechanics,* Cambridge University Press, New York

Julien, P. Y., and Wargadalam, J. (1995). “Alluvial channel geometry: theory and applications.” *Journal of Hydraulic Engineering*, American Society of Civil Engineers, 121(4), 312–325.

Makar, P., Massong, T., Bauer, T., Tashjian, P., and Oliver, K J. (2006). “Channel Width and Flow Regime Changes along the Middle Rio Grande NM.” Joint 8th Federal Interagency Sedimentation Conference and 3rd Federal Interagency Hydrologic Modeling Conference, Reno, Nevada.

Massong, T., Paula, M., and Bauer, T. (2010). “Planform Evolution Model for the Middle Rio Grande, NM.” *2nd Joint Federal Interagency Conference, Las Vegas, NV, June 27 - July 1, 2010*.

MEI. (2002). *Geomorphic and Sedimentologic Investigations of the Middle Rio Grande between Cochiti Dam and Elephant Butte Reservoir*, Mussetter Engineering, Inc., Fort Collins, CO, 220 p.

Mortensen, J.G., Dudley, R.K., Platania, S.P., and Turner, T.F. (2019). Draft report. *Rio Grande Silvery Minnow Habitat Synthesis,* University of New Mexico with American Southwest Ichthyological Researchers, Albuquerque, NM.

Posner, A. J. (2017). Draft report. *Channel conditions and dynamics of the Middle Rio Grande River,* U.S. Bureau of Reclamation, Albuquerque, New Mexico.

Scurlock, D. (1998). “From the Rio to the Sierra: an environmental history of the Middle Rio Grande Basin.” *General Technical Report RMRS-GTR-5. Fort Collins, CO: US Department of Agriculture, Forest Service, Rocky Mountain Research Station, 440 p.*

Shah-Fairbank, S. C., Julien, P. Y., and Baird, D. C. (2011). “Total sediment load from SEMEP using depth-integrated concentration measurements.” Journal of Hydraulic Engineering, 137(12), 1606–1614.

U.S. Bureau of Reclamation. (2012). “Middle Rio Grande River Maintenance Program - Comprehensive Plan and Guide.” Albuquerque Area Office, Albuquerque, New Mexico, 202p.

U.S. Fish and Wildlife Service. (2007). “Rio Grande Silvery Minnow (Hybognathus amarus).” Draft Revised Recovery Plan, Albuquerque, New Mexico, 174 p.

Varyu, D. (2013). *Aggradation / Degradation Volume Calculations: 2002-2012*. U.S. Department of the Interior, Bureau of Reclamation, Technical Services Center, Sedimentation and River Hydraulics Group. Denver, CO.

Varyu, D. (2016). *SRH-1D Numerical Model for the Middle Rio Grande: Isleta Diversion Dam to San Acacia Diversion Dam*. U.S. Department of the Interior, Bureau of Reclamation, Technical Services Center, Sedimentation and River Hydraulics Group. Denver, CO.

Yang, C.Y. (2019). *The Sediment Yield of South Korean Rivers*, Colorado State University, Fort Collins, CO.

Yang, C.Y. and Julien, P.Y. (2019). “The ratio of measured to total sediment discharge.” *International Journal of Sediment Research*, 34(3), pp.262-269.

Yang, C.Y., LaForge, K., Julien, P.Y., and Doidge, S. (2019). Draft Report. *Isleta Reach: Hydraulic Modeling and Silvery Minnow Habitat Analysis*, Colorado State University, Fort Collins, CO.

Appendix A

Subreach Delineation

The following figures were used to aid subreach delineation.

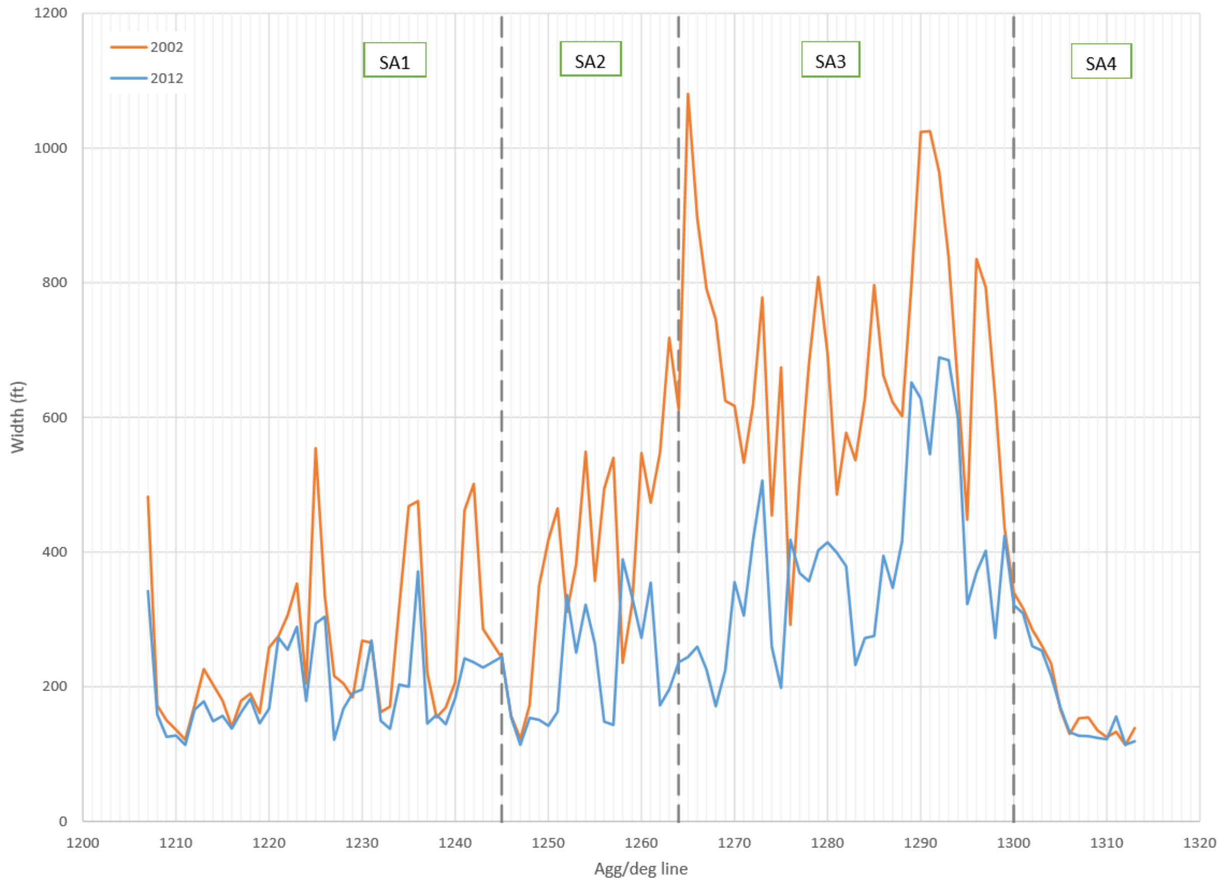

Figure A- 1 Subreach delineation width

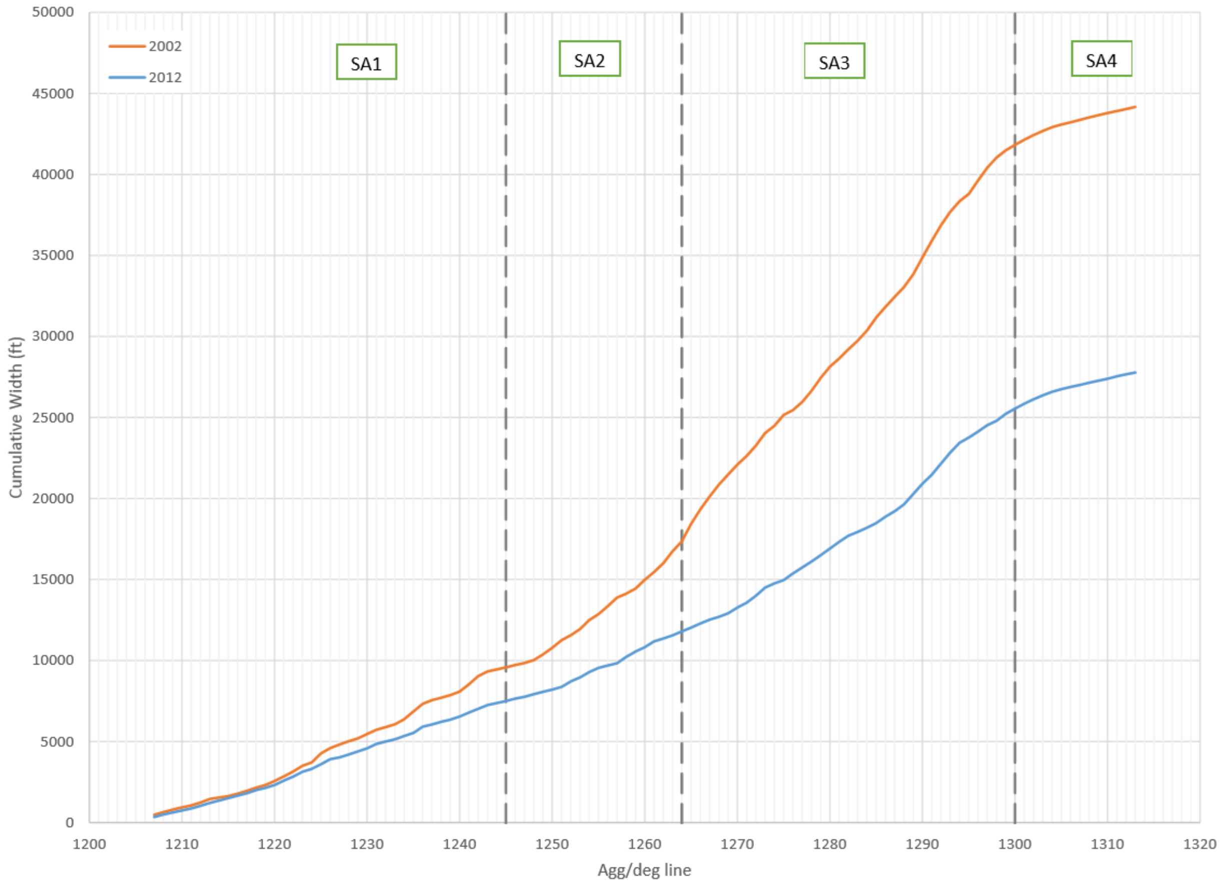

Figure A- 2 Subreach delineation cumulative width

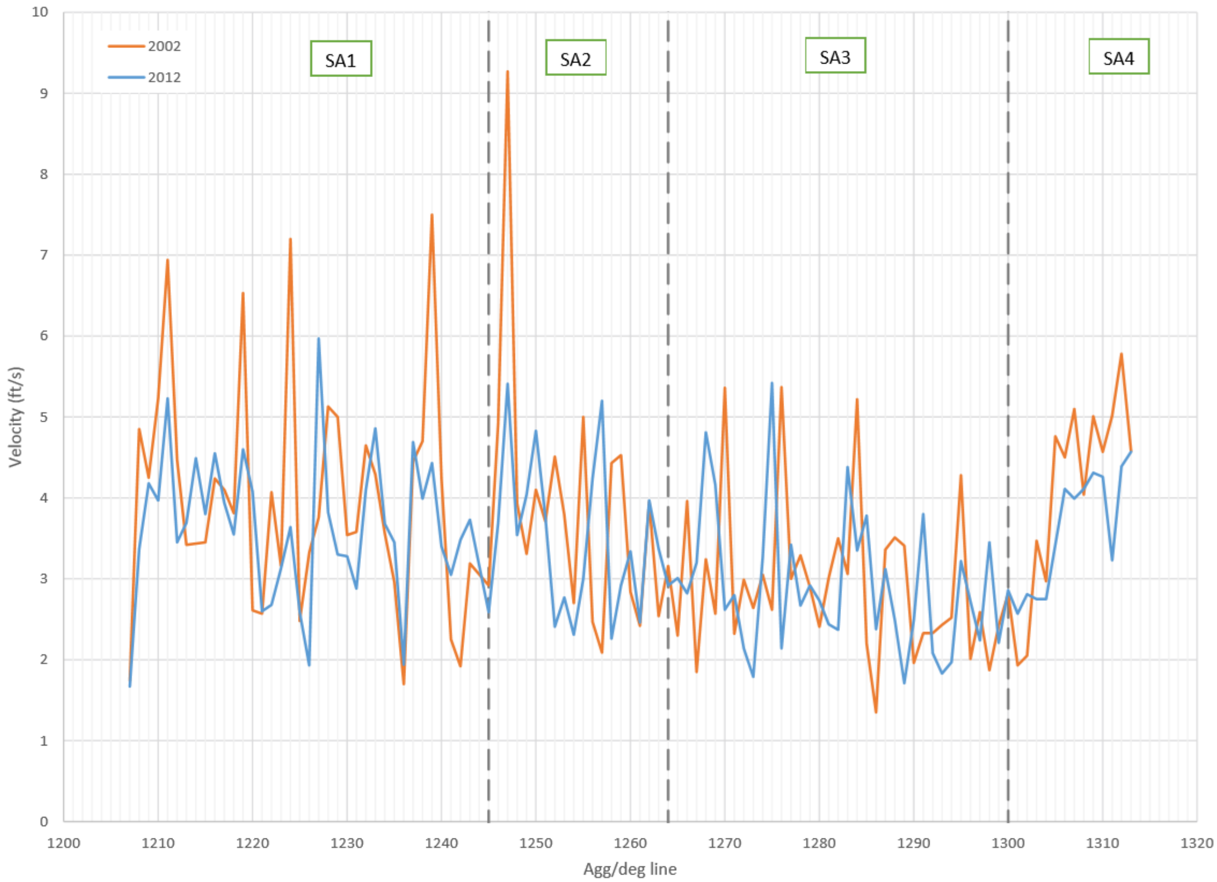

Figure A- 3 Subreach delineation velocity

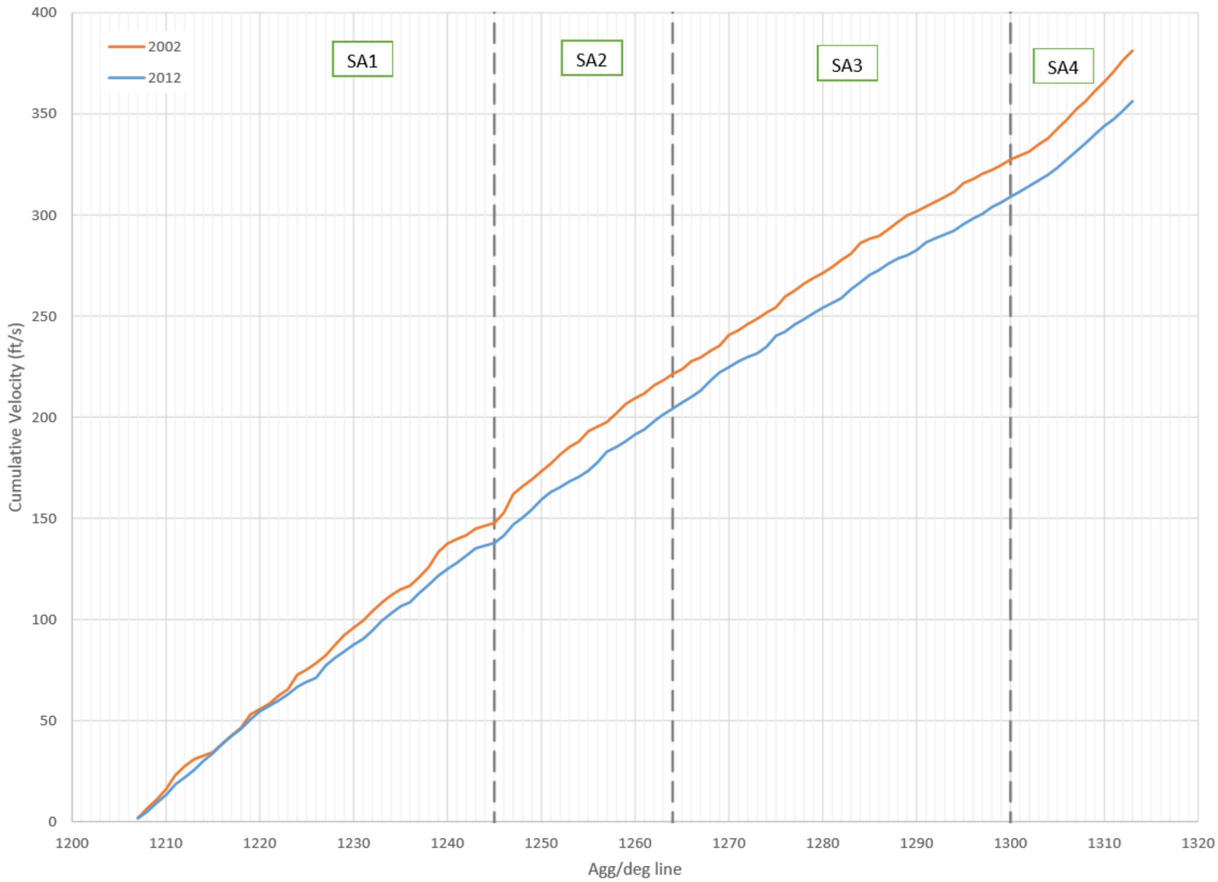

Figure A- 4 Subreach delineation cumulative velocity

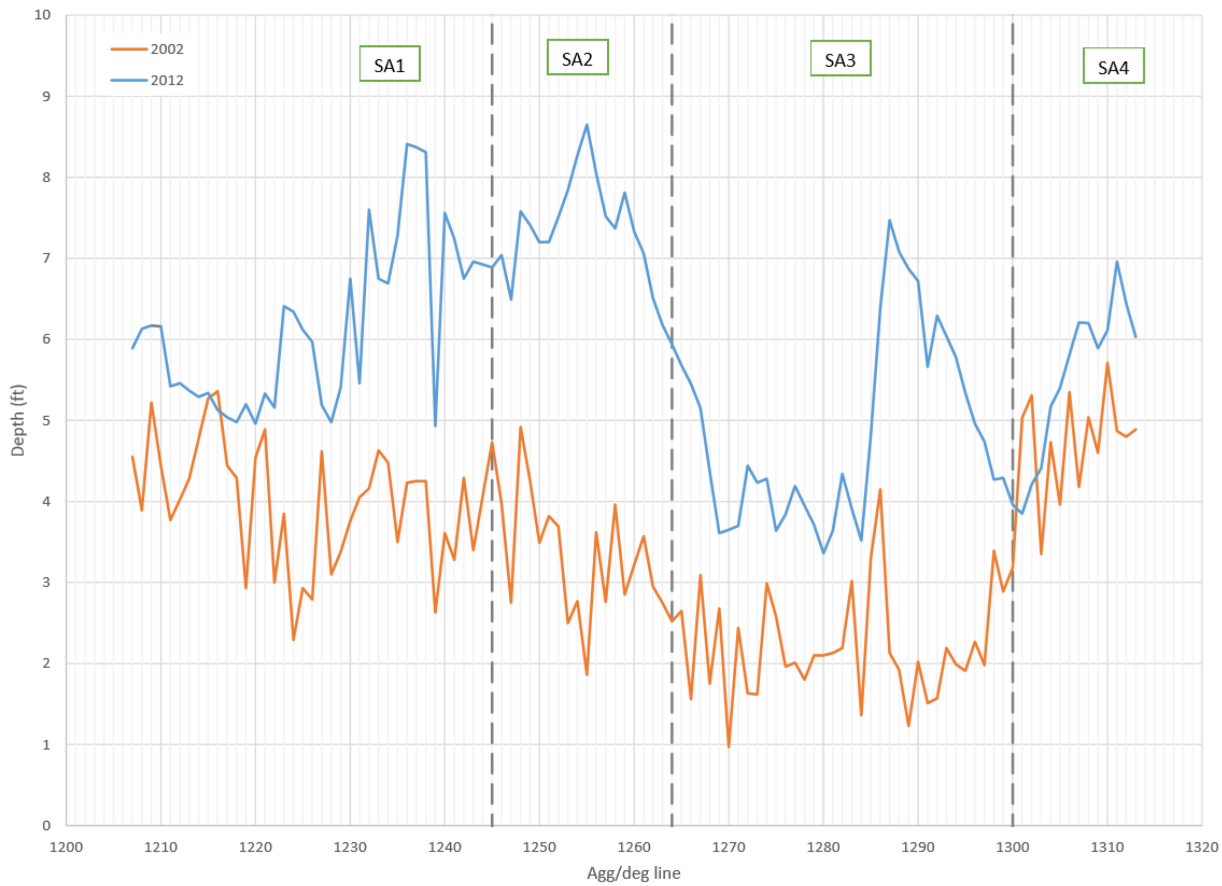

Figure A- 5 Subreach delineation depth

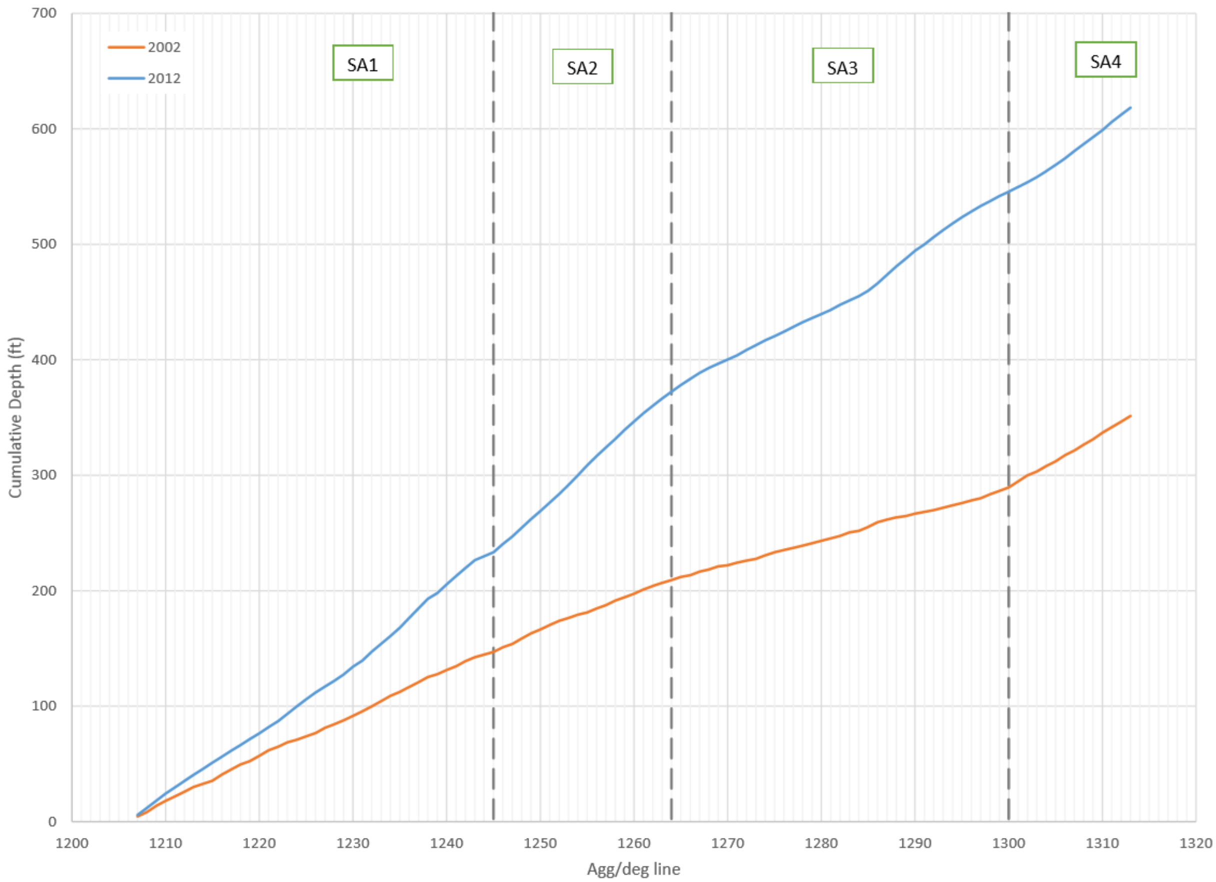

Figure A- 6 Subreach delineation cumulative depth

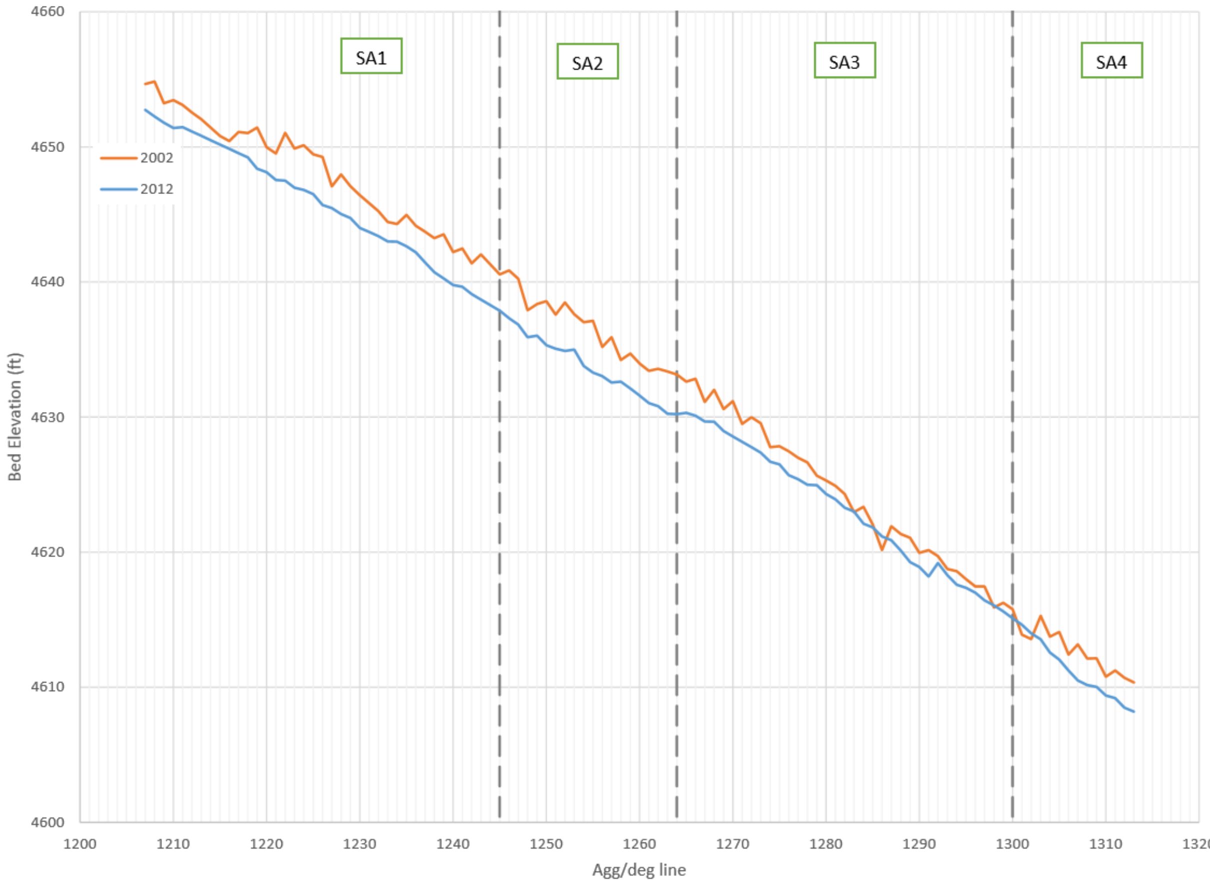

Figure A- 7 Subreach delineation bed elevation

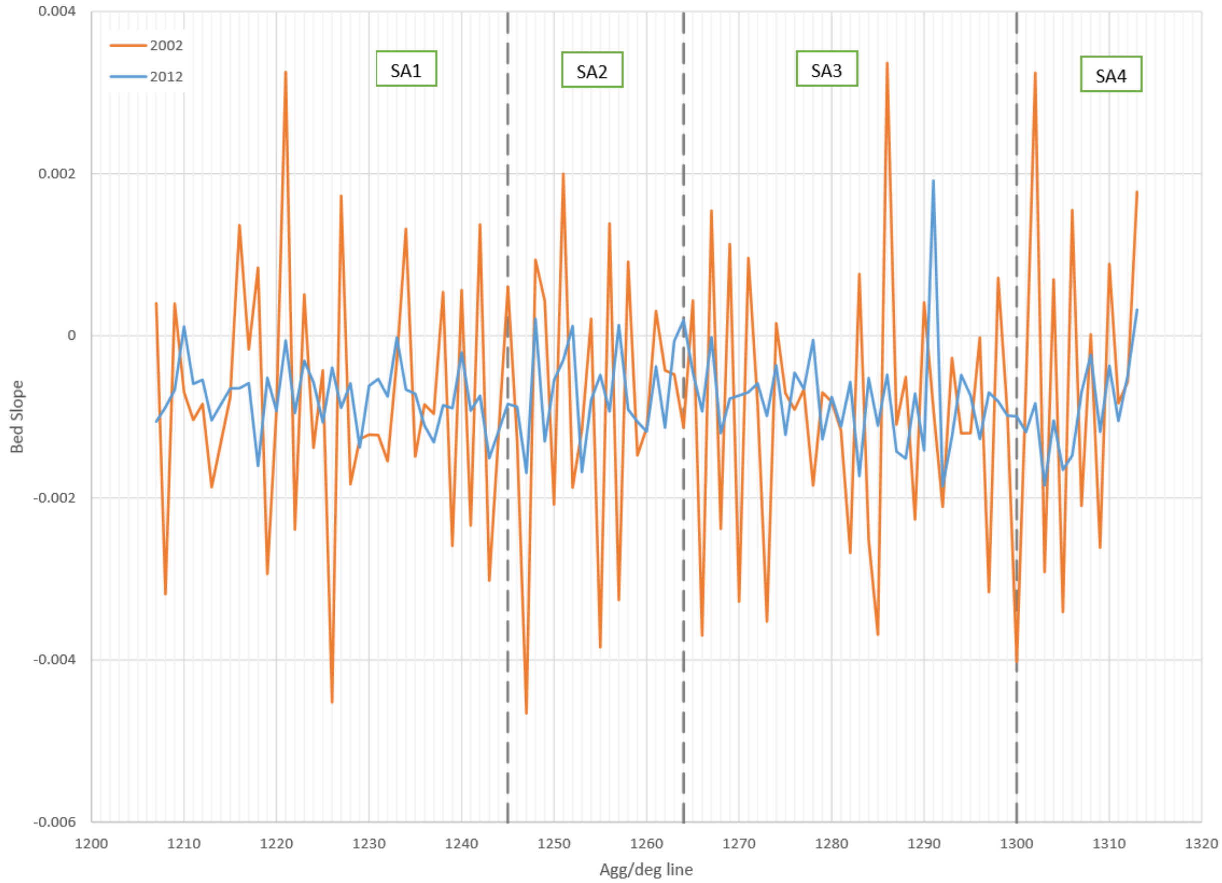

Figure A- 8 Subreach delineation slope

Appendix B

Total Sediment Load Using SEMEP Analysis

The Series Expansion of Einstein Procedure (SEMEP) was used in this study to estimate the total sediment load. The method was developed at CSU with the procedure detailed in Shah-Fairbank et al. (2011) as a function of shear velocity u_* and fall velocity ω. Fall velocity is based on D_{50} and $u_* = \sqrt{gRS}$ where g is gravity, R is the hydraulic radius, and S is the bed slope. It was recently tested by Yang (2019) with applications on 35 rivers in South Korea. In this report, SEMEP is applied at three stations on the Rio Grande, at San Acacia gage 08354900, as well as Albuquerque and Bernardo at gages 08330000 and 08332010. The number of field samples calculated by the SEMEP are respectively 306, 211, and 173 samples at gages 08330000, 08332010, and 08354900. For these stations, the values of u_*/ω range from 1.5 to 37,600. According to Shah-Fairbank et al. (2011), SEMEP performs accurately when $u_*/\omega > 5$, so good results are expected from this application.

It can be seen in

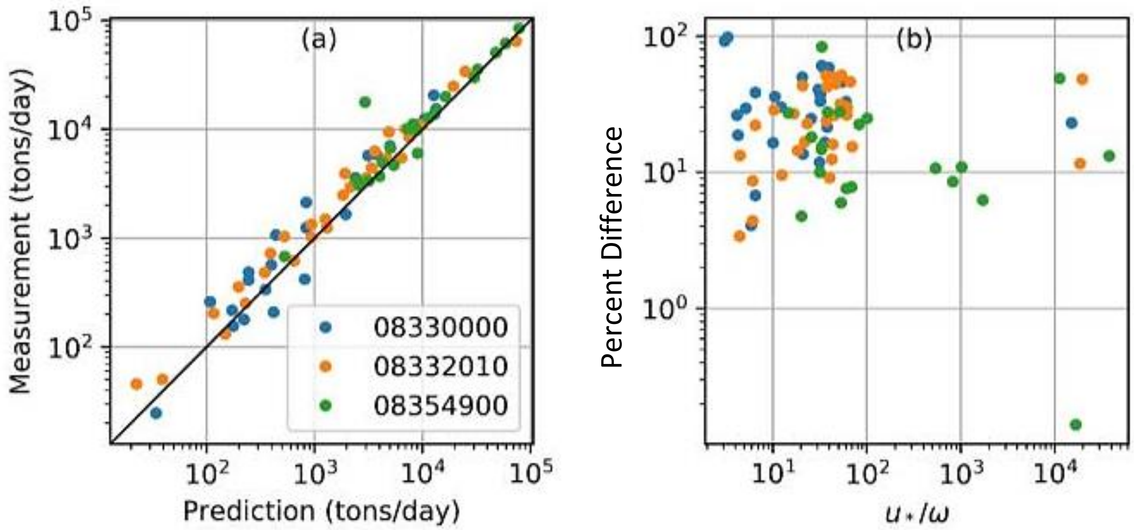

Figure B- 1 that the SEMEP predictions and total sediment load measurements fall close to the 45-degree line of perfect agreement.

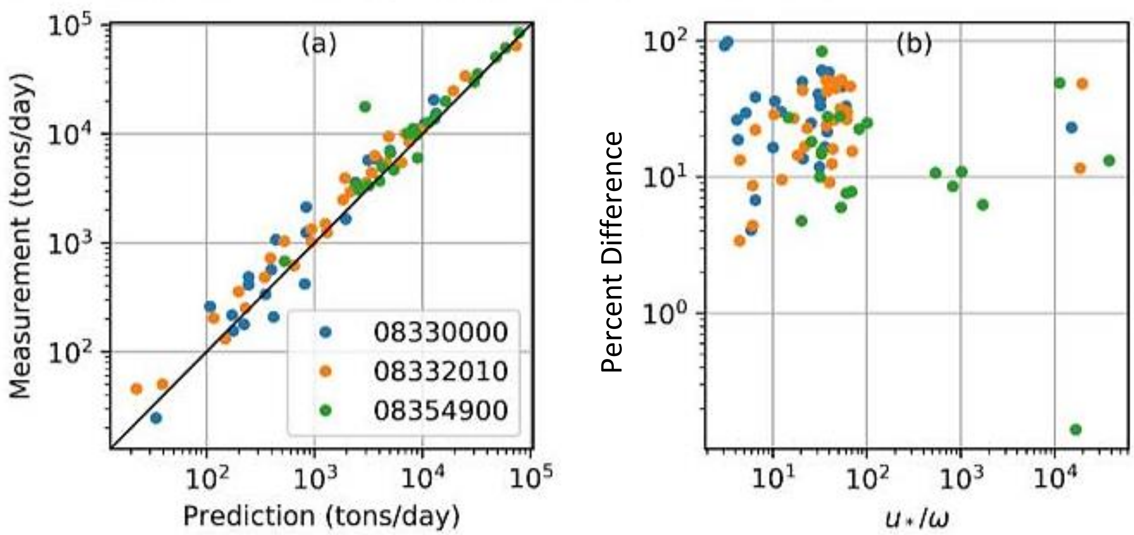

Figure B- 1 also shows the prediction errors between SEMEP calculations and measurements as a function of u_*/ω. The mean absolute percent difference is 27%. Figure B- 2 shows the sediment rating curves for total sediment discharges at gage 08354900.

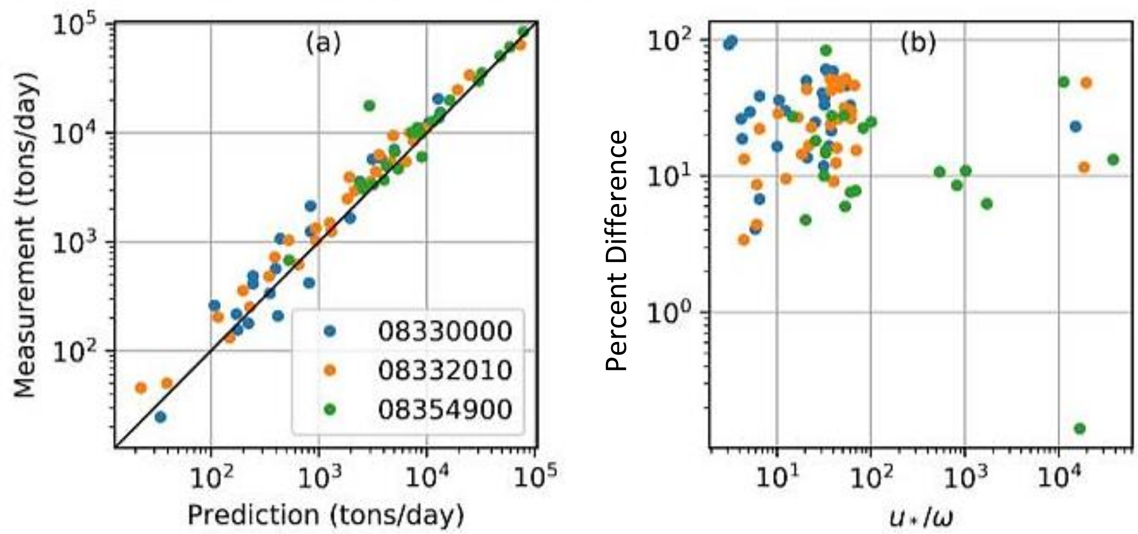

Figure B- 1 (a) Comparison between predicted and measured total sediment load, and (b) percent difference vs u_*/w

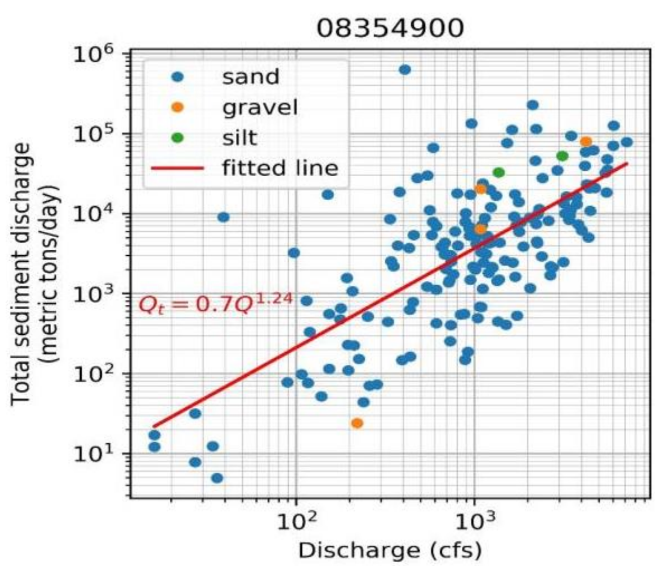

Figure B- 2 Total sediment rating curve at the San Acacia gage

The ratio of measured to total sediment discharge is a function of flow depth h, grain size d_s, and Rouse number Ro (Ro = $\omega/2.5u_*$) according to SEMEP (Shah-Fairbank et al. 2011; Yang and Julien 2019). In addition, the ratio of suspended to total sediment discharge is a function of the ratio h/d_s and Ro (Yang and Julien 2019). The calculated ratio Q_m/Q_t and the ratio Q_s/Q_t are plotted with the analytical solutions in Figure B- 3 for the San Acacia gaging stations, where Q_m is the measured sediment discharge, Q_t is the total sediment discharge, and Q_s is the suspended sediment discharge. As expected, when the value of Ro is low (Ro < 0.3), the ratio Q_s/Q_t is close to 100% during floods when h/d_s > 100.

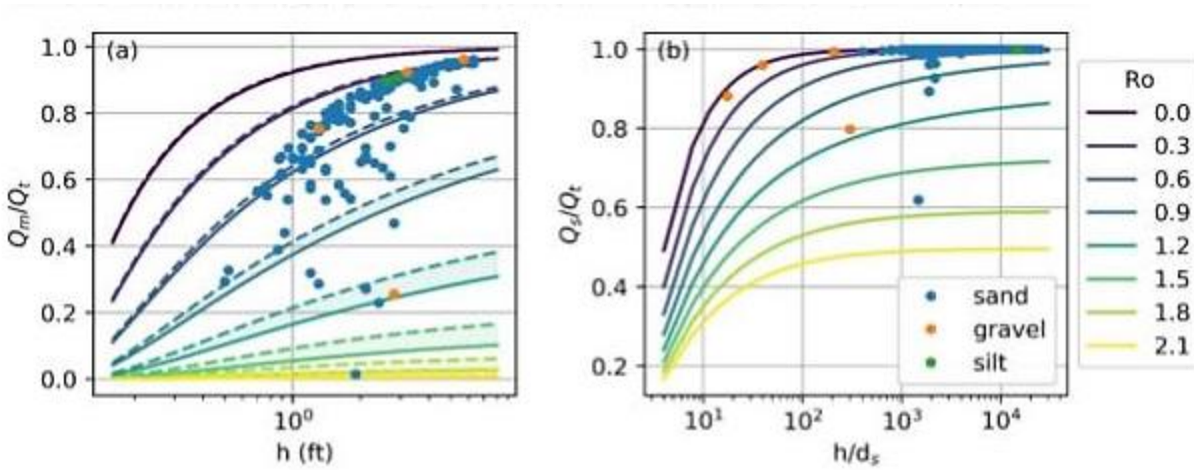

Figure B- 3 (a) the ratio of measured to total sediment discharge vs depth; and (b) the ratio of suspended to total sediment discharge vs h/d_s at the San Acacia gage

Appendix C

Additional Figures

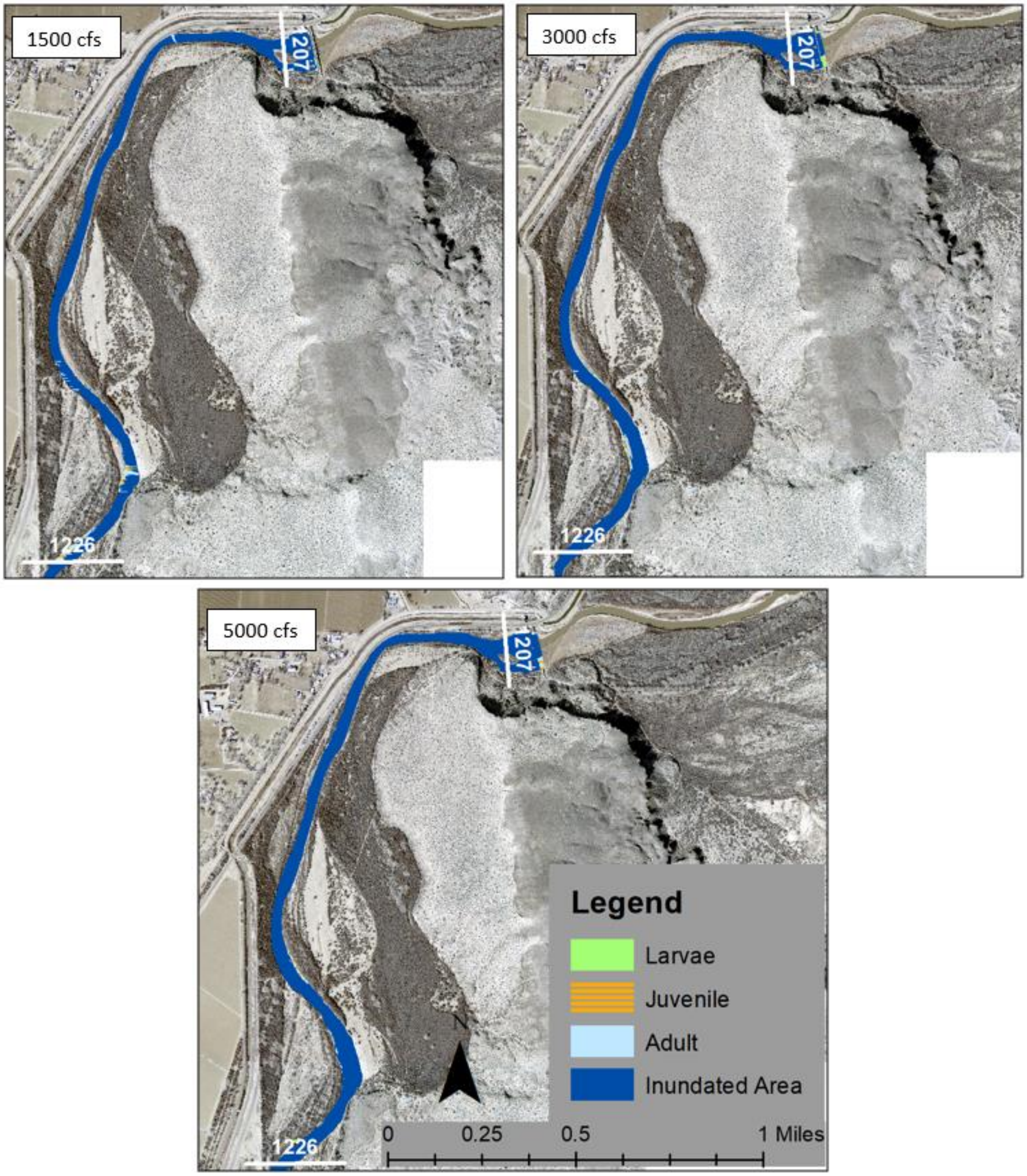

Figure C- 1 SA1(a) maps showing larvae, juvenile, and adult habitat. Inundated area refers to habitat that is unsuitable for all life stages. Flow direction is from top to bottom

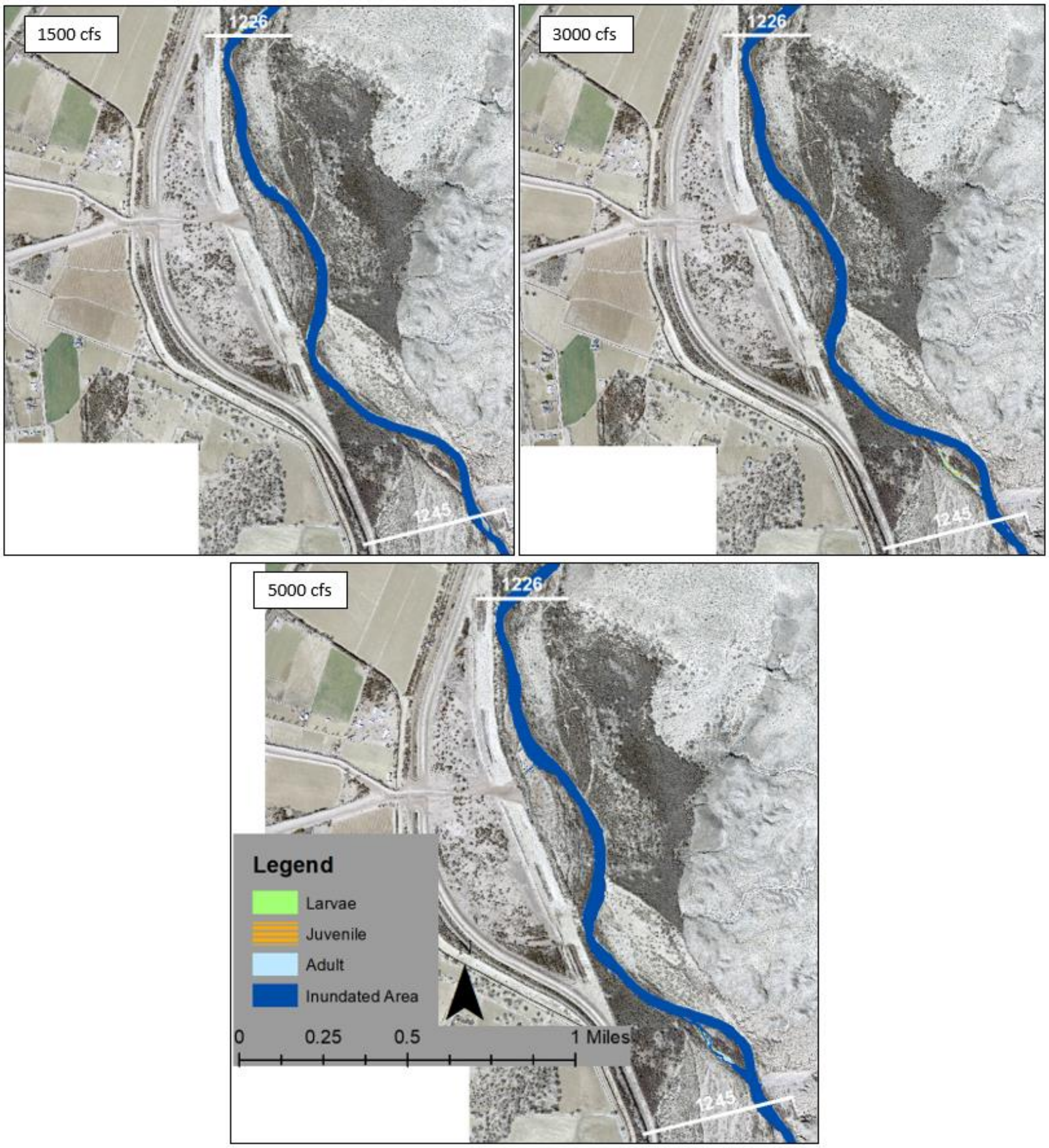

Figure C- 2 SA1(b) maps showing larvae, juvenile, and adult habitat. Inundated area refers to habitat that is unsuitable for all life stages. Flow direction is from top to bottom

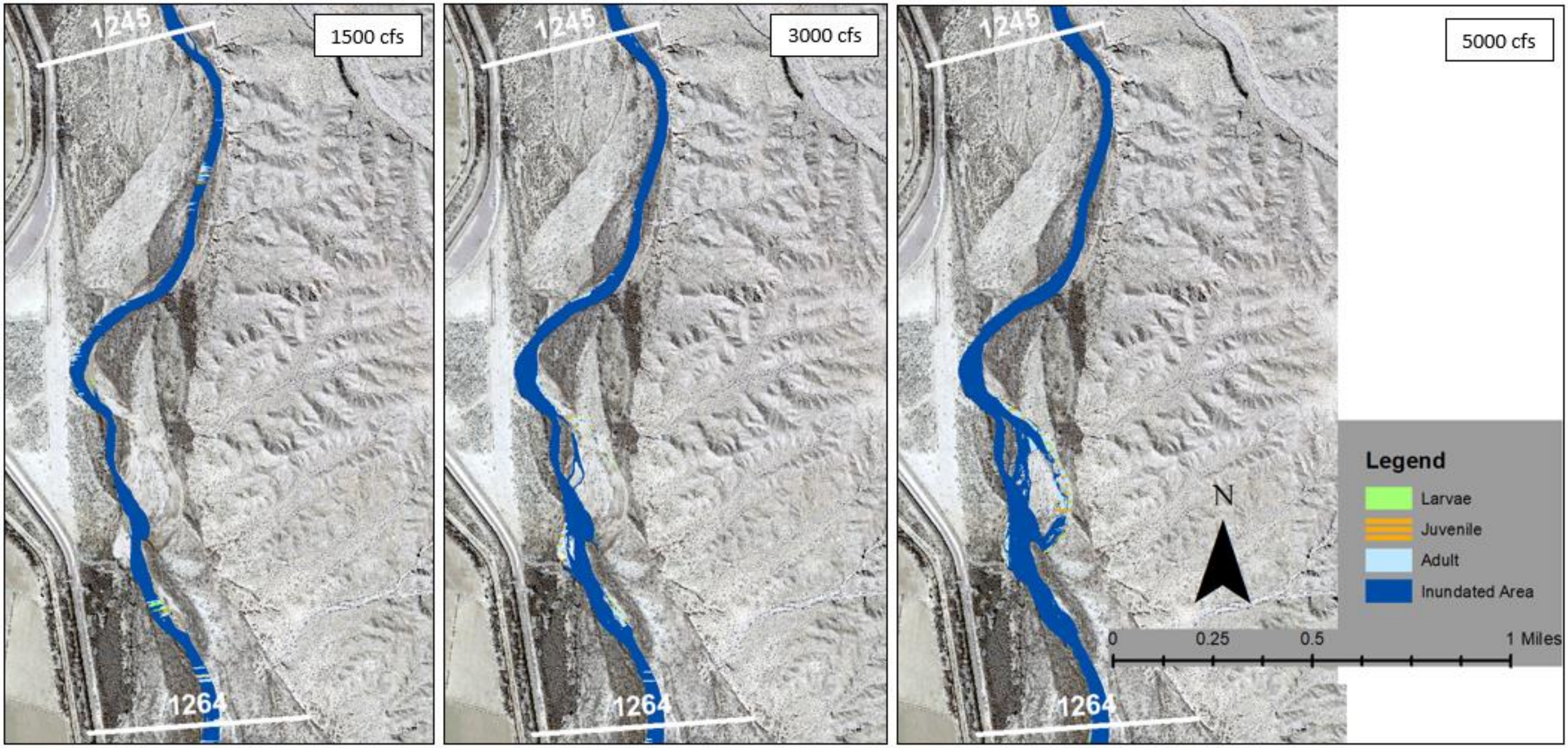

Figure C- 3 SA2 maps showing larvae, juvenile, and adult habitat. Inundated area refers to habitat that is unsuitable for all life stages. Flow direction is from top to bottom

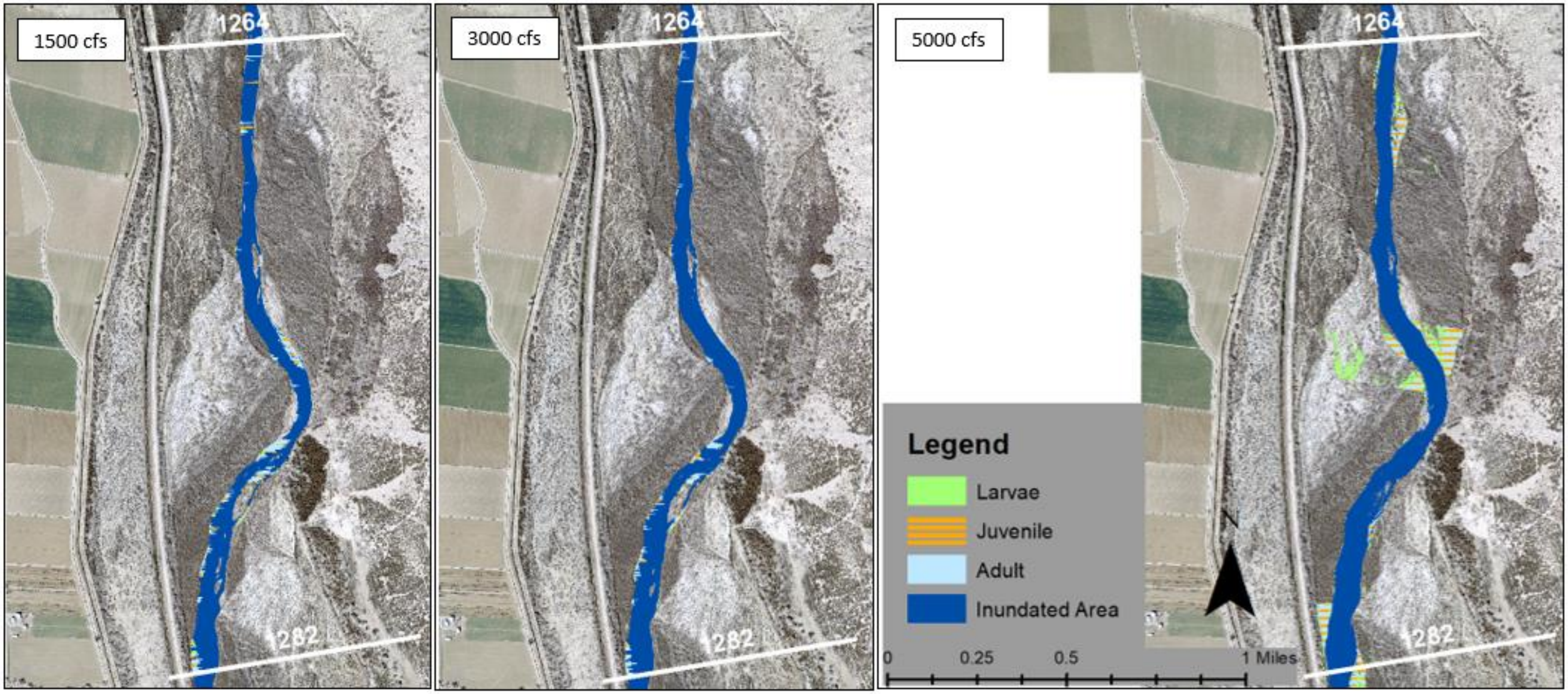

Figure C- 4 SA3(a) maps showing larvae, juvenile, and adult habitat. Inundated area refers to habitat that is unsuitable for all life stages. Flow direction is from top to bottom

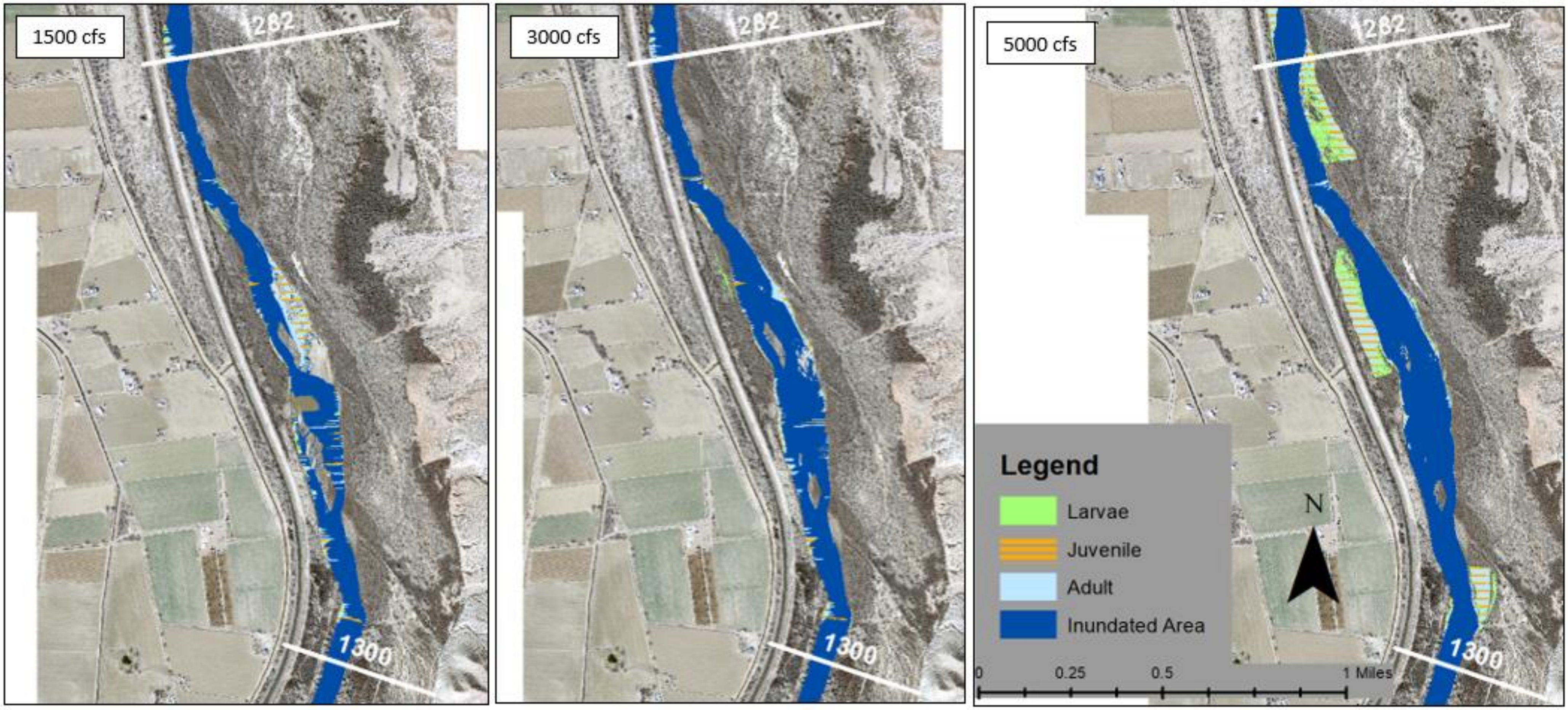

Figure C- 5 SA3(b) maps showing larvae, juvenile, and adult habitat. Inundated area refers to habitat that is unsuitable for all life stages. Flow direction is from top to bottom

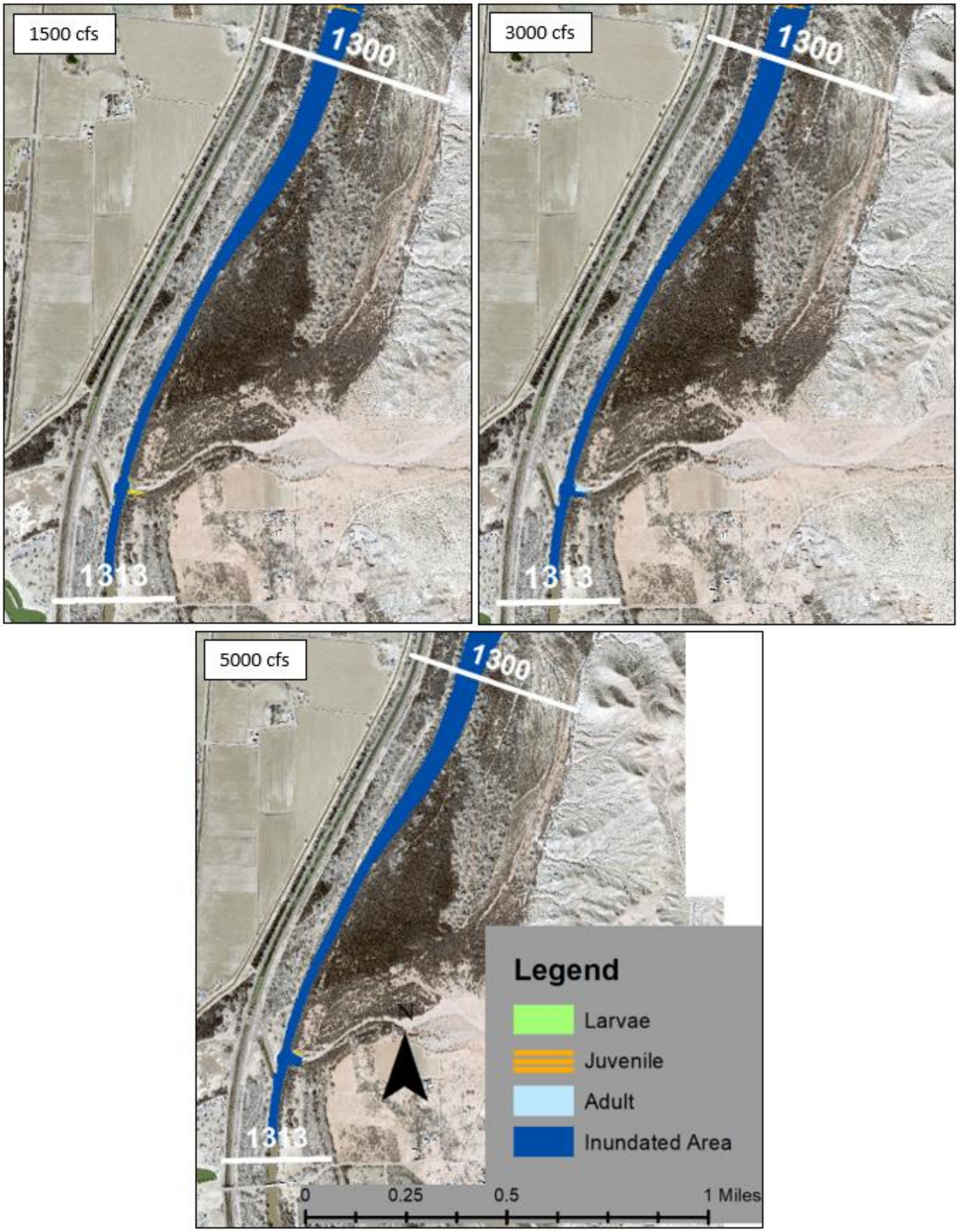

Figure C- 6 SA4 maps showing larvae, juvenile, and adult habitat. Inundated area refers to habitat that is unsuitable for all life stages. Flow direction is from top to bottom

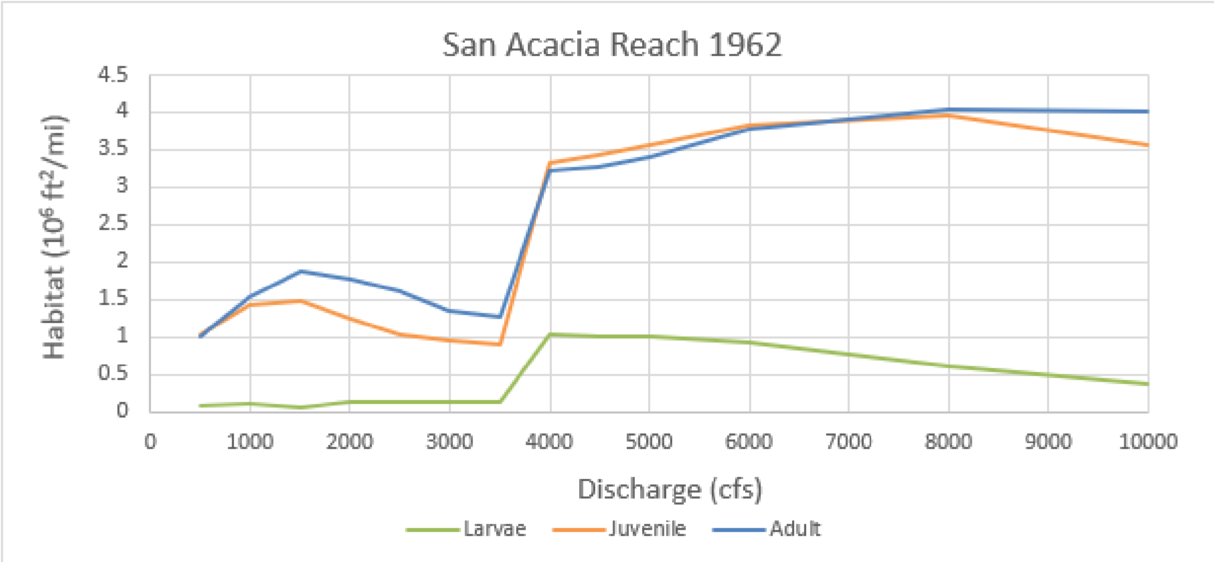
San Acacia Reach 1962
Habitat (10^6 ft^2/mi)
Discharge (cfs)
Larvae
Juvenile
Adult

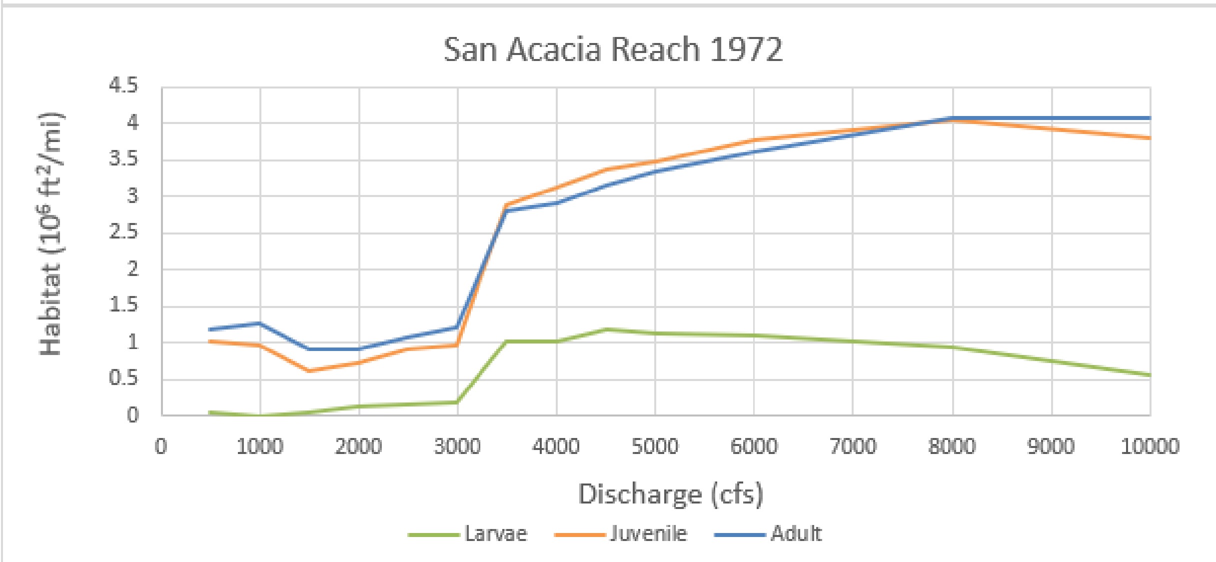
San Acacia Reach 1972
Habitat (10^6 ft^2/mi)
Discharge (cfs)
Larvae
Juvenile
Adult

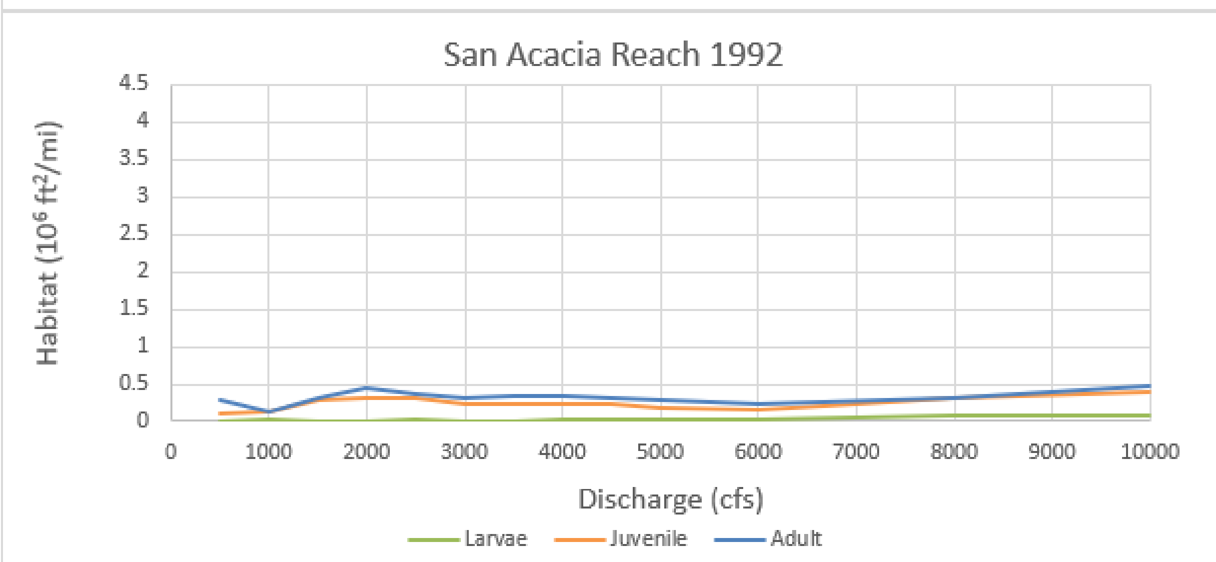
San Acacia Reach 1992
Habitat (10^6 ft^2/mi)
Discharge (cfs)
Larvae
Juvenile
Adult

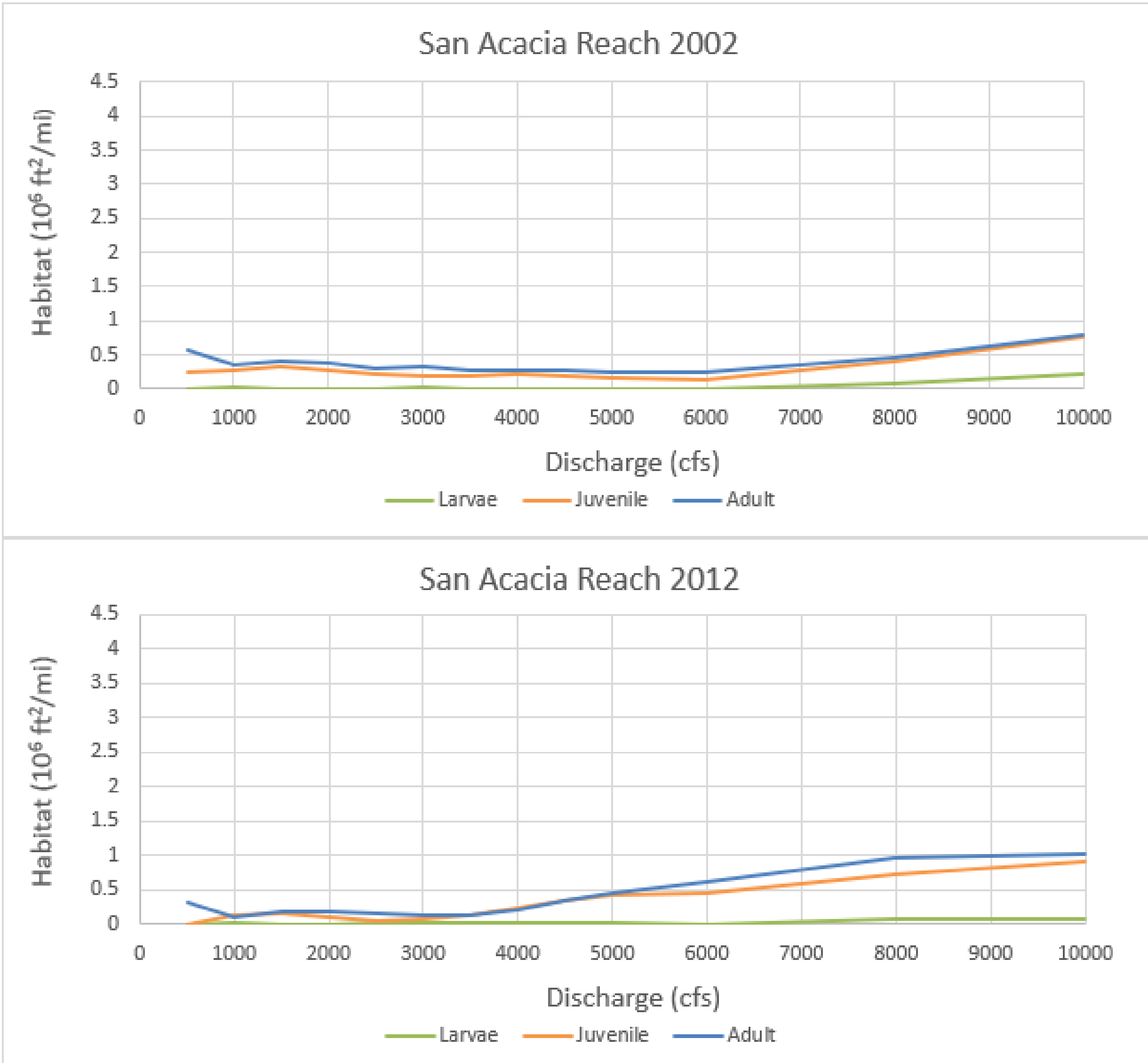

Figure C- 7 San Acacia reach habitat curves for larvae, juvenile, and adult

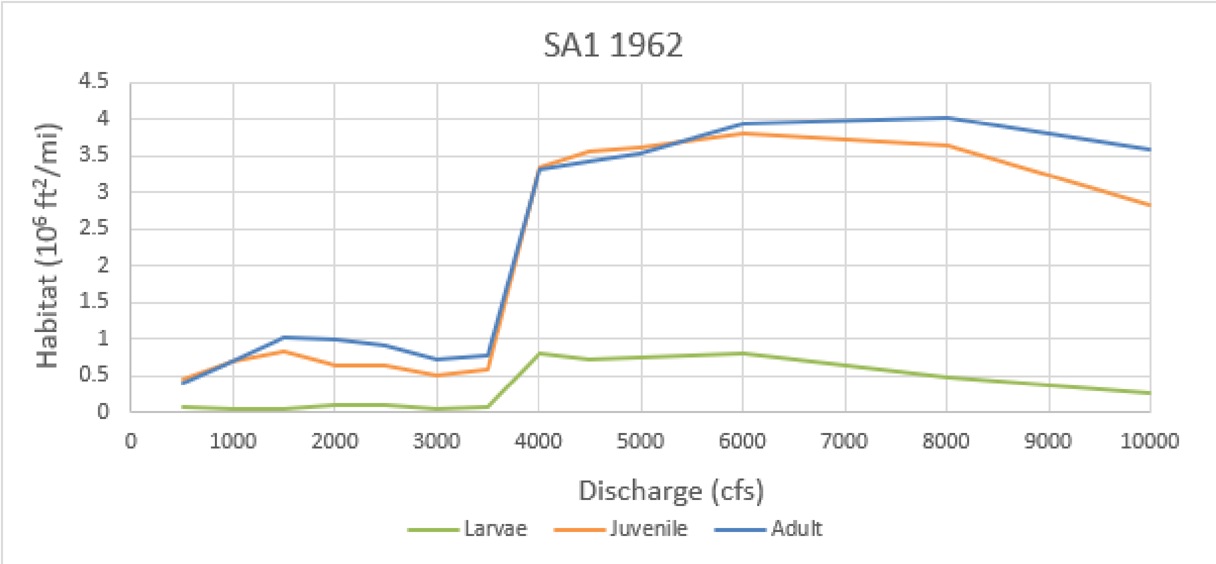
SA1 1962
Habitat (10^6 ft^2/mi)
Discharge (cfs)
Larvae
Juvenile
Adult

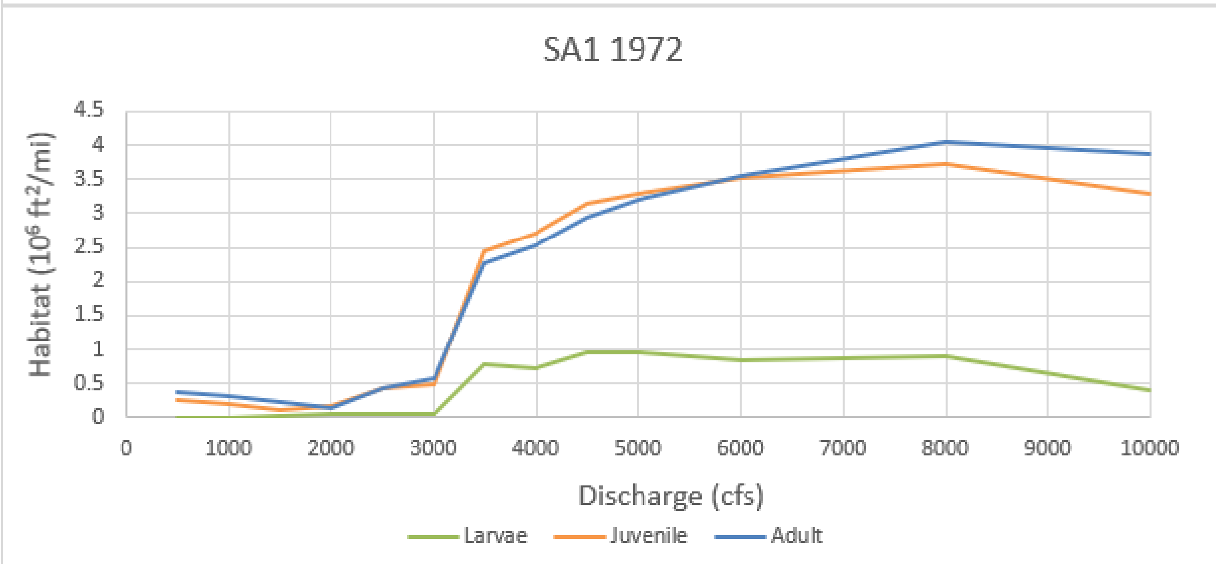
SA1 1972
Habitat (10^6 ft^2/mi)
Discharge (cfs)
Larvae
Juvenile
Adult

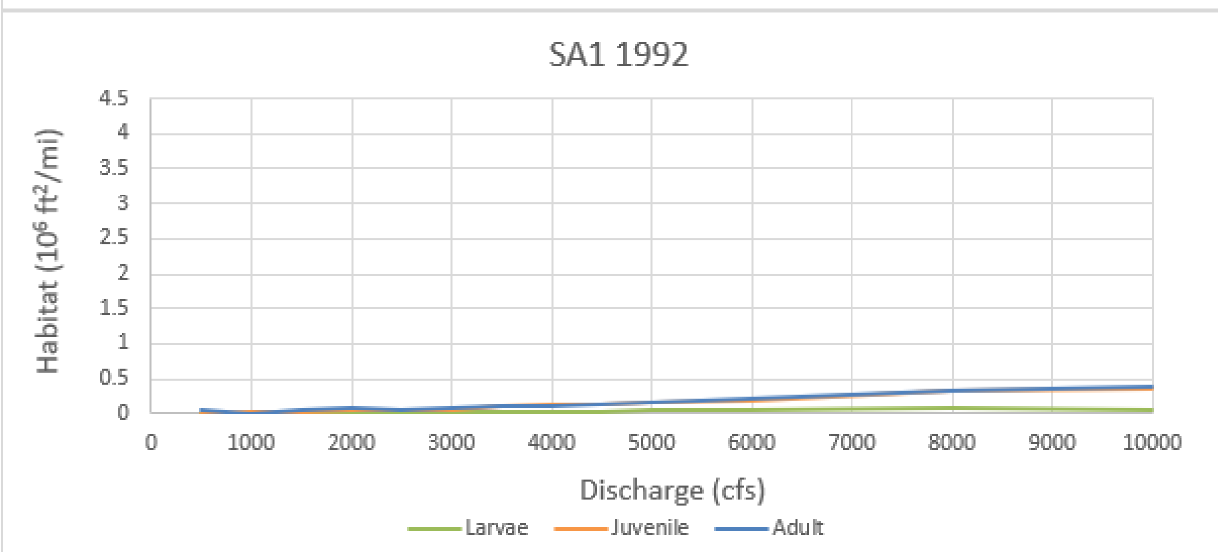
SA1 1992
Habitat (10^6 ft^2/mi)
Discharge (cfs)
Larvae
Juvenile
Adult

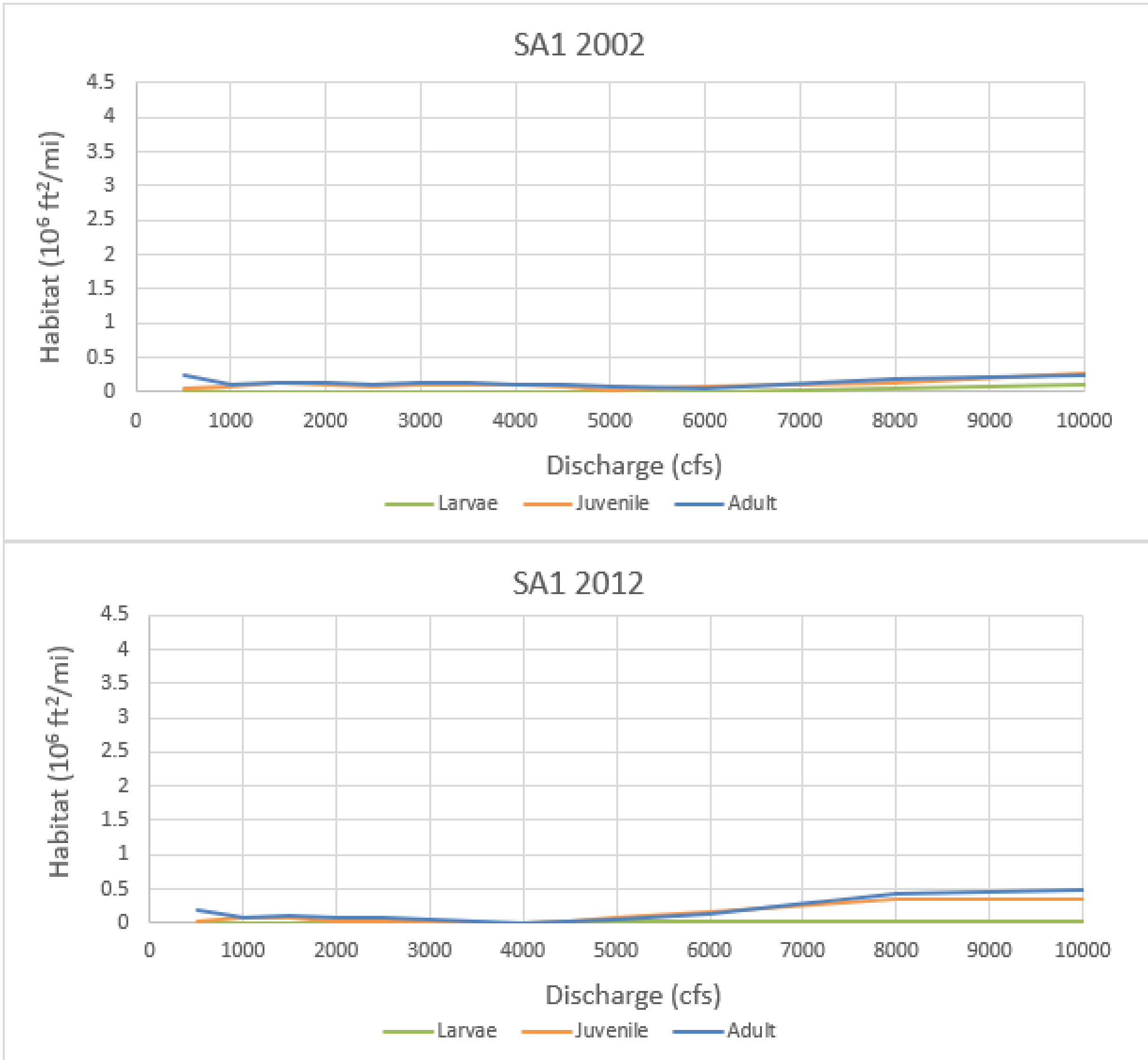

Figure C- 8 SA1 habitat curves for larvae, juvenile, and adult

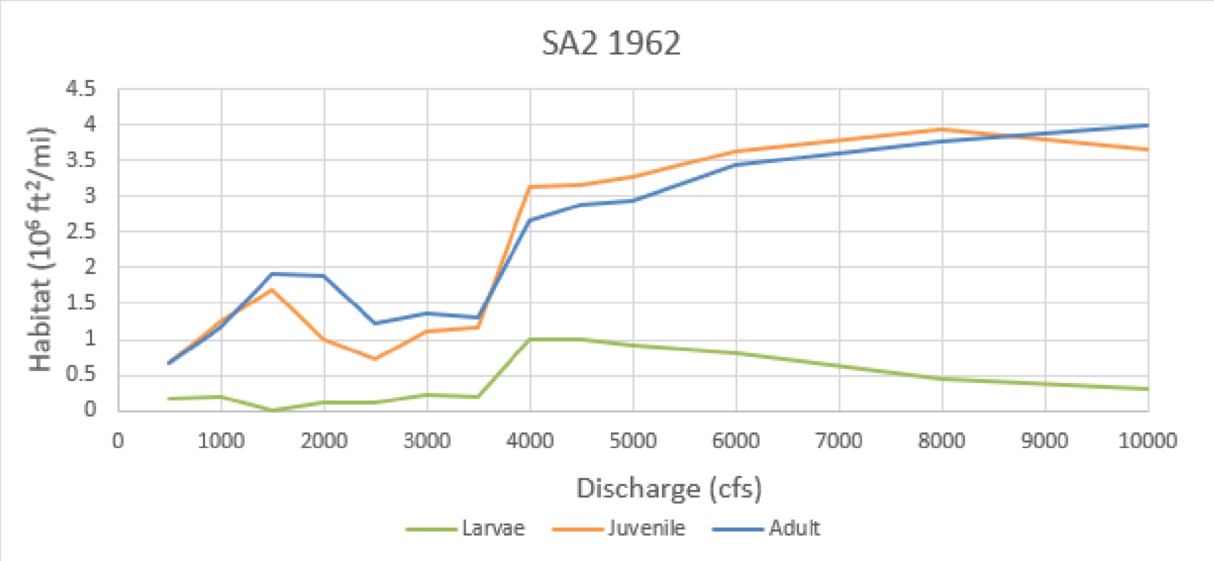
SA2 1962
Habitat (10^6 ft^2/mi)
Discharge (cfs)
Larvae
Juvenile
Adult

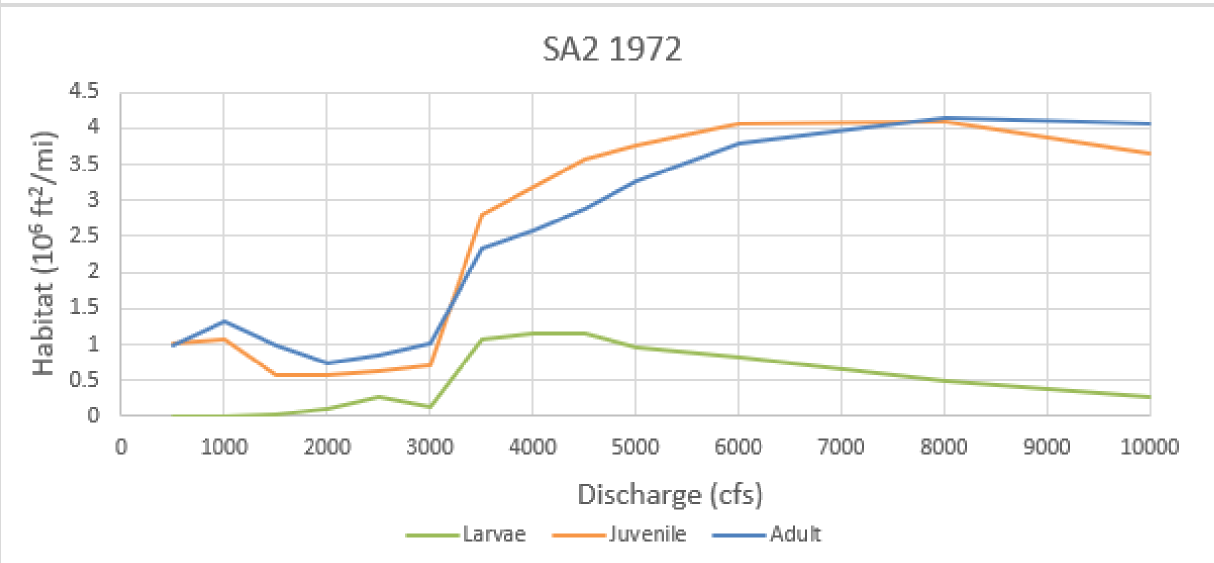
SA2 1972
Habitat (10^6 ft^2/mi)
Discharge (cfs)
Larvae
Juvenile
Adult

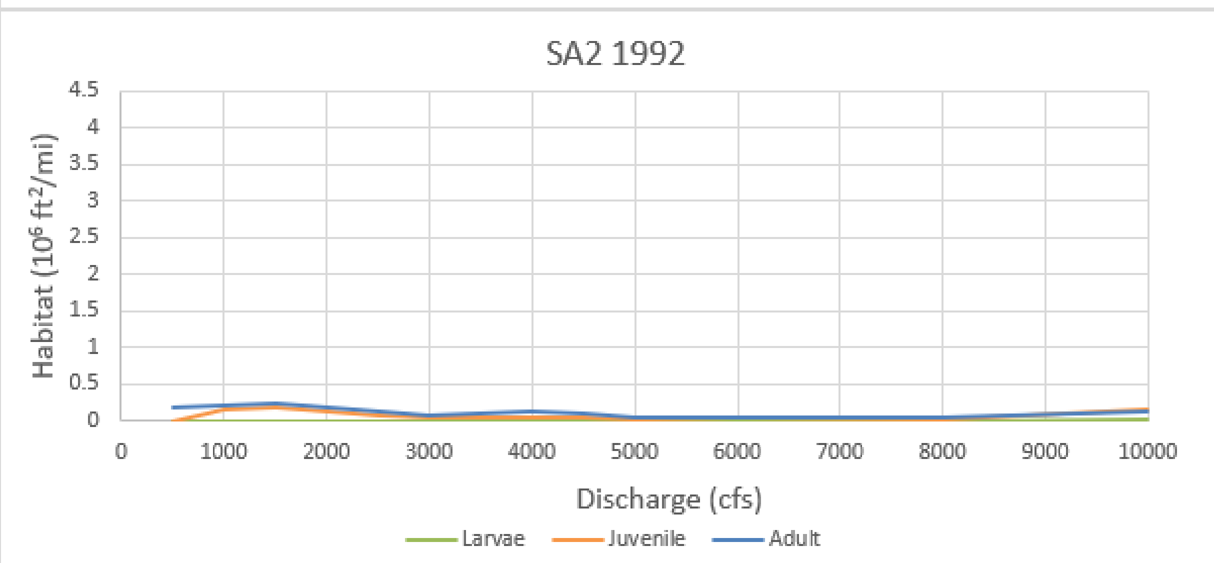
SA2 1992
Habitat (10^6 ft^2/mi)
Discharge (cfs)
Larvae
Juvenile
Adult

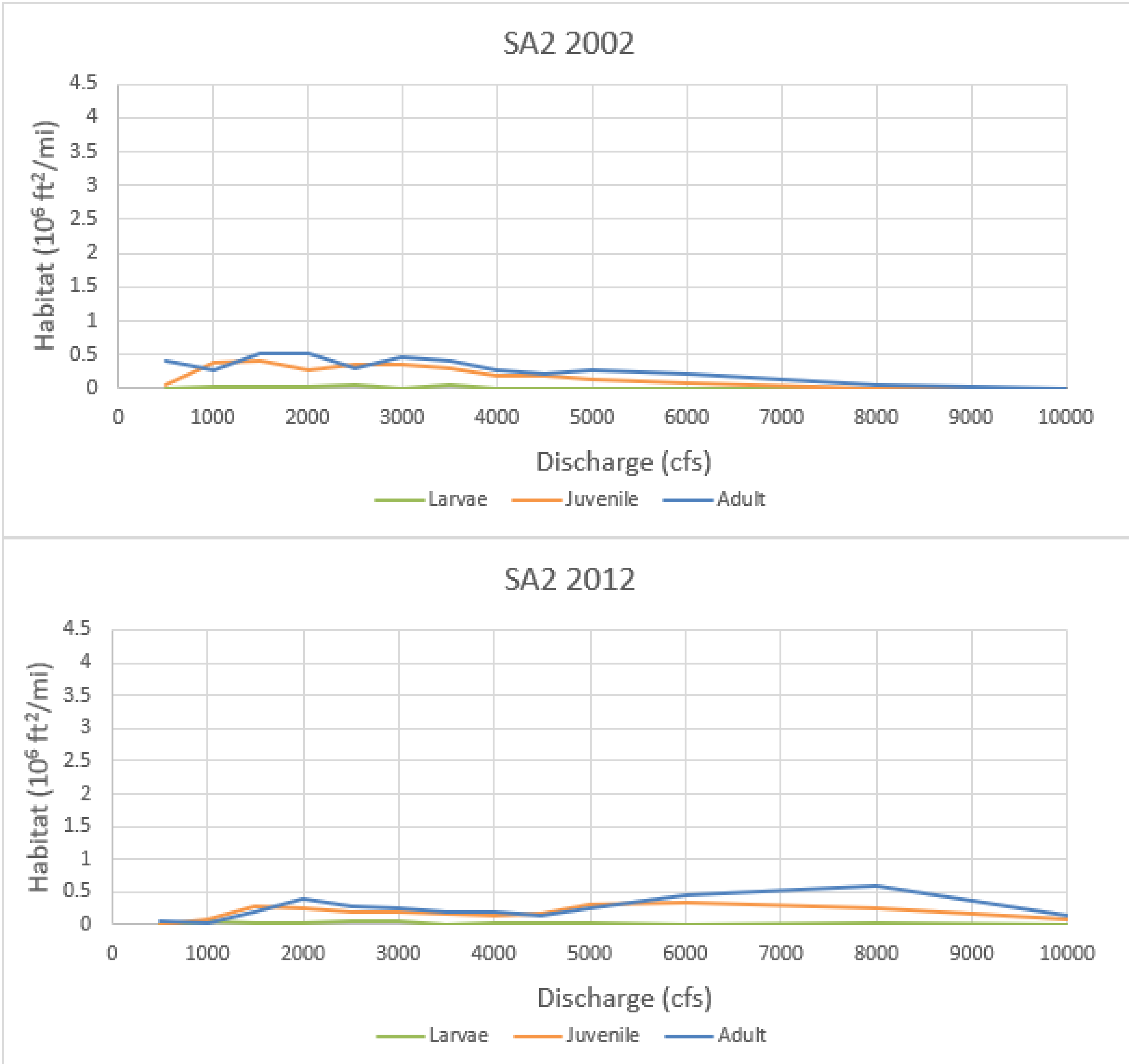

Figure C- 9 SA2 habitat curves for larvae, juvenile, and adult

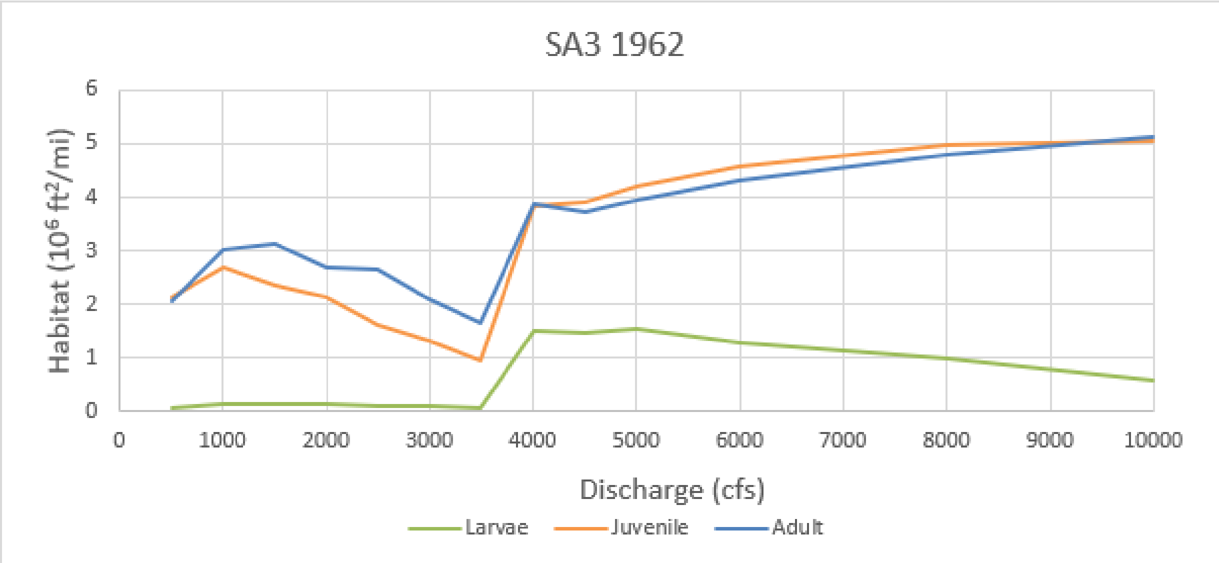
SA3 1962
Habitat (10^6 ft²/mi)
Discharge (cfs)
Larvae
Juvenile
Adult

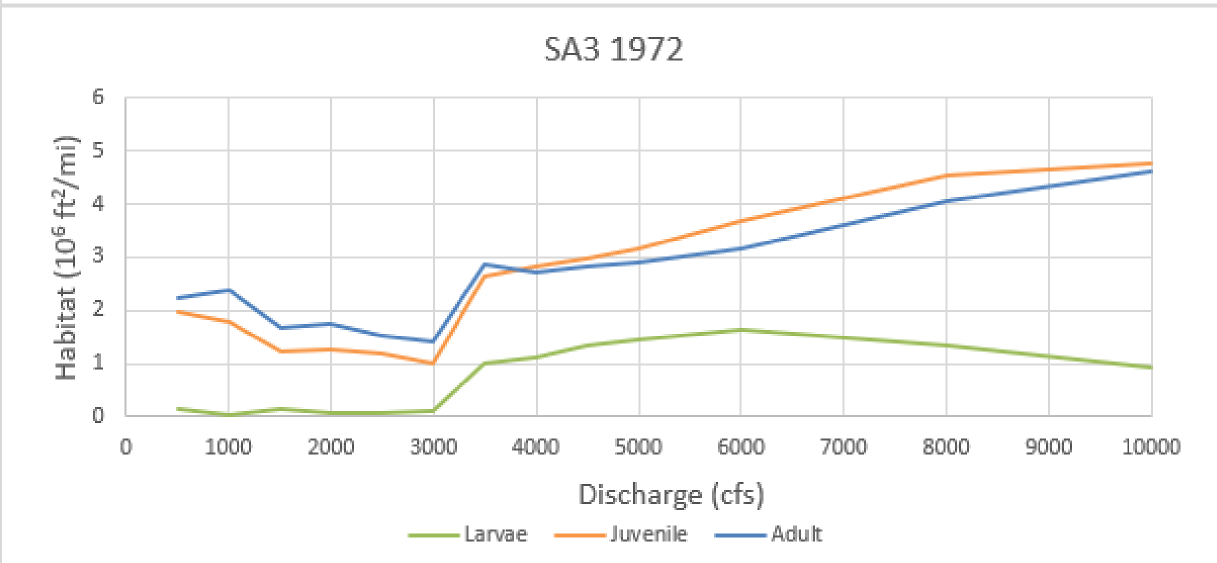
SA3 1972
Habitat (10^6 ft²/mi)
Discharge (cfs)
Larvae
Juvenile
Adult

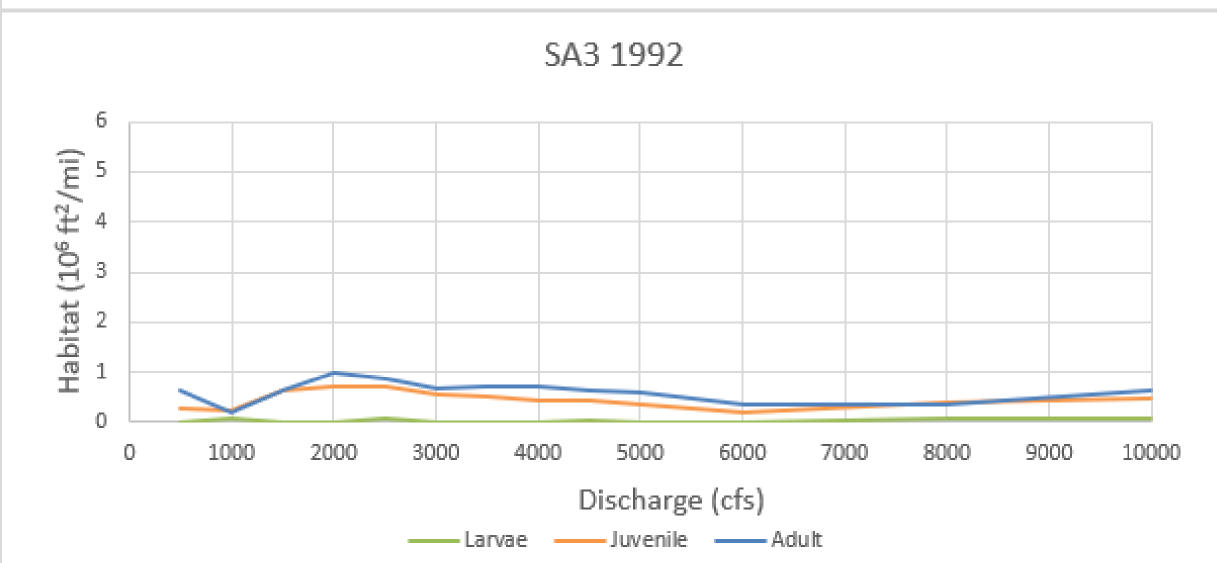
SA3 1992
Habitat (10^6 ft²/mi)
Discharge (cfs)
Larvae
Juvenile
Adult

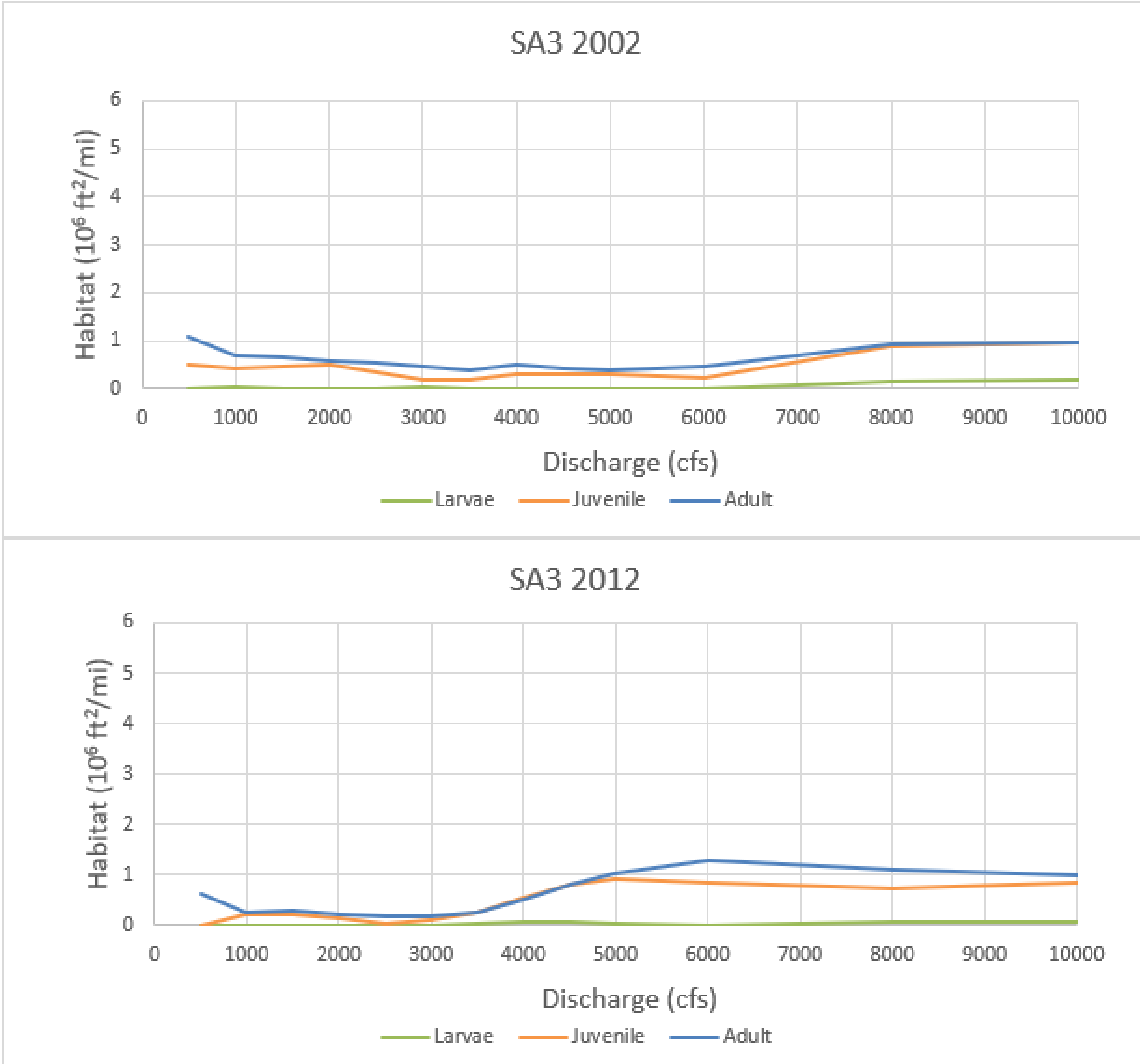

Figure C- 10 SA3 habitat curves for larvae, juvenile, and adult

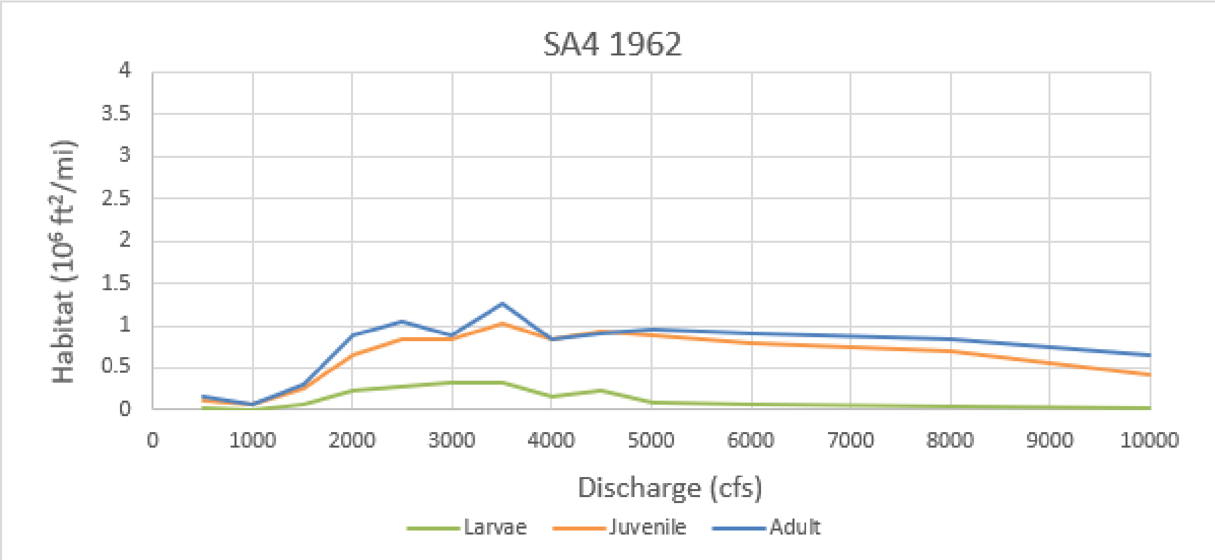
SA4 1962
Habitat (10^6 ft^2/mi)
Discharge (cfs)
Larvae
Juvenile
Adult

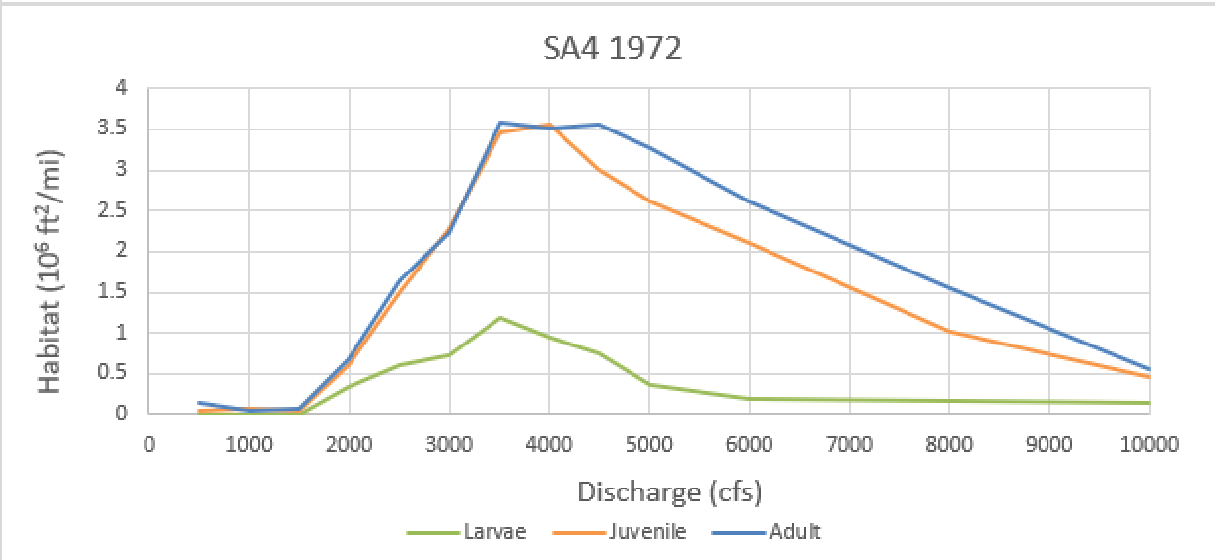
SA4 1972
Habitat (10^6 ft^2/mi)
Discharge (cfs)
Larvae
Juvenile
Adult

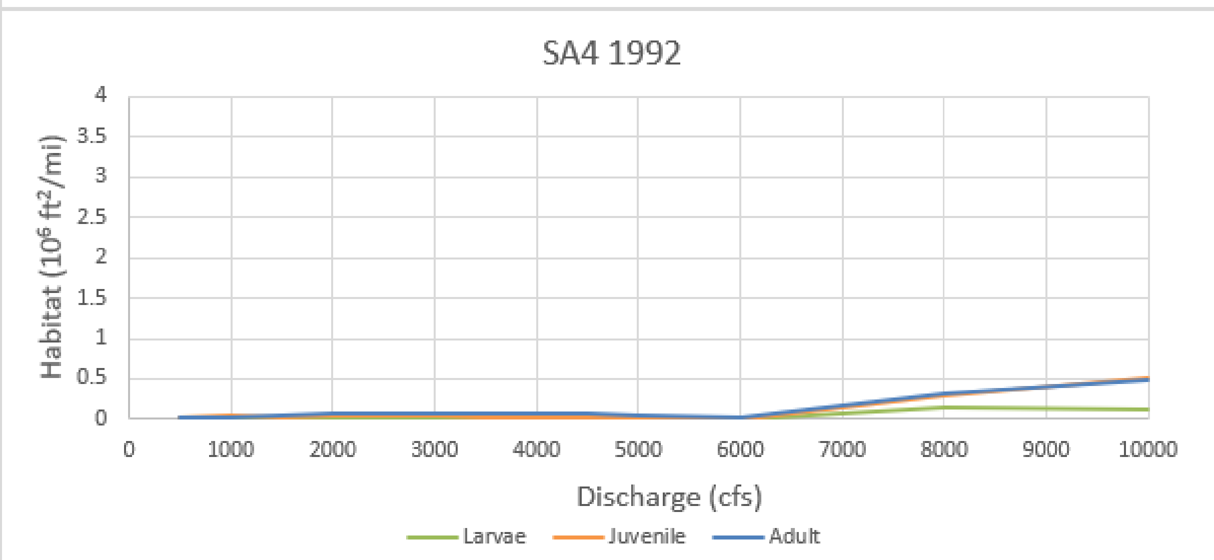
SA4 1992
Habitat (10^6 ft^2/mi)
Discharge (cfs)
Larvae
Juvenile
Adult

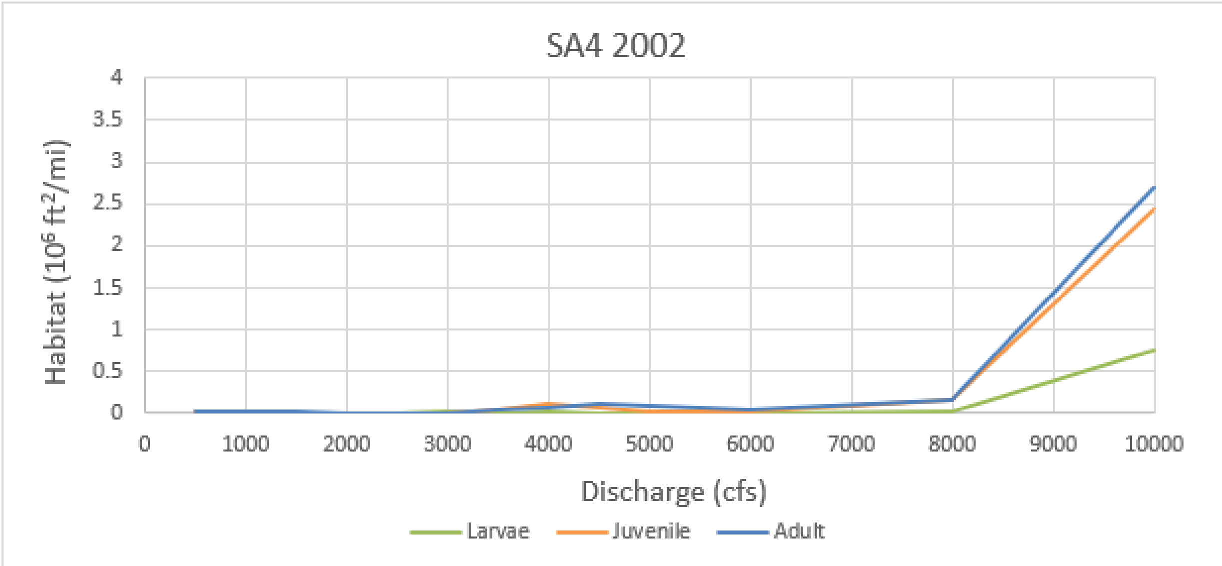

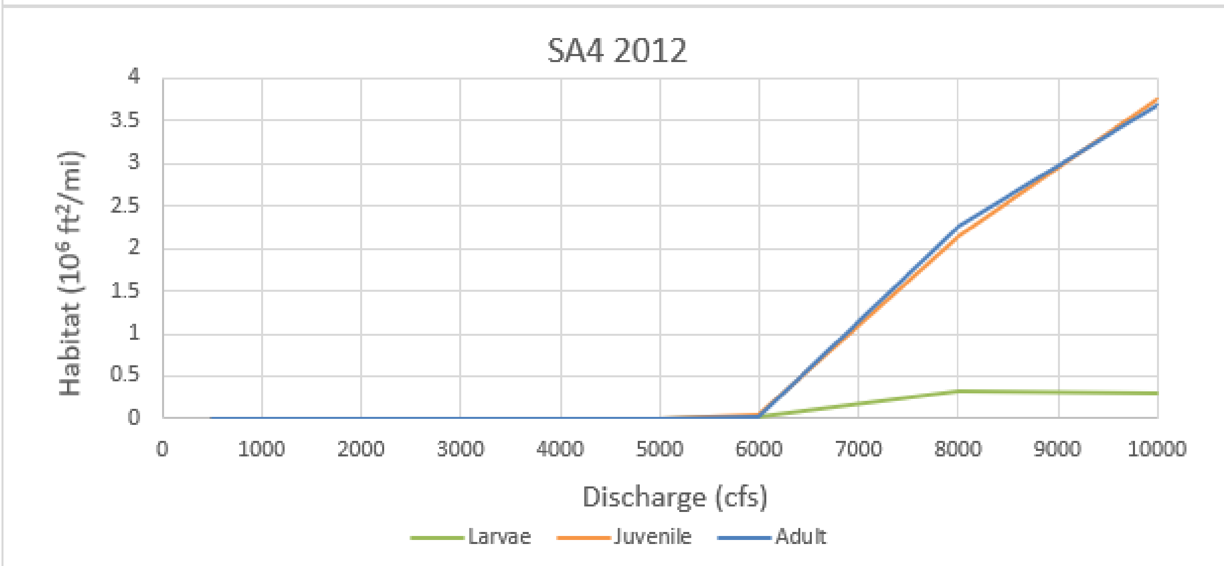

Figure C- 11 SA4 habitat curves for larvae, juvenile, and adult

Appendix D

Levee Placement

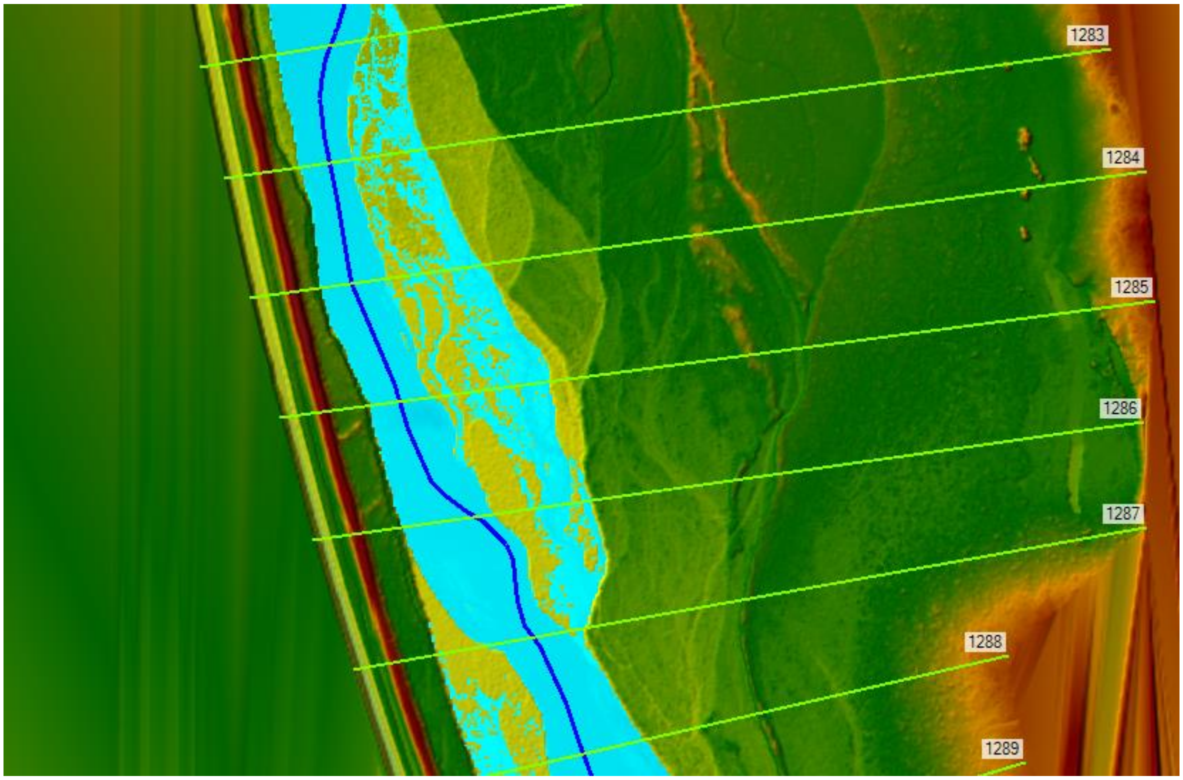

Figure D- 1 RAS-Mapper results at 3,000 cfs with levees in default positions

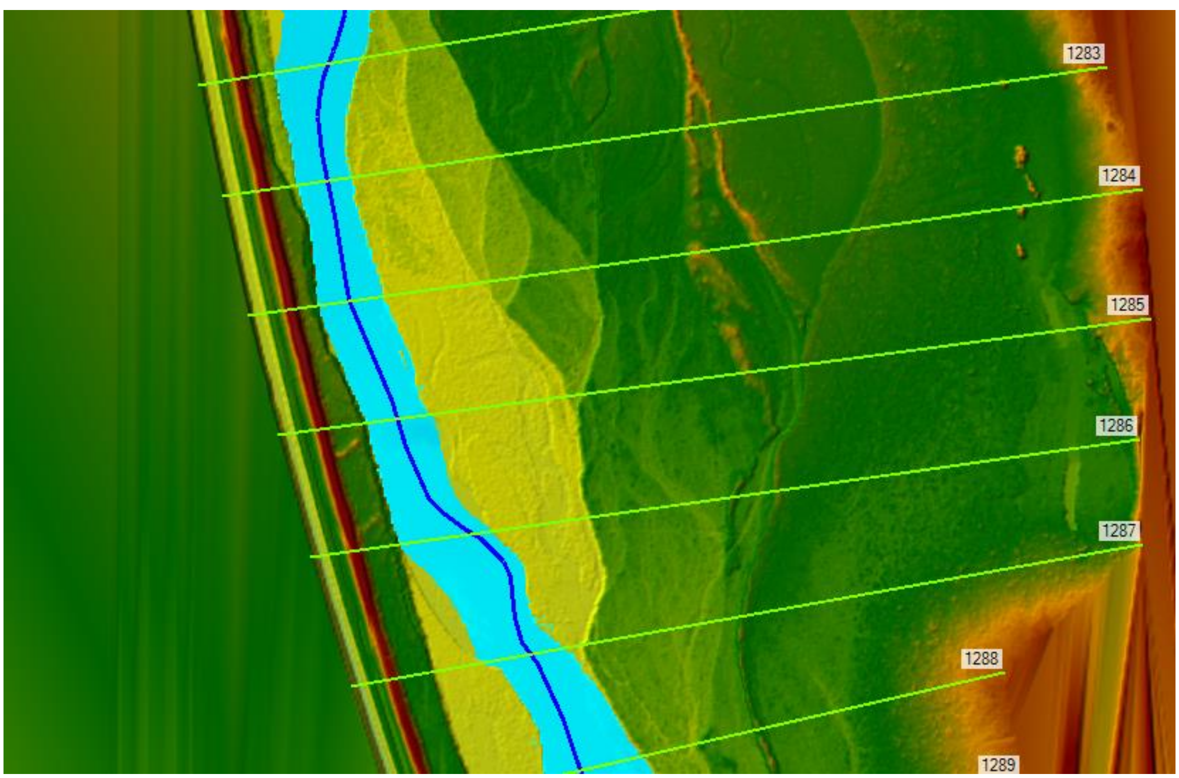

Figure D- 2 RAS-Mapper results at 3,000 cfs with levees lowered for flows below 4,000 cfs

Appendix E

Width Slices Sensitivity Analysis

A simple test was performed on the 1992 results to test the sensitivity of the width slices method. Originally, each cross-section was split into 45 sections, with 15 on the left bank, 15 in the main channel and 15 on the right bank. The same method was done for every other year. However, the locations of the bank stations vary dramatically from 1992 through 2012 which can impact the width of each slice, particularly in the main channel, where the flow is mostly confined in 1992. For example, at a discharge of 500 cfs, the average width of each slice in 2012 was 19 ft. In 1992, that number was 37 ft. To understand what impact this was having, the 1992 results were reprocessed using a new scheme to divide the slices between the bank stations. Where initially 15-15-15 was used, 10-25-10 was used (meaning 10 slices on the left overbank, 25 in the main channel and 10 on the right overbank). This caused the average width of a slice for 1992 to drop to 22 ft.

These results (1992 with 15-15-15 and 1992 with 10-25-10) were then compared and presented in Figure E- 1. Adult habitat is the most similar, but poor trends are found for larvae and juveniles. Larvae was much higher using 10-25-10 above 3,000 cfs. The R^2 value was 0.168. Juvenile habitat was much lower at every discharge (R^2 of 0.0375). The high R^2 value (0.88) for adult habitat may be explained by the fact that the adult criteria are much broader and less sensitive than the criteria for juveniles and larvae (see Figure E- 2).

The results are very sensitive to changes in model set up and the ways of proportioning the slices, which indicates that considerable caution should be used in extrapolating from the results provided by the 1-D method (except for the results for adults).

This method has since been updated to use 20 slices in each floodplain and 5 slices in the channel due to the RGSM’s dependence on the lower depths and velocities that often occur in the floodplains.

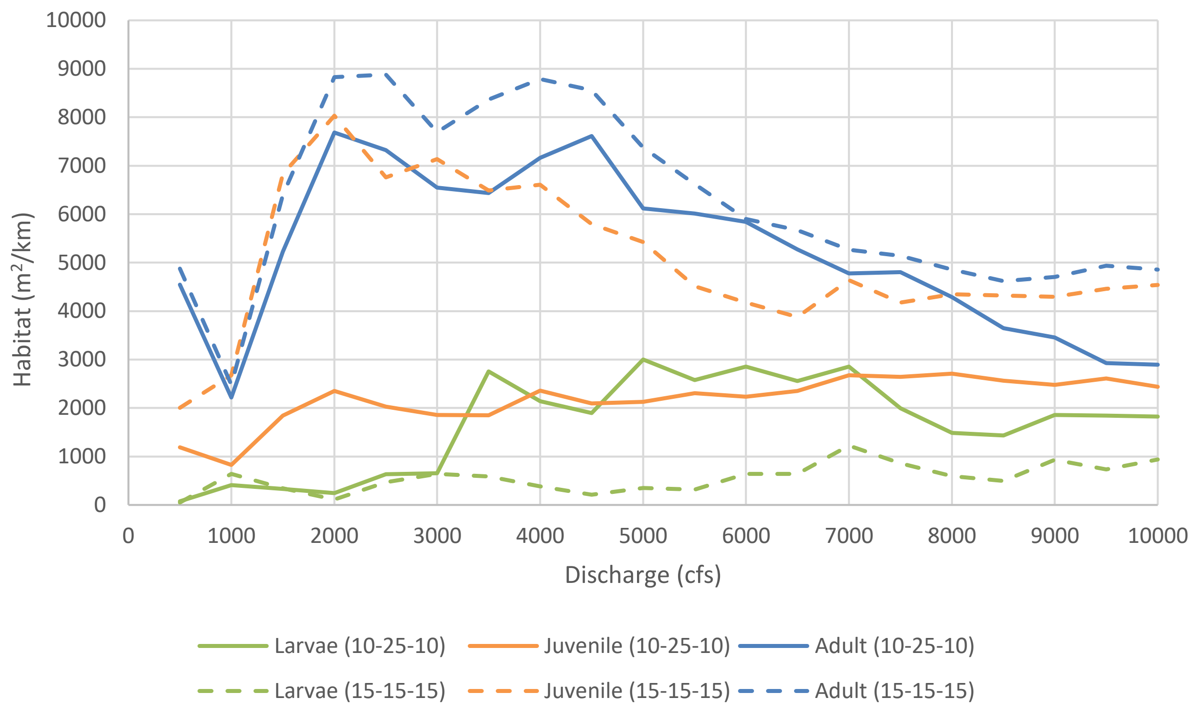

Figure E- 1 Comparing 1992 results using 10-25-10 vs 15-15-15 width slices distribution

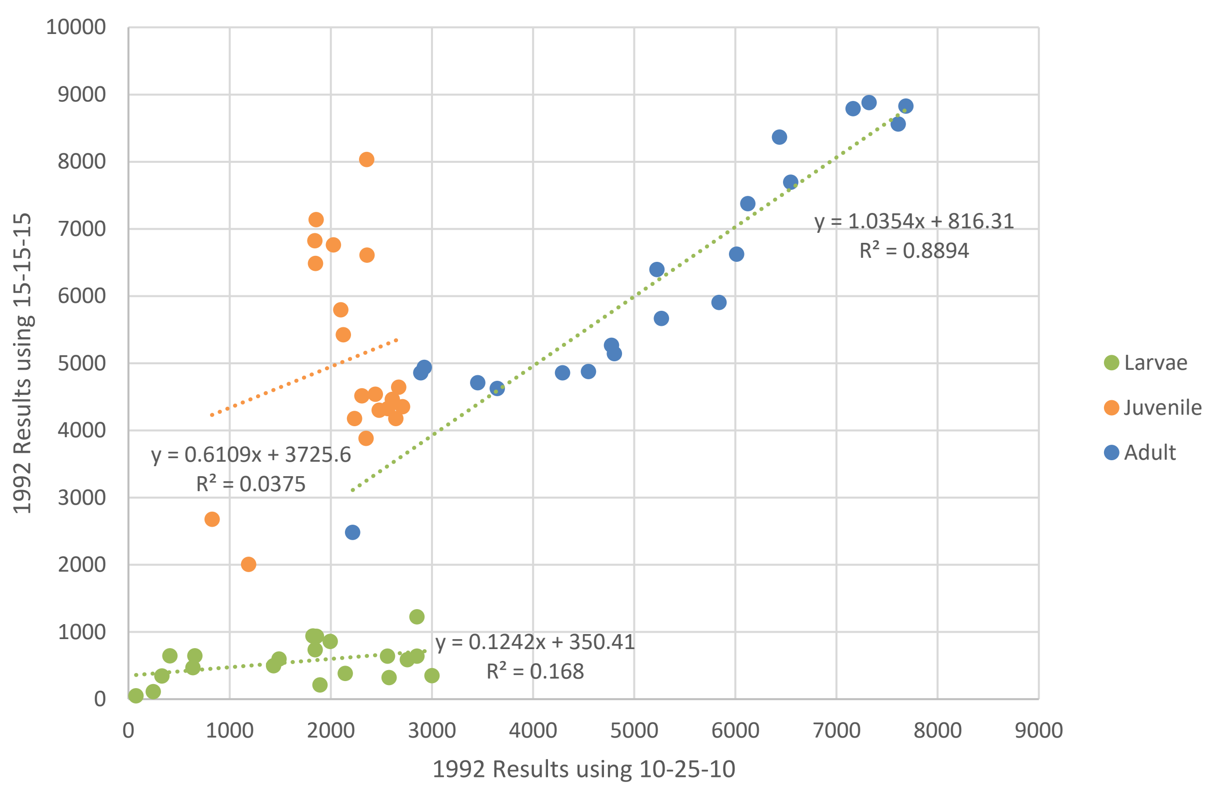

Figure E- 2 Comparing 1992 results using 10-25-10 vs 15-15-15 width slices distribution

Figure E- 3 shows the results of the comparison between the width slices and RAS-Mapper methods for 2012. For better comparison with the RAS-Mapper results, the width slices results were multiplied by 500 feet (the average distance between cross-sections) to obtain units of ft^2/mile. Figure E- 4 shows the correlation between the 2012 RAS-Mapper and width slices results. R^2 values are the best for juveniles at 0.80 compared to adults at 0.77. The R^2 value is the lowest for larvae at 0.72. All values are relatively high, indicating that this is an acceptable method to bridge the gap in data between 1992, 2002 and 2012.

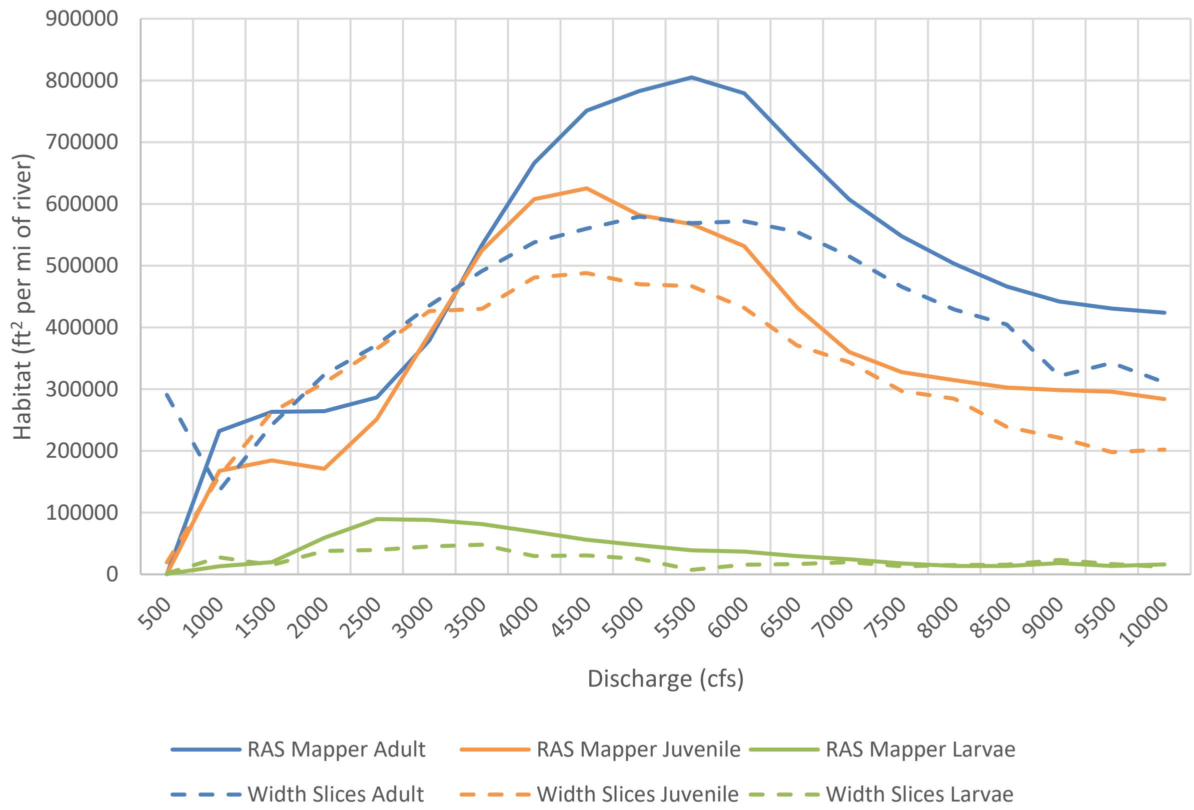

Figure E- 3 Comparison between width slices and RAS-Mapper habitat results for larvae, juvenile, and adult

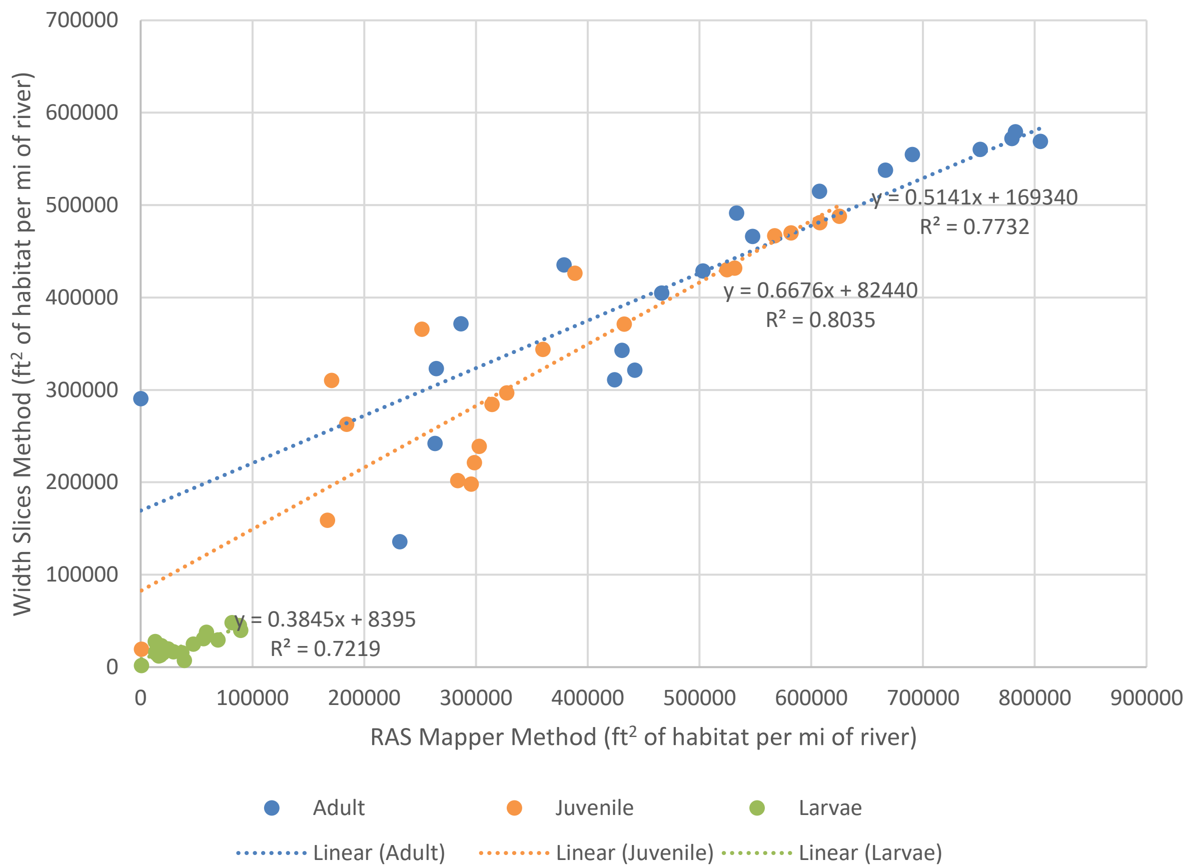

Figure E- 4 Correlation between width slices method and RAS-Mapper method

Appendix F

Habitat Versus Velocity and Depth in 2012

Areas produced by the RAS-Mapper method were also broken apart into their component parts, looking at velocity and depth across areas individually. Figure F- 1 through Figure F- 3 shows a comparison of the areas meeting depth and velocity criteria individually versus combined. In most areas, the velocity is the limiting factor, which indicates that areas where the depth criteria are met may still have velocities that are too high for the RGSM. The overall shape of the velocity curve more closely resembled the actual habitat availability curve that considers both depth and velocity. However, the depth only curve shows two peaks, with the first occurring around 1,500 cfs. Figure F- 4 shows that for some discharges, almost 100% of the areas meeting velocity criteria become overall acceptable habitat (meeting both velocity and depth criteria).

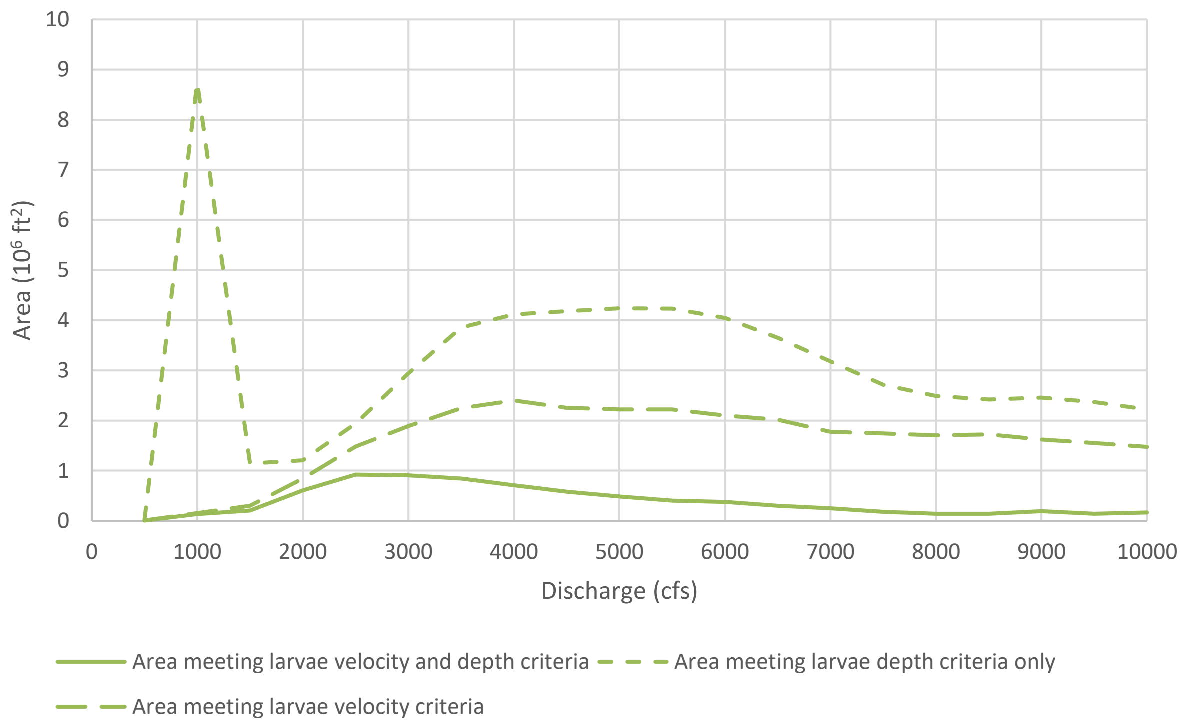

Figure F- 1 Comparison of areas meeting depth and velocity criteria individually and combined for larvae

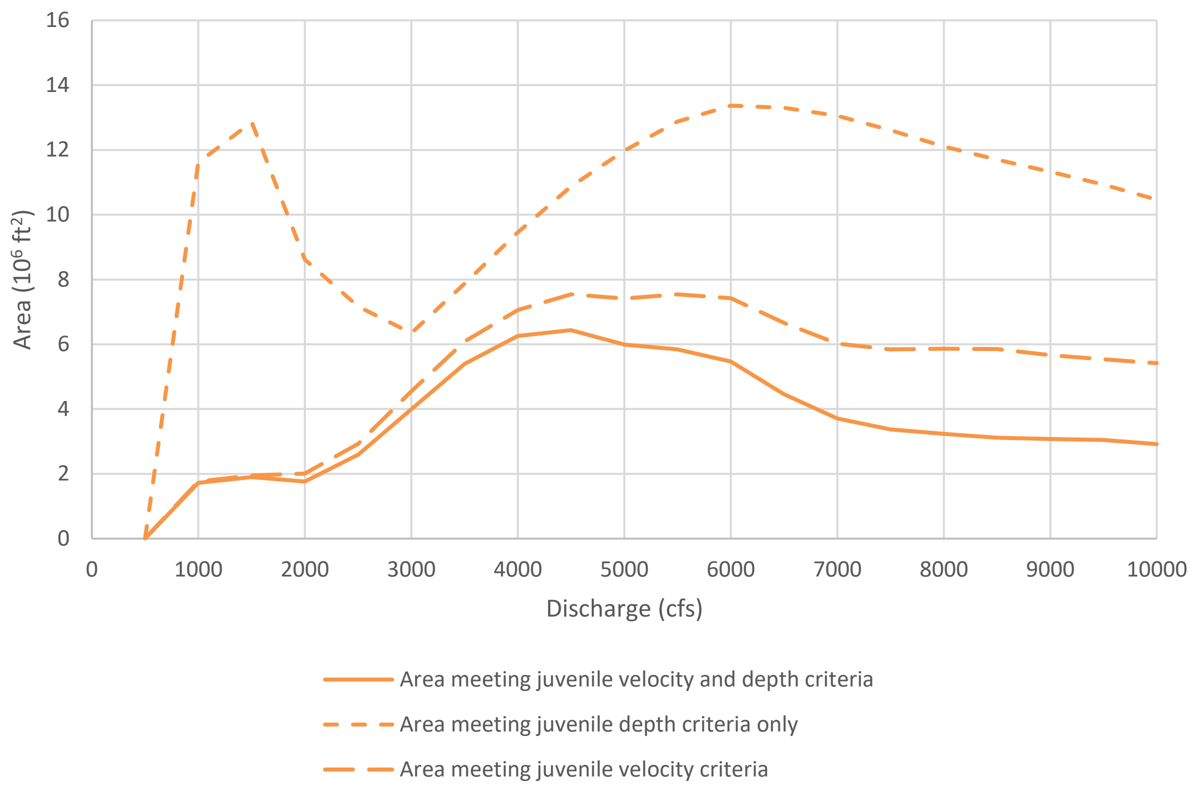

Figure F- 2 Comparison of areas meeting depth and velocity criteria individually and combined for juveniles

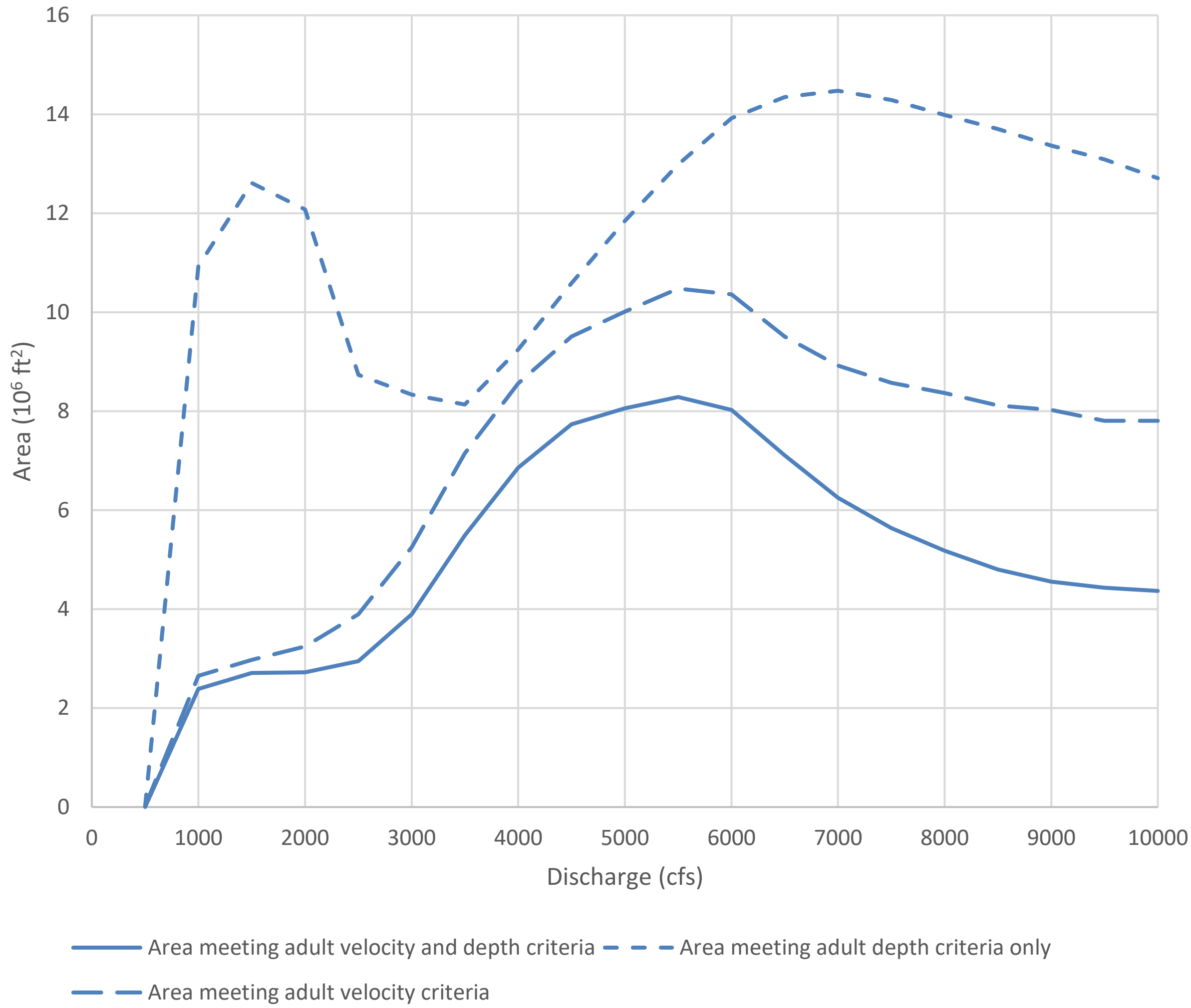

Figure F- 3 Comparison of areas meeting depth and velocity criteria individually and combined for adults

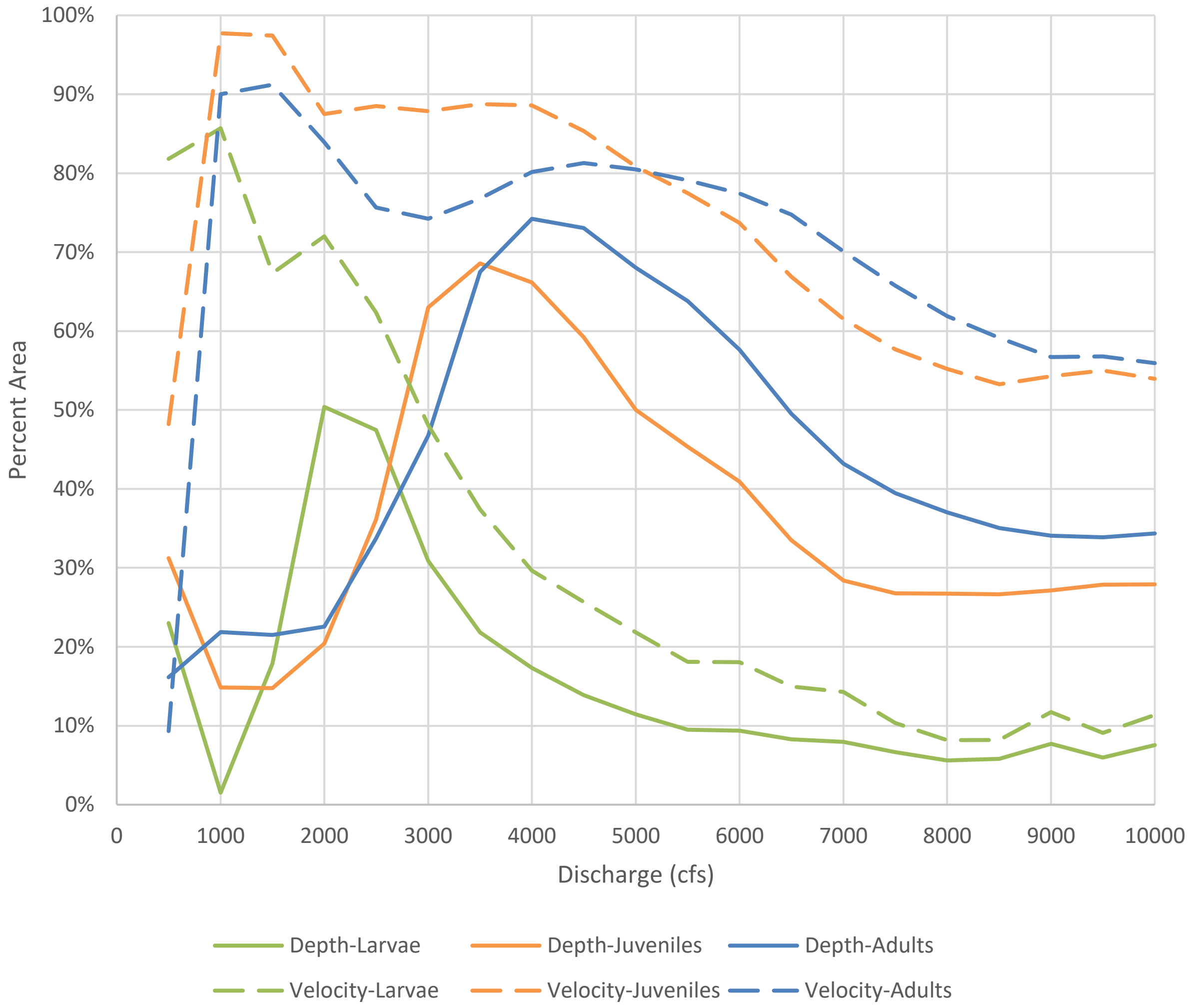

Figure F- 4 Percent of areas meeting depth and velocity criteria over the total acceptable habitat area

In 2012, the limiting factor for habitat availability was velocities, not depths. This is particularly true at discharges at or below 3,000 cfs. For example, of the areas meeting velocity criteria for adults alone, 91% ultimately became areas that fit velocity and depth criteria. In contrast, only 21% of the areas meeting depth criteria for adult alone were utilized. This suggests that there are many areas where depths are acceptable for RGSM habitat in the channel, but velocities are too high. Further investigation is needed, but restoration efforts could potentially focus on creating areas of low velocity in places where the existing depths meet criteria for RGSM.

Appendix G

Spatially Varying Habitat Charts for Future Process Linkage Report

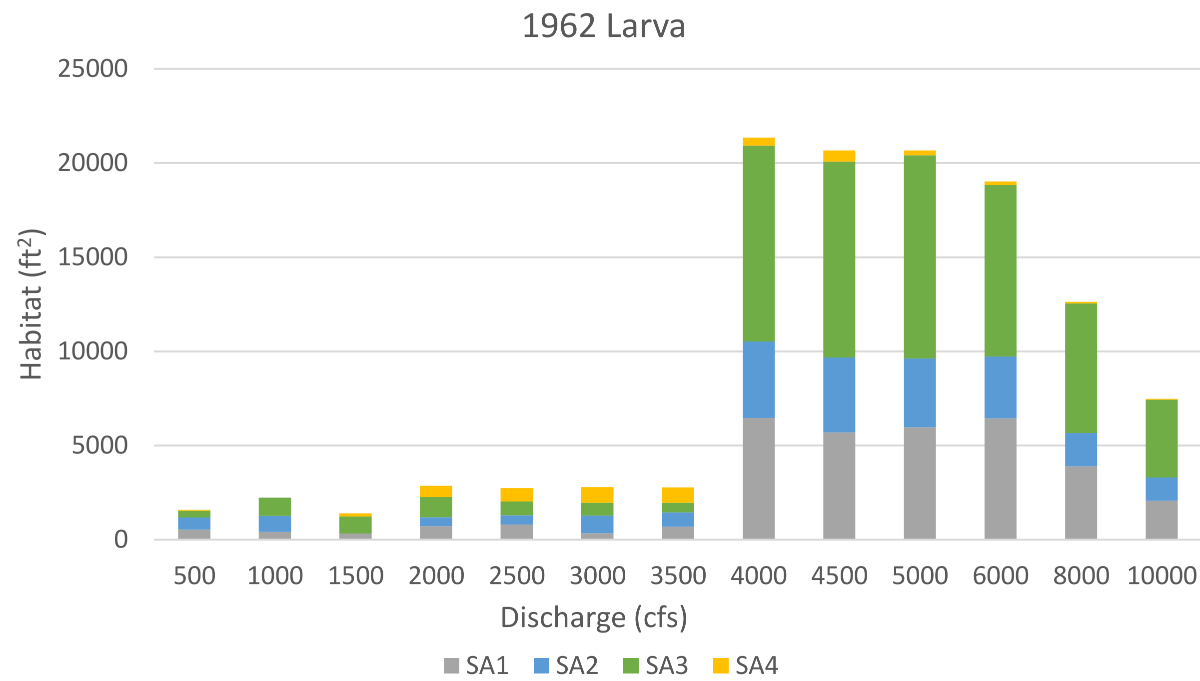

Figure G- 1 Spatially varying larva habitat throughout San Acacia reach in 1962

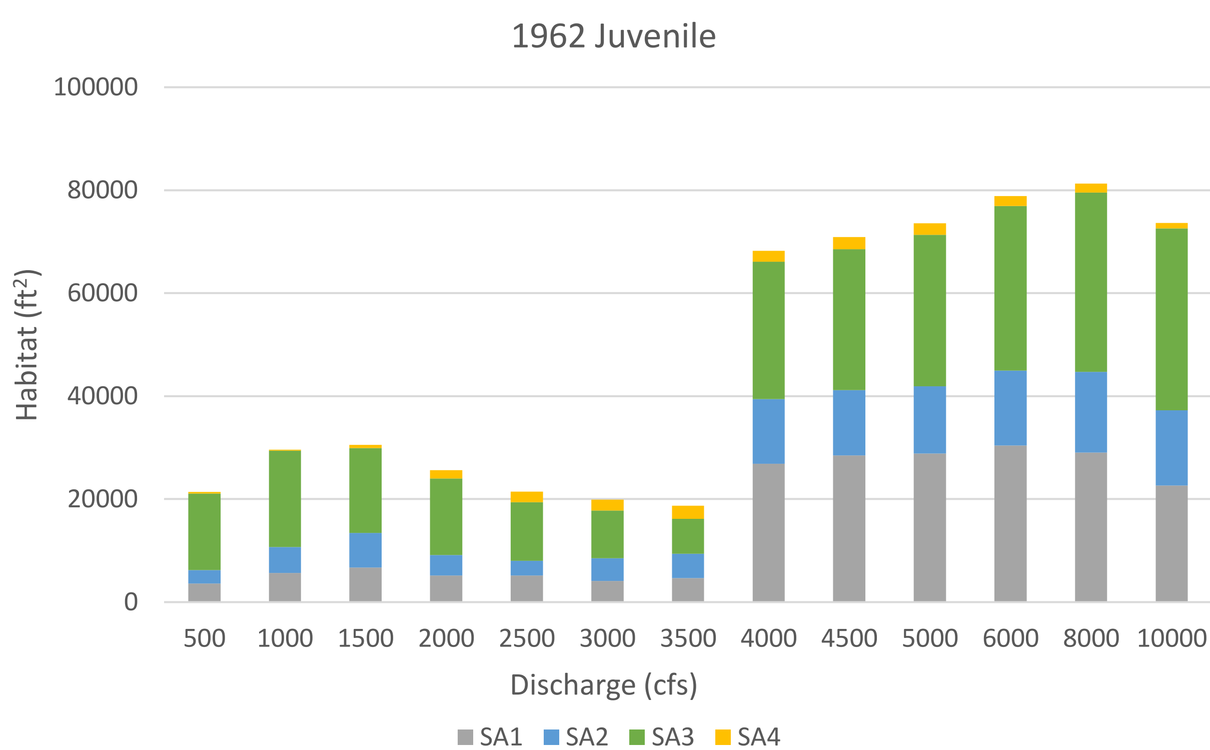

Figure G- 2 Spatially varying juvenile habitat throughout San Acacia reach in 1962

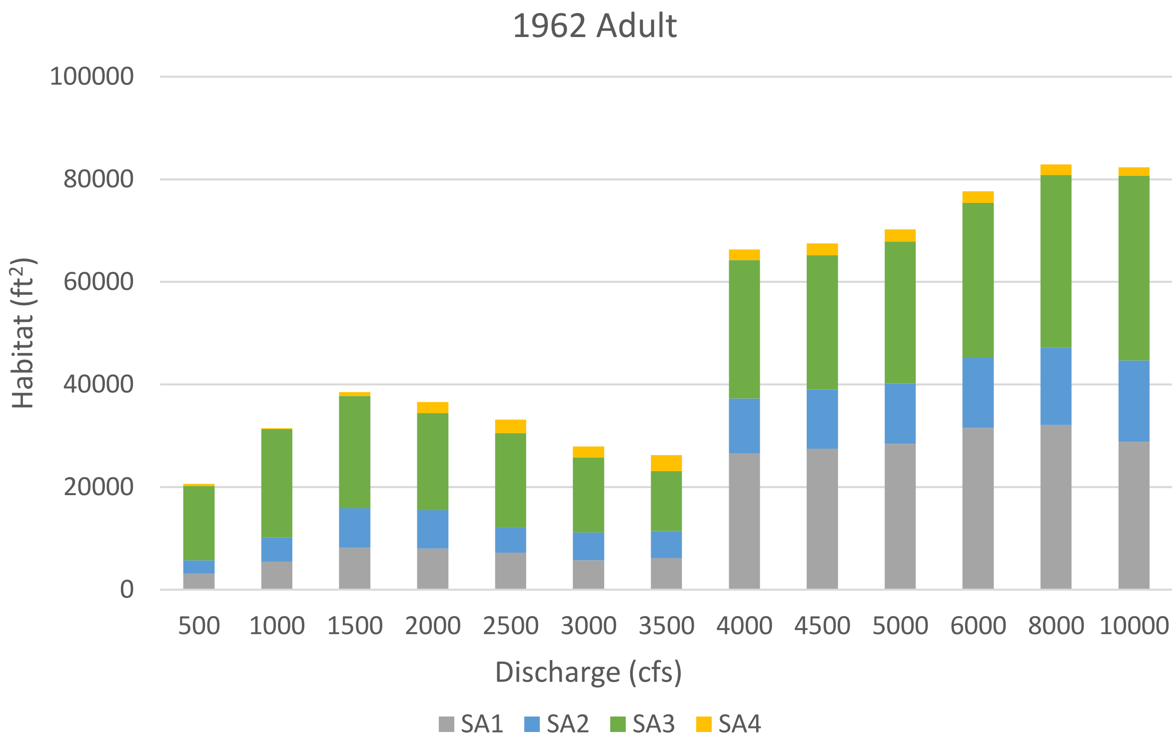

Figure G- 3 Spatially varying adult habitat throughout San Acacia reach in 1962

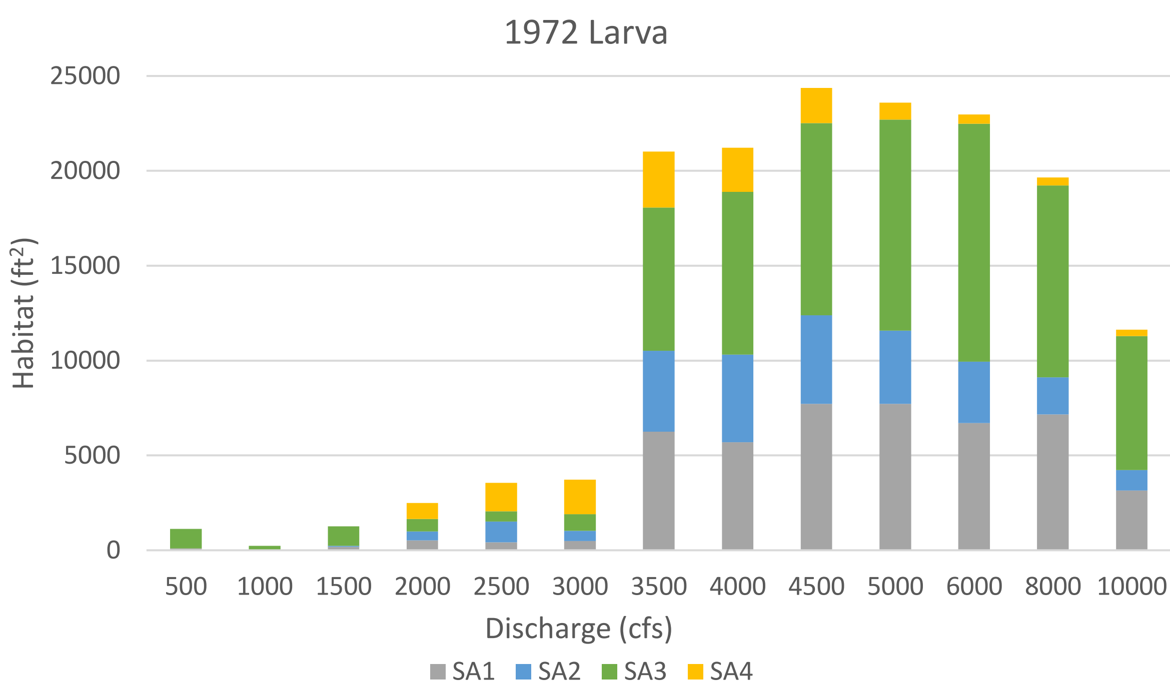

Figure G- 4 Spatially varying larva habitat throughout San Acacia reach in 1972

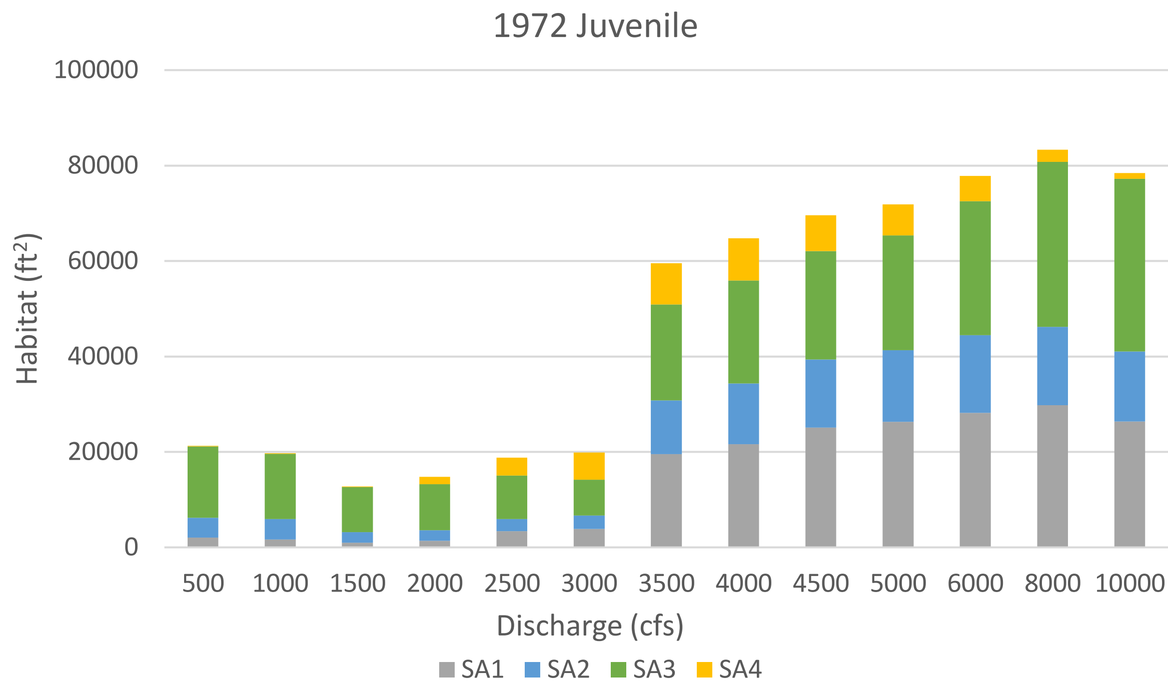

Figure G- 5 Spatially varying juvenile habitat throughout San Acacia reach in 1972

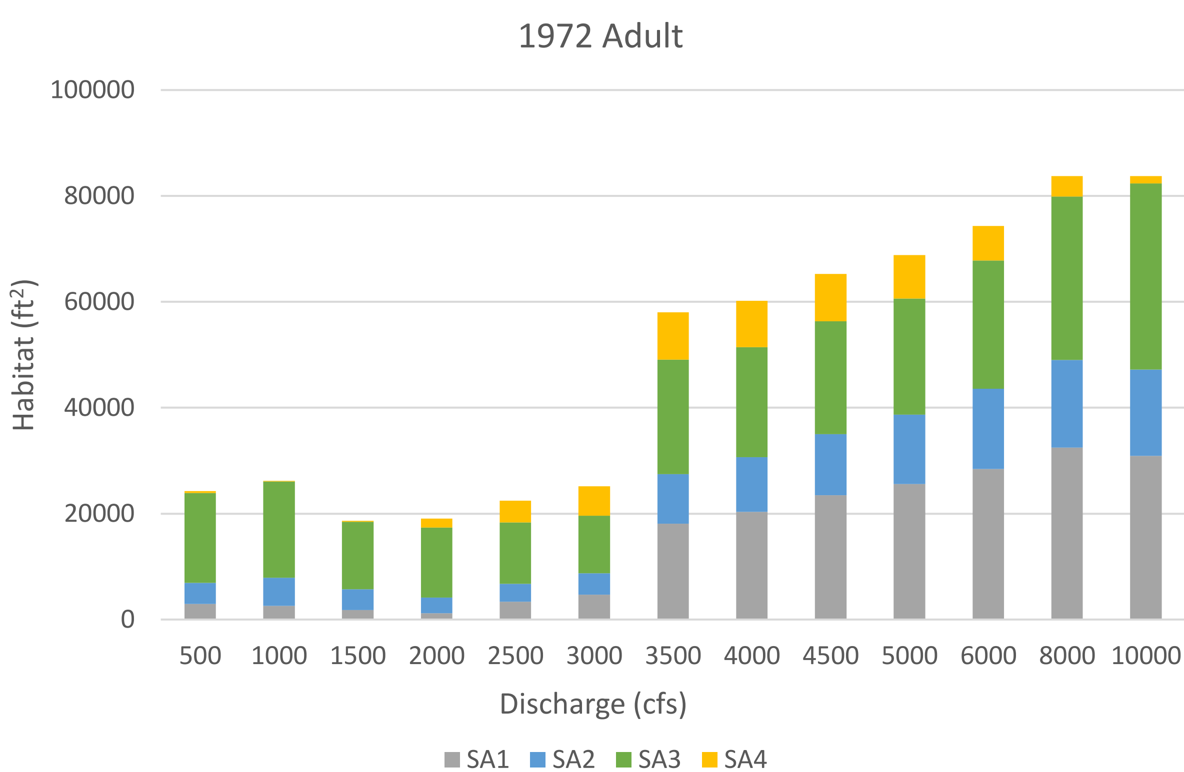

Figure G- 6 Spatially varying adult habitat throughout San Acacia reach in 1972

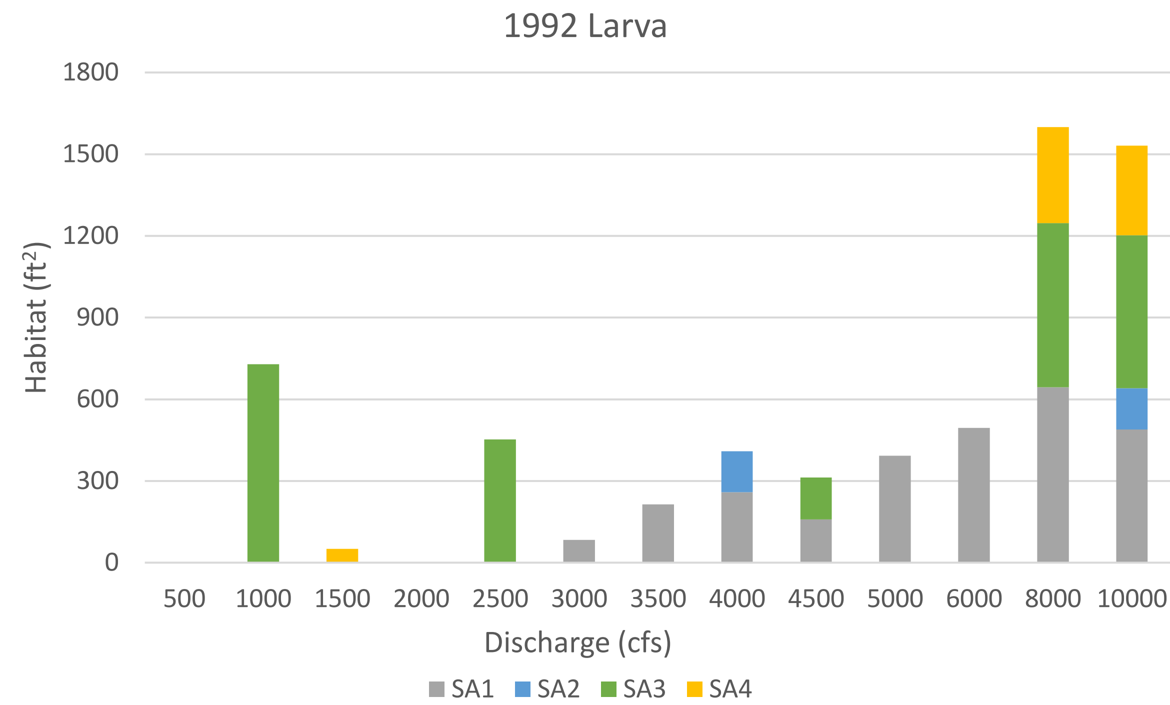

Figure G- 7 Spatially varying larva habitat throughout San Acacia reach in 1992

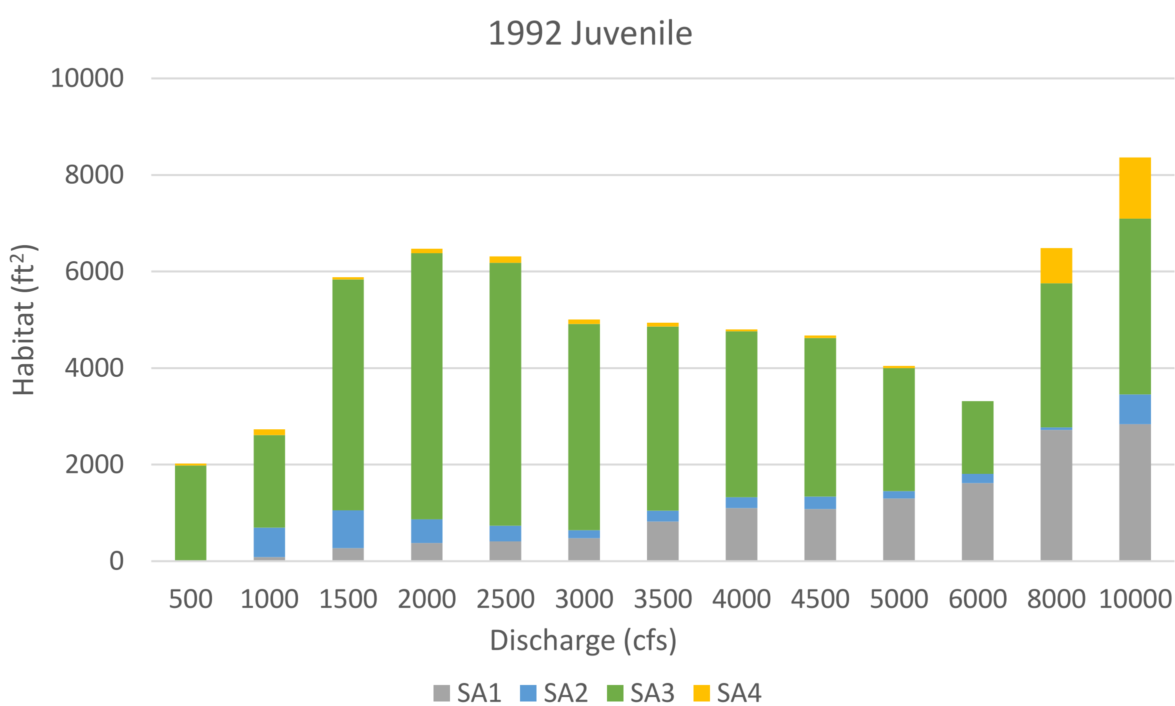

Figure G- 8 Spatially varying juvenile habitat throughout San Acacia reach in 1992

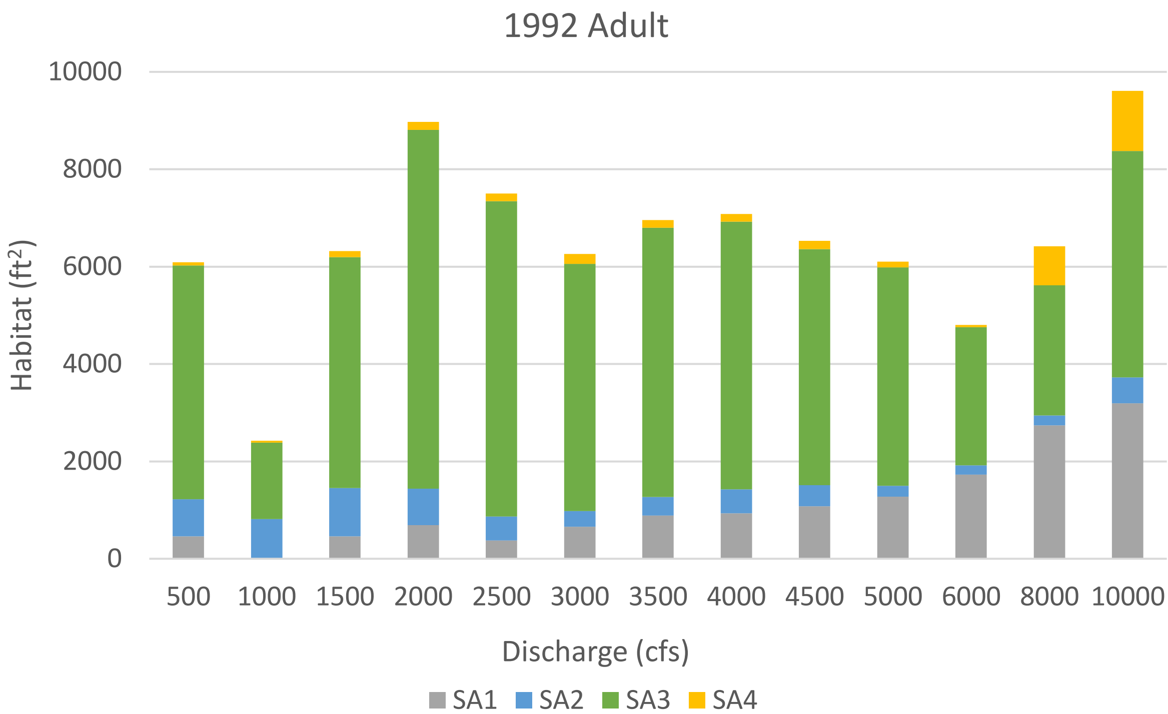

Figure G- 9 Spatially varying adult habitat throughout San Acacia reach in 1992

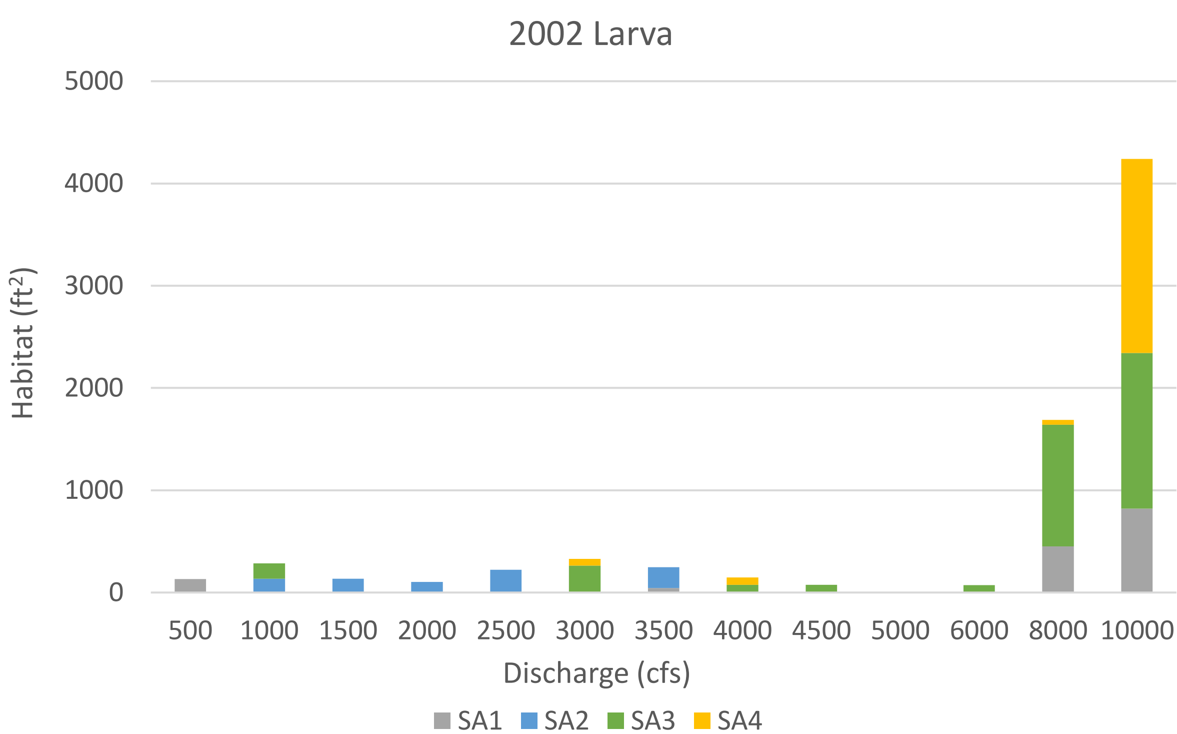

Figure G- 10 Spatially varying larva habitat throughout San Acacia reach in 2002

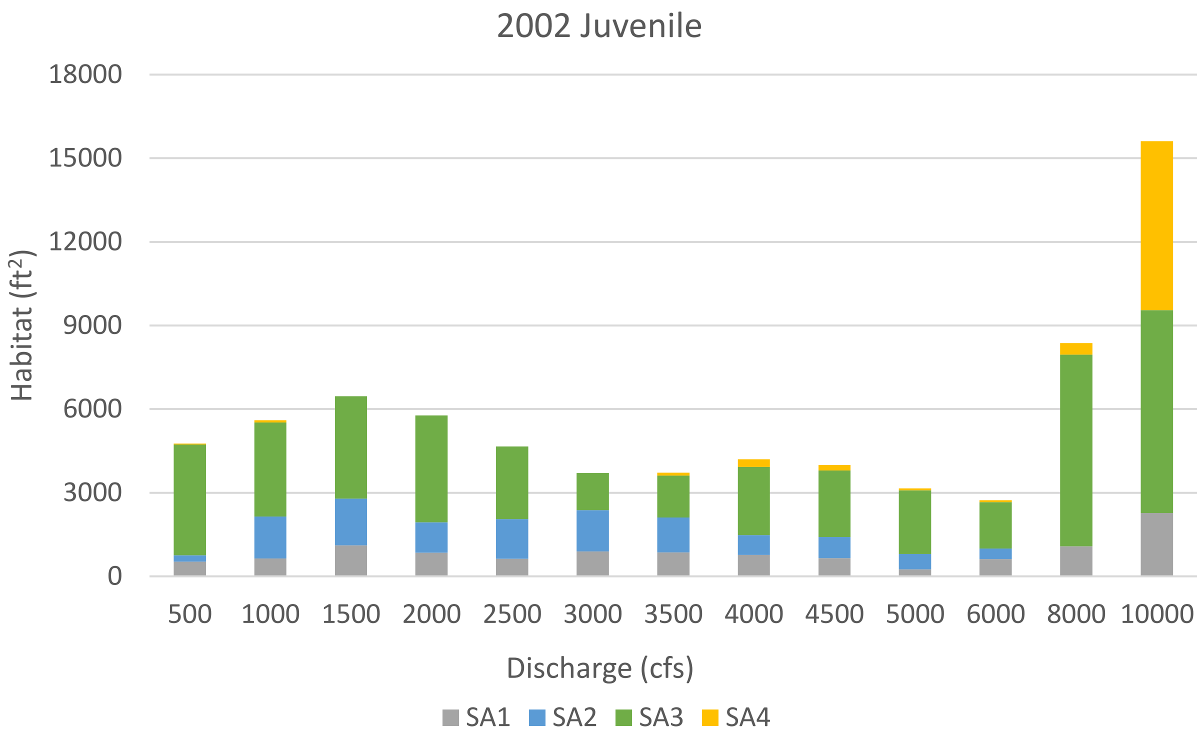

Figure G- 11 Spatially varying juvenile habitat throughout San Acacia reach in 2002

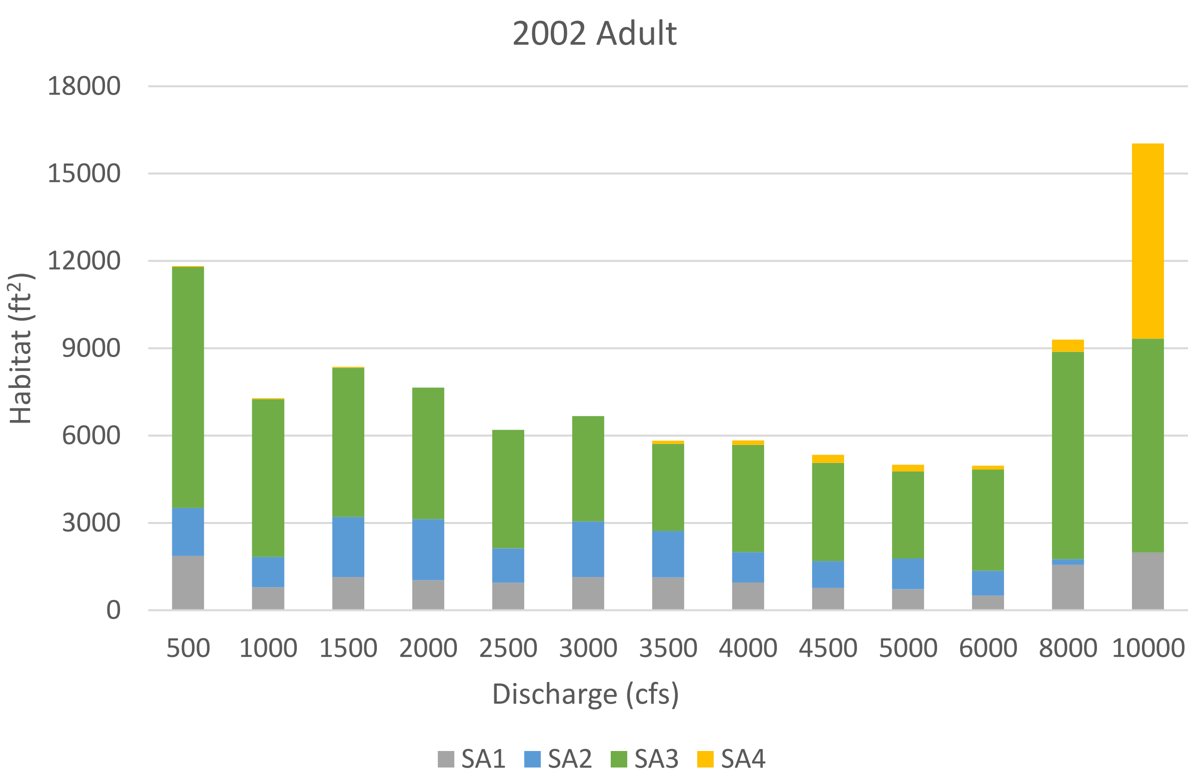

Figure G- 12 Spatially varying adult habitat throughout San Acacia reach in 2002

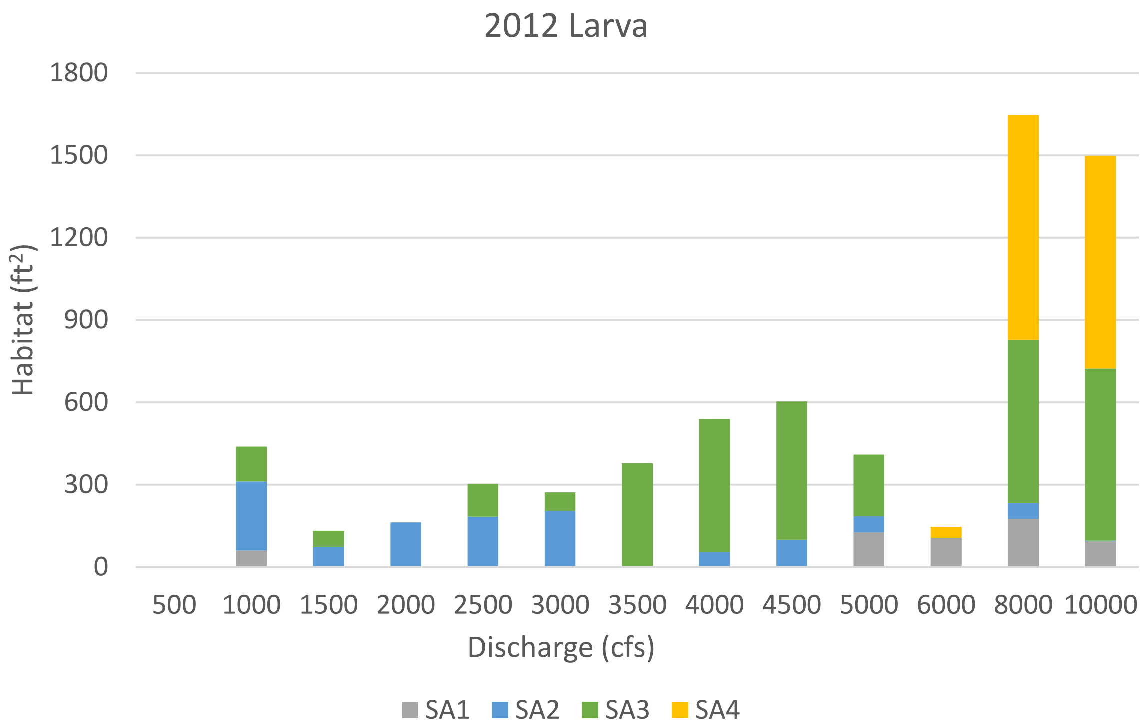

Figure G- 13 Spatially varying larva habitat throughout San Acacia reach in 2012

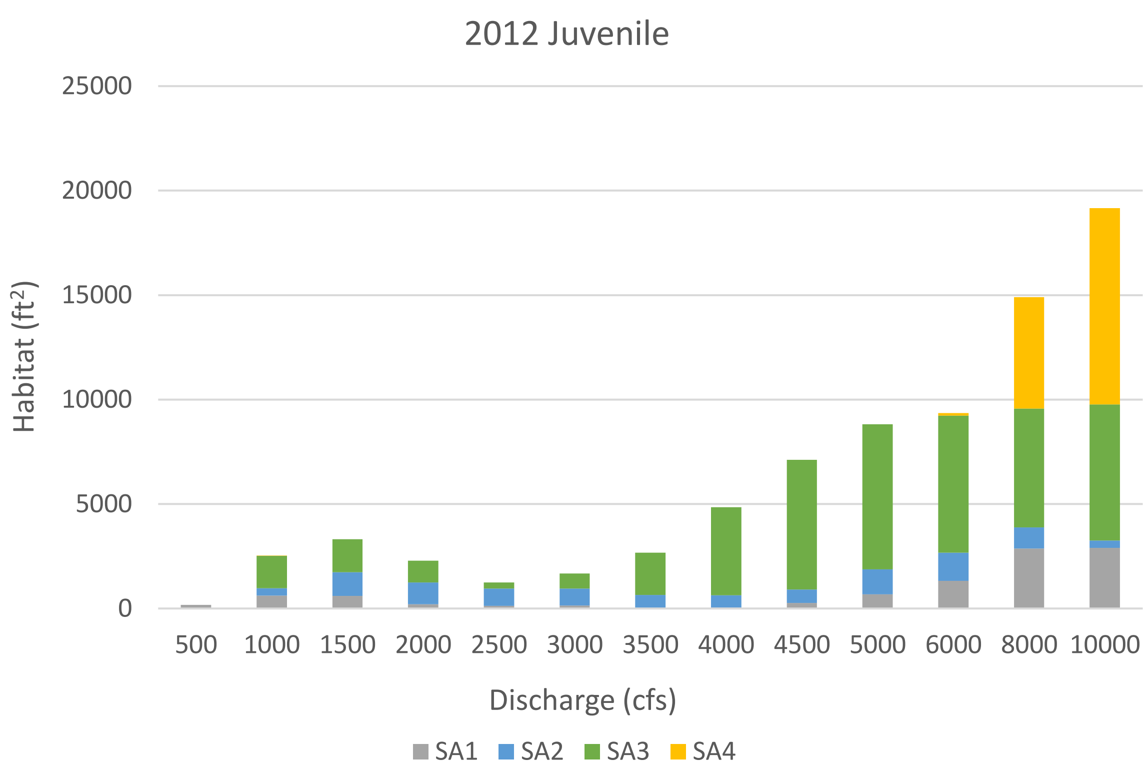

Figure G- 14 Spatially varying juvenile habitat throughout San Acacia reach in 2012

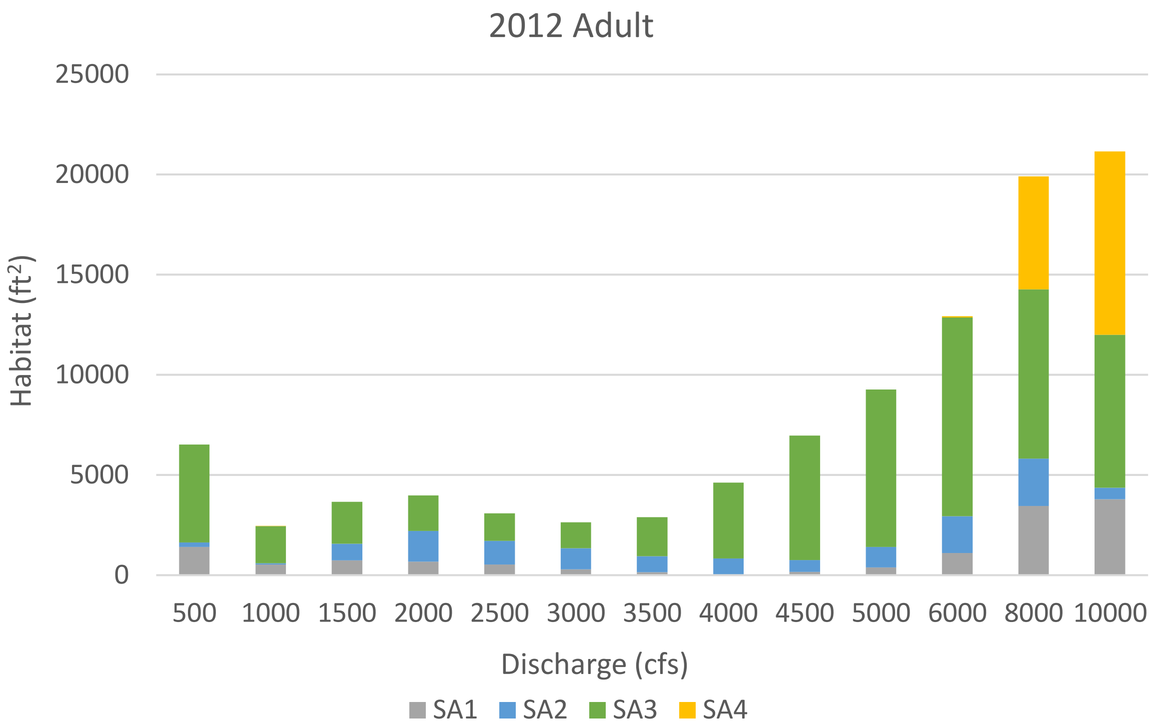

Figure G- 15 Spatially varying adult habitat throughout San Acacia reach in 2012